PHYSICAL AND MECHANICAL PROPERTIES OF ROCKS EXPOSED TO MICROWAVE IRRADIATION: POTENTIAL APPLICATION TO TUNNEL BORING

Pejman Nekoovaght Motlagh

Department of Mining & Materials Engineering
McGill University, Montreal

February 2015

A Thesis Submitted to the Faculty of Graduate Studies and Research
In partial fulfilment of the requirements for the degree of
Doctorate of Philosophy

Dedication

I dedicate this dissertation to my parents for their priceless and extreme love, devotion, support, dedication, encouragement and kindness.

Abstract

Mining companies and the market today are advancing toward faster, more efficient and productive continuous excavation within mining and civil applications. Explosives are not used in continuous excavation in hard rock formations; therefore, the interaction between mechanical rock breakage or cutter tools and the natural rock become increasingly important to understand. Rock cutter tools are highly advanced in terms of material quality, but limited in performance when they cut natural hard rocks. Comprehensive and collaborative research between McGill University and Natural Resources Canada on all possible explosive-free rock breakage techniques demonstrated that the use of microwaves in rock breakage techniques is highly advantageous and efficient. Microwave-assisted rock breakage machines, specifically tunnel boring machines or TBMs, represent a potential new avenue of rock cutting and breaking technology. This thesis research introduces the microwave-assisted TBM concept, describes the selection of the appropriate microwave wave guide applicator for the design (i.e., multi-mode vs. open ended), and quantifies the influence of microwave irradiation on temperature distributions and mechanical properties (i.e., uniaxial compressive and Brazilian tensile strength, CERCHAR abrasiveness index) of specimens of hard rock. Influencing parameters such as power level, distance from the antenna and exposure time were evaluated, as well as the physical damage that microwaves induce to the rock. Microwave irradiation with an open ended applicator was shown to heat the rock from the surface inward, when the rock is a good energy absorber. The failure mechanism (biaxial compression vs. shear failure) depended on the temperature difference inside the rock has been observed. A benchmark numerical model was developed for both types of

microwave applicators, simulating the influence of microwave energy on the temperature profile under various conditions. Results of this study show that microwave-assisted rock breakage system is potentially viable in continuous hard rock excavation.

Résumé

Les compagnies minières et le marché aujourd'hui avancent rapidement vers l'excavation continuelle, car la technique est plus efficace et productif dans des applications minières et civiles. Les explosifs ne sont pas utilisés dans l'excavation continuelle dans des formations de roches dures; par conséquent, l'interaction entre les outils mécaniques de coupe et la rupture de la roche naturelle devient de plus en plus important de comprendre. Des outils de coupe de roche sont aujourd'hui très avancés en termes de qualité des matériaux, mais limitées dans la performance quand ils coupent les roches dures naturelles. La recherche globale et compréhensible de collaboration entre l'Université McGill et de Ressources naturelles Canada sur toutes les techniques possibles de rupture des roches sans explosifs a démontré que l'utilisation de micro-ondes en tant qu'un technique de rupture est très avantageuse et efficace. Les machines mécaniques pour la rupture des roches assistée par micro-ondes, en particulier les machines de forage à tunnel ou TBM, représentent une nouvelle voie potentielle de la coupe des roches et une technique de rupture. Cette recherche de thèse introduit le concept de TBM assistée par micro-ondes, décrit la sélection du guide d'onde des micro-ondes approprié pour la conception (multimodes vs. guide ouvert), et quantifie l'influence de l'irradiation des micro-ondes sur la distribution de température et des propriétés mécaniques (la résistance de compression uni-axiale, la résistance à la traction Brésilienne et l'indice d'abrasivité de CERCHAR) de spécimens de roche dure. Les paramètres influencent, tels que le niveau de puissance, la distance d'antenne et du temps de l'exposition ont été évalués, ainsi que les dommages physiques que les micro-ondes induisent à la roche. Lorsque la roche est un bon absorbeur d'énergie, irradiation de micro-ondes avec un applicateur de guide ouvert a été montrée qui chauffe la roche de la surface vers l'intérieur. Le mécanisme de défaillance (compression bi-axiale vs. rupture par cisaillement) dépendait de la différence de température à l'intérieur de la roche a été appris. Un modèle numérique de référence est développé pour les deux types d'applicateurs de micro-ondes. La simulation de l'influence de l'énergie de micro-ondes sur le profil de température dans différentes conditions est aussi évaluer. Les résultats de cette étude montrent que le système de rupture de roche assistée par micro-ondes est potentiellement fiable dans l'excavation continuelle de roche dure.

Acknowledgement

Words cannot describe nor actions show how to thank my lovely parents who supported and given me endless and priceless love, motivation and encouragement throughout this research even my life. By dedicating this dissertation to them, I hope I may return a tiny fraction of all they have given to me. I also offer my deep sincere appreciation to my wife, Ms. Roya Safari, for her love and support.

I would like to thank my research supervisor Professor Ferri P. Hassani – without whom this project would not be realized – for all of his support: financial, technical and moral.

I would also like to thank Dr. Nima Gharib for his kind assistance in the simulation and numerical modelling section of this research, as well as Mr. Amir-Arash Rafie for his help regarding the economics of the mineral processing.

I was extremely fortunate to work with highly motivated members associated with my supervisor's research group. I would especially like to thank Dr. Ali Ghoreishi, Dr. Farzan Abbasi, Mr. Fan Liu, Mr. Lei Jin, Dr. Mehrdad Kermani, Mr. Hamed Rafezi, Dr. Leyla Amiri, Dr. Mohammed Hefni, Mr. David Gomezdiaz, Mr. Jeff Templeton, Mr. Kelvin Creber, Ms. Maureen Mcguinness, Mr. Eric Moulton, Mr. Arash Zarassi and Mr. Jonathan Cioffi for their help throughout the years. I give thanks to the administrative and technical staff of the Mining and Materials Engineering offices for their help, especially Ms. Marina Rosati and Ms. Barbara Hanley.

I would also like to extend my gratitude to Dr. Marc Betournay from Natural Resources Canada (NRCan) for his kind help in my research.

This work was generously sponsored by the Natural Sciences and Engineering Research Council of Canada (NSERC), Vale Canada, IAMGOLD, Glencore Xstrata and the Faculty of Engineering at McGill University.

Table of Contents

List of Tables

Table of Figures

Nomenclature

E	Electric field (V/m)
B	Magnetic field
$\varepsilon_\circ$	Permittivity of free space (8.86×10^{-12} F/m)
ρ	Density (kg/m^3)
t	Time (s)
J	Current per unit area
$\mu_\circ$	Permeability of free space ($4\pi \times 10^{-7}$ H/m)
μ^*	Complex electrical permeability
μ'	Real part of complex permeability
μ''	Imaginary part of complex permeability
σ	Electrical conductivity (S/m)
ε	Emissivity
ε'	Real part of complex permittivity
ε''	Imaginary part of complex permittivity (loss factor)
ε^*	Complex dielectric permittivity
ω	Angular frequency ($2\pi f$)
f	Frequency (Hz)
λ	Wave length (cm)
$\tan \delta$	Loss tangent
P	Power (W)
E_{rms}	Root mean square of the electric field
m	Mass (kg)
C_p	Specific heat capacity (J/kg°C)

ΔT	Temperature difference (°C)
e	Euler number (2.74)
α	Attenuation factor
β	Phase factor
z or d	Distance from and normal to the antenna (cm)
D_p	Depth of penetration (m)
σ_s	Stress (GPa)
E_{el}	Modulus of elasticity (GPa)
P_{rev}	Penetration per revolution
F_n	Normal force (N)
σ_{Bt} or σ_T	Brazilian tensile strength (MPa)
σ_{ucs} or σ_c	Uniaxial compressive strength (MPa)
CAI	CERCHAR abrasiveness index
R	Electrical resistivity (Ω-m)
K	Thermal conductivity (W/m°C)
A	Cross-sectional area (mm^2)
W	Power flux density (W/cm^2)
M	Total dipole moment per unit volume (C.m)
M_e	Electric dipole moment per unit volume (C.m)
M_i	Ionic dipole moment per unit volume (C.m)
M_o	Orientational dipole moment per unit volume (C.m)

Chapter 1 Introduction

Since the Stone Age, humans have increasingly used various rock breakage techniques. Today rock breakage is common in mining and civil applications, where it can present challenges, especially regarding extremely hard rock types. To facilitate breakage of hard rocks, many techniques have been developed and applied, such as explosive, mechanical, thermal, fluid, sonic, chemical, electrical and laser. Using explosives has disadvantages that limit the productivity and advancement rates of a project. Mechanical techniques remain the most efficient and economical, but the search for novel hard rock breakage techniques continues, particularly in light of economic factors today.

Microwave technology has been exploited since the end of World War II and today is widely used in the medical, food and telecommunication industries. In the early stages of technology development, it was found that an alternating electric field can alter the energy content of dipolar substances. This energy would be released in the form of heat (Osepchuck, 1984; Cao, 2012). Research on the dielectric and thermal properties of various materials is crucial to predict the energy absorbed and the heat generated.

The use of microwave technology as an electrical technique to break natural rocks without a mechanical tool involved was first proposed by Maurer (1968). Since the technology required a large amount of energy to break rocks as the only tool, it was not economically viable.

Today underground excavation projects require to be completed in a shorter period of time, efficiently and continuously. Currently, many major corporations (e.g., Atlas Copco, Anglo American, Rio Tinto, Sandvik, Robbins Company) whether individually or in collaboration try to develop explosive-free mechanical equipment to continuously break rocks and excavate more efficiently, quickly, and productively. Continuous excavators called tunnel boring machines (TBMs) are widely used in civil applications. Mining industries are trying to develop continuous excavators to increase productivity (Robbins Company, 2012). Whereas TBMs are very effective, heavy wear of cutting tools during use in hard rocks necessitates costly replacements. Microwave-assisted TBMs represent a potential new avenue to improve the economics of TBMs in mining and civil engineering projects. The higher capital costs of microwave systems could be offset by lower operating costs and higher productivity considering mine to mill process in mining applications.

This thesis introduces the concept of microwave energy in combination with TBM. The material of disc cutters as the primary tools to break rocks on TBMs are immensely improved at their highest strength possible in order to perform efficiently. Nonetheless, performance of TBMs in hard rocks still remains limited, where microwave-assisted TBM can potentially show positive efficient performance. By eliminating the need for explosives, much of the heavy equipment for drilling, loading or hauling can also be eliminated. Weakening of the rock by microwaves means that in the mineral processing plant, a smaller crusher can be used, reducing energy consumption during processing (Walkiewicz et al., 1988, 1991, 1993; Marland et al., 2000; Wang and Forssberg, 2000; Vorster et al., 2001; Kingman et al., 2004a, 2004b; Amankwah et al., 2005).

1.1 Objectives

To investigate the feasibility of microwave-assisted TBMs, it is necessary to understand the influence of microwaves on the physical and mechanical properties of hard rocks. Thus, the project has the following objectives:

- Understand microwaves in terms of how they are generated, the mechanism(s) by which they heat the material being exposed, and the microwave parameters influencing the material being irradiated.
- Compare the effect of microwave power in a multi-mode cavity in the laboratory on rock uniaxial compressive strength (UCS), CERCHAR abrasiveness index (CAI) and Brazilian tensile strength (BTS).
- Determine how microwave radiation in a multi-mode cavity interacts with the material physical dimension and water saturation to influence the temperature distribution within rock and understand the mechanism of damage induced to the rock.
- Study the proper microwave applicator type that adapts in the conceptual design of a microwave-assisted TBM.
- Determine the electrical properties of rock samples, and how they are influenced by microwave frequency and water saturation.
- Investigate the influence of microwave irradiation on the surface of a rock mass, in terms of damage density, depth of penetration and temperature distribution.
- Understand the mechanism of rock failure after microwave irradiation, as well as the influence of the power level and distance from the antenna.
- Calculate the penetration rate and performance of a TBM by microwaves.
- Numerically simulate all experimental microwave testing conditions to develop and calibrate a model to test the effect of distance, power level, frequency and exposure time on the temperature distribution within the rock mass.

- Understand the power and electric field intensity distribution inside the microwave applicators, as well as the rock mass subjected to microwave irradiation.

1.2 Statement of originality

I declare that the text and the work presented in my thesis is original and that no sources other than those mentioned in the text and its references have been used in creating it.

Chapter 2 Microwave Heating of Materials

Since their discovery during World War II, microwaves have been increasingly used for a variety of applications. Communication applications include telecommunication and satellite data transmission (Osepchuk, 1984). In addition to medical and domestic uses, microwaves have also been used in industry for heating purposes in industries such as rubber extrusion, plastic manufacturing, and the treatment of foundry core ceramics (Kingman et al., 1998b). Gwarek and Celuch-Marcysiak (2000) categorize industrial microwave applications as:

- Food processing (heating, thawing, biological deactivation, quality control)
- Industrial material drying (paper, wood, explosive wood drying)
- Chemical reaction enhancement (micro-reaction control, fluidized beds)
- Melting of industrial materials (glass, rubber, sludge)
- Sintering (ceramics, metal powders)
- Plasma generation
- Mineral processing (rock crushing, comminution)
- Waste treatment and recycling

The most common microwave frequency used worldwide for heating applications is 2.45 GHz. This frequency falls in the range of S band microwaves (2 to 4 GHz), which is commonly used for weather radar, surface ship radar, communication satellites and devices, microwave ovens, radio astronomy, mobile phones, wireless LAN, Bluetooth, global positioning systems, oil extraction, medical applications (Bond et al., 2003), food industry, chemical laboratories (Arrieta et al., 2007), agricultural industries (Jing Tao & Tianxing 2011) and mineral processing industries (Atomic Energy of Canada, 1990). The frequency 915 MHz is another frequent frequency used for industrial microwave heating applications especially food industry.

The major advantages of microwave heating are the short start-up time, precise control on specifications and volumetric heating (Ayappa et al., 1991). In mineral processing, additional advantages are non-contact heating, energy transfer instead of heat transfer, rapid heating, material-selective heating, heating initiation from the interior of a material, and a high level of safety and automation (Haque, 1999).

2.1 Electromagnetic Theory

Since microwaves affect rocks by heating, a thorough understanding of electromagnetic theory is of paramount importance.

2.1.1 Electromagnetic Waves in Free Space

In a vacuum, electromagnetic theory can be described by Maxwell's four equations (Griffiths, 1999):

$$\nabla \cdot E = (1/\varepsilon_o)\rho_c \tag{1}$$

$$\nabla \cdot B = 0 \tag{2}$$

$$\nabla \times E = -\partial B/\partial t \tag{3}$$

$$\nabla \times B = \mu_o J + \mu_o \varepsilon_o (\partial E/\partial t) \tag{4}$$

where E is the electric field, ε_o is the permittivity of free space, ρ_c is the charge density, B is the magnetic field, μ_o is the permeability of free space, and J is the current per unit area-perpendicular-to-flow.

Equations 1–4 constitute a set of coupled, first order, partial differential equations for E and B. However, both vector functions E and B satisfy the wave equation with speed $v = \frac{1}{\sqrt{(\varepsilon_0 \mu_0)}}$ or 299,792,458 m/s, the speed of light in a vacuum, also written c.

2.1.2 Electromagnetic Waves in Matter

Equations 1–4 describe dynamics for electromagnetic waves propagating through free space or insulating material (such as glass). When conductors and dielectrics are involved, the form of Maxwell's equations change, as well as the solutions, bringing about new dynamics. Maxwell's equations in the presence of linear media are (Griffiths, 1999):

$$\nabla \cdot E = (1/\varepsilon)\rho_f \tag{5}$$

$$\nabla \cdot B = 0 \tag{6}$$

$$\nabla \times E = -\partial B/\partial t \tag{7}$$

$$\nabla \times B = \mu\sigma E + \mu\varepsilon(\partial E/)\partial t \tag{8}$$

For conducting material, the free charge ρ_f almost immediately flows to the surface, and for insulators, there is no free charge available, as it is tightly bound to atoms and molecules. Equation 5 therefore reads $\nabla \cdot E = 0$.

2.2 Dielectric Properties of Materials

Polarization is the main phenomenon responsible for dielectric loss in a material exposed to an alternating electric field.

2.2.1 Polarization in Linear Dielectrics

Even if materials are electrically neutral, their constituents are not! All atoms, ions and dipoles in materials tend to orient themselves so as to align with the electric field. Each of atom, ion and dipole obtains a dipole moment that is proportional to the electric field (Metaxas et al., 1983) (Meredith, 1998). Since atoms, ions, and dipoles obtain dipole moments in different ways, each has its own polarizability, given by α_e, α_i and α_o, respectively. Therefore, materials become polarized by three mechanisms within an electromagnetic field (Griffiths, 1999) (Saxena, 2009).

a) Electronic (atomic) polarization

b) Ionic polarization

c) Orientational (dipolar) polarization

In bulk material, all individual atoms, ions and dipoles align in the same direction to polarize the material. A convenient way to measure this is with the vector M, defined as the dipole moment per unit volume. The total polarization, M is the sum of the contributions of the realignment of all the atoms, ions and dipoles as given in equation 9.

$$M = M_e + M_i + M_o \tag{9}$$

where the subscripts e, i, and o correspond to electronic, ionic, and orientational polarization, respectively.

2.2.2 Complex Permittivity and Permeability

Saxena (2009) modelled the complex behaviour of electric and magnetic waves in matter (equations 10 and 11) by considering the permittivity and permeability of the material to be complex. The complex permittivity (ε^*) and permeability (μ^*) are calculated as follows:

$$\varepsilon^* = \varepsilon' + i\varepsilon'' \tag{10}$$

$$\mu^* = \mu' + i\mu'' \tag{11}$$

The real parts of ε^* (ε', the dielectric permittivity constant) and μ^* (μ', the dielectric permeability constant) are responsible for the normal dynamics inside the material, such as the speed of the wave. However, the complex (imaginary) parts are due to losses arising from the response of the material (the "load") to the electric (ε'', the permittivity loss factor) and magnetic (μ'', the permeability loss factor) fields. It is interesting to note that most dielectrics do not couple strongly with the magnetic field, and, as a result, $\mu'' = 0$ and μ^* becomes real, written as $\mu = \mu'$ (Saxena, 2009). The permeability of free space is $\mu_{\circ} = 4\pi \times 10^{-7}$ H/m. The relative complex permittivity of a material is calculated by dividing the complex permittivity by the permittivity of free space ($\varepsilon_{\circ} = 8.86 \times 10^{-12}$ F/m).

The constant permittivity (ε') is the real part of the complex permittivity and the loss factor (ε'') is the imaginary part of the complex permittivity.

2.2.3 Electrical Conductivity

The relationship between a material's electrical conductivity and loss factor is a function of the electromagnetic frequency, as described in equation 12 (Gabriel, et al., 1998):

$$\sigma = \omega\varepsilon_{\circ}\varepsilon'' = 2\pi f\varepsilon_{\circ}\varepsilon'' \qquad (12)$$

where σ is the electrical conductivity, $\omega = 2\pi f$ is the angular frequency in Hz, $\varepsilon_{\circ}$ is the free space electrical permittivity (8.86×10^{-12} F/m) and ε'' is the material's loss factor at the appropriate frequency.

2.2.4 Loss Tangent

The loss tangent is an indicator of the amount energy that could be lost within a material and is calculated as follows (Gabriel, et al., 1998) (Sutton, 1989):

$$\tan\delta = \varepsilon'' / \varepsilon' = \sigma / 2\pi\varepsilon_{\circ}\varepsilon' \qquad (13)$$

where tan δ is the loss tangent, ε' is the dielectric constant, ε'' is the loss factor and σ the effective conductivity of the material (S/m).

2.2.5 Power Absorption Density

Energy is transported through space by electromagnetic waves. The power flow through a closed surface can be calculated by the power density generated by the electric field, as well as the magnetic field. Although the electric field can be quite difficult to determine inside a material, it can be approximated by assuming that it is constant in the calculated area (Metaxas, et al., 1983). The power density of a unit volume absorbed by a material being exposed in an electromagnetic field is calculated by:

$$P = 2\pi f \varepsilon_o \varepsilon'' |E|_{rms}^2 + 2\pi f \mu_\circ \mu'' |E|_{rms}^2 \tag{14}$$

where P is the power density of a unit volume (W) absorbed by the dielectric, E_{rms} (V/m) is the root mean square value of the electric field inside the material, and f is the frequency (Hz) of the electromagnetic wave. Since nonmagnetic materials have $\mu'' = 0$, their power density is then calculated by only considering the first part of the combination.

According to the first law of thermodynamics, the power dissipated and absorbed within a specific mass of material increases the temperature of that material from $T_\circ$ at $t_\circ$ to T after t seconds. The rate at which the material temperature rises is $\Delta T/\Delta t$ (Meredith, 1998). Therefore the following equation is applied:

$$P = mC_p(\Delta T/\Delta t) \tag{15}$$

Where P is the power dissipated (W), m is the mass of the material (kg), C_p is the specific heat capacity of the material (J/kg°C), $\Delta T = T - T_\circ$ is the temperature difference (°C) and $\Delta t = t - t_\circ$ is the time interval during which power is emitted to the material (s).

2.2.6 Electric Field Intensity

The intensity of the electric field emitted by an electromagnetic device diminishes exponentially when it enters a medium (e.g., air, a dielectric) (Metaxas, et al., 1983) in accordance with equation 16. Therefore, the power dissipated due to that electric field also decreases exponentially (equation 17).

$$E = E_{max} \,.\, e^{-\alpha z}\, e^{j(\omega t-\beta z)} \tag{16}$$

$$P \approx e^{-2\alpha z} \tag{17}$$

where E_{max} is the initial electric field (V/m), α is the attenuation factor of the wave propagating into the medium, β is the phase factor of the wave propagating into the medium and ω is the angular frequency ($2\pi f$, in which f is the frequency (Hz)).

2.2.7 Depth of Penetration

The amplitude of the electromagnetic wave diminishes exponentially once it enters a dielectric, until it disappears. The depth at which the power of the electromagnetic wave attenuates to 1/e (where e is Euler's number = 2.72) the value at the surface is called the penetration depth, also known as the skin depth l (Griffiths, 1999), given by:

$$D_p = \frac{1}{\alpha} = \frac{1}{2\omega}\sqrt{\frac{\frac{2}{\mu'\varepsilon'}}{\sqrt{1+(\frac{\varepsilon''}{\varepsilon'})}-1}} \tag{18}$$

In most materials ε” << ε’; therefore, equation 18 can be Taylor expanded and reduces to:

$$D_p = \frac{\lambda_{\circ}\sqrt{\varepsilon'}}{2\pi\varepsilon''} \tag{19}$$

where $\lambda_{\circ}$ is the free space wavelength.

2.3 Health and Safety Standards of Microwaves

Although a great deal of research has been conducted regarding the hazards of microwave exposure for human health, no concrete conclusions have been drawn. According to the World Health Organization (WHO) international standard of electromagnetic emission safety, IEEE International Committee on Electromagnetic Safety (SCC39) (2006) and the U.S. Bureau of microwave radiation safety (U.S. Standards C95.1, 1966) (Steneck, et al., 1980), the maximum range allowable electromagnetic energy to be emitted to protect human health is 5 – 10 mW/cm^2 (Steneck, et al., 1980), as in commercial microwave ovens (Klauenberg & Miklavčič, 2000).

2.4 Factors Influencing Dielectric Properties of Materials

2.4.1 Frequency of the Applied Field

The permittivity of a material varies with the frequency of an alternating electric field (Saxena, 2009). This is due to the ability of the atoms, ions, and dipoles to align and realign with the alternating electric field. All properties of a dielectric material are connected by a complex permittivity, which is frequency-dependent, according to the Griffiths model (Griffiths, 1999).

2.4.2 Temperature of the Material

A material's loss factor determines the part of the microwave radiation that is lost into the material and transferred to heat. The loss factor is proportional to temperature and it decreases as the temperature of the material increases (Schön, 2004).

2.4.3 Porosity and Moisture Content of the Material

Water is known to be an excellent absorber of microwave energy (Gabriel et al., 1998); it normally has higher electrical permittivity than any other materials. Moisture within a material subjected to microwave irradiation will cause the temperature to rise significantly, since water will be first to absorb microwave energy. Porosity differs among natural rocks. Hard igneous rocks have 0.5 – 1% porosity, therefore they have very low water content. Micro- and macro-factures (cracks) enhance the water retention abilities of a given rock.

2.5 Microwave Heating of Rocks

2.5.1 Background of Microwave Heating in Rock Breakage Applications

Microwave exposure transfers electromagnetic energy into rock and upon its properties the energy transforms as heat. The relative transparency of minerals to microwave energy determines their behavior when exposed to microwaves. Chen et al. (1984) measured the temperature of 40 purified (99% pure) minerals, weighing 0.5 - 1g, were exposed to microwave irradiation for 3 – 5 minutes at 150 W applied energy (power) and a frequency of 2.45 GHz. Most silicates, carbonates and sulphates, and some oxides were transparent to microwave radiation: the microwaves passed through them without producing heat. By comparison, most sulphides, arsenides, sulphosalts, sulphoarsenides, and metal oxides were microwave absorbers, heating strongly, emitting fumes and fusing. These findings were also supported by a subsequent investigations by Walkiewicz et al. (1988) Haque (1999) and Jones et al. (2002).

By treating minerals with microwaves, thermally-assisted liberation of minerals was introduced by Fitzgibbon et al. (1990) and Veasey et al. (1991). As a result of the heat generated due to the influence of microwave irradiation the grindability efficiency and liberation of valuable minerals from gang was increased. Furthermore, Veasey et al. (1991) and Walkiewicz et al., (1991) emphasized more on the usefulness of microwave irradiation in mineral processing.

Church et al. (1988) also classified six classes of minerals commonly found in natural ores, grouped by their chemical composition: (oxides, carbonates, silicates, phosphates and sulfates, haloids and tungstates) as low loss minerals (weak absorbers), since their temperatures did not increase significantly when exposed to microwave radiation. Powdered minerals were exposed to microwave irradiation at frequencies ranging from 0.3 to 1 GHz.

Further to Chen et al. (1984) research, more natural minerals commonly found in nature were treated with microwave energy by Ulaby et al. (1988) and Walkiewicz et al. (1988). The authors not only confirmed the major groups introduced by Chen et al. (1984) they also demonstrated that minerals' loss factor are independent of frequency change. Moreover, micro-cracks were observed at microscopic scale when minerals were treated with microwaves.

Typically, rocks contain several minerals, some of which are transparent to and some absorb microwaves. In addition, thermal expansion coefficients differ among mineralogical species; therefore thermal gradients and stresses are created in rocks, leading to inter- or trans-granular cracks (Kingman and Rowson, 1998a; Passchier et al., 2005).

Gray (1965) described the influence of heat on the mineral spallation process, using a conductive surface heating device. Increasing the surface temperature of materials created a stress distribution within the heated area. The stress field caused cracks to grow and propagate rapidly, so the surface began to fall apart in the form of very thin discs (spall). Maurer (1968) evaluated the performance of all known possible novel drilling systems or technologies, and categorized them as mechanically induced stresses, thermally induced stresses, fusion and vaporization, and chemical methods. Lauriello (1974a), Lauriello and Fritsch (1974b) investigated thermal weakening of some rock types such as limestone and granite as spallable specimen and basalt as a non-spallable rock type, using a flame torch as the conductive heat source. The samples' thermal characteristics were analyzed according to the results from spallable and non-spallable rocks. The author showed an increase in the penetration rate of drilling in limestone by using a conductive heat source (flame torch) within the drill system. The author's research demonstrated that the surface of the rock can be fractured and spall off due to the quick rise in temperature.

Thermally-assisted grinding and liberation of minerals from ore using microwave energy as the heat source was introduced by Fitzgibbon et al. (1990). Santamarina (1989) investigated rocks characteristic against microwave energy and introduced the potential combination of microwave-assisted mechanical rock breakage machines. Lindroth et al. (1992, 1993), equipped a drag bit with a high-power microwave energy device to examine the effect on the penetration rate of a tungsten carbide spade bit into St. Cloud gray granodiorite and Dresser basalt. The samples were exposed to variable microwave power (up to 25 kW) and time of irradiation to reach the wanted temperature. The microwave apparatus was an open-ended rectangular waveguide emitting 2.45 GHz of frequency microwaves at power levels up to 25 kW. The rocks were exposed for one minute while drilled with a rotary tapered drill bit by putting 401 kg of thrust and applying 36 rpm torque speed. The microwave energy was being radiated from a steady rectangular waveguide to the surface of the rock.

It was concluded that the drilling penetration rate increased with increasing temperature. In addition, negligible wear on the bit was observed. Since bit temperatures remained low, no destruction of the carbide-to-steel brazing occurred (Lindroth et al., 1993). This concept of microwave-assisted hard rock cutting was patented by Lindroth et al. (1991); however, no experimental data was found on preconditioning the surface of rocks prior to be cut.

Previous studies to date are mostly related to the use of microwave technology in mineral processing. It was once introduced to break rocks with microwave as the only method of rock breakage system (Maurer, 1968). Moreover, microwave-assisted drilling was investigated (Lindroth et al., 1993) and showed that there was an improvement in drilling performance. A microwave treated scratching system on the surface of rock is also patented but without any experimental data. Furthermore, the industrial application of explosive-free rock breakage technology including continuous miners, road-headers and TBMs are also introduced by Hartman (1992). The current research investigates the concept of a mechanical rock breakage machine combined with microwave technology for the purpose of continuous excavations.

2.5.2 Influence of Microwave Radiation on Material Strength Properties

Microwave cavities "…are mechanically simple, closed metal boxes, consisting of two dimensions of several wavelengths long which support many modes" (Kingman, 2005). Microwave cavities can be multi-mode and single-mode. "A mode is a defined pattern of distribution of the electric and magnetic field components of an electromagnetic wave excited in a closed cavity" (Kingman et al., 2004). The heat generated in the dielectric material (the "load") in a multi-mode cavity is affected by several parameters, such as the dimensions and mechanical properties of the load, and the configuration of microwave feeds in the apparatus (Kingman et al., 2004). "A single-mode cavity is a metallic enclosure which supports only a single mode to localize the microwave radiation into a small volume and generate a high electric field" (Kingman, 2005). In single-mode cavities, the volume of energy absorbed by the dielectric directly depends on the electric field provided by the electromagnetic energy, which leads to rapid heating (Kingman, 2005).

The nature of the material being irradiated strongly influences the effect of microwave treatment on mechanical properties. For example, andesite rock samples treated in a 2.45 GHz frequency multi-mode microwave completely melted after being exposed to 1350 W of power for 10 minutes, followed by 2700 W of power for 30 minutes (Znamenácková et al., 2003). X-ray diffraction analyses showed that the basic chemical composition of andesite was unchanged, without any losses in weight, but the structure of andesite turned amorphous (Znamenácková et al., 2003).

Jerby et al. (2000) designed an apparatus that drives the microwave energy from a 1 kW power magnetron into the material through a waveguide, such that the microwave irradiation is localized into a predetermined spot on the material. The subjected material is exposed to microwave irradiation as long as the microwaved area on the material is melted, and the heat-resistant tungsten electrode can be inserted into the melted zone (Jerby et al., 2002, 2004). As the electrode is pushed into the molten material, a hole is formed. A hole of two millimeters in diameter and two centimeters in depth has been drilled in the materials mentioned above within less than a minute. This apparatus is still at the bench scale and has been successfully applied to a variety of materials such as glass, basalt, concrete, ceramics and silicon (Jerby et al., 2002, 2003, 2004).

Whittles et al. (2003) and Jones et al. (2007), used numerical modeling to investigate the influence of the power density on the strength of the material. Both authors simulated a 30 × 15mm pyrite-hosted calcite sample in FLAC simulator software and examined the effect of microwave radiation on the strength of the numerically designed sample. Whittles et al. (2003) used the simulated sample to model irradiation to the normal constant microwave energy in various conditions, such as different times of exposure and power levels of microwave energy. Whereas, Jones et al. (2002 and 2007) studied the influence of pulsed microwave energy on the strength of the same simulated pyrite hosted calcite sample. Jones et al. (2007) used five times of exposure from 0.1 to 10 seconds. Both researchers evaluated the influence of the energy on the unconfined compressive strength of the rock sample and showed a significant reduction either by exposing the simulated sample to constant or pulsed microwave energy. For Whittles research, small pyrite particles were distributed randomly throughout the calcite host model. Both multi-mode and single-mode microwave applicators were used. Pyrite is considered absorbent and calcite transparent to the microwave radiation. In this numerical simulation, where no practical experiment were conducted, two different microwave conditions were used with the same frequency of 2.45 GHz. In the first condition, the sample was exposed to 2.6 kW of power in a multi-mode cavity producing power density between 3×109 W/m^3 at 300°K and 9×109 W/m^3 at 600°K. The time of exposure in the first condition was 1, 5, 10, 15 and 30 seconds (Whittles et al., 2003). After heat treatment, uni-axial compressive strength (UCS) and point load test (PLT) were performed in order to compare the strength of sample irradiated by microwaves. Eventually the strength of the simulated material drops significantly sharp as the time of exposure increases. Since the power density is directly proportional to the magnitude of the electric field, specimens heated up more quickly than in the multi-mode cavity. The pyrite particles heated before the calcite host and expanded, releasing stress at shear planes (Kingman et al., 1998). Hence, although calcite was heated by conduction from pyrite particles in the multi-mode cavity, the high power density in the single mode cavity was much more effective in terms of rapid and significant strength reduction (Whittles et al., 2003).

The nature of the grain boundaries between minerals is not well understood, but it has been suggested that it is an area of disorder between two ordered species, which can be a potential area of weakness within rock (Passchier & Trouw, 2005). Previous researches done by Chen et al. (1984), Haque (1999) and Jones et al. (2002) determined that different minerals have different reactions to microwave radiation. Some absorb or absorb little the radiation and some are transparent. With respect to different mechanical properties, minerals heat at different rates in an applied microwave field, which will increase the level of volumetric expansion at the grain boundaries (Res et al., 2003). It is assumed that this rise in the volumetric expansion will hence create potential stress in the grain boundaries that can weaken the material via inter-granular and trans-granular cracks. An investigation of the effect of microwave on massive Norwegian Ilmenite ore performed by Kingman et al. (1998, 2000) confirmed the presence of inter- and trans-granular cracks after microwave treatment created within the minerals. Another investigation also showed reduction in Bond Work Index (BWI) of up to 90% (Kingman et al., 2004). Similarly, Vorster et al. (2001) determined the influence of microwave energy on the BWI reduction of two kinds of copper ores from Neves Corvo, Southern Portugal. The samples were massive copper ore and massive copper-zinc ore. The authors exposed the samples being irradiated for 90s by microwave energy of 2.6 kW of power level and 2.45 GHz of frequency in a multimode cavity. The results of treated tests compared to the untreated samples shows almost 70 % reductions in Bond Work Index. Quenching the treated samples in water enhanced strength reduction by 15 %, which was attributed to the steep temperature gradient between the hot samples and the water causing a shock of expansion ratio of grains that led to micro-fracturing within particles (Vorster et al., 2001). Detailed investigations regarding the influence of microwave treatment in a multi-mode cavity on basalt strength conducted at McGill University showed reduction in strength with increasing time exposure (Satish, 2005; Satish et al., 2006). Satish (2005, 2006) exposed basalt core samples to the microwave irradiation of 750 watts for 60, 120, 180 and 320 seconds in a multi-mode cavity. Longer exposure times (180 and 320 s) causes the sample to spall and chip off locally under the point load test.

Modelling studies have helped improve our understanding of the mechanisms of strength reduction in rock exposed to microwaves. Satish (2005) refined Whittles et al. (2003) simulations using finite element method (FEM) in modelling of the energy density of the microwave field in the cavity, instead of assuming a power density as did Whittles et al. (2003). In his simulations, Satish used the same material as Whittles et al. (2003), but used a single pyrite particle hosted calcite in the shape of a sphere, to show the generation of stress within the grain boundaries. Because of the axes of symmetry of the model, the model could be reduced to the two dimensional quadrant. The simulations showed that the transparency difference between the two minerals meant that a large amount of potential stress could be generated at the particle boundaries of the particles, leading to strength reduction. Furthermore, to be able to better understand how rapid heating generates stresses among particles due to differential volumetric expansion (Wang et al., 2005) performed a numerical modeling investigation on the mechanism of microwave assisted rock breakage. By using the discrete element method (DEM), they developed a model showing the breakage density at the boundary of a single pyrite particle hosted by calcite. Wang et al. (2005) used two different power levels to conduct his experiment. They realized that by increasing the power level and exposure time, the density of breakage increases in the area of the particles boundaries.

The potential for microwave-assisted strength reduction exists not only at the mining face, but in the processing plant. Kingman et al. (2004) investigated the influence of microwave irradiation on ore comminution within a processing plant. The author used actual lead and zinc ore from a mine in Sweden. One kilogram samples were exposed to microwave radiation in two different conditions.

In both multi-mode and single-mode cavity conditions in Kingman`s et al. (2004) research, the frequency of microwave is 2.45 GHz. Samples were irradiated with 5, 10 and 15 kW power for 1, 5 and 10 seconds each in multi-mode cavity; and 5, 7.5 and 10 kW power for 0.1, 0.5 and 1 second in single-mode cavity. Ore samples were not exposed to the radiation of 15 kW in single-mode cavity because of melting of the sample. The strength of samples was determined by the point load testing before and after microwave treatment. This study showed that rapid and significant failure can happen in single-mode applicators due to the high electric field strength concentration. In other words, the higher the microwave power level, the more the strength of the sample was reduced. Hence, this experiment on actual rock samples proves numerical experiments from Whittles et al. (2003) and Jones et al. (2007). Similarly, Scott (2006) investigated on the impact of microwave energy on copper ore liberation from South Africa. The author exposed 1kg batches of crushed samples into 10.5 kW power level of microwave irradiation of 2.45 GHz frequency for 0.5 sec. The result shows a significant strength reduction through mills within the processing plant after microwave treatment and an increase in the potential of copper liberation from its host during flotation (Scott et al., 2008). However, this study also specifies that coarse particle size (106 – 300 μm) improved the efficiency of the liberation process (Scott 2006; Scott et al., 2008).

Recent studies also demonstrate the benefits of using microwave technology in producing, demolishing and recycling concrete (Gary Ong and Akbarnezhad, 2015). It is also highlighted that as the frequency increases the thermal impact as a result of higher power intensity increases. Furthermore, higher frequency has shorter wavelength and requires smaller waveguide (in terms of physical dimensions) to travel through.

2.6 Thermal Properties of Materials

Every material, including natural rocks, requires a certain amount of energy per unit mass to increase its temperature one degree Celsius. This is known as the “thermal specific heat capacity” of that material, denoted as c_p. The specific heat capacity of rocks is temperature dependent and increases as the temperature rises (Somerton, 1992) (Schön, 2004). This means, more energy is required at higher temperature to increase the temperature of the material. Heat causes thermal expansion and thermal expansion causes internal thermal stress (σ_s) within the material (Somerton, 1992) (Schön, 2004) calculated by:

$$\sigma_s = \alpha E_{el} \Delta T \tag{20}$$

where α is the coefficient of thermal expansion ratio of the material (1/°C), Eel is Young’s modulus of the material (MPa) and ΔT is the temperature difference within the material (°C).

In natural rocks that have no magnetic susceptibility, combining equations 14, 15 and 20, the thermal stress induced within the material can be calculated by:

$$\sigma_s = \frac{2\pi f \varepsilon_o \varepsilon'' |E|^2 \Delta t \alpha E_{el}}{m C_p} \tag{21}$$

Equation 21 shows that the thermal stress induced in material exposed to microwave energy is independent of temperature. However, the thermal stress is directly dependent on the electric field intensity and exposure time that the material is exposed to microwave radiation.

The sintering point of materials (0.5 – 0.9 of the melting point) is the temperature at which the grains in a material begin to deform: the material has entered the plastic stage before melting ensues (DeJonghe, et al., 2003). At temperatures cooler than the sintering point, the material remains brittle and can be affected by the differential of expansion ratio of the grains. The melting point of most rocks is approximately 1200°C (Tarbuck et al., 2011). Between 500 and 700°C, rocks remain brittle. These are the optimum temperatures for fracturing (Gray, 1965) (Hasselman, 1969) (Tarbuck et al., 2011).

2.7 Tunneling in Hard Rocks

A common mechanical method of tunnelling though rocks without using explosives is using a tunnel boring machines, commonly known as TBM. The TBM cutter discs cut the surface of the rock by applying a huge amount of thrust on the cutters. In hard to very hard rock types, the penetration rate of TBMs is very low. Cutting hard rock by grooving instead of fracturing (Heiniö, 1999) would improve the penetration rate by fracturing the rock surface.

Among the many parameters involved in predicting the performance of a TBM, intact rock and rock mass parameters are significant (Cigla et al., 2001). The uniaxial compressive strength (UCS) (McFeat-Smith, 1977) (Roxborough et al., 1975) (Pang et al., 1989) and Brazilian tensile strength (BTS) (Fowel et al., 1976) (Blindheim, 1979) (Howarth et al., 1986) tests are commonly conducted to predict TBM performance (P_{rev}) in milimeters per revolution (equations 22 and 23). The CERCHAR abrassivity index value, also known as CAI, is a good predictor of cutter tool wear (equation 24) (Wijk, 1992) (Frenzel et al., 2008).

$$P_{rev} = 624 \frac{F_n}{\sigma_{Bt}} \tag{22}$$

$$P_{rev} = 3940 \frac{F_n}{\sigma_{ucs}} \tag{23}$$

$$\mathrm{L} = \mathrm{Dw}^3 \frac{\cot(\theta)}{\mathrm{F}\sqrt{\sigma_C \sigma_{PLT}}(\mathrm{CAI})^2} \tag{24}$$

where L is the life of the disc cutter measured by meters cut (m), D is the diameter of the disc cutter (m), w is the width of the cutter's edge (m), θ is the half angle of the cutter's edge, σ_c is the UCS of the rock (MPa), σ_{PLT} is the point load of the rock (MPa), F_n is the thrust applied to the disc cutter (N) and CAI is the CERCHAR abrasiveness index value of the rock.

Chapter 3 Methods and Experimental Setup

3.1 Rock Samples

A vast variety of natural rock types exist in nature. To investigate the influence of microwave energy on natural rocks, especially hard rocks, various rock samples were required to have a reasonable comparison study. 10 rock samples were chosen (Figure 3-1) to be within from three rock classes: igneous (granite, norite, two basalts, felsic and mafic granophyres), sedimentary (dolomite, sandstone and limestone) and metamorphic (gneiss).

Table 3-1 Some characteristics of rock samples used in the study

Rock sample	Location	Country	Density (gr/cm3)	Emissivity	Type	Grain size	Weak plane	Uniformity	Homogeneity
Granite	Vermont	USA	2.65	0.97	Igneous	coarse	No	Yes	Yes
Norite	Sudbury	Canada	2.8	0.98	Igneous	coarse	No	Yes	Yes
Dolomite	Polkowice County	Poland	2.61	0.98	Sedimentary	very fine	Yes	No	No
Basalt #1	Chifeng (Inner Mongolia)	China	2.89	0.99	Igneous	fine	No	Yes	Yes
Sand stone	Polkowice County	Poland	2.62	0.89	Sedimentary	fine	No	Yes	Yes
Basalt #2	California	USA	2.78	0.94	Igneous	fine	No	Yes	Yes
Limestone	Quebec	Canada	2.69	0.98	Sedimentary	very fine	Yes	No	No
Felsic Granophyre	Sudbury	Canada	2.62	0.97	Igneous	semi coarse	No	Yes	Yes
Mafic Granophyre	Sudbury	Canada	2.82	0.97	Igneous	semi coarse	No	Yes	Yes
Gneiss			2.89	0.98	metamorfic	very fine	No	No	No

Some rocks were received from active mines either as cores or as boulders extracted by drill and blasting methods. Potential discontinuities existed in boulders received due to blasting shocks. Limited amount of rock sample were available in the Geomechanics lab at McGill University in the form are either core or intact blocks cut from quarries. The discontinuities already existed in rock samples received from active mines were considered during testing; however, rock samples available in the lab were completely intact and did not anticipated any discontinuities. Some other rock samples were received from active mines in the form of cores that has been drilled for exploration purposes. Some other rocks such as granite and basalt #1 were undisturbed blocks extracted from quarries by diamond saws. Therefore, blasting shocks did not disturb them nor cause the development of potential planes of failure within the blocks; however, the blocks already contained planes of weakness and joints.

All blocks and boulders were cored with a radial drill machine in the McGill Geomechanics laboratory. Core samples either prepared from the core drill machine or received as cores from the mine site were precisely cut into cylinders to the appropriate shape in order to perform the tests for the present research. In order to cut the samples in the appropriate shape and dimensions, a 4-inch wet diamond saw was used to cut and size rock specimens according to standard procedures. The geometry shape of the samples would have an influence on the test results, therefore, samples were cut precisely to the shape needed in unconfined compressive strength and Brazilian tensile strength tests.

Core samples were prepared and cut in two sizes of cylindrical and disc shapes. For unconfined compressive strength (UCS) tests, samples were prepared in a cylindrical shape respecting the height to diameter ratio of 2:1 for the sample length depending on core diameter prior to be treated in microwave irradiation. Disc shaped specimens were prepared for Brazilian tensile strength (BTS) test respecting to have the length between $0.5D < L < D$. CERCHAR abrasiveness index (CAI) test are performed on the flatten face of disc shape specimen prepared for Brazilian tensile strength test.

At first, a series of specimens had been prepared to be irradiated with microwaves at three power intensity (0.8, 1.2 and 3 kW), five different time of exposure (ranging from zero to 120 seconds) and at least three runs for each. Of course, a set of untreated specimens are kept to be tested for every rock samples in order to have a control to compare the results.

Cylindrical core specimens were extracted and prepared from all rock samples. The cylinder ends were cut and polished according to the techniques and standards of ISRM suggested techniques (1978, 1979) and ASTM (D3967-05, D7012-04). A diamond wheel grinder machine was used to precisely flatten both ends of the cylinders and disc shaped specimens prepared or cut by the diamond saw, to ensure the applied load was evenly distributed during uniaxial compressive strength testing, the end of the specimen must be completely and precisely flat.

A separate set of rock sample was prepared to better understand the temperature distributions inside specimens. Cylindrical specimens were sliced into 1 cm thick discs, 10 of which were stacked to the same height as the intact cylindrical specimens used for UCS testing (Figure 3-1). This made it possible to measure the temperature between discs and plot the temperature distribution inside the cylindrical specimen after exposure. In order to understand the temperature profile within the rock specimens after being microwaved, the cylindrical shaped specimens were slice cut in thin discs of 1 cm height. All the thin discs were completely flatten in both sides so they would sit on top of each other with minimum amount of air within the gap in between. Ten disc were stacked on top of each other and were exposed to 3 kW microwave irradiation for 40, 50, 60, 70 and 80 s. The temperature of each layer were measured right after the microwave was turned off.

Figure 3-1 Stacked and intact disc basalt #1 specimens at the same height and diameter

Whereas as the cylinders and disks prepared above were to be subjected to microwave treatment in enclosed cavities, a set of rock samples was prepared for exposure to microwave radiation from a pyramidal open-ended horn antenna, to simulate conditions at the tunnel face. Basalt #2 (Table 3-2) was cut into 40 cm (l) × 40 cm (w) × 2 cm (h) slabs, which were stacked on top of each other to stimulate a rock mass. These samples were also used to examine the temperature distributions and density and distribution of macro-cracks caused by different thermal expansion ratios among rock constituent minerals.

Table 3-2 Electrical and physical properties of basalt #1

	Symbol	Value	Unit	Reference
Thermal conductivity	K	0.6	W/m°C	(Carmichael, 1988)
Electrical conductivity	σ	0.00005	S/m	(Carmichael, 1988)
Specific heat capacity	Cp	1.37	kJ/kg.K	
Electrical resistivity	R	20000	Ω.m	(Carmichael, 1988)
Density	d	2870	kg/m^3	

The surface temperature of each specimen was measured with an infrared gun immediately after each exposure to microwave irradiation. In order to have a good comparative study all dry specimens were randomly chosen to be treated by microwave energy.

All the specimens treated/irradiated by microwave energy were first left in the room to get cooled down to the ambient temperature before conducting any tests. The unconfined/uniaxial compressive strength test, Brazilian tensile strength test, CERCHAR (Centre d' Études et Recherches de Charbonnages de France) abrasivity index scratch test are the main tests that had been conducted in the ambient temperature.

The Brazilian tensile strength test was conducted by using a mechanical gearbox press machine and the unconfined compressive strength test with a servo-controlled press machine.

Diamond saw would never give a precise flat surface; therefore a diamond wheel grinder machine is used to smoothly flatten both end of the cylindrical specimen in order to obtain accurate uniaxial compressive strength results.Cylindrical rock samples were 50 mm in diameter with a height of 100mm for the uni-axial tests and 25 mm for the tensile tests. The results of the first phase of the experiments showed high variation of energy absorption by each rock sample. X-ray fluorescence (XRF) analysis was performed to determine the mineralogy and mineral distribution within each sample (Table 3-3).

Table 3-3 Mineralogy of rock samples.

	Granite	Norite	Basalt #1	Limestone	Basalt #2	Dolomite	Sandstone	Gneiss	Mafic Granophyre	Felsic Granophyre
SiO_2	70.70	58.34	49.43	3.54	63.14	1.04	69.16	82.13	60.17	75.10
TiO_2	0.3819	0.6231	2.3373	0.039	0.221	0.018	0.108	0.412	0.717	0.135
Al_2O_3	14.75	16.82	13.19	0.87	5.86	0.35	3.04	6.43	14.79	13.64
Fe_2O_3	2.2331	7.0088	12.5428	0.33	16.15	0.72	0.56	1.12	8.12	1.64
MnO	0.0372	0.1129	0.1642	0.026	0.041	0.393	0.238	0.012	0.108	0.027
MgO	0.85	4.83	8.38	1.53	1.07	16.79	0.29	1.31	5.05	0.25
CaO	1.52	6.59	8.66	48.11	2.75	30.56	13.02	2.45	5.92	1.35
Na_2O	3.9990	3.0455	3.0092	0.11	1.61	0.02	3.80	0.04	3.13	3.43
K_2O	4.55	1.71	1.23	0.08	1.28	0.01	1.27	1.04	1.63	4.89
P_2O_5	0.119	0.152	0.436	0.112	0.083	0.022	0.036	0.395	0.180	0.061
BaO	1022	603	318	15.7	299.4	351.5	269.5	394.2	575.0	925.6
Ce	56	71	71	18	21	23	34	45	62	57
Co	39	40	60	<d/l	45	<d/l	<d/l	10	35	<d/l
Cr_2O_3	17	273	371	14.3	27.3	12.8	54.1	157.5	415.9	66.9
Cu	9	49	94	23	10068	35	40911	23	245	21
Ni	<d/l	34	216	<d/l	<d/l	<d/l	<d/l	12	56	<d/l
Sc	10	24	32	<d/l	<d/l	<d/l	<d/l	<d/l	16	<d/l
V	44	125	212	13.1	56.1	10.1	16.2	96.8	128.3	10.6
Zn	31	42	88	<d/l	253	27	899	50	51	<d/l
LOI	0.84	0.79	0.91	41.29	7.39	41.90	9.84	4.64	0.64	0.20
Total	100.100	100.150	100.440	96.040	100.670	91.870	105.580	100.060	100.610	100.830

The CWPI Normative mineralogy of the rock samples was calculated from XRF results (Table 3-4). An advantage of the XRF analysis as well as the CWPI Normative mineralogical calculation is that it shows the exact distribution of ten common oxide compounds and their relative minerals within the sample. The minerals distribution computed by the CWPI Normative mineralogical calculation of all rock samples are according to the Table 3-3.

Table 3-4 The CWPI Normative mineralogy of the rock samples

	Granite	Norite	Basalt #1	Limestone	Basalt #2	Dolomite	Sandstone	Gneiss	Mafic Granophyre	Felsic Granophyre
Plagioclase	41.04	53.72	45.11	1.64	20.49	0.84	9.34	10.48	48.1	35.29
Orthoclase	27.18	10.22	7.39		8.33		8.21	6.44	9.63	28.78
Diopside		3.76	17.66		7.87		2.24		3.64	
Hypersthene	4.74	19.51	10.33		23.49			3.41	10.92	0.62
Olivine			12.15	2.7		29.38				
Ilmenite	0.74	1.2	4.52	0.06	0.46	0.04	0.23		0.2	0.05
Magnetite	0.33	1.03	1.86		2.57	1.04				
Apatite	0.28	0.35	1.02	0.25	0.21	0.05	0.09	0.95	0.42	0.14
Quartz	24.93	10.2			36.57		44.41	75.32	17.47	33.1
Corundum	0.77							1.79		0.33
Nepheline				0.5		0.09				
Kalsilite				0.27		0.03				
Larnite				73.14		46.65				
Hematite				0.33				1.17	8.14	1.63
Perovskite				0.01						
Wollastonite							28.22			
Acmite							1.76			
Na2SiO3							5.53			
Chromite							0.01	0.03	0.09	0.01
Rutile								0.43		0.1
Sphene									1.51	

3.2 Measurement of Rock Electrical Properties

There are five ways to measure the dielectric properties of a materials described as follow. The coaxial cable apparatus is used to measure the dielectric properties of all rock samples; however, the resonant cavity apparatus is used to measure a certain rock samples for three different frequencies (915, 2450 and 5800 MHz) in order to compare the results with the coaxial cable.

3.2.1 Coaxial Probe

The coaxial probe apparatus was used to measure the dielectric properties of all rock samples prepared for BTS testing. This technique is commonly used for lossy materials in the liquid, powder or solid and semi-solid state; it is not accurate nor recommended if applied to loss-less materials. A coaxial probe is attached to a data analyzer by a coaxial cable (Figure 3-2). Since electromagnetic energy is transmitted and arced within the material, the smoothness of the material’s surface significantly influences the accuracy of the measurement. Therefore, one end of the disc specimens is polished to an accuracy of 5–10 microns of surface roughness. Dielectric properties are measured by firmly pressing the probe to the smooth flattened surface of the specimen. Experience showed that the material had to be at least 1.5 times thicker than the diameter of the probe. The range of frequency on the network analyzer was set to measure the real and imaginary part of the material permittivity between 1 and 10 GHz. One surface on the specimens is polished to have minimum gap of air when setting the coaxial probe of the surface. A tiny space in between the specimen and the probe reduces the measurement’s accuracy significantly. On the another hand, the coaxial probe method is strongly recommended not to be used and referenced for loss-less materials, since the accuracy limit of the method is 0.1.

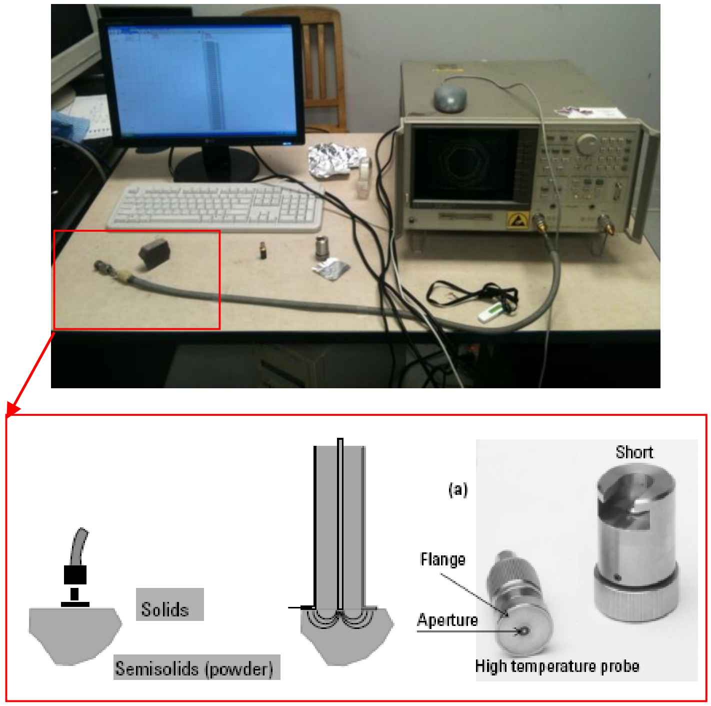

Figure 3-2 Coaxial probe measurement device. From left to right in the magnified box: pressing the probe to the smooth surface; cross-section of the probe and dielectric showing how the microwave signal penetrates the material and reflects back; the probe components and probe short.

Since the electromagnetic energy is transmitted and arced within the material, the smoothness of the material's surface has a significant influence on the accuracy of the results obtained. Ideally the center of the aperture and the flange has to be completely in contact with the surface of the material to avoid any possible air gap in between. Furthermore to the perfectly polished surface of the material, the stability of the coaxial cable as well as the sample thickness have also a great influence on the results to be measured.

3.2.2 Free Space

Similar to the concept as the transmitted line method, the specimen's dielectric properties are measured by computing the difference between the transmitted and the reflected energy. Unlike the transmission line, the thickness of the specimen must be small compared to its length and the surface area must be larger than the cross-section of the antenna aperture. Further, the specimen must be located at a distance close to $2d^2/\lambda$ from the antenna, where d is the largest diameter of the antenna aperture and λ is the wavelength of the electromagnetic wave in free space (12.2 cm for 2.45 GHz).

3.2.3 Resonant Cavity (Cavity Perturbation)

The resonant cavity apparatus was used to measure a subset of rock samples at three frequencies (0.915, 2.45 and 5.80 GHz) for comparison with the coaxial probe method (Figure 3-3a). It is considered very accurate for loss-less materials. In this method, a cavity is designed with dimensions based upon the wavelength of a specific frequency. A small, thin, rod-shaped specimen is inserted in the empty cavity (Figure 3-3b).

a) 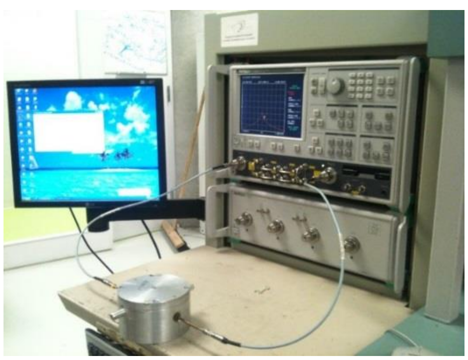 b) 

Figure 3-3 a) Spectrometer connected to a resonant cavity and b) rod-shaped rock specimen

When the electromagnetic waves are transmitted from the data analyzer, a peak is observed on the graph, which is the exact frequency of the empty cavity. Once a material is inserted into the cavity, the impurity of the empty cavity is change; therefore, the resonance of cavity changes. As a result of the changes in the cavity's resonance the peak of the graph shifts into another phase that indicates another frequency (Figure 3-4). By calculating the changes in resonance and frequency, the dielectric properties of the specimen are computed. It has to be noted that since the physical dimensions are crucial (Figure 3-5), knowing the exact volume of the empty cavity and the specimens is extremely important.

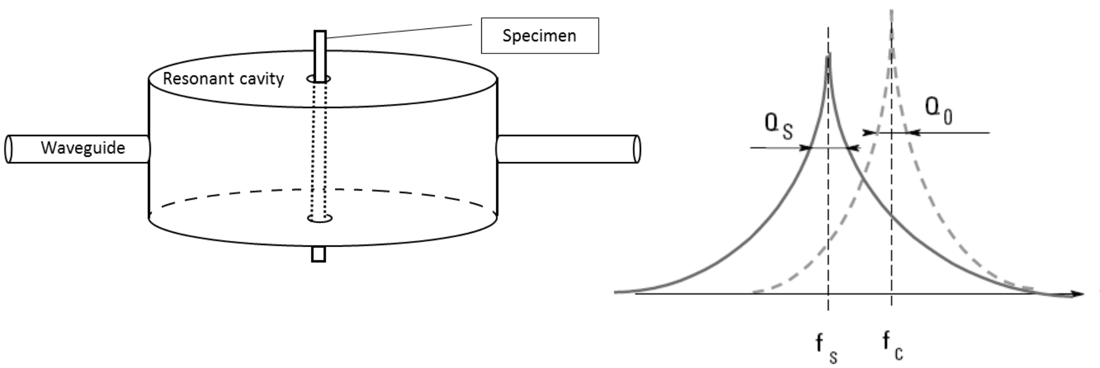

a) b)

Figure 3-4 a) Position of the sample in the resonant cavity and b) perturbation of frequency shifting from the cavity (f_c) to the sample (f_s) when the sample is located in the resonant cavity

This technique allows only the measurement of a specimen's dielectric properties at a certain specific frequency. If other frequencies are required, other cavities must be designed and built (Figure 3-5).

a) b) c)

Figure 3-5 The resonant cavity constructed for frequencies of a) 0.915, b) 2.45 and c) 5.80 GHz

3.2.4 Transmission Line

In this method, the material is precisely cut to the size of the waveguide, which is designed to contain small-sized material. The specimen is inserted into the closed end waveguide (Figure 3-6). Once the specimen will be subjected to the electromagnetic energy inside the waveguide, the specimen reflects, absorbs and transmits some of the emitted energy. By computing the difference impedance, the amount of energy reflected, transmitted, and absorbed is calculated, which permits calculation of the specimen dielectric properties. This method was performed by IDS Corporation (Ingegneria Dei Sistemi Corporation) to confirm study results obtained.

a) 

b) 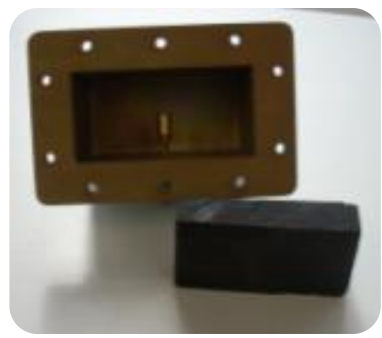

Figure 3-6 a) Waveguide or transmission line apparatus to measure dielectric properties of a material for frequencies between 8 and 12.4 GHz and b)Waveguide and specimen cut to size (after IDS Corporation)

3.2.5 Parallel Plate

The parallel or capacitive method requires a very thin disc-shaped specimen to be inserted between two plates connected to a data analyzer (Figure 3-7). The aperture used in this method simulates the functionality of a capacitor filled with the specimen. By knowing the default parameters of the aperture and transmitting the energy, the dielectric properties of the specimen can be calculated. This method was performed by IDS Corporation to confirm study results obtained.

a)  b) 

Figure 3-7 Parallel plate of capacitive set-up apparatus to measure dielectric properties from 10 to 1000 MHz of frequency (left), specimens cut to size (right) (after IDS Corporation)

3.3 Microwave System Components

Based on the literature review, several authors have used various microwave conditions prepared for treating rock samples. They mostly exposed rock samples to the microwave irradiation in a single mode cavity and evaluating the influence of microwave energy on rock comminution in mineral processing industries. To evaluate and conclude that the microwave energy has a great impact on rock materials in order to be able to use it in assistance of TBM machines, first, the examination of the influence of microwave energy on rock materials is necessary. Obviously, the microwave energy emitting to the face of the tunnel by TBM is categorized as plane wave exposure.

Basically, within this research, samples are planned to be exposed to three different microwave power levels and five different time durations of exposure for each power. In other words, samples are treated to the energy within the microwave ovens for 15, 30, 60, 120 and 240 seconds in three power levels used as 0.8, 1.2 and 3 kilowatts individually.

Among a variety of applications that microwave is used in, the microwave system for heating purposes is the main focus in the entire current research, in which it will be referred to a microwave system or device. The choice of microwave system (choosing the appropriate components to build a complete system) depends highly on the frequency to be used and the application. The location where the system will be used can have a significant influence on its design as well. In order to distinguish the systems from one to the other we can categorize all microwave systems for heating purposes into two main commercial and industrial groups. Commercial microwave ovens, which are mostly used in restaurants and houses, vary in design among manufacturers. Industrial microwave systems are mainly custom-made. Within the present research, microwave facilities used for the study to treat the rock cylinders and discs are commercial microwave ovens. Kitchen microwave ovens have a multi-mode cavity. Initially, commercial microwave ovens have been used to evaluate the influence of microwave radiation on mechanical properties of rock samples. The results obtained from using the commercial microwave ovens led to research using more powerful industrial microwave systems for potential field applications. All microwave system used in this research are having constant 2.450 GHz of frequency. Commercial ovens also have the standard components but designed in a compact architecture.

A standard microwave system (either being commercial or industrial) has the following components (Figure 3-8):

- The cavity is a metallic closed box with dimensions several times the wavelength of the energy.
- The power generator generates the power specified by the manufacturer.

- The magnetron converts the high voltage electricity into electromagnetic energy and radiates microwave energy.
- The isolator or dummy load ensures one-way flow of energy from the waveguide. It protects the magnetron from reflected energy waves by absorbing them.
- The waveguide is a hollow metallic tube that guides the energy moving through it.
- The power meter measures the amount of emitted and reflected power.
- The tuner adjusts the efficiency of the modes travelling through the waveguide.

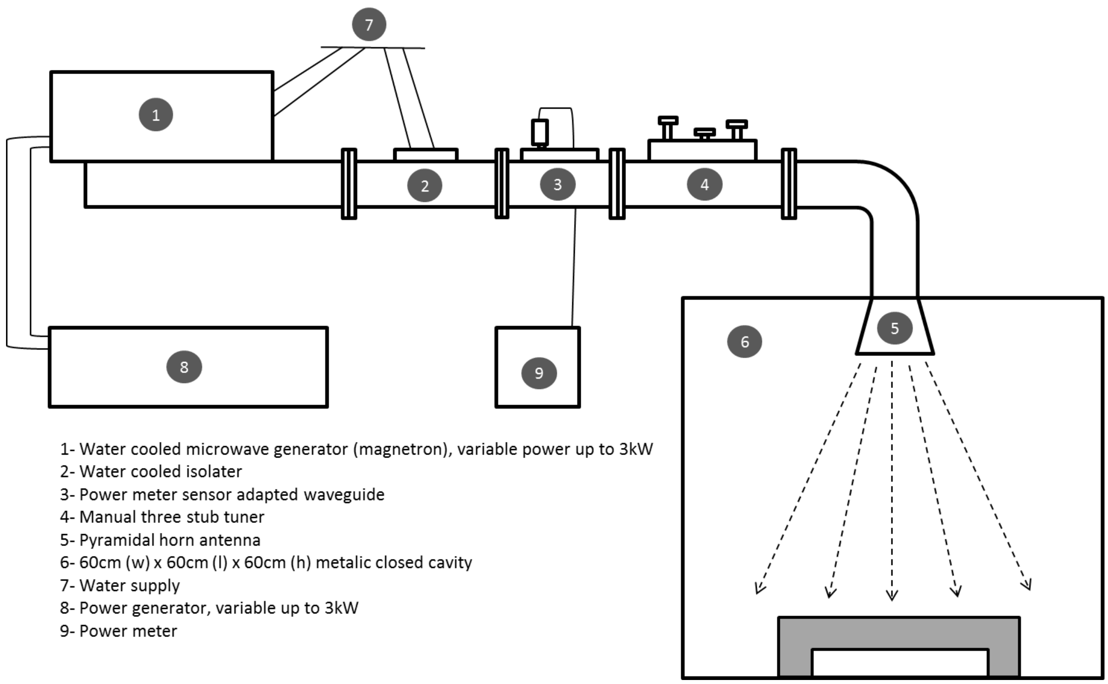

Figure 3-8 A schematic view of an industrial microwave system components

As an electromagnetic wave propagates, some nodes of energy are created by its alternations. Those nods of energy, in which more energy is concentrated, are known as modes of energy. The distance between each node is directly related to the wavelength of the standing wave. The physical dimensions of the area where the wave is propagating also play an important role. Waveguides always have two dimensions that are smaller than the wavelength, which causes the wave to travel in the third direction. Therefore, only one node of energy is generated. If the end of the waveguide is closed and a specimen is located at the energy node, a single-mode cavity is created. When two or three dimensions of a closed cavity are longer than one wavelength, more than one node of energy concentration is created: this is called a multi-mode cavity. Since electromagnetic waves alternate constantly, the nodes inside the cavity constantly change location and cannot be controlled nor being calculated. This causes a non-uniform distribution of energy inside of the cavity. To make the energy distribution within the close metallic box (called cavity) uniform, a device inside of the cavity is used to constantly scatter the microwave energy in all directions, such as a turntable, mode stirrer, or rotating antenna.

3.3.1 Microwave Cavities and Power Levels

To treat rock cylinders and discs, three commercial, single-mode 2.45 GHz microwave ovens were used that differ in cavity dimensions and power. All of the commercial microwave ovens operated at maximum power capacity. The automatic power adjustment on a commercial microwave oven’s control panel is not suitably adjustable for this study. Although the control panels of these microwave ovens state that power can be adjusted in 10% increments, the actual power input to the magnetron is always at full capacity. Changing the power output on the panel causes the oven to automatically adjust itself by turning the magnetron on and off. Thus, the total amount of power emitted remains as the amount adjusted at the first place within the time given.

The Panasonic NN-S335WF oven has internal cavity dimensions of 32 cm (l) × 31 cm (w) × 19 cm (h) (Figure 3-9). A sole magnetron generates 0.8 kW of power. A turn table mechanism is used inside of the cavity so the load constantly turns while being microwaved in order to be exposed to microwave radiation uniformly.

Since the turn table is in glass, a 15 cm diameter × 1 cm thick alumina silica-based ceramic plate (ZAL-45AA) was used as a spacer between rocks samples and the turntable. The ceramic plate is completely transparent to microwave radiation and is heat-resistant up to 1200°C; therefore it prevented heat conduction to the glass turntable and damage to the oven.

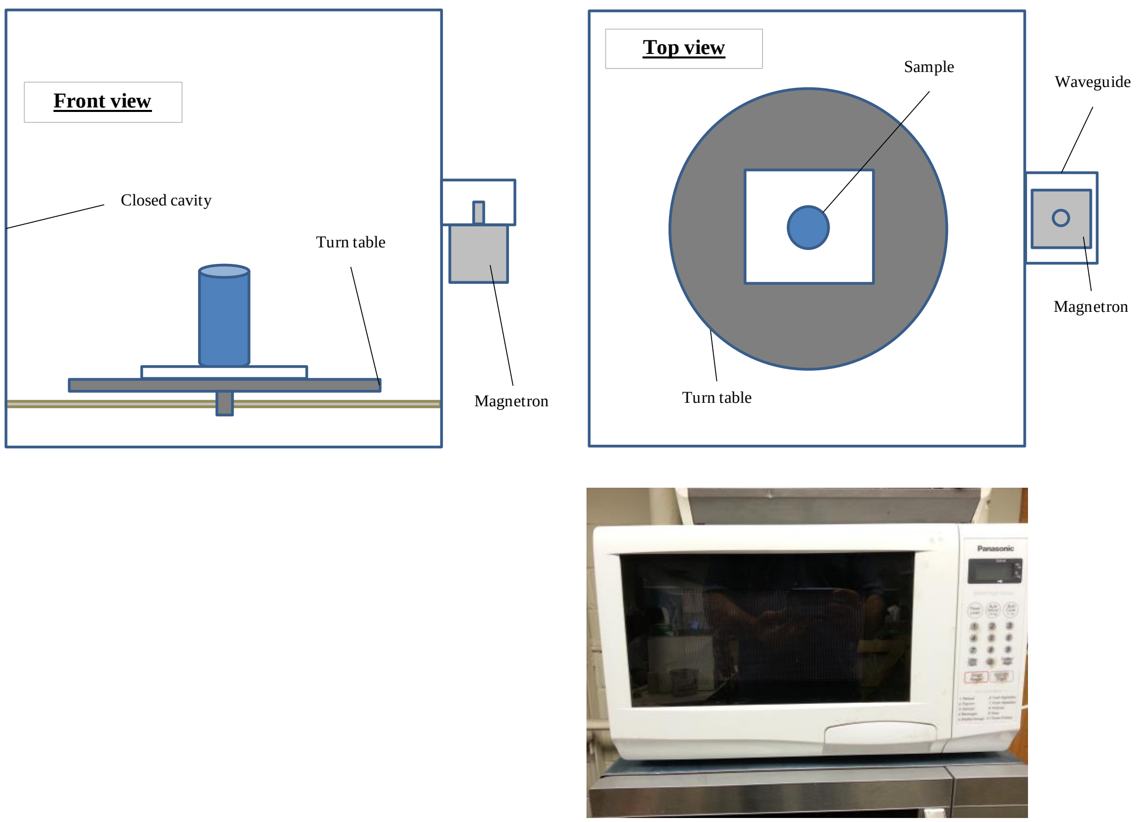

Figure 3-9 Front and top views and photograph of the 0.8 kW single-mode commercial microwave oven used in this study

The Litton Moffat MG0873 microwave oven has internal cavity dimensions of 37 cm (l) × 30 cm (w) × 25 cm (h) and generates 1.25 kW of power through a single magnetron (Figure 3-10). The waveguide is positioned such that the microwaves hit the angled wings of a mode stirrer, which turns freely and constantly while the microwave is on. The mode stirrer in front of the waveguide and on top of the cavity allows the platform of the microwave cavity to be static. Microwaves hitting the mode stirrer create a huge chaos of energy inside the cavity; whereas, a turntable give more chance to the load to be irradiated by microwaves more uniformly.

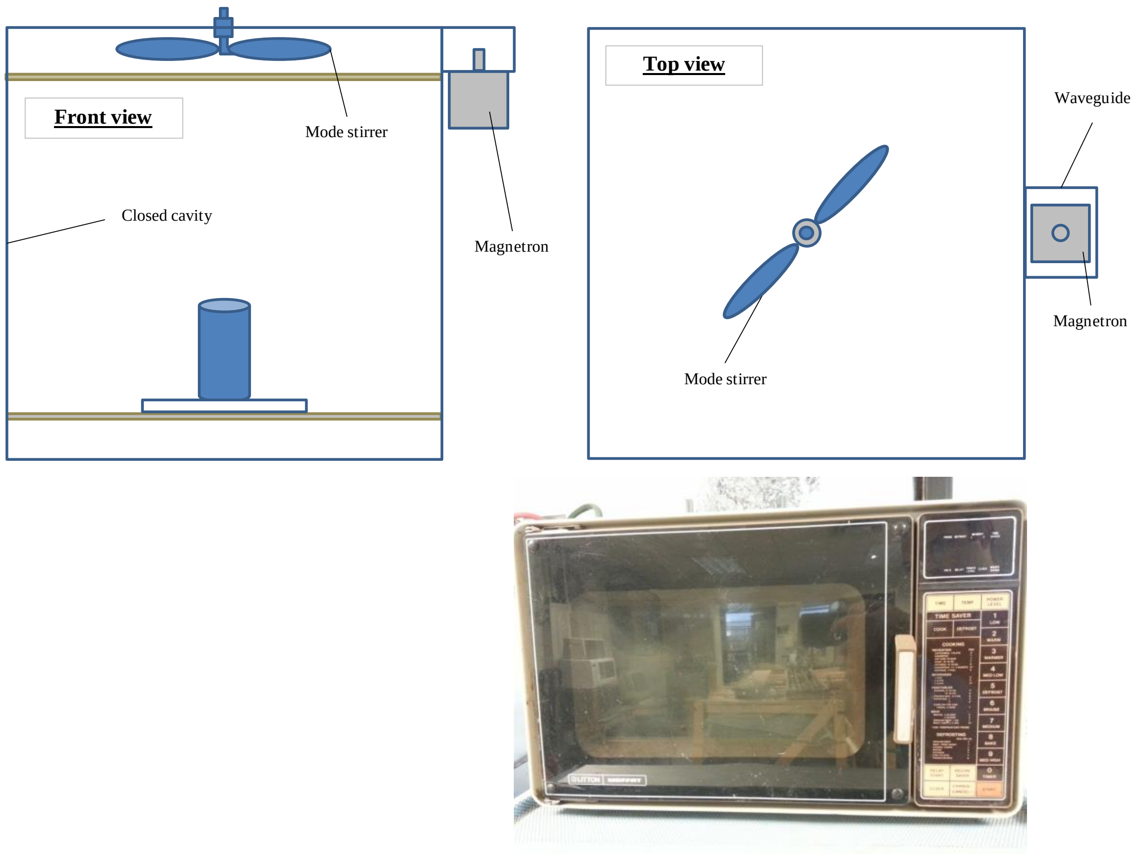

Figure 3-10 Front and top views and photograph of the 1.25 kW single-mode commercial microwave oven used in this study

The third commercial microwave oven (Amana RC30S) has internal cavity dimensions of 33 cm (l) × 38 cm (w) × 32.5 cm (h), excluding the ceramic plate at the bottom and the cover cap on top (Figure 3-11). Three 1 kW magnetrons generate 3 kW of power. This microwave oven has three 1 kW magnetrons, two of which are located on top of the cavity and the third one is at the bottom generating microwave energy. Unlike the other two commercial ovens, the magnetrons of this model do not radiate microwaves directly into the cavity. Instead three rotating antennas with 90° phase difference transmit the energy from the waveguides to the cavity. The rotating antennas play the same role as a mode stirrer. One antenna is located at the bottom of the cavity, immediately beneath the ceramic platform where the load sits. Two antennas are positioned at the top of the cavity. This can cause non-uniform microwave irradiation of the sample, which is very close to the bottom antenna and is bombarded from two antennas from the top.

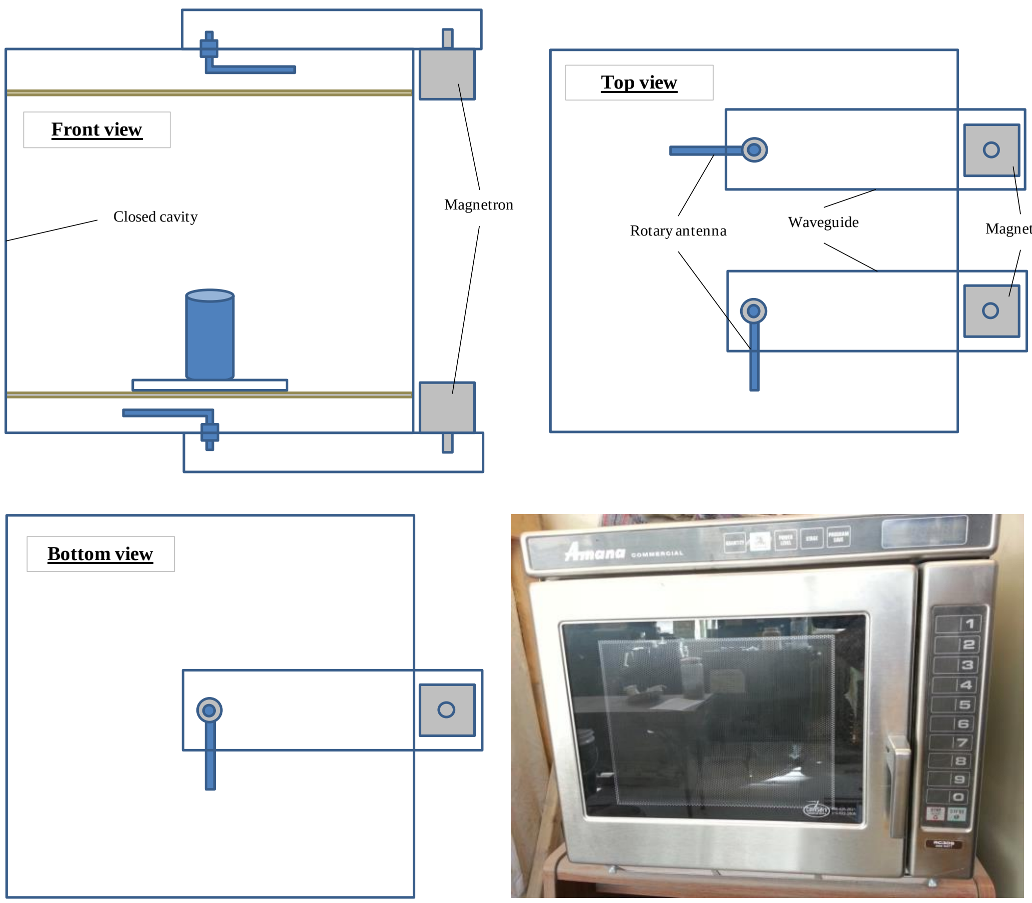

Figure 3-11 Front and top views and photograph of the 3 kW single-mode commercial microwave oven used in this study

In addition to the commercial ovens above, powerful industrial ovens were required to be used in order to irradiate rock samples with higher power intensity. Although all three microwave ovens were similar in design, the inside dimensions of their cavity were completely different. The fact that each one of the cavities are multi-mode cavity in terms of energy by using different mechanism, makes the microwave exposure not uniform; therefore, an industrial 2.45 GHz multi-mode microwave system were used. The advantage of these systems is that the power can be adjusted. The first oven was available at Hydro-Quebec: it has variable power up to 6 kW, and cavity dimensions of 70 cm (l) × 70 cm (w) × 70 cm (h) (Figure 3-12). The microwave system at Hydro-Quebec had the same standard components of a microwave system mentioned earlier. The advantage of this equipment is that the cavity remains the same while the power can be adjusted.

Figure 3-12 Industrial multi-mode, variable power (up to 6kW) microwave system at Hydro-Quebec facility

The second industrial microwave oven was custom made in the Geomechanics laboratory at McGill University. It has variable power (up to 3 kW) always at 2.45 GHz of frequency. This oven has the same components and design as shown in Figure 3-8 with an internal closed cavity dimensions of 60 cm (l) × 60 cm (w) × 60 cm (h) as shown in Figure 3-13. The system is water cooled: a water flow of 10 L/min circulates through the isolator (acting as dummy load) to absorb reflected waves, and through the magnetron to cool the microwave generator components. The energy produced by the magnetron exits into a much larger area (metallic closed cavity) via a pyramidal horn waveguide (acting as an antenna). The waveguide extends the internal dimensions of the standard rectangular WR-340 waveguide from approximately 9 cm (w) × 4.5 cm (h) to approximately 15 cm (w) × 9 cm (h). This makes the pyramidal horn waveguide approximately 10 cm long.

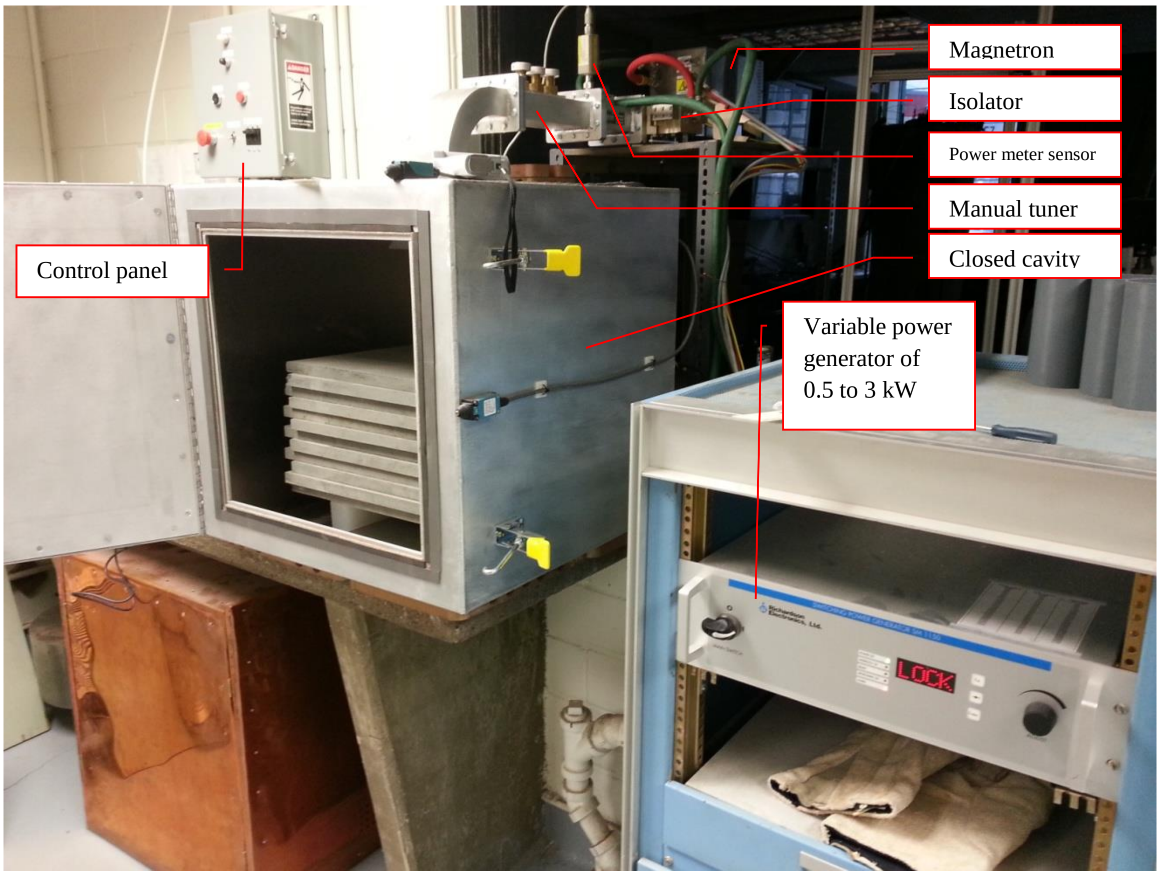

Figure 3-13 Industrial multi-mode, variable power (up to 3 kW) microwave apparatus in the Geomechanics laboratory at McGill University

The results of the variable 3 kW power industrial microwave on the slabs of basalts led the research to especially design a third custom made industrial oven in the Geomechanics laboratory at McGill University. It has variable power up to 15 kW. This microwave system has the same standard components mentioned earlier and is also water-cooled. Since it is much powerful than other systems, individual components are larger (Figure 3-14). This equipment has also a multi-purpose cavity that can be turned into a multi-mode cavity from an open ended waveguide cavity type. Three configurations are possible: two multi-mode configurations that includes a mode stirrer and one directional wave configuration from the top.

Figure 3-14 Industrial multi-purpose, variable power (up to 15kW) microwave system in the Geomechanics laboratory at McGill University

Furthermore, this system has the ability to generate pulsed waves in addition to continuous waves. Commercial microwave ovens generate continuous waves: when the magnetron is turned on, it stays on for the amount of time defined by the operator and instantly turns off at the time of shut down. During the time the system is on, the magnetron generates microwaves continuously. In industrial microwave systems, the magnetron reaches the maximum defined power intensity gradually, during the ramp-up or warm-up period (Figure 3-15). At maximum power, the power fluctuates as the current of electricity constantly alternates. Since the magnetron heats during operation, its irradiation efficiency declines over time.

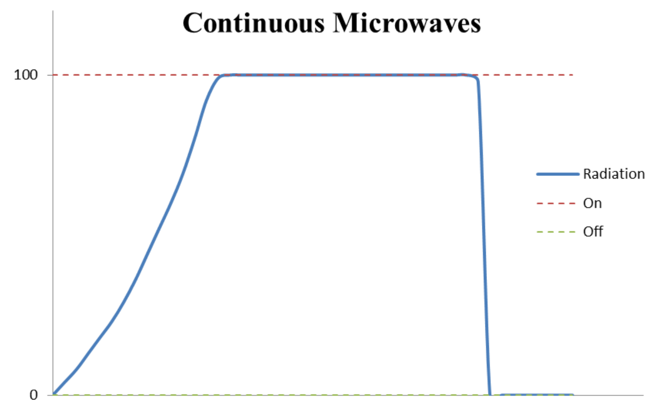

Figure 3-15 Continuous waves generated from the magnetron when the microwave is turned on

Unlike commercial microwave ovens, industrial systems can support a pulsing mechanism, whereby the power intensity is stored in a capacitor, then released at 100% intensity in defined on/off pulsating sequences (Figure 3-16). The on/off sequences are in the order of milliseconds, and can be adjusted by the operator prior to turning the system on. In pulsing mechanism the power intensity of the system is at its 100% capacity during ON time and turns off (0%) during OFF time. This mechanism makes it possible to irradiate rock samples at 100% power.

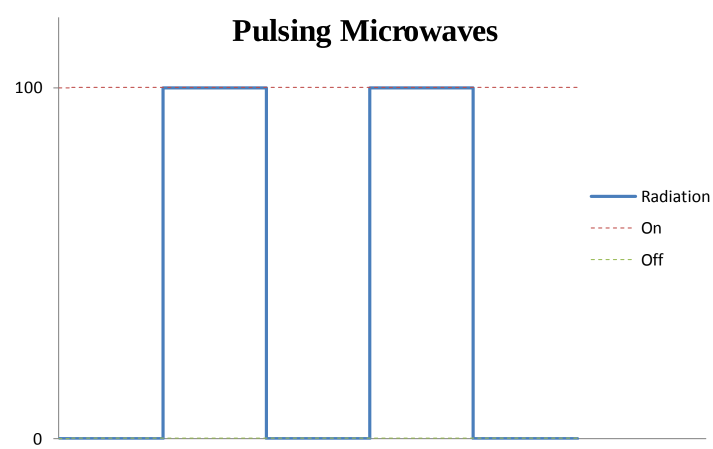

Figure 3-16 Pulsing waves in an on/off sequence

3.3.2 Type of Waveguides

Microwave wave guides are hallow tubes made of aluminum and allow the microwaves radiated travel through it. They can be circular or rectangular hallow tubes. Waveguides are designed with geometries that precisely suit a given range of frequencies. The dimensions are standardized. For instance, the waveguide used for this research is known worldwide as WR340, in the U.S. military as RG112(b) or RG113(a), and according to British standards as WG9A. The internal dimensions of a rectangular WR340 waveguide are 8.636 cm (w) × 4.318 cm (h). Microwaves with a frequency between 2.20 and 3.30 GHz travel through a WR340 waveguide without losing intensity. Depending on the dimensions, waveguides can transmit electric (transverse electric or TE) or magnetic (TM) fields, or both types of fields (TEM). The existence of one of multiple modes inside the waveguide is shown with a subscripted 0 and 1. The rectangular WR340 waveguide used to guide the microwave radiation from the generator to the cavity is a TE_{01}. Transverse Electric term is a term given to waveguides that have no electric field component in the direction of wave propagation.

A pyramidal horn antenna on the end of a rectangular waveguide prevents microwave energy from randomly scattering in all directions (Figure 3-17). It allows the microwaves to gradually move into a larger area after leaving the rectangular waveguide. In the current research, the microwaves gradually radiated into a much larger space (large cubic cavity) as if radiating into the open air. In that situation, the microwaves radiating from the horn waveguide radiate as plane waves.

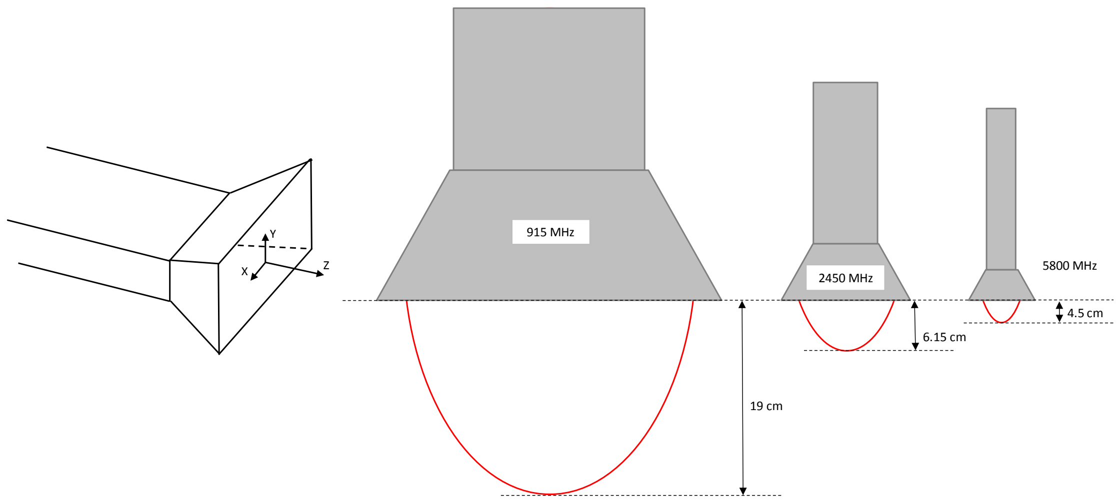

Figure 3-17 TE_{01} rectangular waveguide followed by a pyramidal horn waveguide for 0.915, 2.45 and 5.80 GHz frequencies, and reactive zone for each

The lower the frequency, the longer the wavelength and the larger the dimensions of the waveguide. Although a pyramidal horn waveguide gradually guides the waves in a specific direction, the waves are exiting to a much larger area than their own wavelength. This creates two zones of power intensity. Close to the aperture of the antenna is the near field zone or the reactive zone (Figure 3-17). Waves that just exited the antenna have a constant power intensity. Beyond in the far field zone, the waves exponentially lose power intensity. To estimate the power flux density (W in watts/cm^2) of the microwave radiation via a pyramidal horn waveguide as plane waves, equations 25–27 can be used (Pfafflin, 1992):

$$W = \frac{4P}{A} \qquad \text{Near field} \qquad (25)$$

$$z = \frac{A}{2\,\lambda} \qquad \text{Intersection of near to far field zones} \qquad (26)$$

$$W = \frac{AP}{\lambda^2 z^2} \qquad \text{Far field} \qquad (27)$$

where P is the average output power (watts), A is the effective area of the antenna's aperture (cm^2), z is the distance from the antenna aperture (cm) and λ is the wavelength (cm). These simplified equations do not account the reflected waves from surfaces.

3.4 Microwave Treatments

Cylindrical specimens were randomly assigned in triplicate to microwave treatment trials. Microwave treatments were conducted in three phases.

In the first phase, the three commercial microwave ovens (0.8, 1.2 and 3 kW power levels) were used for five exposure times (15, 30, 60, 120 and 240 s) to treat samples of the ten rock types from Table 3-1. Rock specimens were placed on the alumina silica ceramic plate and positioned in the middle of the cavity on top of the turntable (see Figure 3-9). A perforated plastic cover (transparent to microwave radiation) larger than the specimens prevented damage to the oven from rock fragments when samples burst. The perforations allowed air to circulate, avoiding the creation of hot air pockets around specimens from convective heating. The chamber, size and energy distributer of all three initial microwave ovens used are known as mode stirrer to be completely different. Although this oven has a ceramic platform, the alumina silica ceramic plate have also being used, since the ceramic platform of the oven is not heat resistant, hence, it may crack at high temperature conduction.

The results of the first phase of experiments led the second phase examined higher power intensities (1.2, 3 and 5 kW) and four exposure times (0, 60, 90 and 120 s). Four rock samples out of the many samples used in the first phase, had been chosen to be treated at higher power microwave energy. The four rock types are: basalt #1 and #2, norite and granite. At least three runs is also considered for each test in order to calculate the square regression of the means.

In the first phase of experiments the difference of size and mode stirrer methods highly affects the treatment conditions. In the second phase of the experiments a 6 kW power industrial microwave oven at Hydro-Quebec was used. The treatment variable was the sample volume to cavity volume ratio.

Tests within all experiment were performed on specimens cooled down at ambient temperature. The results of the second phase of the experiments revealed that high power intensity influences the rock's destruction more rapidly. Since the application of this research is microwave-assisted tunnel boring machines, a third phase of experiments was required to represent field conditions, where the surface of the rock mass in underground openings is exposed to microwave energy as directional plane waves. The rock mass in front of the machine can be considered as layers (Figure 3-18).

Although all tests were performed in a single oven and it mode stirrer method was the same, the filling ration of the oven and load also influences the treatment condition which was very low. The ration of the cavity's volume to the sample's volume was very high.

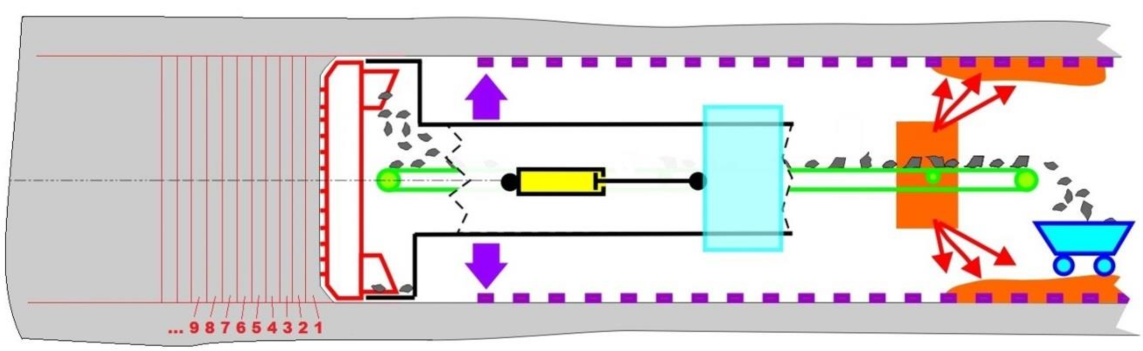

Figure 3-18 Tunnel boring machine with rock mass shown as layered rocks to the left

In order for the laboratory scale to be representative to the field, this phase of experiment studies the influence of Continuous microwave energy at 3 kW power was radiated from a pyramidal open-ended horn antenna for two exposure times (60 and 120 s) onto basalt #2 large slab stacks at six distances from the waveguide (3, 6, 9, 12, 15, and 20 cm) (Figure 3-19). The stacked slabs on top of each other stimulates a block of rock mass in front of the horn wave guide antenna. Stacked slabs permitted measurement of the temperature of each layer after microwave exposure. The slab dimensions (40 cm (l) × 40 cm (w)) were chosen to be at least two times larger than the aperture of the waveguide base to aid determination of the footprint of the microwave irradiation. The distances were chosen to fall in different sections of a wavelength (12.2 cm) from 3 cm to 20 cm with an interval of 3 cm.

The slabs used to be exposed to microwaves by previous equipment explained earlier will also be used to be irradiated with this high power microwave apparatus as well. The slabs will also be stacked on top of each other in order to irradiate the surface of the rock via and open ended waveguide according to the arrangement in Figure 3-19. In the continuous mode three powers (to be 5, 10 and 15 kW) are chosen to irradiate the stacked slabs of rocks for two times of 60 and 120 seconds at six distances from the horn waveguide (to be 3, 6, 9, 12, 15, 20 cm).

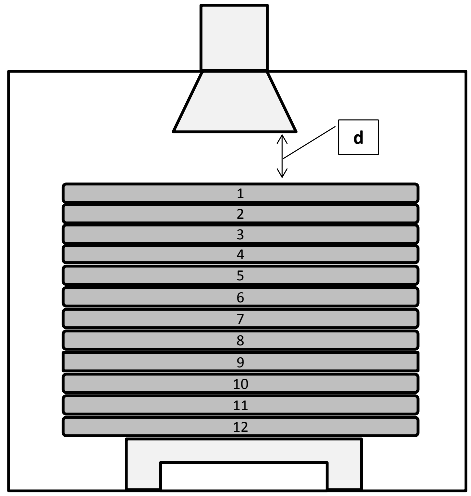

Figure 3-19 Arrangement of basalt #1 slabs stacked inside the microwave cavity relative to the pyramidal open-ended horn antenna

To test the effect of water (a very good absorber of microwave energy) on the temperature of basalt #1 after microwave treatment, this experiment was conducted using both dry (as was used for all other tests) and wet samples. The water content of basalt #1 measured with a standard vacuum chamber. The sample's water content has then been measured to be < 1.5%, which indicates that the rock is not permeable and porosity is extremely low. Basalt #1 slabs were completely submerged in water for at least 72 h in ambient conditions (too large to fit into a standard vacuum chamber). Spacers between each slab allowed water to circulate around the slabs.

Since the water is a very well absorber of microwave energy, it is then expected that the rock obtains a much higher temperature at it surface as well as its depth. The excess water in between the slabs was wiped out with a wet towel before the slabs were stacked in the cavity under the antenna. However, since the porosity and the permeability of the rock are extremely low, only a thin surface layer of water remained on specimens after submersion.

Stacked dry or wet rock slabs were positioned under the horn antenna such that the antenna's aperture was localized in the middle of the rock surface to emit the energy. This allowed to the largest dimension of the horn aperture to be much smaller than the width of the slab; hence, wave propagation would be more concentrated on the rock surface rather than propagating in the cavity randomly. The high-power industrial system (see Figure 3-14) has a powerful magnetron with a 7 s ramp-up time (to reach maximum power) period, during which the temperature of samples increased only 20°C from the initial room temperature. The ramp-up period was ignored during experiments (Appendix E).

After microwave treatment, the surface temperature of the middle of each slab was measured with an infrared gun along the z axis shown in Figure 3-19, directly in front of the horn antenna. The distances were chosen to fall in different sections of a wavelength (12.2 cm) from 3 cm to 20 cm with an interval of 3 cm in between. All recorded temperature measured with an infrared gun were plotted versus the distance from the surface of the rock towards the depth along the z axis.

In addition to the 3 kW dry/wet experiments, a series of directional plane-wave experiments was conducted on stacked slabs with using three higher power levels: 5, 10 and 15 kW. Both cavities of the low and high power directional plane-wave microwave systems have the same dimensions and conditions. The only difference is the power generator. Stacked slabs forming blocks of rock were exposed to 15 kW power to two modes of irradiation: continuous and pulsed. Two pulsing conditions were defined: 1) pulsed energy at 20 Hz, equivalent to a 74% duty cycle; and 2) pulsed energy 200 Hz, equivalent to a 53% duty cycle. A duty cycle is defined as the percentage of the total period that a signal is active (ON) to the total period of the signal multiply by 100. As the frequency of energy irradiation increases, the duty cycle decreases. As the duty cycle decreases (to have higher frequency of pulsation), the power of the microwave irradiation decreases because the amount of time that the energy remains inactive increases; therefore, less energy will be irradiated to the load. When the duty cycle is 100%, the energy will be pulsed once (1 Hz), in other words, continuously.

In every test, the amount of microwave energy reflected back to the magnetron from the surface of the rock was measured by a power meter on the waveguide. The high-power microwave has an automatic tuner controlled by software that records the energy reflected.

3.5 Temperature of Rock Samples

Since convection of heat to the surrounding air occurs quickly, heat starts to convey to the surrounding air of the specimen just right after microwave is shut down; therefore, rapid temperature measurement was crucial in these experiments. The average time spent to measure the temperature right after the microwave is shut down barely exceeds 45 seconds; hence, negligible amount of heat could be dissipated to the ambient air. The surface temperature of each specimen was measured with a Raytec Raynger MX4+ high performance infrared gun before and immediately after microwave treatment (Figure 3-20a). The infrared gun is able to measure the minimum, maximum and average temperature emitted from the specimen, which has been set to measure and show the average temperature. The device emits infrared light to the surface of the specimen at 18 points from a distance of 0.1 to 1 m (Figure 3-20b) and calculates the average temperature from those points. The technique relies on the principle that emissivity—a measure of the ability of a material to emit infrared energy—differs among materials. Emitted energy from the object specifies the temperature of the object. Emissivity can have a value from 0 (shiny mirror surface) to 1.0 (dark body). Most organic, painted, or oxidized surfaces have emissivity values close to 0.95 (Raytec, 1999). Since the test material was rock, the infrared gun was calibrated with the emissivity of non-metallic materials. The amount of emitted energy is related to the temperature of the object. Emissivity values were converted to temperatures by heating representative samples of each rock type in a conventional furnace at 100°C for three days until the temperature stabilized. Surface temperatures were measured and compared by infrared emission with a TC-K thermocouple and the infrared gun. By comparing those two methods the emissivity of each rock sample were calculated. Emissivity values ranged from 0.89 for sandstone to 0.99 for basalt #1 (see Table 3-1).

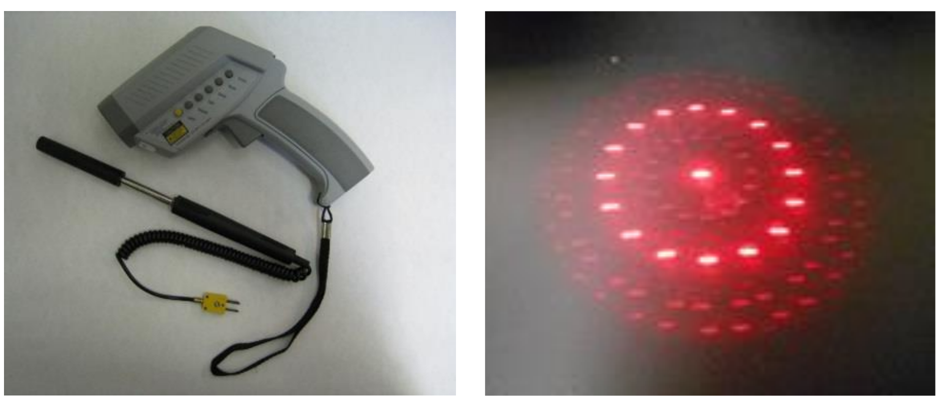

a) b)

Figure 3-20 a) Raytec Rayngel MX4+ high performance infrared gun and b) infrared dots

3.6 Strength Testing

Strength tests were performed on both untreated and treated specimens. Each treated specimen was cooled to ambient temperature before testing.

3.6.1 Uniaxial Compressive Strength

The unconfined compressive strength (UCS) is a very important predictor of TBM penetration rate or performance. Generally, the UCS test is the most commonly used test by tunneling application contractors. The procedure subjects a cylindrical specimen with a diameter of D and length of L, which should be at least equal to 2D, to a vertical load, longitudinal to the specimen, until failure based on ISRM 1979. Figure 3-21 shows the UCS measurement apparatus used in the study.

Figure 3-21 Computerized MTS uiaxial compression strength apparatus in the Geomechanics laboratory at McGill University

The UCS (σ_c in MPa) of the rock sample is calculated from equation 28:

$$\sigma_C = \frac{F}{A} \tag{28}$$

Where F is the load applied by the machine (kN), and A is the cross-sectional area of the specimen (mm^2)

3.6.2 Brazilian Tensile Strength

The BTS test has become a common and useful test among tunnelling application contractors for predicting TBM performance, because it is simple and low cost. The BTS test measures the tensile strength of rocks indirectly. The rock sample, in the form of a disc, having a diameter of D and thickness of L is subjected to a vertical load, provided by two upper and lower loading platens until failure vertical to the platens (Figure 3-22). The procedures and experimental setups in this study are based on ASTM D3967-05 and ISRM 1978 (Figure 3-23).

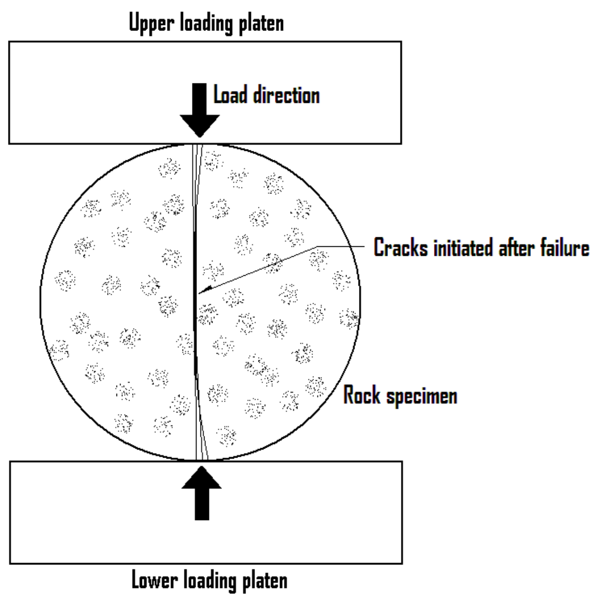

Figure 3-22 Sketch of Brazilian tensile strength test mechanism

Figure 3-23 Brazilian tensile strength apparatus in the Geomechanics laboratory at McGill University

The Brazilian tensile strength (σ_T in MPa) of the rock sample is calculated from equation 29:

$$\sigma_T = \frac{2F}{\pi DL} \tag{29}$$

where F is the load applied from the machine causing failure (kN), D is the diameter of the specimen (mm), and L is the length or the thickness of the specimen (mm).

3.6.3 CERCHAR Abrasiveness Index

The mineralogy and petrography of the rocks significantly influence the CAI of rocks. There is a good relationship between the quartz (SiO_2) content, the most abrasive mineral, and the abrasiveness of the rock (Suana & Peters, 1982) (Table 3-5). Figure 3-24 shows the CERCHAR apparatus used for the current study.

Table 3-5 CERCHAR abrasiveness index of rocks relative to quartz content (Suana & Peters, 1982).

Minerals	Quartz equivalence
Quartz	100%
Feldspar	70 - 80%
Olivine	57 - 60%
Pyroxenes	50 - 53%
Amphiboles	47 - 53%
Serpentinites	23 - 30%
Carbonates	17 - 34%
Claystone	up to 41%

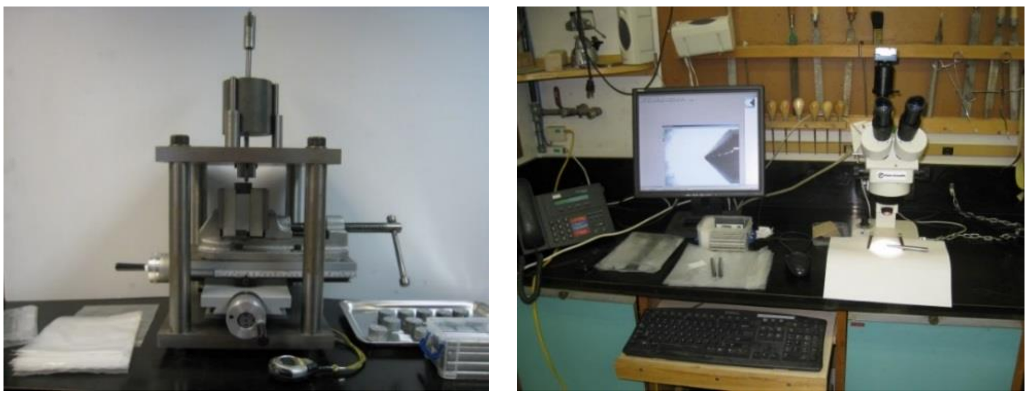

a) b)

Figure 3-24 a) CERCHAR apparatus in the Geomechanics laboratory at McGill University and b) stereo-master zoom microscope

Scratching a metal tool across the fresh surface of the rock over a distance of at least 10 mm under a constant load of 70 N yields an estimate of the wearing rate of a cutter tool on a TBM (Plinninger et al., 2003, 2004) (Plinninger and Restner, 2008). The tool is a metal rod with a diameter of 1 cm and a length of at least 7.5 mm. The rod is flat at one end and has a precise sharp 90° cone at the other end. The most suitable and representative steel type for the test is EN24, heat treated to a Rockwell hardness of HRC 40 V, which also has the least deviation among other types of steel (West, 1989; Michalakopoulos et al., 2006). CAI tests were performed on the flattened face of each disc, at three locations and in three directions. Each scratch on each specimen should be made with a fresh tool tip (Plinninger et al., 2003). The tools should be scratched on a fresh surface of the rock then the worn area of the tool is determined under a microscope (Figure 3-24b). After each use, the tool was sharpened with a cutter grinder machine (Figure 3-25a). Before and after each use, the tool was measured under a 10x Zeiss microscope (Figure 3-25b). A worn area of 0.1 mm on the tool represents 1 CAI.

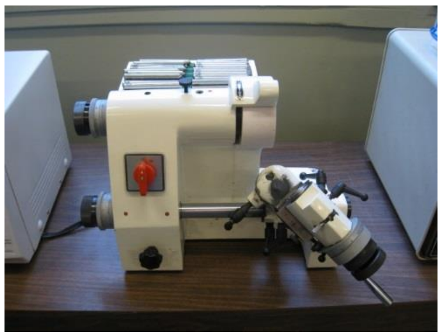

a)

b)

Figure 3-25 a) Cutter grinder machine and b) Zeiss microscope 10x

3.7 Macro-Crack Density and Distribution

When the stacked slabs of basalt #2 forming a block of rock inside of the closed multi-mode cavity being exposed to microwave radiation through the pyramidal horn antenna, a spot in the center of each slab beneath the antenna was heated. Therefore, a 5 cm × 5 cm area was cut from the center of each slab underneath the horn antenna to be observed for macro-crack density determination (Figure 3-26a). All visible cracks on the surface of the specimens were considered macro-cracks. The 25 cm2 area cut out of each slabs in dry and wet (saturated) condition at various depth was photographed with a high-resolution 15-megapixel digital camera (Figure 3-26b). An additional layer on the photo was created in Photoshop software, and a red line with thickness of 9-point was drawn on each visible crack observed. The remaining area was filled with a gray color once the boundary of the subjected surface area is drawn and specified. The number of pixels occupied by each color in the complete surface was counted and the proportion of red pixels was calculated, in other words (i.e., the density of red lines or the macro-crack density within the total surface area). The background of the resulting picture (Figure 3-26c). In Figure 3-26c, in which the red lines (referring to the cracks observed) are shown intentionally white in this thesis, to avoid color confusion for the reader.

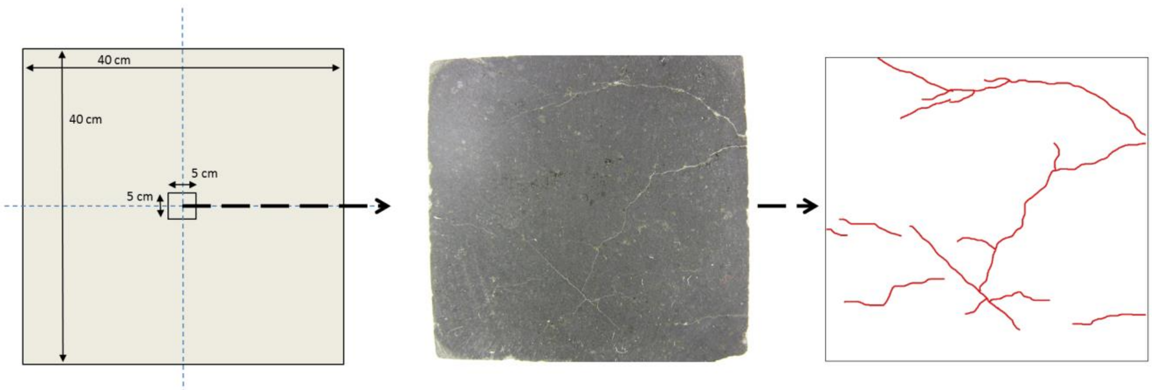

a) b) c)

Figure 3-26 a) 25 cm^2 square cut out of the b) polished 40 cm × 40 cm slab, and c) macro-cracks generated drawn in red

3.8 Numerical Modelling

COMSOL Multiphysics® commercial software was used to study parameters that are difficult to empirically measure and to design a comprehensive experimental matrix. The software has a general-purpose platform with more than 30 add-on modules that can be installed on top the main core if required. The RF module was used to model microwave propagation and the electric field distribution in the cavity, power dissipation in the load, and temperature distribution in the rock at both 2.45 GHz and 0.915 GHz.

Reproducing the experimental results obtained of the treatments with commercial and industrial 3 kW microwave ovens was the first objective of the numerical modelling. The model of the 3 kW industrial oven was applied to the 15 kW industrial microwave system since the dimensions of their cavities and their microwave concepts are the same.

Mesh generation

The commercial 3 kW power as demonstrated in Figure 3-11 has three waveguides: two on the top and one at the bottom. To model this cavity, vertical waveguides (Figure 3-27) needed to be drawn that do not exist in the physical system, where the horizontal waveguides are welded to the main cavity (see Figure 3-11). The vertical waveguides were required in the model to avoid generating too fine mesh at the horizontal waveguide exit, which would cause the software to run very slowly and not converge on a solution. A moderate mesh size is considered for this model. The vertical waveguides were also designed to be long enough that at least one node of energy could be generated. In addition, both commercial and industrial models used basalt #1 (with properties from Table 3-1) specimens constructed in the modelling software. Both intact cylinders and stacked discs of same height were designed and constructed in the model, as in the laboratory experiments. Extremely small gaps between the stacked discs were avoided because they resulted in a very high mesh density, which disrupted the computational process by occupying a large portion of CPU and memory. Hence, the tiny distance in between discs are avoided.

3.8.1 Commercial 3 kW Oven

Boundary conditions

The modelled 2.45 GHz commercial microwave Amana RC30S oven cavity dimensions are 32 cm (l) × 33 cm (w) × 37.5 cm (h). The system has three magnetrons (two on top and one at the bottom), each capable of delivering 1 kW of power (see Figure 3-11). The waves generated from the magnetron inside the waveguide exit through three rotating rod antennas into the cavity; uneven rotation of the antennas inside of the cavity creates a chaotic electric field distribution.

Figure 3-27 shows the COMSOL model of the oven: in the numerical modeling the oven is constructed out of aluminum with three attached rectangular ports (each 4.5 cm (l) × 9 cm (w)). The oven walls and ports were set to "impedance boundary condition", which is used for metallic materials with a very small penetration depth. This boundary condition reflects all waves emitted to it. COMSOL software does not have the functionality to model rotating antennas; thus, the rectangular ports were considered to be stationary and excited by transverse electric (TE) waves. For the subjected commercial microwave oven the excitation frequency is 2.45 GHz. In numerical modelling, only the first propagating TE_{10} mode is considered.

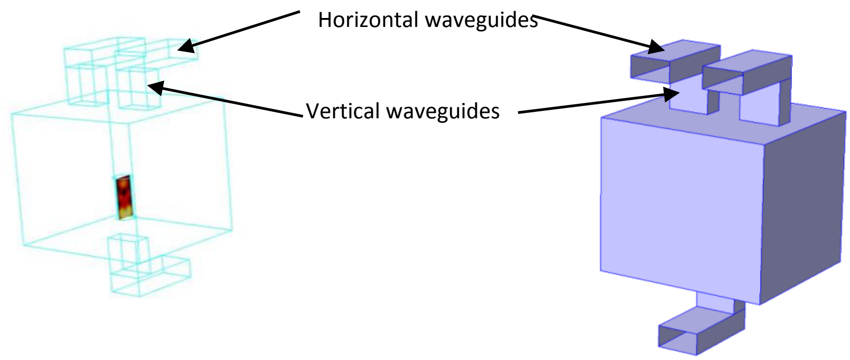

Figure 3-27 COMSOL model of the commercial 3 kW microwave oven with three magnetrons (position of rock sample in the cavity is shown on left)

3.8.2 Industrial Microwave Oven (Directional Plane Wave)

Boundary conditions and wave propagation in two and three dimensions

The two industrial microwave ovens generating directional plane waves have the same metallic box dimensions and conditions and variable power capability (1–3 and 5–15 kW) power. Microwaves generated from the magnetron travel through the waveguides and exit from an open-ended pyramidal horn waveguide. Several modelling runs were performed to determine the influence of port shape and position on wave propagation.

Two terms identify the boundary conditions of the cavity and waveguides: perfect electric conductor (reflects all electromagnetic waves) and scattering electric conductor (transmits all electromagnetic waves). When the cavity is empty, all boundaries must be defined as perfect electric conductors, whereas when a dielectric load (i.e., rock sample) is inside the cavity, all of the waves are concentrated towards the load to be absorbed. Thus, the side and bottom boundary conditions are defined as scattering electric conductors. Four scenarios were investigated (Figure 3-28):

1. Both the horn waveguide and cavity are perfect electric conductors and the horn is inside the cavity

2. A scattering electric conductor horn is inside a perfect electric conductor cavity
3. A perfect electric conductor horn is outside a scattering electric conductor cavity; the cavity height is also shortened relative to the horn height
4. Both the horn waveguide and cavity are scattering electric conductors and the horn is inside the cavity

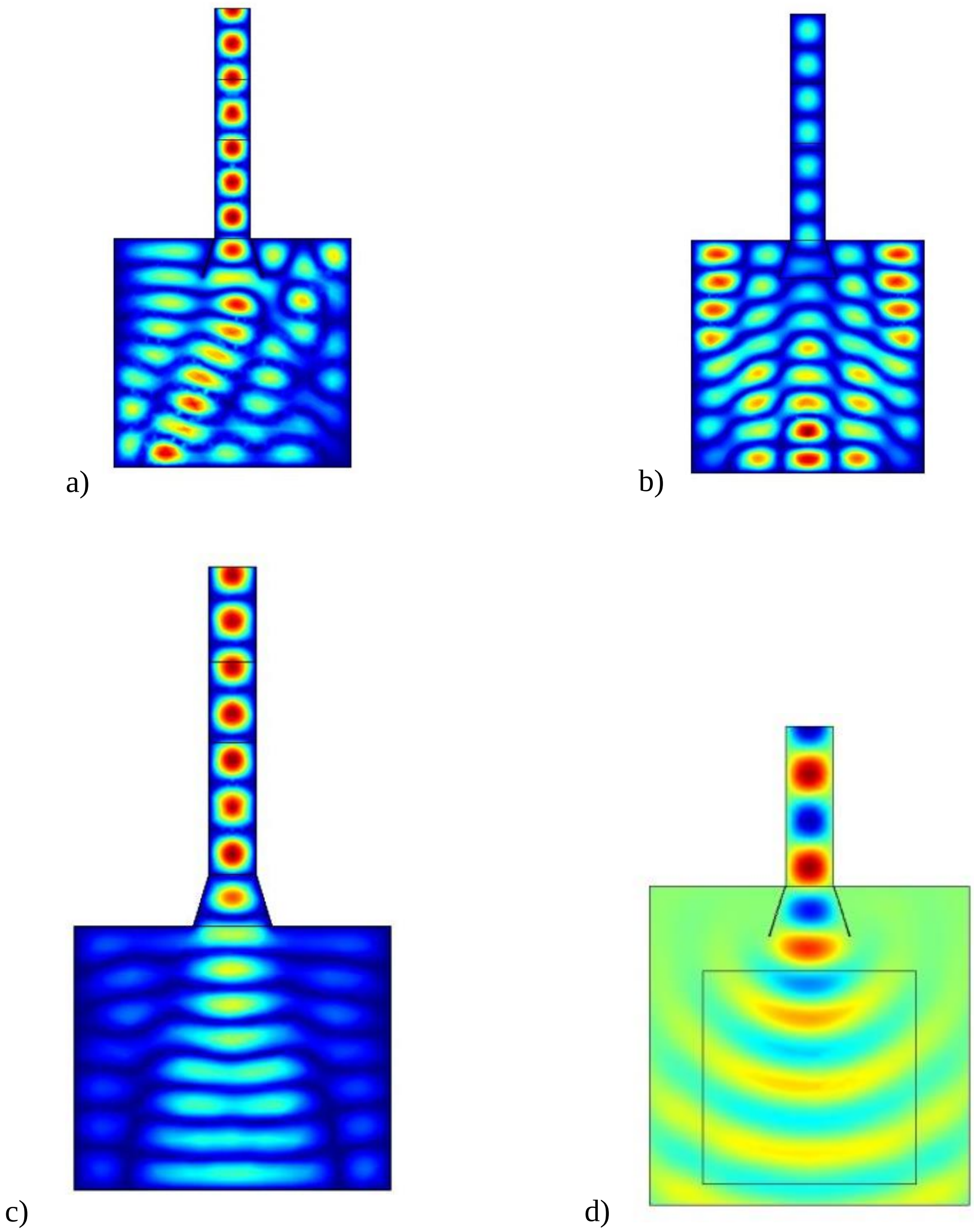

Figure 3-28 Boundary condition and wave propagation of directional plane-wave modelling where: a) the horn waveguide is a perfect electric conductor inside a perfect electric conductor cavity; b) the horn waveguide is a scattering electric conductor inside the perfect electric conductor cavity, c) the horn waveguide is a perfect electric conductor outside a scattering electric conductor cavity, and the cavity is short relative to the height of the horn waveguide; and d) the waveguide is a scattering electric conductor inside a scattering electric conductor cavity

Model calibration for wave propagation

To calibrate the wave propagation inside the cavity, a series of tests was carried out by microwaving marshmallows at different elevations. Marshmallows are very good dielectrics: as they absorb microwave energy, they begin to melt and swell. A Plexiglas® platform (transparent to microwaves) of the same size as the cavity base was placed at four elevations (50, 200, 350 and 500 mm) relative to the antenna's aperture while marshmallows cover the complete platform (Figure 3-29). The elevations chosen with respect to the horn antenna's aperture are: level 1 @ 50 mm, level 2 @ 200 mm, Level 3 @ 350 mm and level 4 @ the base of the cavity. Marshmallows were placed to completely cover the platform and treated for 30 s at 3 kW power.

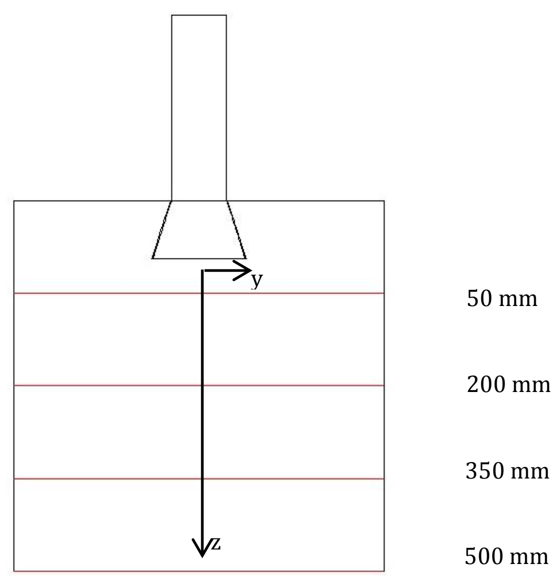

Figure 3-29 Side view of microwave cavity and four elevations relative to the antenna aperture

The graphs in Figure 3-30 are show the energy intensity along the y axis in yz plane at each level. The photographs show all treated marshmallows on the platform; however, the graphs refer only to the line drawn on the treated marshmallows photographs. Each level inside of the cavity shows the energy intensity distribution differed along the y axis at each level, as did the treated marshmallows. The peaks in the graphs of Figure 3-30 are the highest energy intensity and the valleys are the lowest. Comparing the marshmallows affected along the line drawn on the picture and the graphs, it can be understood that the peaks coincided with areas where marshmallows were affected by microwave energy and melted. Superimposing the four images of marshmallows allows visualization of the 3D model of the energy distribution in the cavity. It is important to note that in the marshmallow experiment, the load in the cavity is small; therefore, most of the waves from the waveguide are disturbed and mixed with the reflected waves from the walls of the metallic cavity (perfect electric conductor). The energy intensity here refers directly to the electric field intensity irradiated.

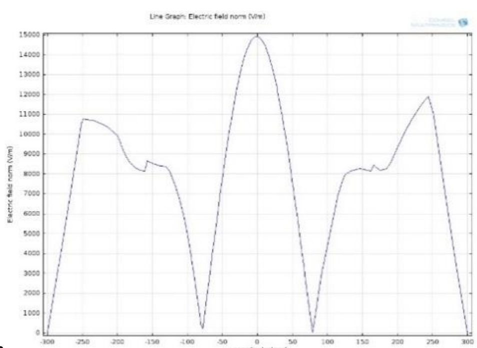

50 mm

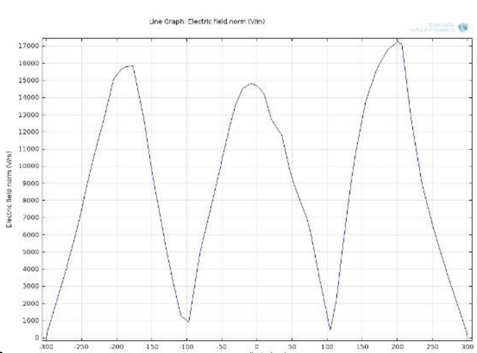

200 mm

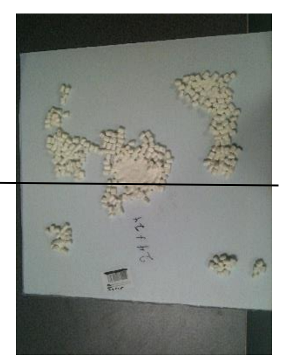

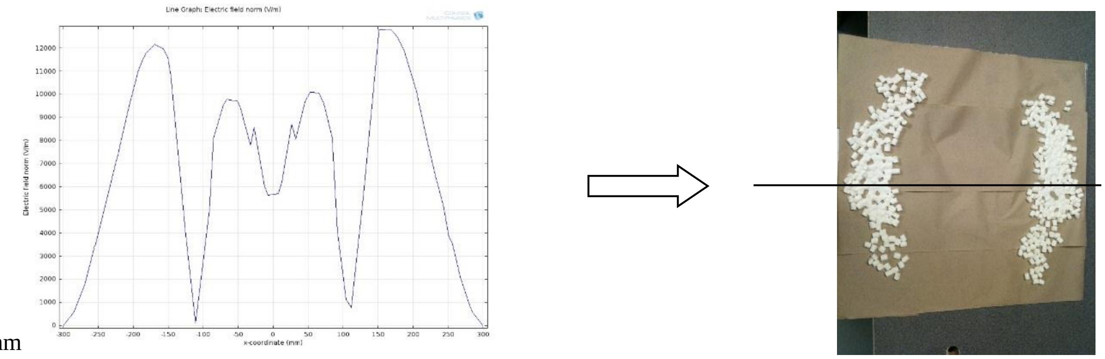

350 mm

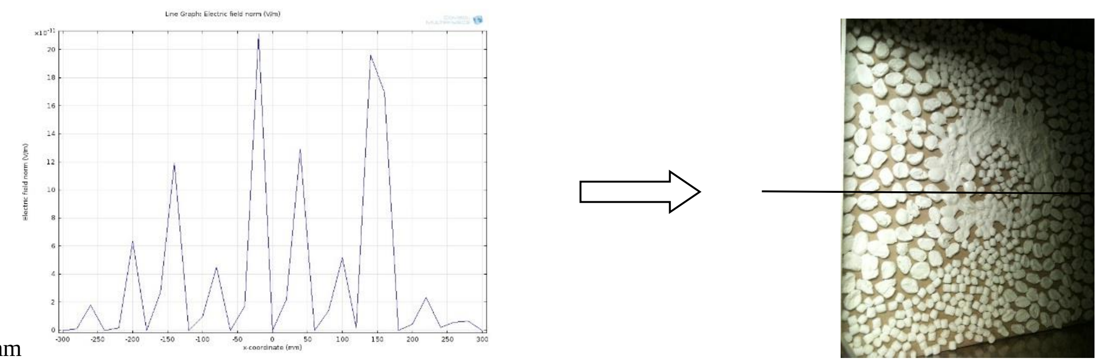

500 mm

Figure 3-30 Energy intensity at each of four levels in the cavity and the affected marshmallows

This calibration finally concluded that wave propagation inside the cavity shown in Figure 3-28 “b” is correct and “a” is incorrect. Results were compared with the numerical electric field distribution and marshmallow test showed the scenario no.1 (Figure 3-28a) is incorrect. Scenario no.3 (Figure 3-28c) runs quickly and is easy to interpret. Therefore, numerical modelling was performed using a perfect electric conductor pyramidal horn waveguide outside a scattering electric conductor cavity, with a short rectangular waveguide attached to it. A three-dimensional (3D) model of the microwave system was constructed based on scenario 3: a 30 cm rectangular transverse electric waveguide was connected to a horn waveguide outside the cavity (Figure 3-31). The cavity height is also shorten the height of the horn waveguide. An intact block of rock and stacked slabs on top of each other without any distance is constructed as well as the dielectric (load). The height of the dielectric load (intact or stacked cylinder) was varied to alter the distance between the antenna's aperture and rock surface.

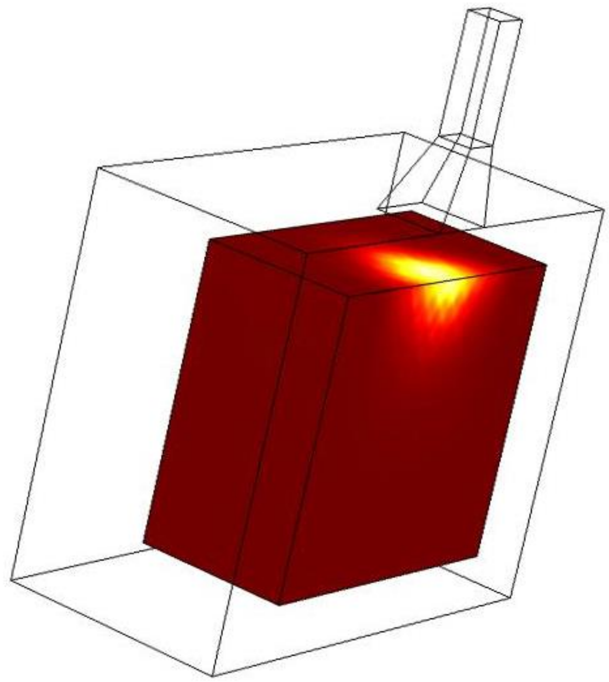

Figure 3-31 3D model of the cavity, waveguide and rock sample

Chapter 4 Results and Discussion

4.1 Effect of Frequency on Electrical Properties of Rocks

The real (ε') and imaginary (loss factor; ε'') permittivities measured with the coaxial probe and resonant cavity (at 0.915, 2.45 and 5.80 GHz) methods are presented in Figure 4-1 for basalt #1, Figure 4-2 for granite, Figure 4-3 for norite, and Appendix A for all other rock types. At the first glance on the results of all samples it is evident that the real permittivity was independent of frequency for all samples (lines are essentially horizontal). The real permittivity values obtained by the two methods were in good agreement with each other. Beyond the accuracy limit of the apparatus (0.1), the results for all rocks except for basalt #1 and #2 fluctuate and became unreliable. This behavior is also rejected by experience as well. The high fluctuation of the results from coaxial probe proof that the material is lossless type. The coaxial probe overestimated the loss factor of granite and norite at the 5.80 GHz frequency, relative to the resonant cavity method. Hence, the rocks except the two basalts are considered loss-less materials. The loss factor of basalts #1 and #2 were approximately 0.5 and 1, respectively, and were independent of frequency: they are considered lossy materials.

a)
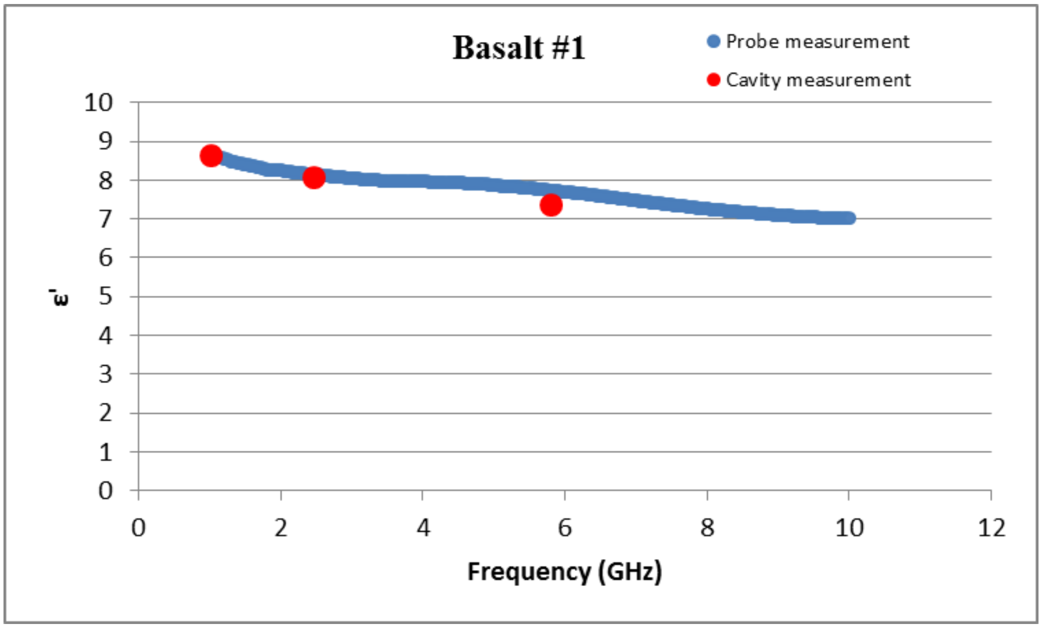

b)
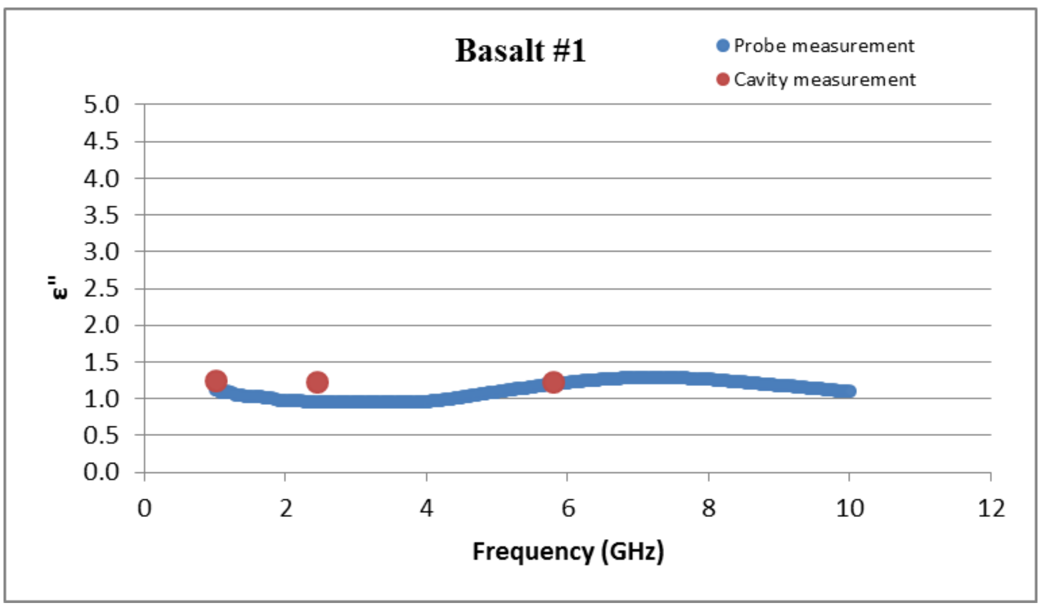

Figure 4-1 a) Real permittivity and b) loss factor of basalt #1 measured with a coaxial probe from 1–10 GHz (blue line) and by the resonant cavity method at 0.915, 2.45 and 5.80 GHz (red dots)

a)

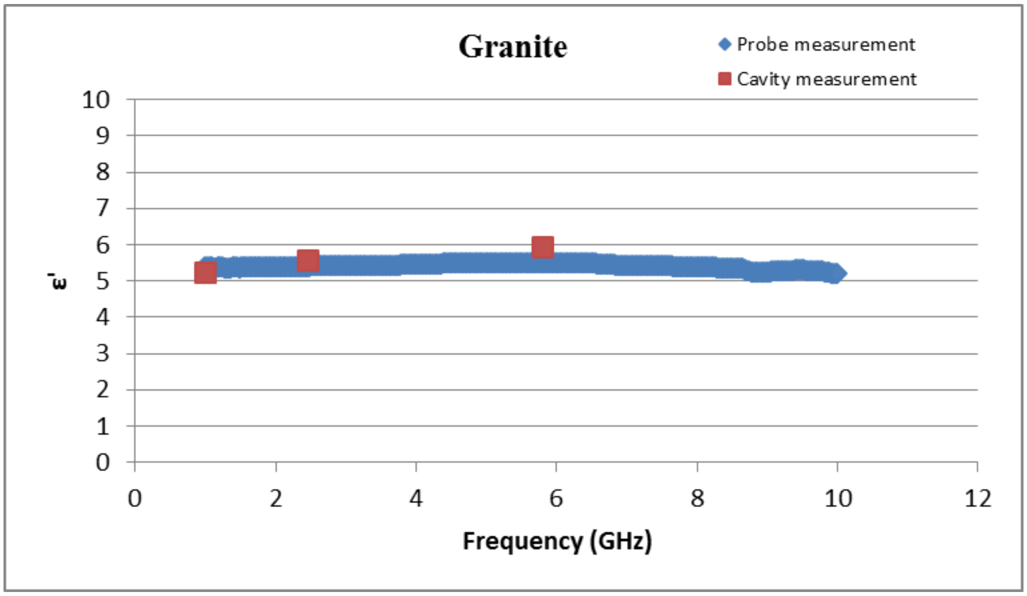

b)

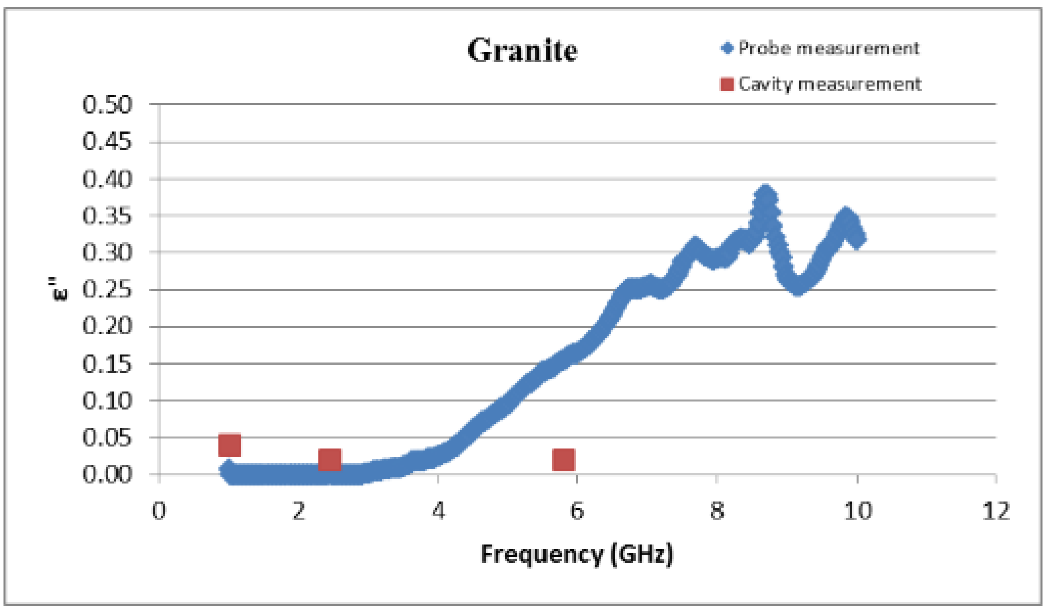

Figure 4-2 a) Real permittivity and b) loss factor of granite measured with a coaxial probe from 1–10 GHz (blue line) and by the resonant cavity method at 0.915, 2.45 and 5.80 GHz (red dots)

a) 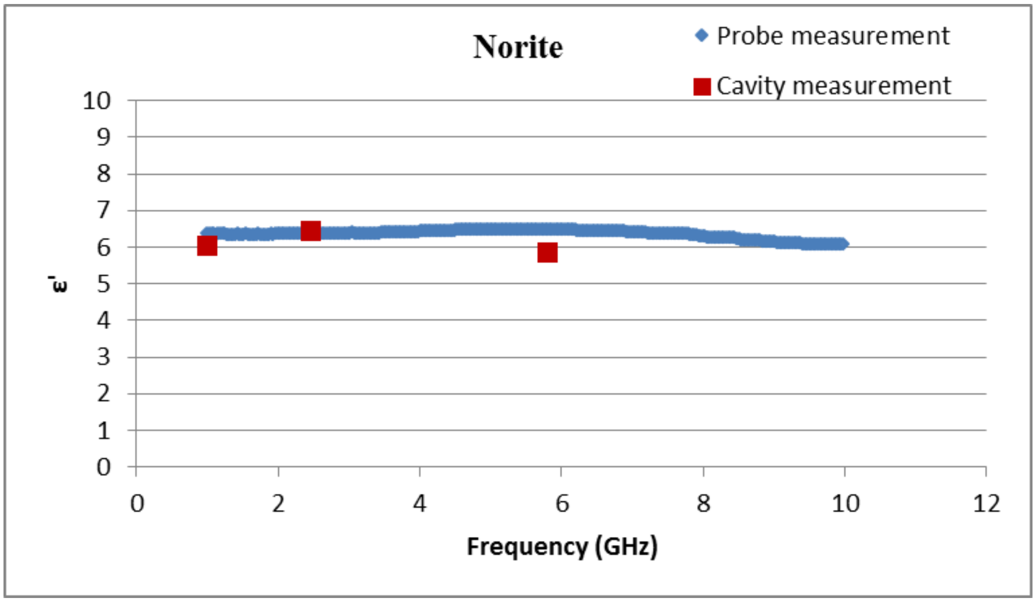

b) 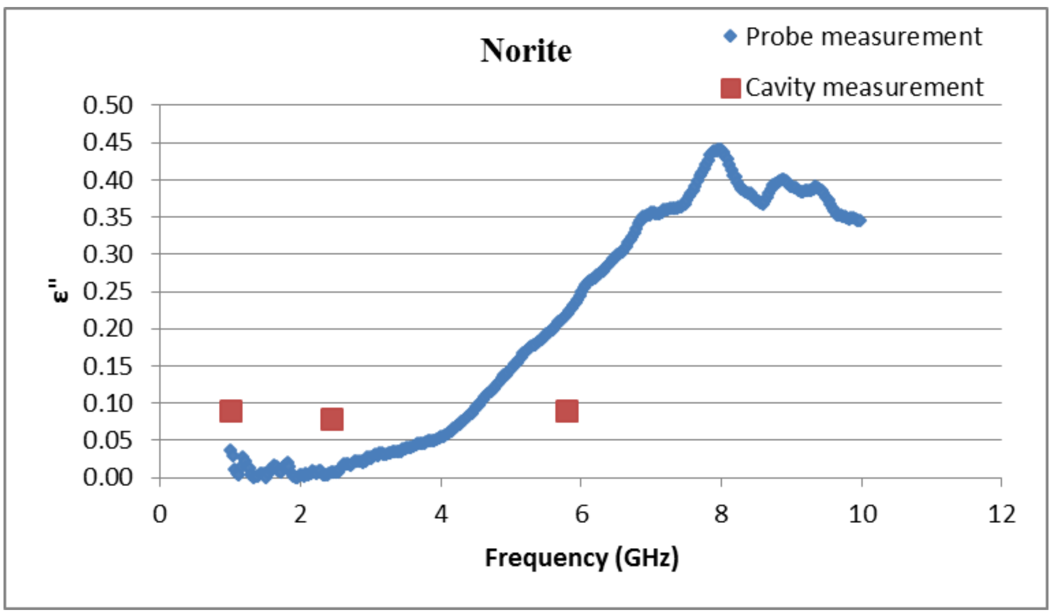

Figure 4-3 a) Real permittivity and b) loss factor of norite measured with a coaxial probe from 1–10 GHz (blue line) and by the resonant cavity method at 0.915, 2.45 and 5.80 GHz (red dots)

As the loss factors of rocks are below or at the accuracy limit of the apparatus, another method of measuring the dielectric properties of rocks is chosen to be used. The resonant cavity attached to a network analyzer is the most recommended and accurate method to measure very low loss factors is a solid state. As explained earlier, this method can only measure the dielectric properties of a material at a certain frequency at a time. Due to this limitation three frequencies had been chosen (0.915, 2.45 and 5.80 GHz) to measure the permittivity of five rock samples (basalt #1, granite, norite, sandstone and dolomite) to compare the results obtained.

The results of the dielectric properties of rocks in the three specific frequencies are plotted in the graphs (red dots) along with the results obtained from the coaxial probe measurement for comparison. By comparing both types of results in graphs good conclusions can be drawn on the electrical properties of rock samples tested. The constant permittivity of rocks are measured correctly by both methods (coaxial probe and resonant cavity). The results from the coaxial probe and resonant cavity measurement match with one another. The resonant cavity revealed that the results of loss factor obtained by the coaxial probe for the loss-less rocks are not correct, since they are under or at the limit of apparatus accuracy. On the other hand, the results for both basal types (#1 and #2) match with one another and shows independency of frequency. The results for loss-less rocks according to resonant cavity measurement also show tendency of being independent of frequency as they are almost showing a horizontal line. All the permittivities, loss tangents and penetration depths according to permittivity of the ten rock types, as well as water, are summarized in Table 4-1 at frequencies of 1, 2.45 and 5.80 GHz. The relationship between the loss tangent and how deep microwaves can penetrate inside are a function of frequency. Rocks with loss factors less than 0.1 are considered transparent and non-absorbent and those with loss factors greater than 0.1 are considered absorbers of microwave energy.

Table 4-1 Real and imaginary permittivities, loss tangent and penetration depth of the ten rock types and water at 1, 2.45 and 5.80 GHz measured by coaxial probe and resonant cavity methods

		Permittivity of dry rocks at frequency of 1 GHz							
		Probe test method				Cavity test method			
	Density (gr/cm3)	e'	e"	Loss tan	Penetration depth (cm)	e'	e"	Loss tan	Penetration depth (cm)
Basalt #1	2.87	8.68	1.13	0.130	13.61	8.65	1.25	0.145	4.59
Granite	2.63	5.38	0.01	0.001	1513.85	5.25	0.04	0.008	111.69
Norite	2.80	6.37	0.04	0.006	360.19	6.07	0.09	0.015	53.38
Sand stone	2.30	2.56	0.05	0.020	162.65	4.29	0.14	0.033	28.85
Dolomite	2.75	7.40	0.14	0.019	102.62	7.65	0.09	0.012	59.92
Basalt #2	2.35	7.48	0.31	0.042	45.59	-	-	-	-
Falsic granophyre	2.44	5.33	0.01	0.002	1507.26	-	-	-	-
Mafic granophyre	3.00	6.60	0.05	0.007	275.81	-	-	-	-
Calcite	3.23	5.39	0.01	0.001	1514.91	-	-	-	-
Gniess	2.59	5.16	0.15	0.029	79.46	-	-	-	-
Green stone	2.96	7.34	0.01	0.001	1768.32	-	-	-	-
Lime stone	2.66	8.23	0.10	0.013	143.05	-	-	-	-
Water (@25 C)	1.00	80.40	4.80	0.060	9.75	-	-	-	-

		Permittivity of dry rocks at frequency of 2.45 GHz								Permittivity of saturated rocks at frequency of 2.45 GHz			
		Probe test method				Cavity test method				Probe test method			
	Density (gr/cm3)	e'	e"	Loss tan	Penetration depth (cm)	e'	e"	Loss tan	Penetration depth (cm)	e'	e"	Loss tan	Penetration depth (cm)
Basalt #1	2.87	8.15	0.95	0.117	5.83	8.09	1.24	0.15	4.47	9.78	1.74	0.178	3.50
Granite	2.63	5.41	0.01	0.001	566.81	5.57	0.02	0.00	230.09	7.29	0.54	0.074	9.77
Norite	2.80	6.39	0.01	0.001	631.90	6.44	0.08	0.01	61.85	8.95	0.71	0.079	8.25
Sand stone	2.30	2.55	0.02	0.006	191.99	3.73	0.09	0.02	41.84	3.06	0.18	0.060	18.65
Dolomite	2.75	7.36	0.10	0.014	52.54	7.09	0.09	0.01	57.69	9.03	0.80	0.089	7.31
Basalt #2	2.35	7.34	0.28	0.039	18.60	-	-	-	-	11.48	1.44	0.125	4.60
Falsic granophyre	2.44	5.41	0.01	0.001	566.79	-	-	-	-	4.21	0.18	0.044	21.72
Mafic granophyre	3.00	6.65	0.02	0.002	304.38	-	-	-	-	7.37	0.50	0.068	10.50
Calcite	3.23	5.41	0.01	0.001	567.06	-	-	-	-	42.52	6.43	0.151	1.98
Gniess	2.59	5.13	0.10	0.020	43.77	-	-	-	-	7.37	0.87	0.117	6.12
Green stone	2.96	7.38	0.01	0.001	662.33	-	-	-	-	6.56	0.30	0.046	16.44
Lime stone	2.66	8.22	0.05	0.006	112.15	-	-	-	-	8.81	0.60	0.068	9.72
Water (@25 C)	1.00	77.10	8.87	0.115	1.93	-	-	-	-	77.10	8.87	0.115	1.93

		Permittivity of dry rocks at frequency of 5.8 GHz							
		Probe test method				Cavity test method			
	Density (gr/cm3)	e'	e"	Loss tan	Penetration depth (cm)	e'	e"	Loss tan	Penetration depth (cm)
Basalt #1	2.87	7.74	1.20	0.155	1.91	7.39	1.23	0.166	1.82
Granite	2.63	5.48	0.16	0.028	12.42	5.94	0.02	0.003	100.32
Norite	2.80	6.48	0.22	0.034	9.50	5.84	0.06	0.010	33.16
Sand stone	2.30	2.59	0.09	0.033	15.46	3.71	0.09	0.024	17.62
Dolomite	2.75	7.41	0.35	0.047	6.39	7.69	0.11	0.014	20.75
Basalt #2	2.35	7.27	0.53	0.073	4.21	-	-	-	-
Falsic granophyre	2.44	5.47	0.14	0.026	13.32	-	-	-	-
Mafic granophyre	3.00	6.74	0.24	0.036	8.85	-	-	-	-
Calcite	3.23	5.48	0.19	0.034	10.29	-	-	-	-
Gniess	2.59	5.14	0.26	0.051	7.07	-	-	-	-
Green stone	2.96	7.51	0.26	0.034	8.83	-	-	-	-
Lime stone	2.66	8.30	0.37	0.044	6.43	-	-	-	-
Water (@25 C)	1.00	-	-	-	-	-	-	-	-

The graphs in Appendix D show the relationship between the penetration depth of microwaves into rocks and the loss tangent at three frequencies. The penetration depth was high in loss-less rocks (i.e., granophyres, granite, norite, calcite, sandstone and dolomite) and low in lossy rocks (i.e., water and basalt #1 and #2). As the microwave frequency is increased from 1 to 2.45 to 5.80 GHz, the penetration depth decreased dramatically, especially in loss-less rocks.

The real permittivity (Figure 4-4a) and loss factor (Figure 4-4b) measured by the resonant cavity method were similar at 1, 2.45 and 5.80 GHz for each of five rock types in the dry condition. A very close similarity in between the results for one rock sample at three different frequencies is observed.

a)
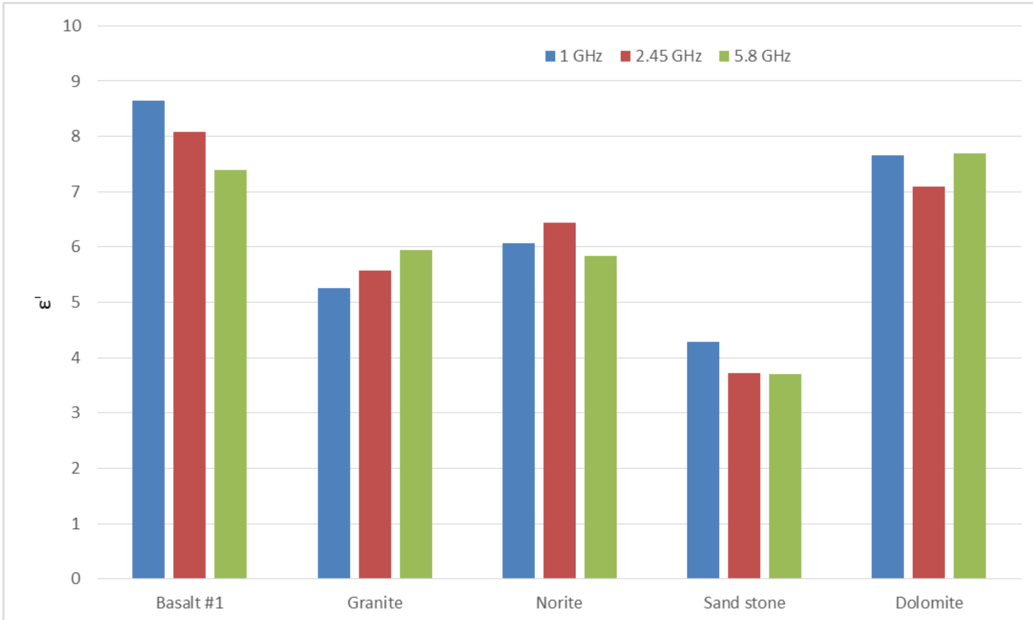

b)
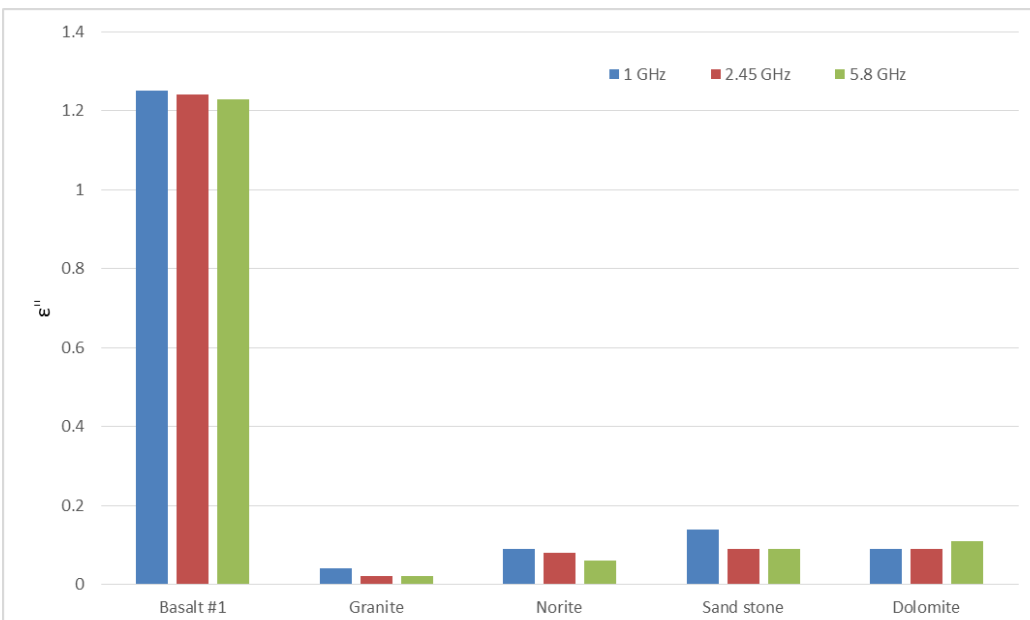

Figure 4-4 a) Real permittivity and b) loss factor of five rock types at 1, 2.45 and 5.80 GHz

The coaxial probe measurements of rocks saturated with water are not considered reliable: all rocks have very low porosity, but a very thin layer of water on the rock surfaces caused overestimated of the real permittivity and loss factor (Figure 4-5).

a)

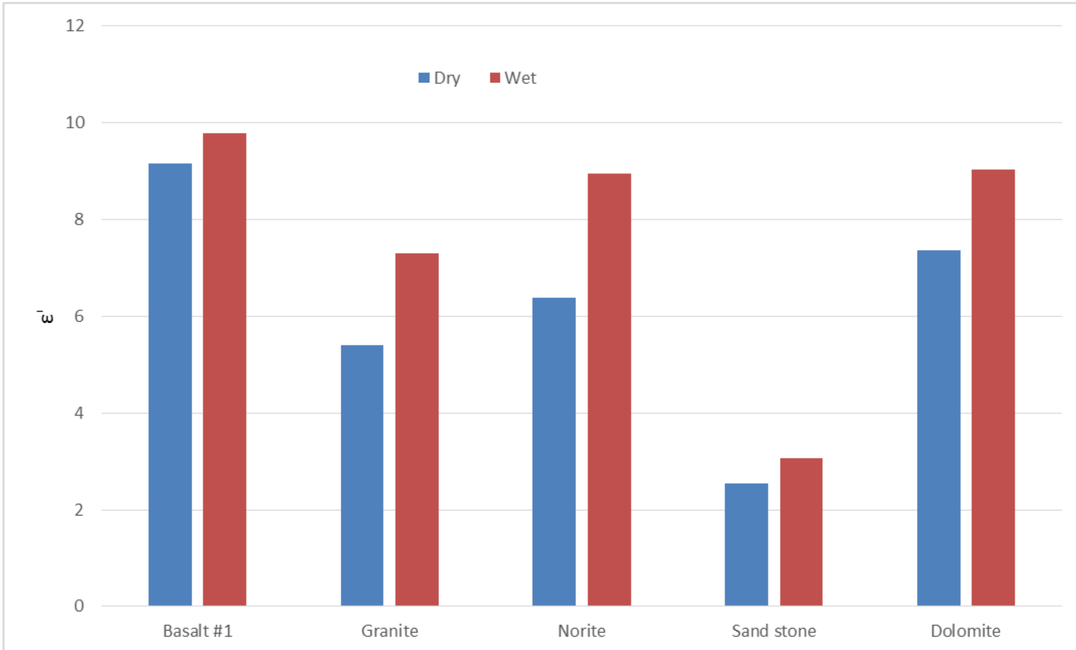

b)

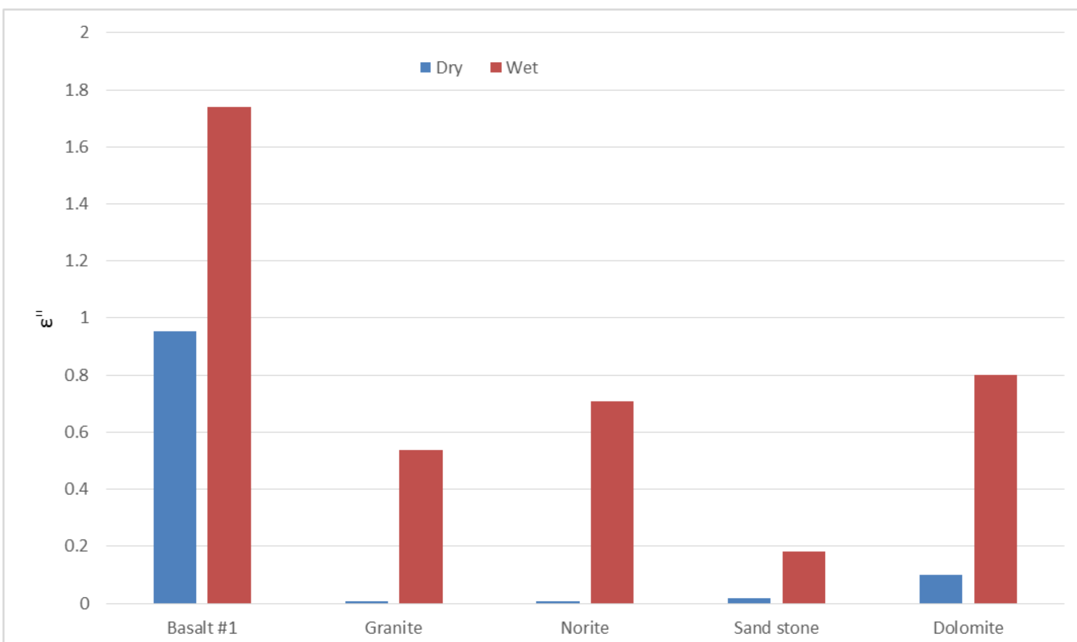

Figure 4-5 a) Real permittivities and b) loss factors of dry and saturated (wet) situation rocks at 2.45 GHz

In order to confirm the accuracy of the results obtained either with the coaxial probe or the resonant cavity, two types of Representative samples (i.e., basalt #1 and granite) were sent to IDS Corporation to verify dielectric property measurements. IDS Corporation also used two different methods measuring the real and imaginary permittivity of rocks within two different ranges. They using the parallel plates and capacitive method to measure dielectric properties from 10 MHz to 1 GHz; and the waveguide X-band from 8.2 to 12.4 GHz. Figure 4-6 and Figure 4-7 show the real and imaginary part of permittivity of granite respectively. Figure 4-8 and Figure 4-9 show the real and imaginary part of permittivity of basalt #1 respectively. Both dielectric properties were independent of frequency, as was observed in the laboratory study. The loss factor of granite showed high fluctuation at low frequencies due to the piezoelectric property of quartz. The peak loss factor in granite at high frequencies is due to the air gap between the specimen and waveguide.

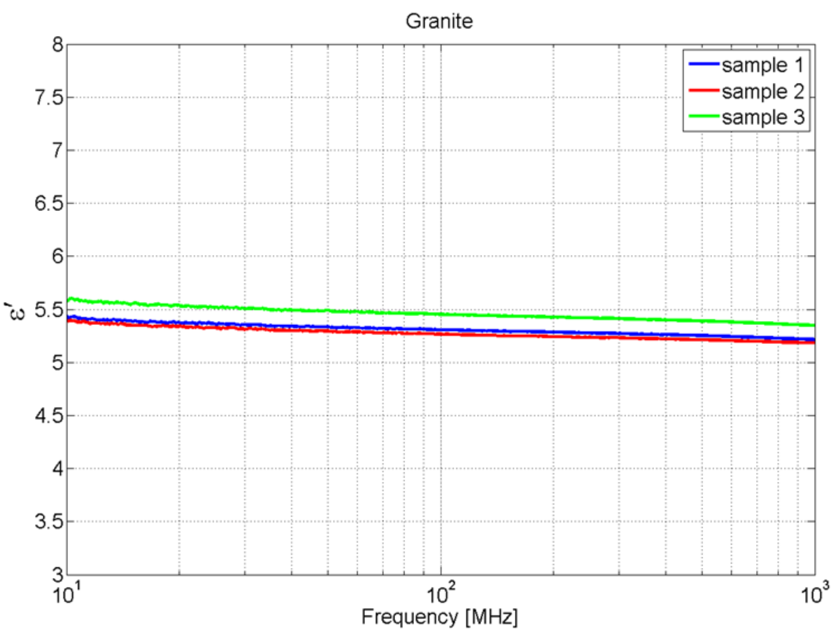

a)

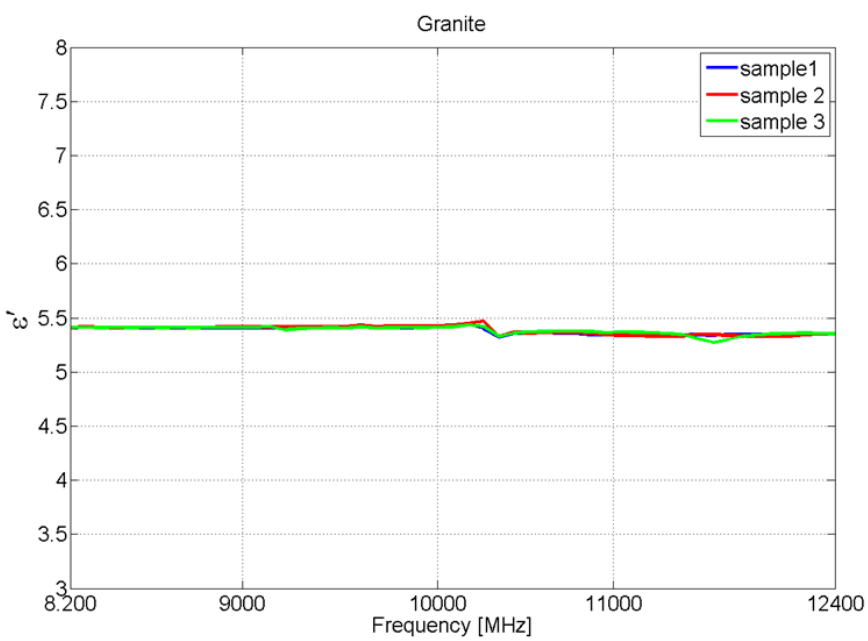

b)

Figure 4-6 Real permittivity of granite measured with the a) capacitive method and b) waveguide X-band method (after IDS Corporation)

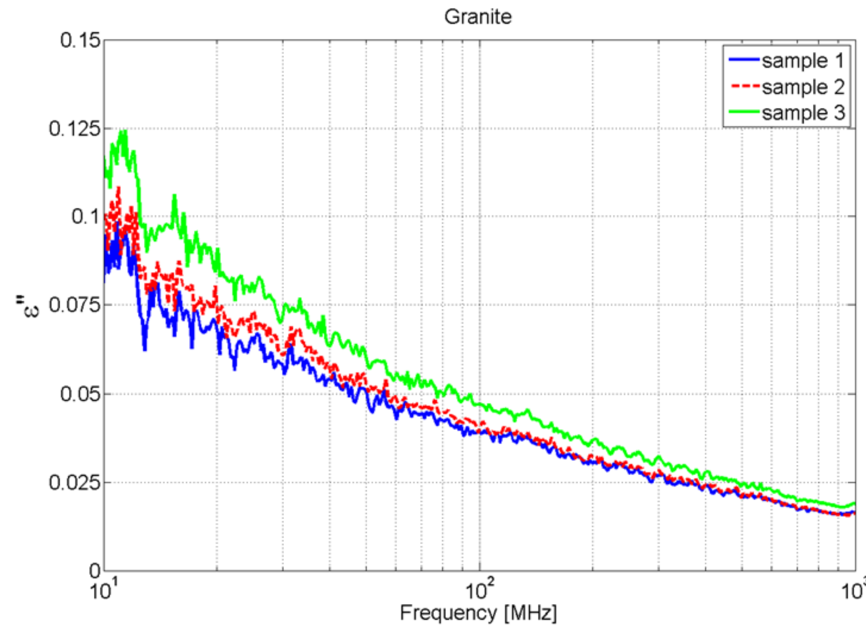

a)

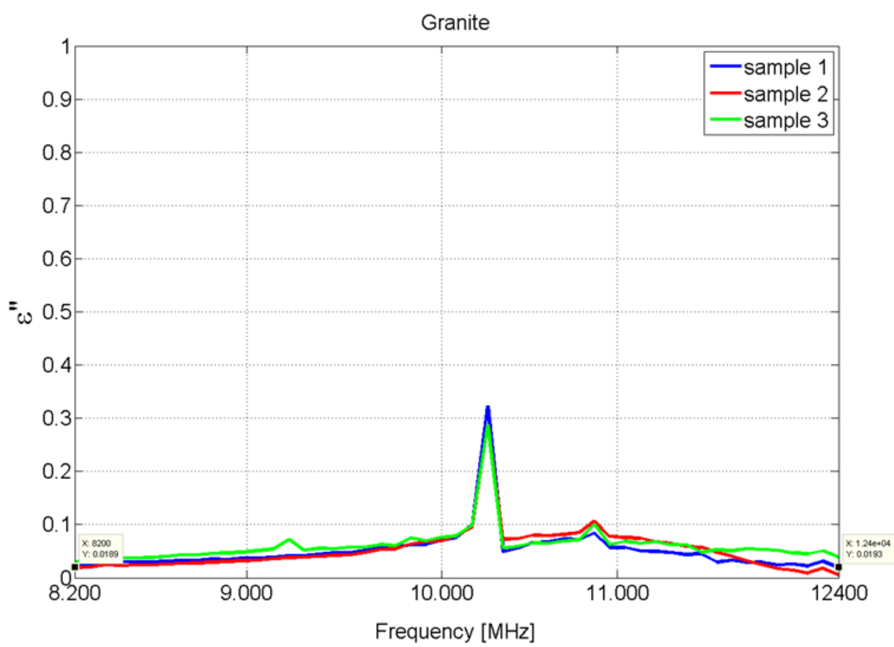

b)

Figure 4-7 Loss factor of granite measured with the a) capacitive method and b) waveguide X-band method (after IDS Corporation)

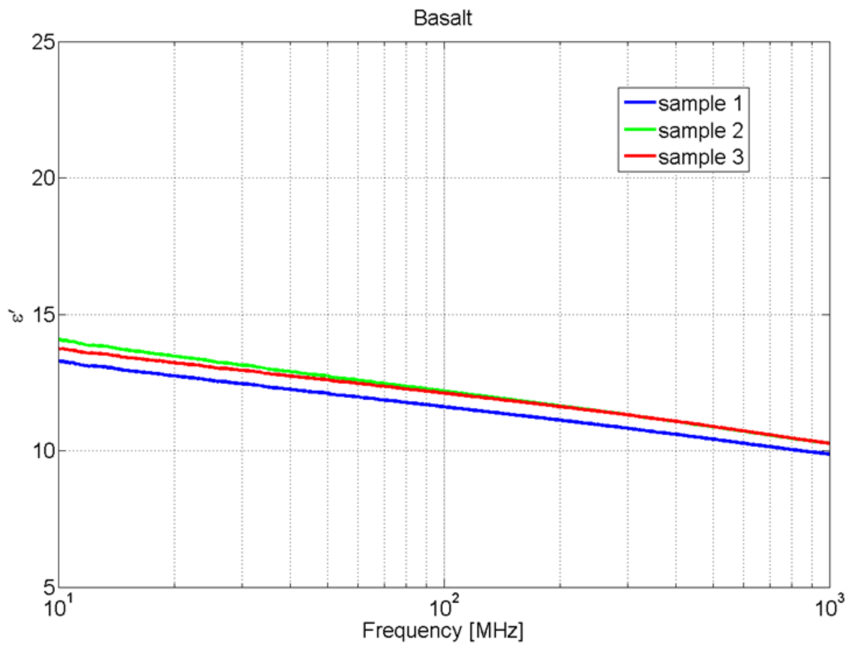

a)

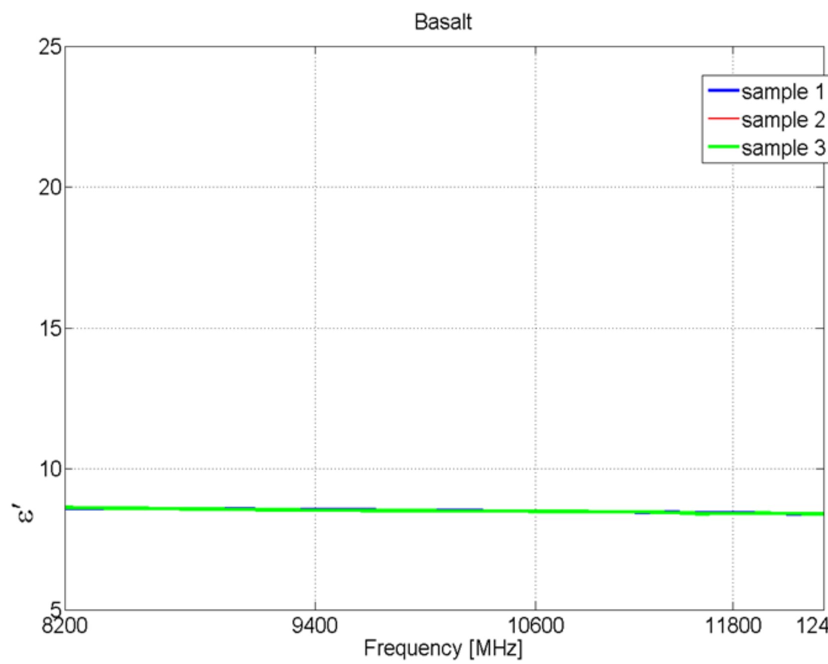

b)

Figure 4-8 Real permittivity of basalt #1 measured with the a) capacitive method and b) waveguide X-band method (after IDS Corporation)

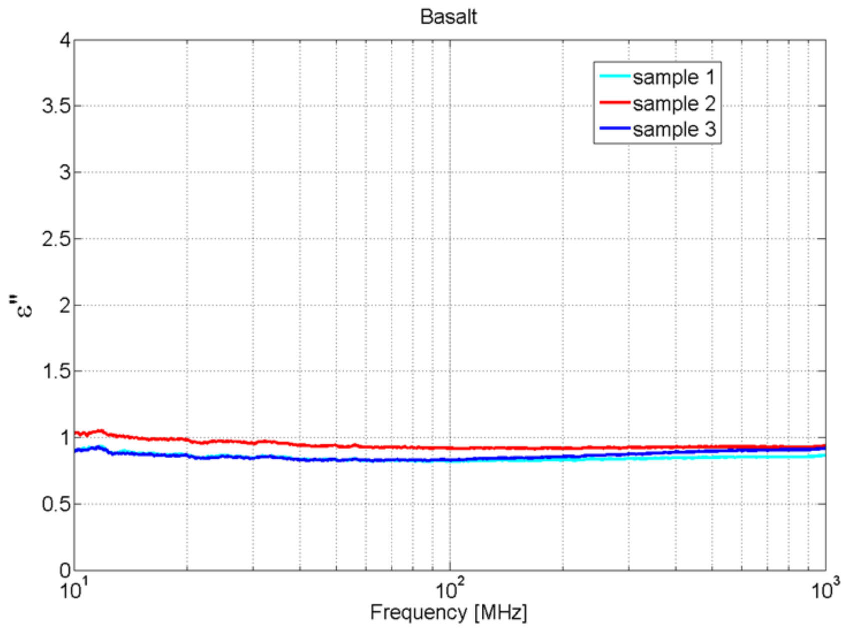

a)

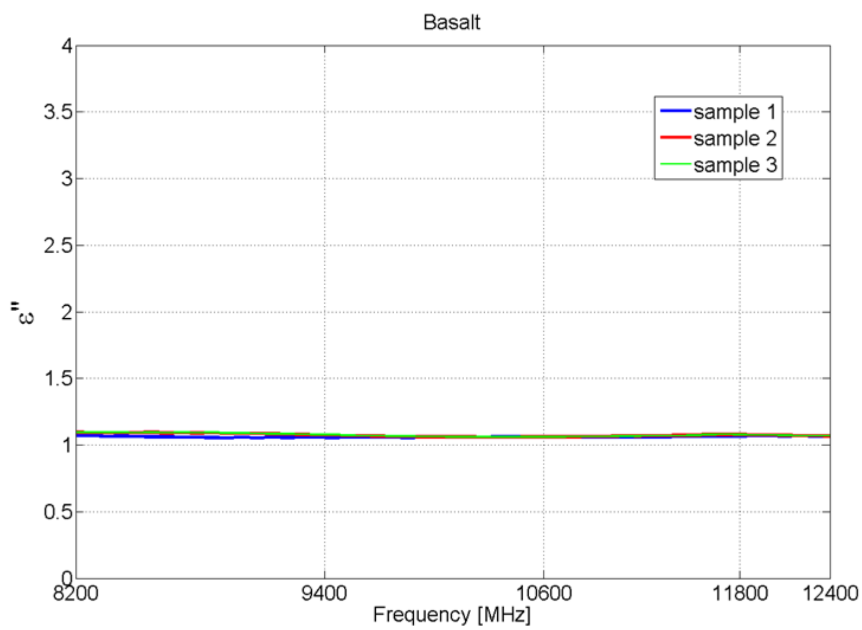

b)

Figure 4-9 Loss factor of basalt #1 measured with the a) capacitive method and b) waveguide X-band method (after IDS Corporation)

The IDS Corporation results complemented the laboratory results (from 1 to 10 GHz) to more comprehensively cover the electromagnetic spectrum. As expected, the measurements in the laboratory study (Figure 4-1 to Figure 4-3) fell between the measurements from IDS Corporation.

- 10 to 1,000 MHz => received from IDS Corp.
- 1,000 to 10,000 MHz => measured in the lab.
- 8,200 to 12,400 MHz => received by IDS Corp.

The constant permittivity of granite in Figure 4-2 goes in between both graphs in Figure 4-6 and matches the values from one end to other. Apart from the results measured by the coaxial probe the loss factor of granite in Figure 4-2 also goes in between both graphs of Figure 4-7 and matches the values.

The constant permittivity of basalt #1 in Figure 4-1 goes in between both graphs in Figure 4-8 and matches the values from one end to the other. Since basalt #1 is considered as lossy type of material the loss factor obtained by coaxial probe in Figure 4-1 also goes in between both graphs in Figure 4-9 and matches the values from both ends. The combination of the results obtained in the lab and received from IDS Corp. concludes that all results are accurate. Moreover, both constant permittivity and loss factor of rocks are independent of frequency.

Previous findings from the microwave-assisted rock breakage research group at McGill University showed that the loss factor of rocks depended on frequency (Nejati, 2014). Further investigation on the same rock samples (explained earlier explicitly in details) the independency of loss factor from frequency is confirmed. In combination with the recommendations of Agilent Technologies Inc. (2006) and Venkatesh and Raghavan (2005), the following conclusions are made:

- The appropriate method has to be chosen to measure the dielectric properties of loss-less materials,
- The coaxial probe is not recommended to measure the dielectric properties of loss-less materials such as granite, since it has very limited accuracy.
- When using a coaxial probe, calibration is recommended for a new measurement, and the range of frequency should be narrow, since a wide frequency range reduces the resolution of the dielectric measurement.
- The resonant cavity and parallel plate methods are recommended to measure the dielectric properties of loss-less materials, the choice of which depends upon the appropriate frequency range.

4.2 Temperature Distribution and Rock Strength after Treatment in Commercial Microwave Ovens at 0.8, 1.2 and 3 kW Power

The temperature distribution of the specimens at different exposure time and power showed unorganized increase. This is also understood that microwaving conditions were not identical at each power level. The 0.8 kW power oven had a turntable and microwaves were irradiated directly from the side to the specimen. The 1.25 kW power oven had a fan in front of the waveguide that act as mode stirrer and microwaves were irradiated indirectly from the top of specimen; therefore, less amount of energy will be emitted to the specimen. The 3 kW power oven had three 1 kW magnetrons (two on top and one at the bottom of the specimen) that irradiated microwaves via rotatable antennas to a stationary specimen in the cavity. The inequality of conditions influences the amount of energy absorption of rock sample.

The tested rocks absorbed little microwave energy, which is evident from the low rise of their temperature; therefore, the results obtained after being microwaved at low power (up to 3 kW in commercial ovens) shows no changes in their mechanical properties.

On the other hand, it has been understood that the subjected rocks are considered as loss-less type of materials due to their extremely low dielectric constants. Therefore, the results obtained from low power microwave treatment were not conclusive and led to experiments at high power microwave energy.

Three strength metrics strongly influence directly the performance and life span of disc cutter in terms of mechanical rock cutters. In predicting the penetration and advancement rate of a TBM, the uniaxial compressive strength and Brazilian tensile strength and CERCHAR abrassivity index value of rocks are the very important predictor parameters.

A series of hard and abrasive rock samples in terms of strength had been subjected to 800, 1250 and 3000 MW microwave power in order to examine the influence of microwave energy on their strength and abrassivity. Commercial microwave ovens (normally used in kitchens) had been used to treat the prepared specimens of relevant samples. Untreated and treated specimen with microwave energy had been subjected to uniaxial compressive strength, Brazilian tensile strength and CERCHAR abrassivity index tests. The results of untreated and treated specimens are shown in the graphs in Appendix C for all rocks samples. The BTS was slightly lower in some microwave treated rock samples than untreated samples, but no changes in the UCS or CAI were observed (Appendix C).

4.3 Treatment in Commercial Microwave Ovens (1.2 to 5 kW)

4.3.1 Temperature Distribution

Rocks treated at higher power levels (1.2, 3 and 5 kW) in an industrial microwave oven show that the rise in temperature was approximately linear with exposure time at each power level. The same was observed for cylinders.

The temperature of discs increased more quickly and had higher maxima than the cylindrical specimen due to the volume of specimens. The power absorption efficiency positively were used at Hydro-Quebec's research laboratory that had variable power adjustment. Here the microwave conditions for the specimens were all identical; however, the ratio of specimen's volume to the cavity's volume is extremely small. That industrial microwave system was a multi-mode cavity at constant frequency of 2.45 GHz. The surface temperature profile of the specimens at mentioned exposure time and power were recorded as in Figure 4-10 for basalt #1, Figure 4-11 for norite, Figure 4-12 for granite and Figure 4-13 for basalt #2. The figures show the temperature distribution of discs and cylindrical specimens of subjected rock samples. By employing the equation (15), the overall temperature of the subjected samples were calculated empirically and compared with their actual results obtained from Figure 4-10 to Figure 4-13. It is interestingly found that upon the rock type and the specimen volume to cavity volume ratio (i.e., sample volume). The mean absorption efficiency of basalt #1 discs was 70%, compared to 80% for cylinders. The difference was more marked for basalt #2 (50% for discs, 100% for cylinders), norite (40% for discs, 70% for cylinders) and granite (18% for discs, 25% for cylinders). Note that the basalt #1 discs could not be treated for more than 90 s at 1.2 kW, 35 s at 3 kW or 20 s at 5 kW, because longer exposure times caused the specimens to spall off their surfaces and finally burst (Figure 4-1). This was also observed by Gray (1965) and Wilkinson and Tester (1993). Basalt #1 has very fine grains and extremely low porosity.

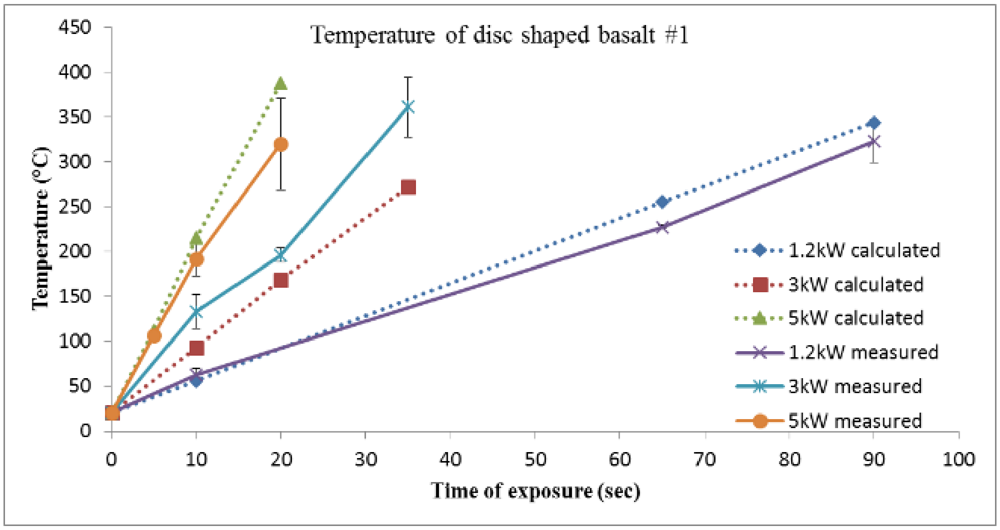

a)

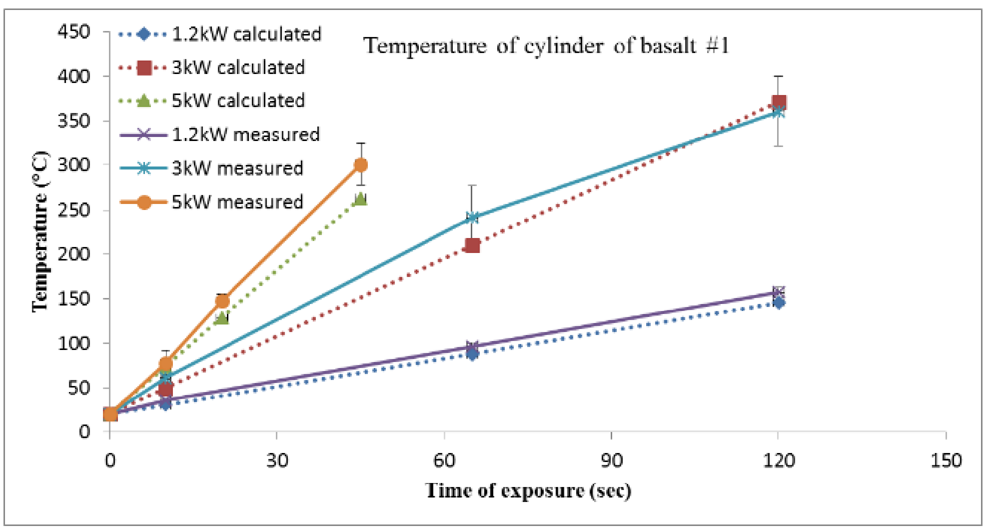

b)

Figure 4-10 Mean (± standard deviation) measured surface temperature and temperature estimated from equation 15 for a) discs and b) cylinders of basalt #1 exposed to 1.2, 3 and 5 kW power in a 2.45 GHz multi-mode industrial microwave

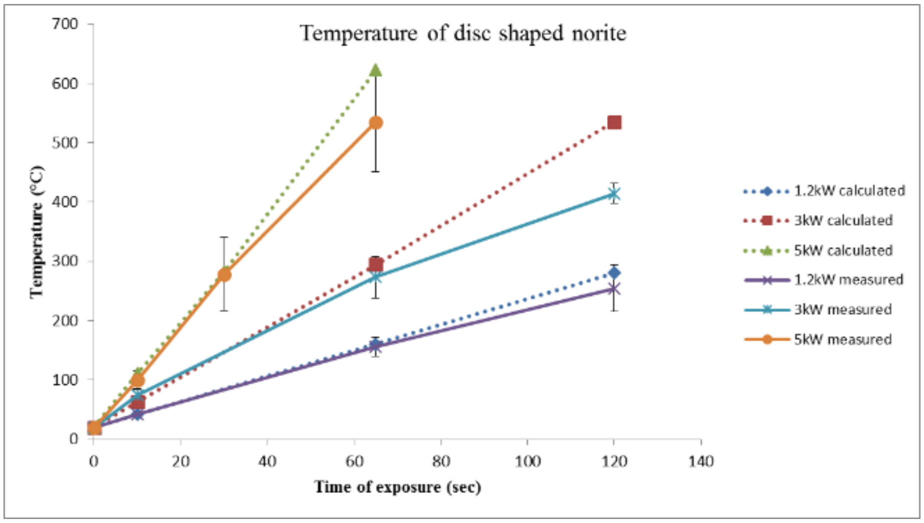

a)

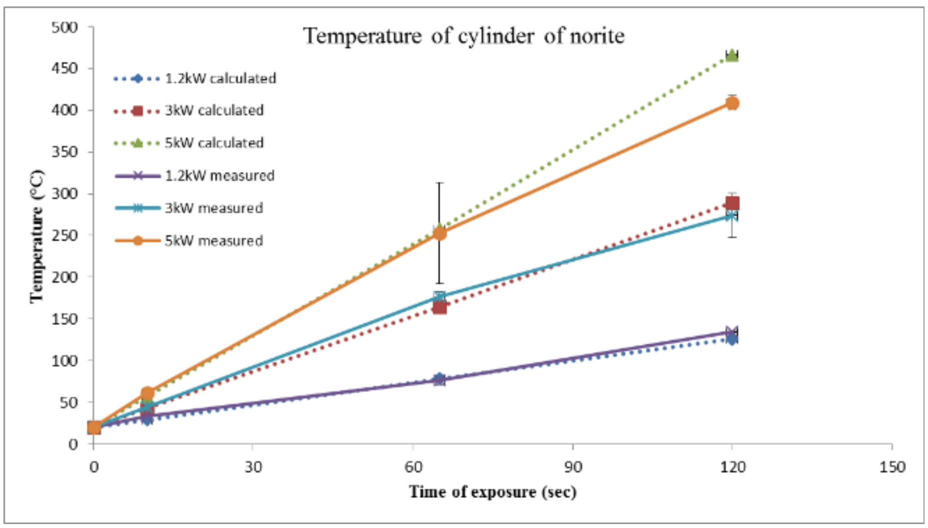

b)

Figure 4-11 Mean (± standard deviation) measured surface temperature and temperature estimated from equation 15 for a) discs and b) cylinders of norite exposed to 1.2, 3 and 5 kW power in a 2.45 GHz multi-mode industrial microwave

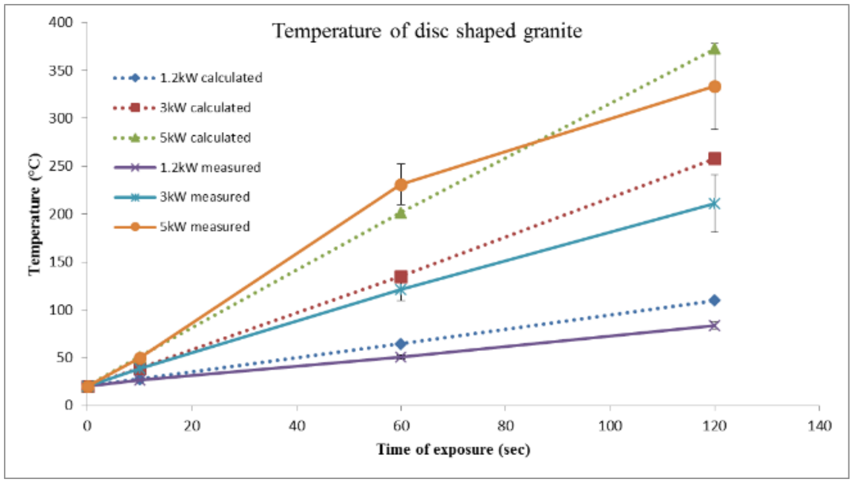

a)

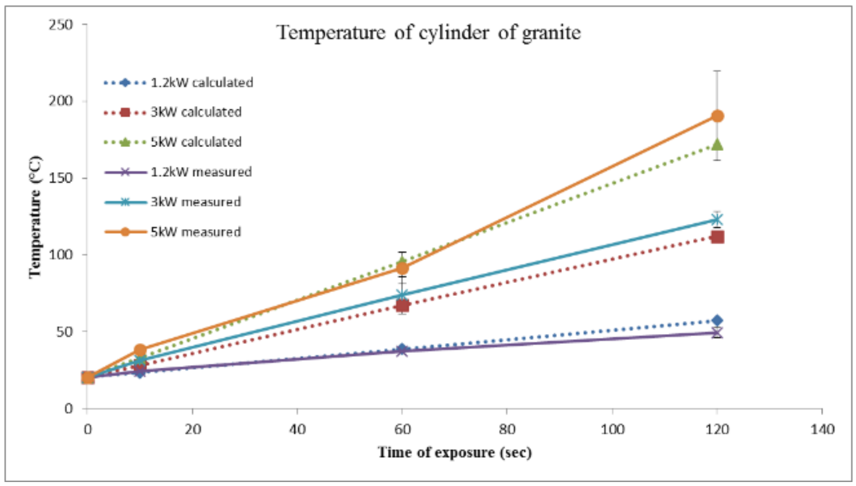

b)

Figure 4-12 Mean (± standard deviation) measured surface temperature and temperature estimated from equation 15 for a) discs and b) cylinders of granite exposed to 1.2, 3 and 5 kW power in a 2.45 GHz multi-mode industrial microwave

a)

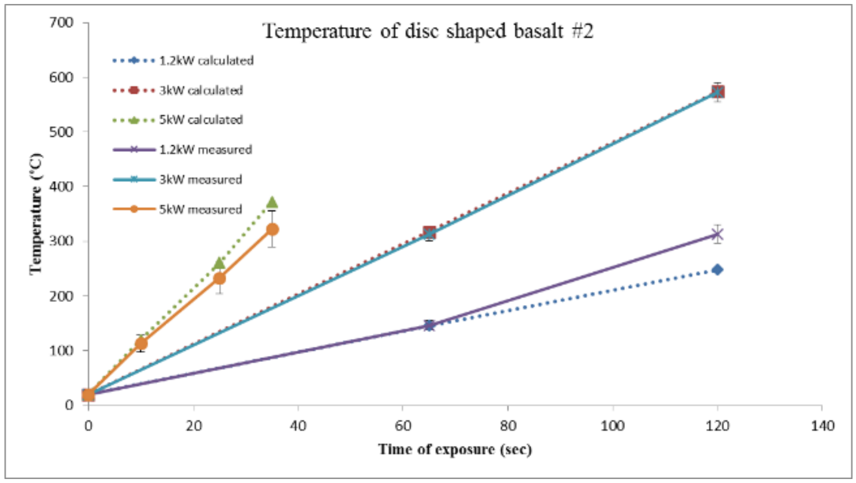

b)

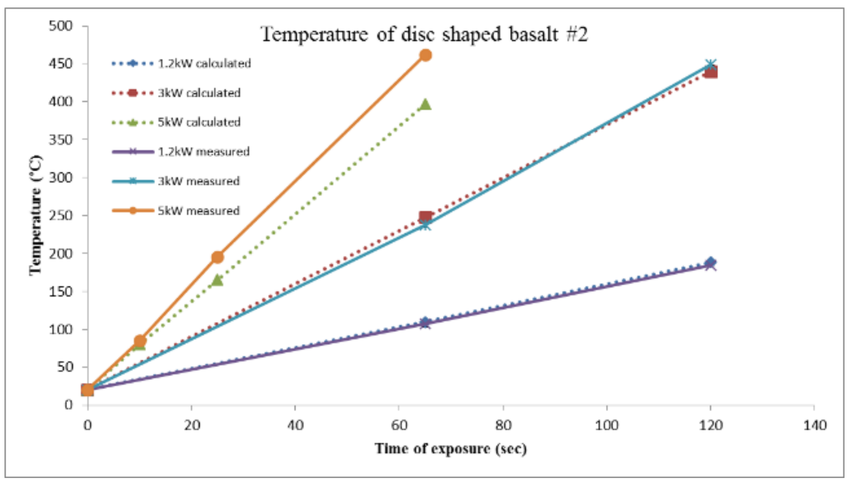

Figure 4-13 Mean (± standard deviation) measured surface temperature and temperature estimated from equation 15 for a) discs and b) cylinders of basalt #2 exposed to 1.2, 3 and 5 kW power in a 2.45 GHz multi-mode industrial microwave

Figure 4-14 Basalt #1 after 35 s of treatment at 3 kW power, showing spalled surface

One norite specimen melted when exposed to 3 kW power within 120 s and one started to melt from the inside at 5 kW power within 35 s. Thus, the higher the power, the earlier the rock specimen reached the melting point, and the higher the power density concentrated in the rock. Norite contains a significant amount of sulfide and mafic minerals, which are considered good absorbers of microwave radiation according to Chen et al. (1984). This causes high absorption ability due to the good energy dissipation. Melting rock samples is not the objective of this study; the rock needs to remain solid so that physical changes within the rock are due to the volumetric expansion of minerals. The start of the melting stage is the upper boundary limit of microwave radiation research.

The temperature distribution in stacked discs of rock type after microwave treatment at 3 kW power showed two peaks, one at the bottom (140–220°C) and the other at 8 cm from the bottom (180–240°C) (Figure 4-15). The lowest temperatures (110–170°C) were observed in the center of the specimen. In the middle of the cylinder the lowest temperature is observed, which shows more than 50 degree Celsius difference with the extremities of the specimen. The surface of the thin discs were polished in order to minimize the air gap in between. It should be noted that when two polished surfaces are heated, the air between the discs lubricates the surface and an air hokey effect happens; therefore, the discs can move and fall from the top. This occurred in the 40 s treatment. The uneven distribution of temperature reveals the reasons why the BTS and UCS varies a lot.

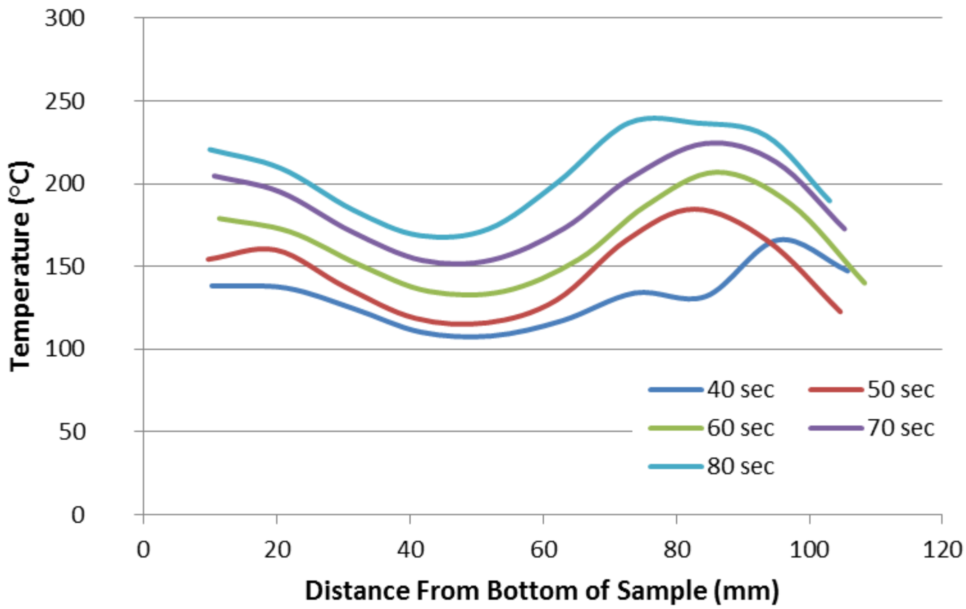

Figure 4-15 Temperature profile of stacked disc specimens along the height of cylindrical specimens

4.3.2 Basalt #1 Strength Parameters

Untreated basalt #1 had a BTS of approximately 12 MPa. The lowest power level had no effect on the BTS (Figure 4-16a), whereas after 20 s exposure at 3 kW power, the BTS was approximately 30% lower than the untreated specimen (Figure 4-16b), and after 20 s exposure at 5 kW power, the BTS was about 30% lower than the untreated specimen (Figure 4-16c). The specimen burst at 35 sec of exposure time at 3 kW. The disc shape specimens were not treated for more than 20 s at 5 kW in order to avoid the specimen to burst. Within that short period of time it can be observed that the tensile strength of the basalt #1 was reduced by about 30 %.

By comparing the power level and the tensile strength value in 10 and 20 s of exposure, it can be observed that in 10 seconds of exposure time the tensile strength value is reduced very little. At 20 s of exposure, the tensile strength was reduced significantly as the power level increased.

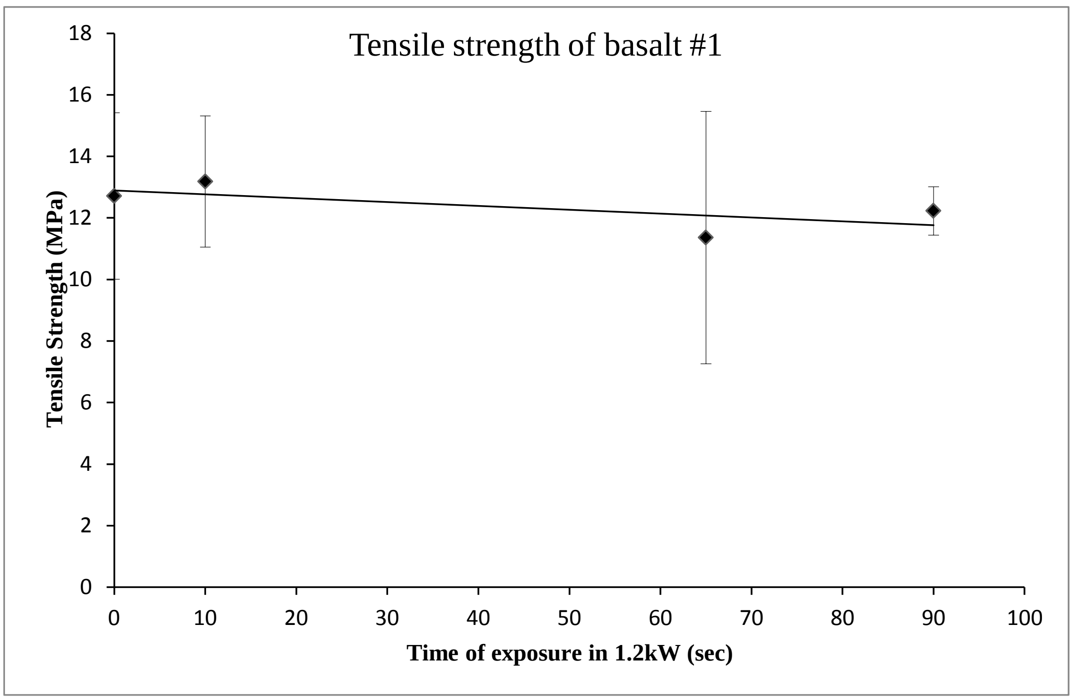

a)

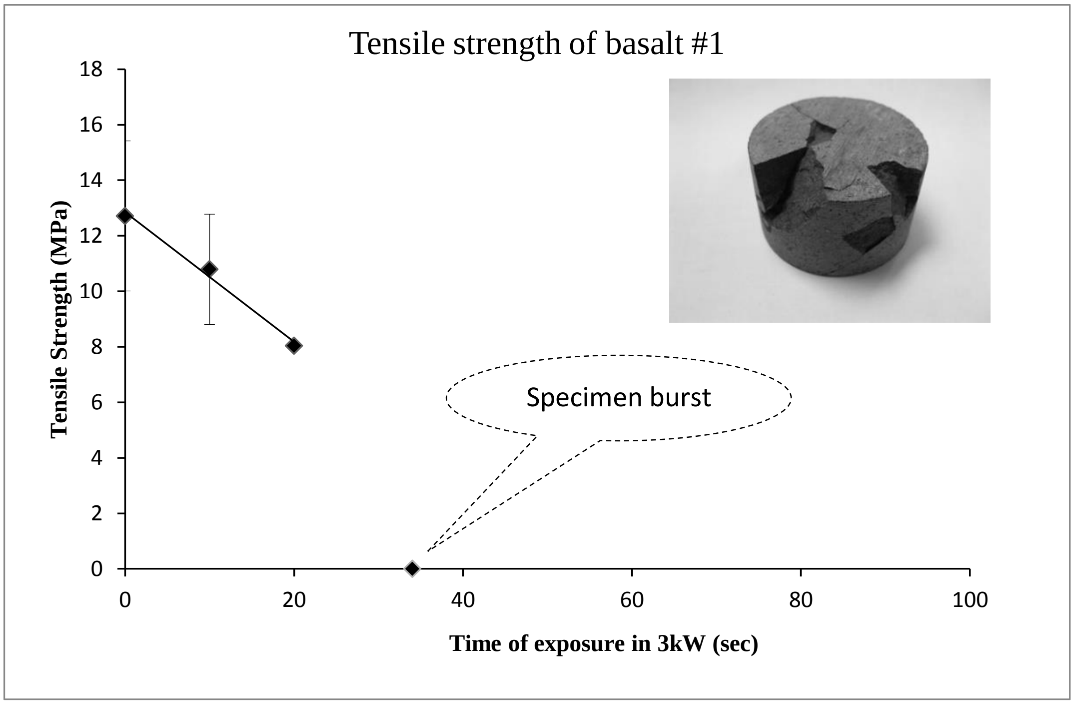

b)

c)

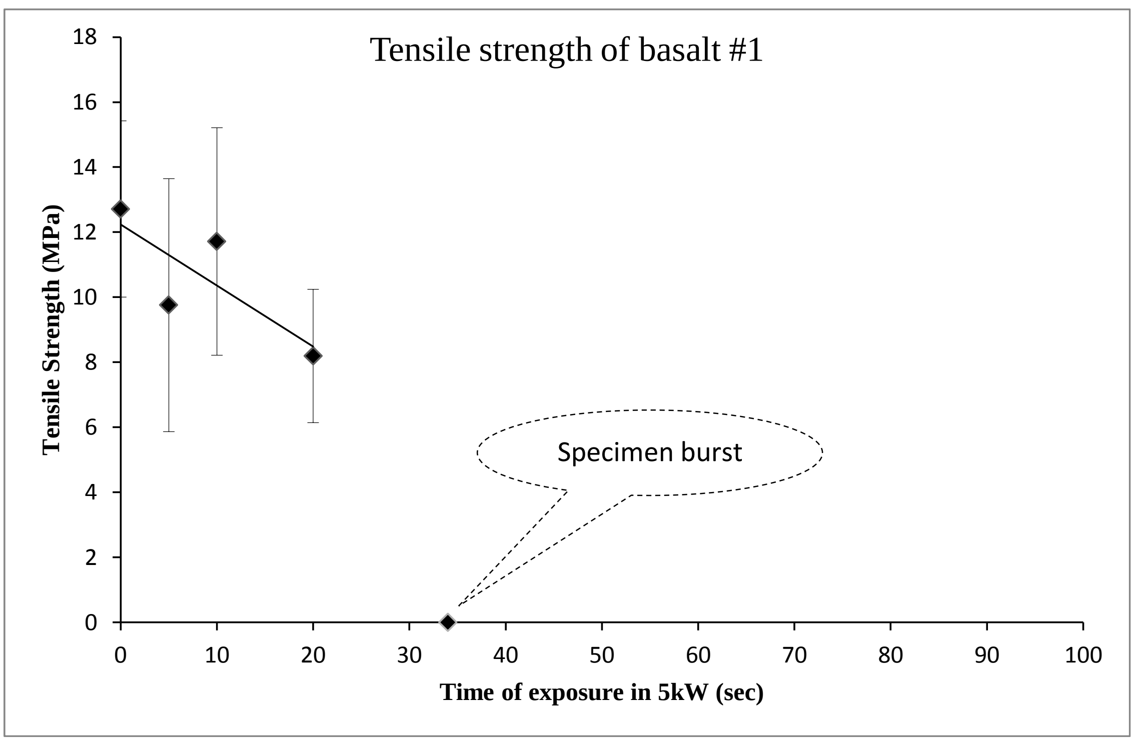

Figure 4-16 Brazilian tensile strength of basalt #1 treated at a) 1.2 kW, b) 3 kW and c) 5 kW microwave power

Some basalt #1 discs were examined under the Scanning Electron Microscope for micro-cracks. The surfaces of untreated specimens appeared to be free of fractures at x50 magnification (Figure 4-17a) but a few micro-cracks were observed at x200 magnification (Figure 4-17b). After exposing a similar specimen to 3 kW microwave energy for a few seconds, the density of the micro-cracks was higher and visible at x50 magnification (Figure 4-18).

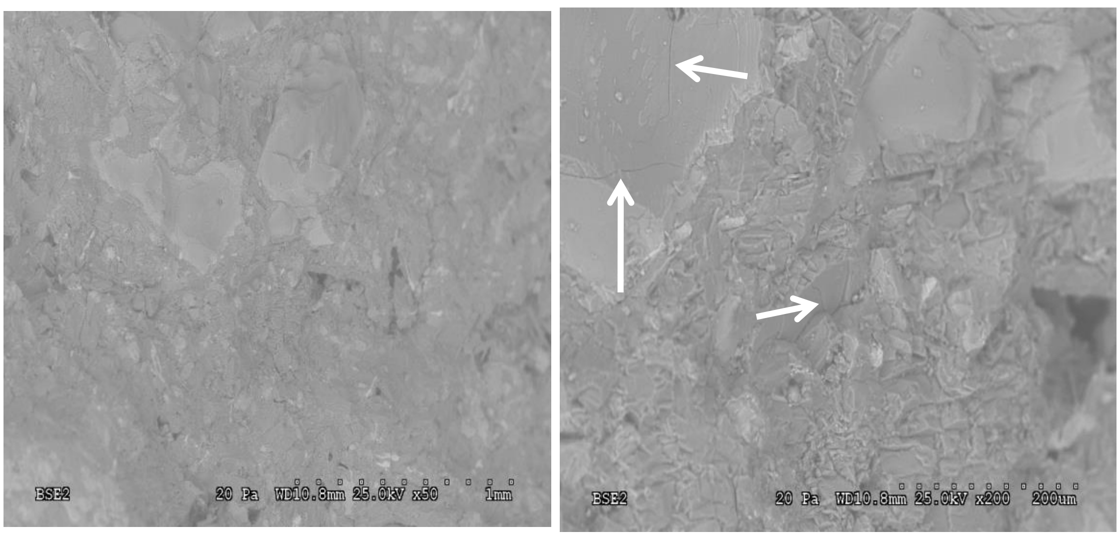

a) b)

Figure 4-17 Scanning electron micrographs of untreated basalt #1 at a) x50 and b) x200 magnification

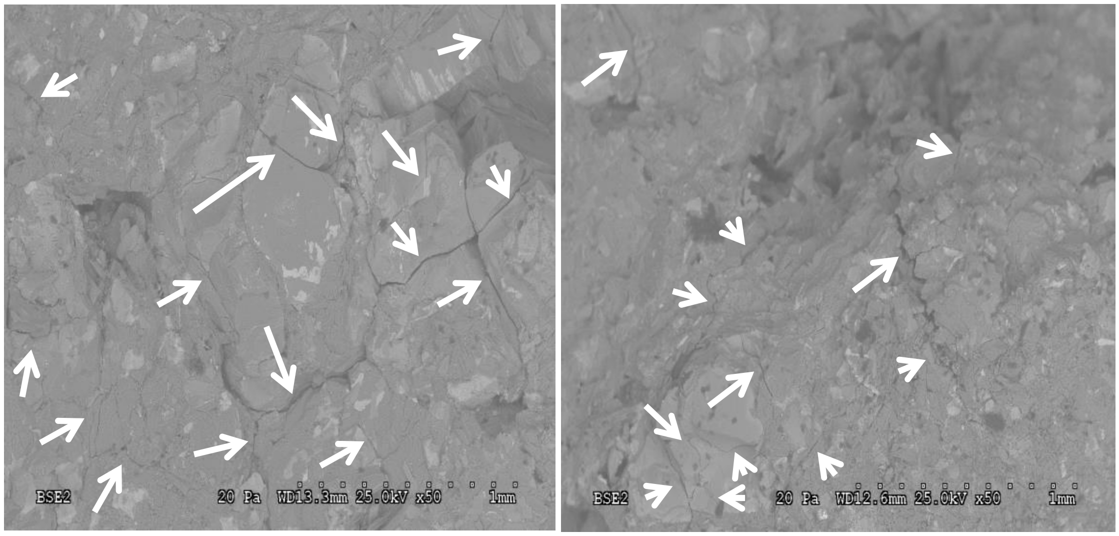

Figure 4-18 Two scanning electron micrographs of basalt #1 exposed to 3 kW microwave energy, x50 magnification

Untreated basalt #1 had a UCS of approximately 230 MPa. Treatment at 1.2 kW power had no effect on UCS up to 120 s exposure time (Figure 4-19a), nor did a power level of 3 kW up to 80 s exposure time (Figure 4-19b). However, the sample burst after being treated for 120 s (Figure 4-19b inset). As the power increases the sample burst earlier when power increases. The UCS was not affected by microwave treatment at 5 kW power for up to 20 s, but specimens burst at 45 s (Figure 4-19c and inset image).

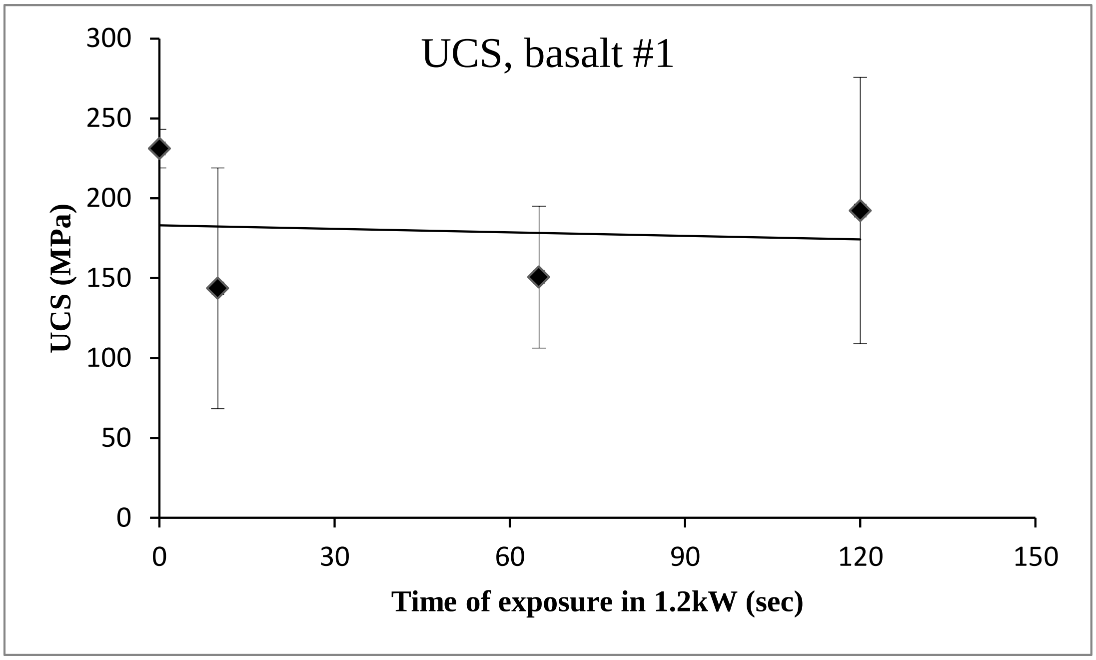
UCS, basalt #1
UCS (MPa)
300
250
200
150
100
50
0
0
30
60
90
120
150
Time of exposure in 1.2kW (sec)

a)

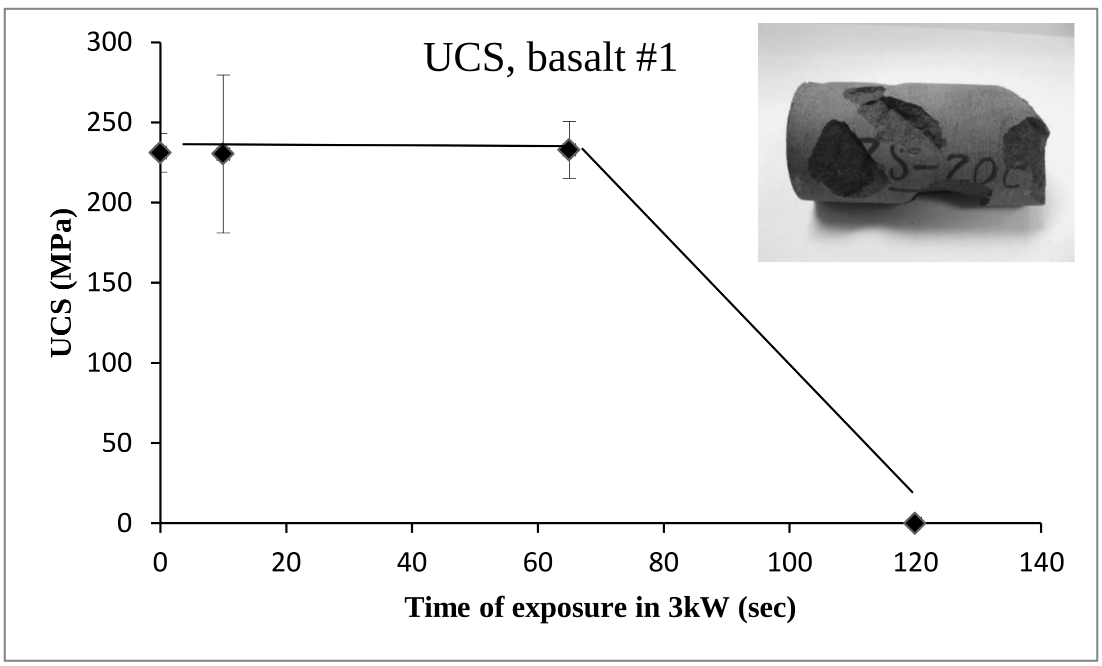
UCS, basalt #1
UCS (MPa)
300
250
200
150
100
50
0
0
20
40
60
80
100
120
140
Time of exposure in 3kW (sec)

b)

c) 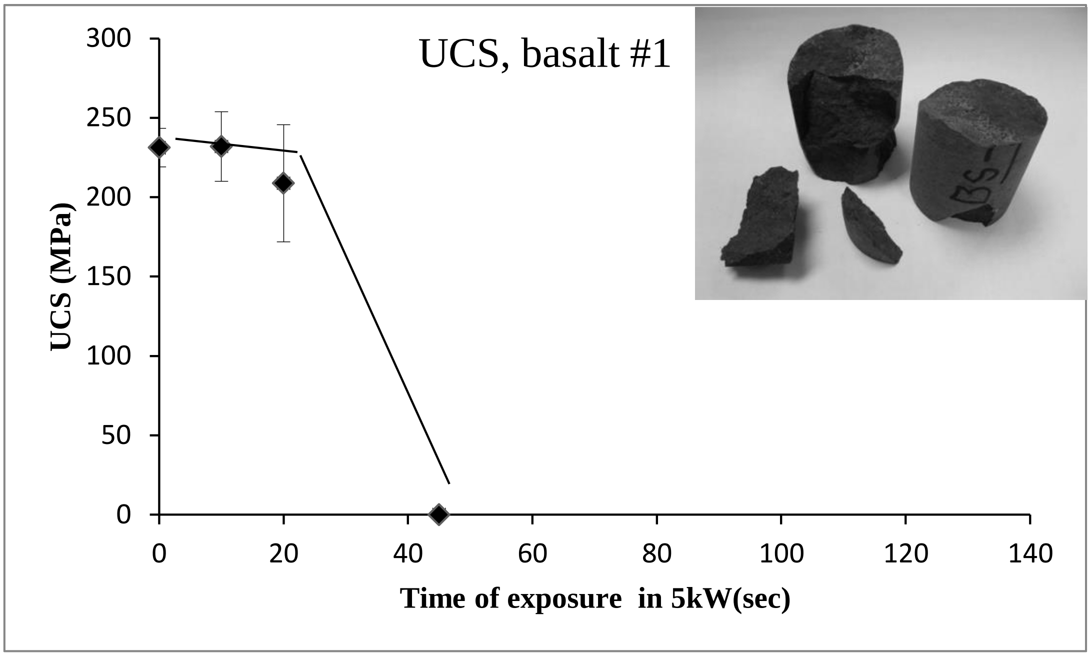

Figure 4-19 Uniaxial compressive strength of basalt #1 treated at a) 1.2 kW, b) 3 kW and c) 5 kW microwave power

Untreated basalt #1 had a CAI of approximately 2.8. The results revealed a significant reduction of tensile strength and a slight reduction in uni-axial compressive strength of the rock samples. Moreover, the longer the specimen is exposed and the higher the microwave power is, the higher the reduction rate of mechanical properties of rocks. The size of the specimen being exposed to microwave energy also influences the heating rate of specimen, hence, the mechanical test results. This is witnessed when the heating rate difference of disc and cylindrical shaped specimens have been observed.

Before performing Brazilian tensile strength test on the disc shape specimens, CEHRCHAR abrassivity test were performed on a flat surface. The CERCHAR abrassivity tests were performed upon it standard explained in earlier chapters. All of the scratches made by the CERCHAR apparatus were made in different directions, from which the average was considered. The CAI was not affected by microwave treatment at

1.2 kW (Figure 4-20a) or 5 kW power (Figure 4-20c). However, a slight reduction in CAI was seen with increasing exposure time at 3 kW power (Figure 4-20b).

Prepared cylindrical and disc shaped specimens of norite sample from Sudbury igneous complex were treated into microwave energy for 10, 65 and 120 seconds at power levels of 1.2, 3 and 5 kW. The disc shape specimens could not be treated in microwave energy of 5 kW more than 35 seconds due to melting. The surface temperature of each specimen was measured with an infrared gun immediately after being irradiated by microwave. The norite contained a significant amount of sulfide and mafic minerals which are considered good absorbers of microwave radiation according to (Chen et al., 1984). This causes high absorption ability due to the good energy dissipation.

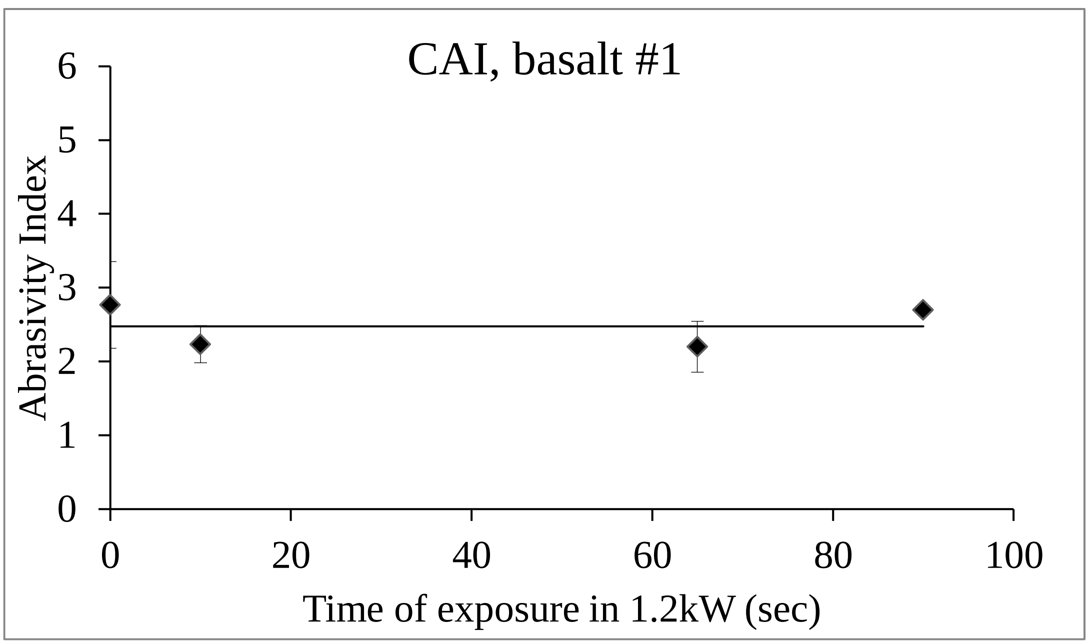

a)

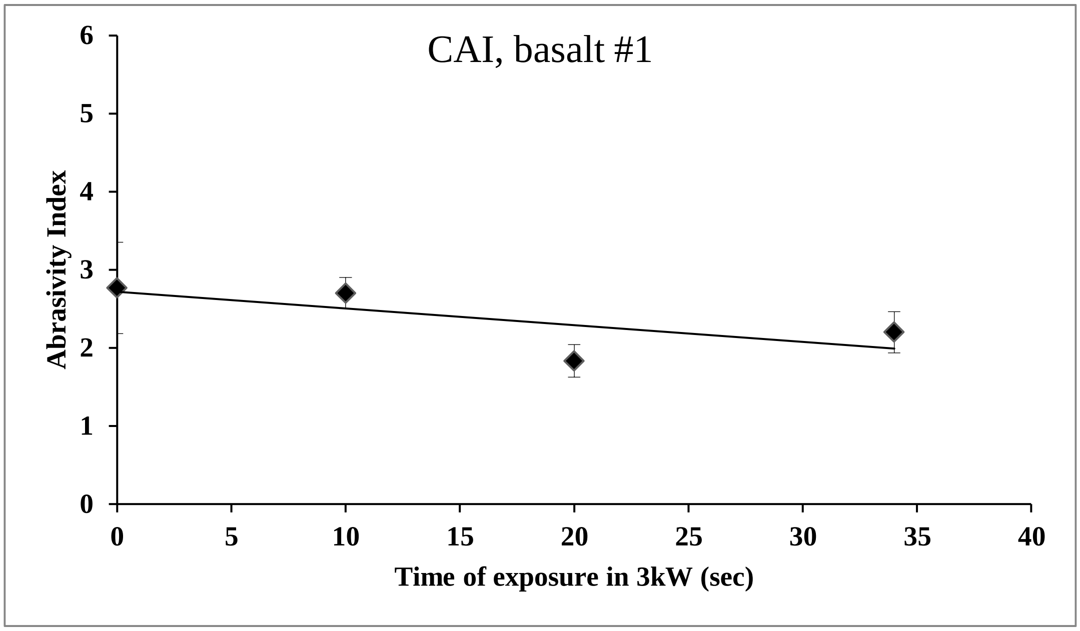

b)

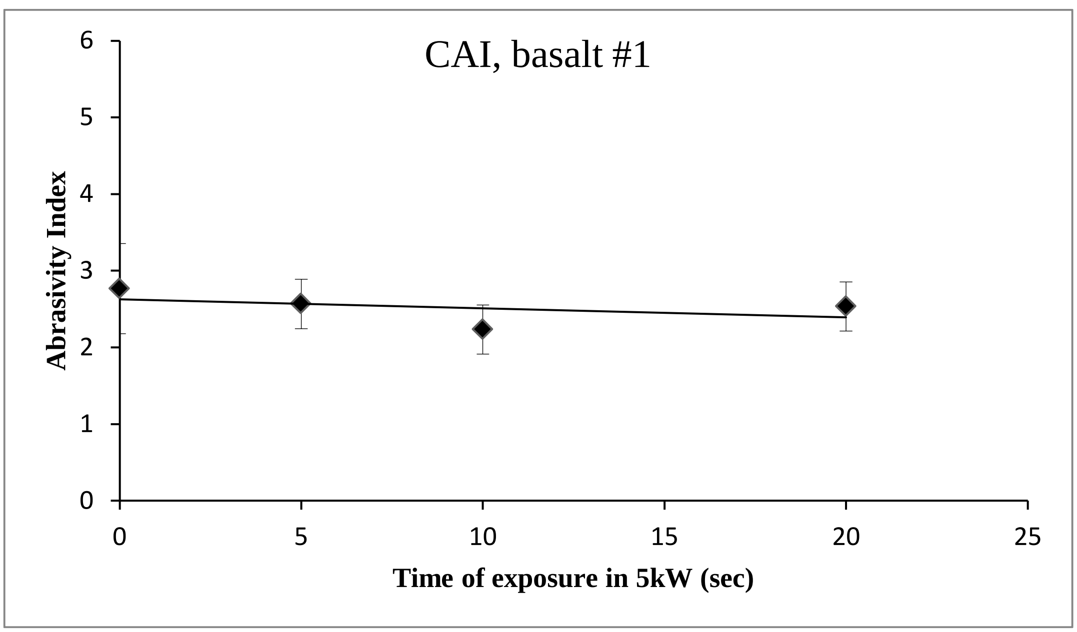

c)

Figure 4-20 CERCHAR abrasiveness index of basalt #1 treated at a) 1.2 kW, b) 3 kW and c) 5 kW microwave power

Considering the multi-mode microwave conditions as a platform of multi-regression analysis, two main controllable parameters or influencing factors are playing a crucial role affecting the rock specimens. Those primary factors are power that varies between 0.8 – 5 kW and exposure time of microwave treatment varying from 10 to 120 seconds.

In order to have a good statistical analysis on the existing data obtained experimentally, a surface response regression is applied using a design of experiment software as an add-ins on Microsoft Excel.

For disc and cylindrical shaped specimens two separate multi-regression analysis has been performed in order to better compare the results. Since CHERCHAR abrassivity index value (CAI) tests are conducted on disc shape specimens, it is considered as a response factor including Brazilian tensile strength (BTS) and temperature. The influencing coefficients of models for both disc and cylindrical shapes are given in Table 4-2.

Table 4-2 Factor coefficients of quadratic models for temperature of discs and cylinders of basalt #1 for CAI, BTS, as well as UCS responses on specimens exposed to microwaves in a multi-mode cavity

Factor	Parameter	Temperature of discs	UCS	Temperature of cylinders	BTS	CAI
Constant		365.34	334.24	188.37	55.548	-12.018
A	Power (W)	172.38	-106.29	188.59	0.22114	-8.079
B	Exposure time (s)	293.15	-237.11	164.17	109.03	-33.322
AB		-301.02	-1014.90	186.78	-0.96929	-19.435
AA		-259.62	-890.64		-163.29	36.719
BB		-11.759	-465.96		66.896	-18.859
AAB		-722.33	-989.47		-402.57	89.357
ABB		-479.85	-935.56		-4.909	-11.128

AABB		-509.19			-243.71	53.187
R^2		0.9722	0.4337	0.9712	0.3282	0.5551

By evaluating the linear regression of coefficients, it is clear that variability was high among the results and a saddle point is given. Hence the results of multi-regression analysis is found to be inconclusive statistically within the confidence level of 0.05. The variability of the results indicates that basalt #1 is not uniformly affected in a multi-mode cavity.

4.3.3 Norite Strength Parameters

The BTS of untreated norite was approximately 15.5 MPa. Mafic norite from the Sudbury igneous complex has large grain structure composed with a fair mixture of quartz and sulfides. Since sulfides are very good absorbers of microwave energy, they get heated quickly and expand relatively fast as well. This phenomenon can be validated from the calcite hosted pyrite samples of (Whittle et al., 2003) (Satish, 2005).

Significant reduction in the decreased with increasing exposure time and power level. At 1.2 kW power, the BTS was approximately 25% lower after 120 s of exposure (Figure 4-21a). At 3 kW power level, this value was 35% (Figure 4-21b). A power level of 5 kW reduced the BTS by more than 50% in only 65 s Figure 4-21c). Discs cracked in the cross section of the radius after 120 s at 3 kW and 30 s at 5 kW. At 65 s of exposure to 5 kW power, the center of the discs turned red (indicative that melting is about to being).

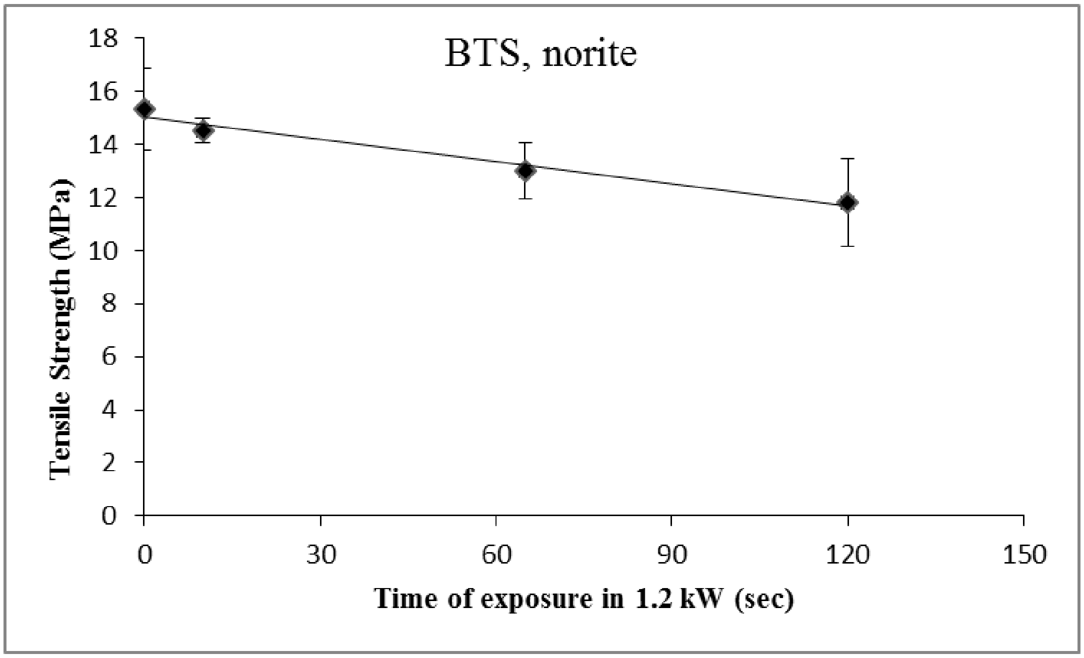
BTS, norite
Tensile Strength (MPa)
Time of exposure in 1.2 kW (sec)
0
2
4
6
8
10
12
14
16
18
0
30
60
90
120
150
a)

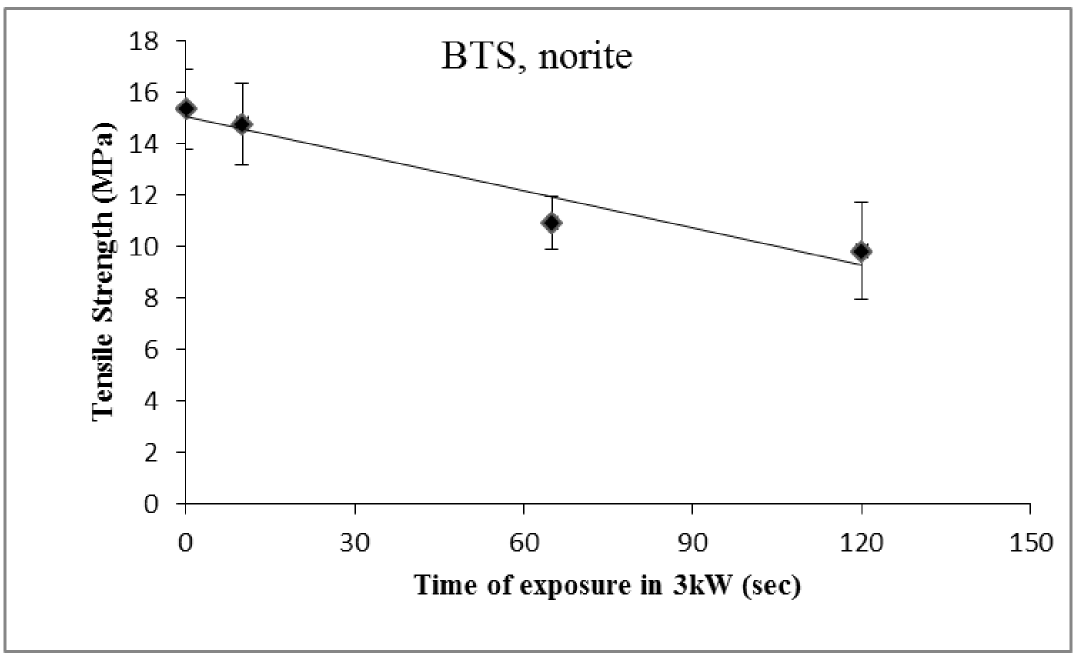
BTS, norite
Tensile Strength (MPa)
Time of exposure in 3kW (sec)
0
2
4
6
8
10
12
14
16
18
0
30
60
90
120
150
b)

c) 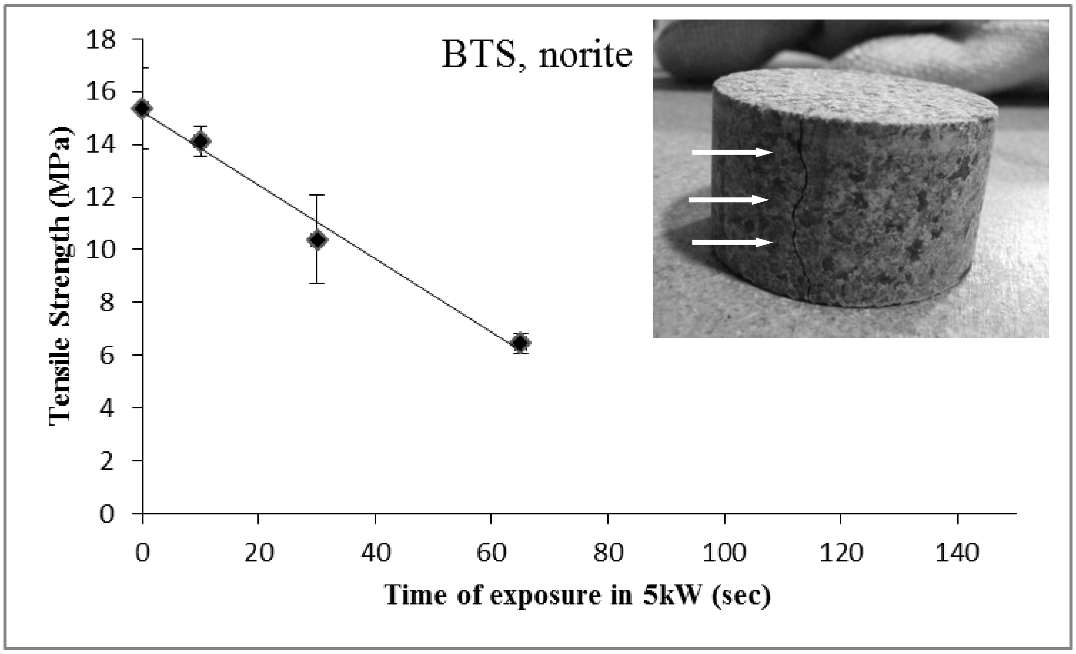

Figure 4-21 Brazilian tensile strength of norite treated at a) 1.2 kW, b) 3 kW and c) 5 kW microwave power

By comparing the power level with the tensile strength values of norite in each exposure time it can be observed that in the first 10 sec the tensile value remain unchanged (Figure 4-22). After 65 and 120 sec of exposure time the tensile strength value of norite reduced significantly more than 30% by increasing power level. Furthermore, it also can be concluded that the reduction of tensile value has a linear relation with the power input as the regression squared of the trends in Figure 4-22 are relatively high.

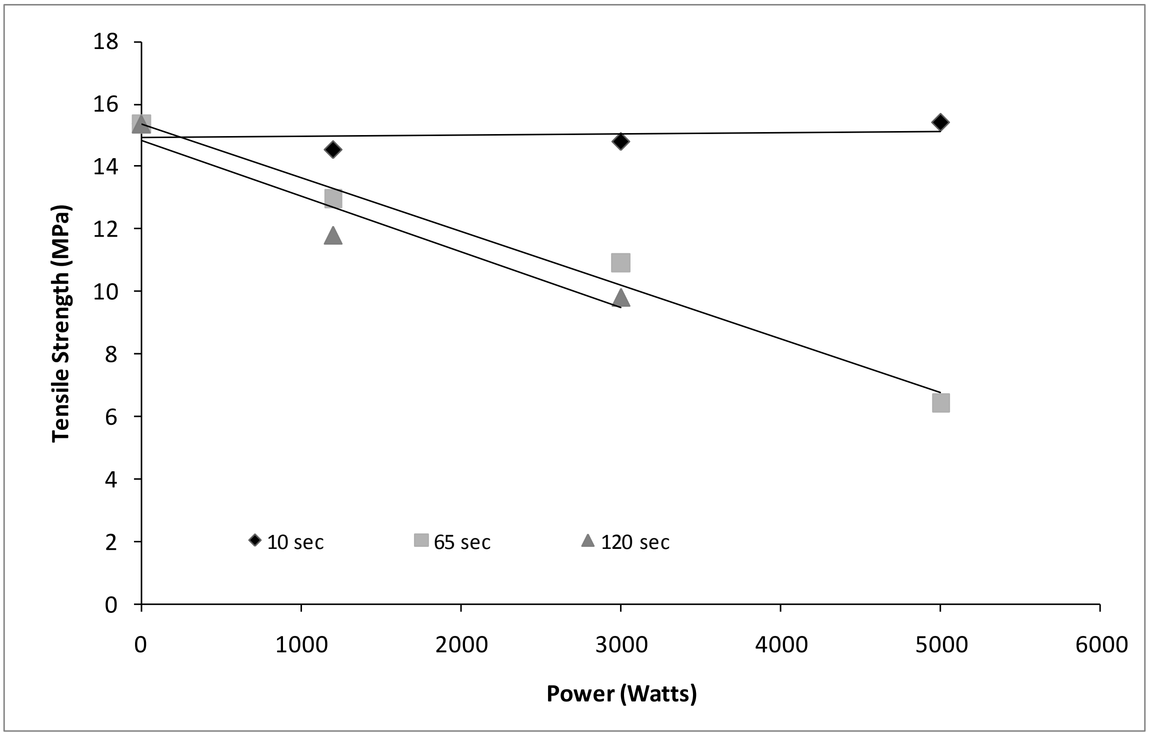

Figure 4-22 Power input of microwave energy versus Brazilian tensile strength value of norite

Where the tensile strength of norite reduces significantly as the power level and exposure time increases, its uniaxial strength remained unchanged in 1.2 and 3 kW of power level. At the 5 kW power level, the uniaxial compressive strength value showed more than a 25% reduction as the exposure time increases. This is demonstrated in Figure 4-23. At lower power microwaves irradiation (1.2 and 3 kW) the uniaxial compressive strength value of norite remains unchanged regardless of the exposure time. At 65 sec of exposure at 5 kW, visual cracks start initiating in cylindrical shaped specimens, which causes the overall uniaxial compressive strength of the sample to be reduced (Figure 4-24). The apparent cracks are basically due to the volumetric expansion of the heated rock, which exceeds the confinement pressure of the actual specimen.

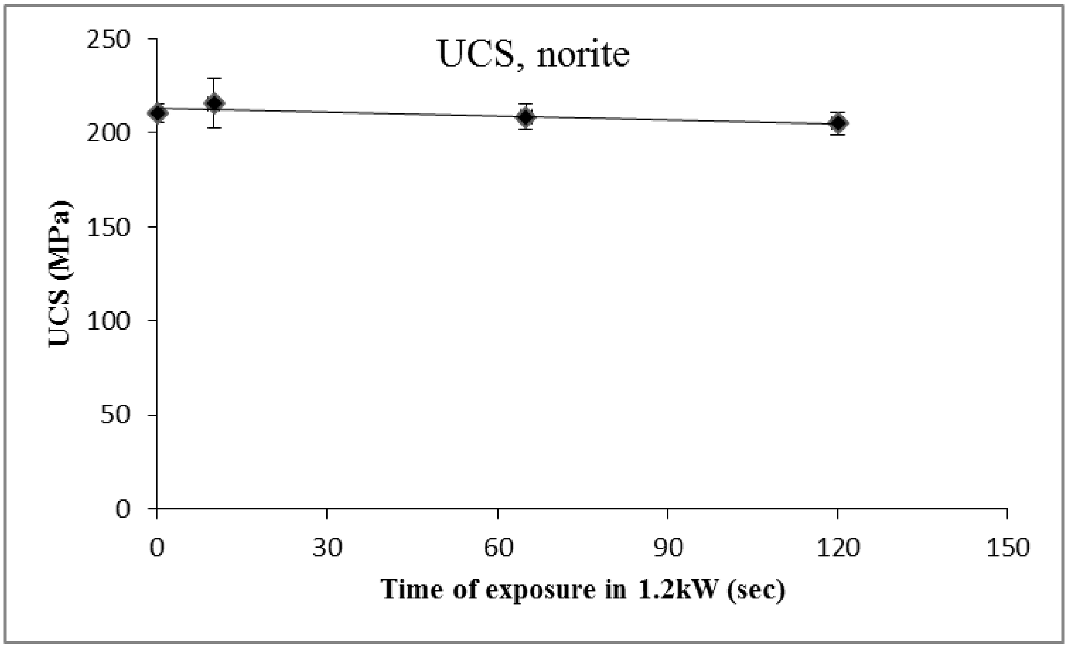

UCS, norite
UCS (MPa)
250
200
150
100
50
0
0
30
60
90
120
150
Time of exposure in 1.2kW (sec)

a)

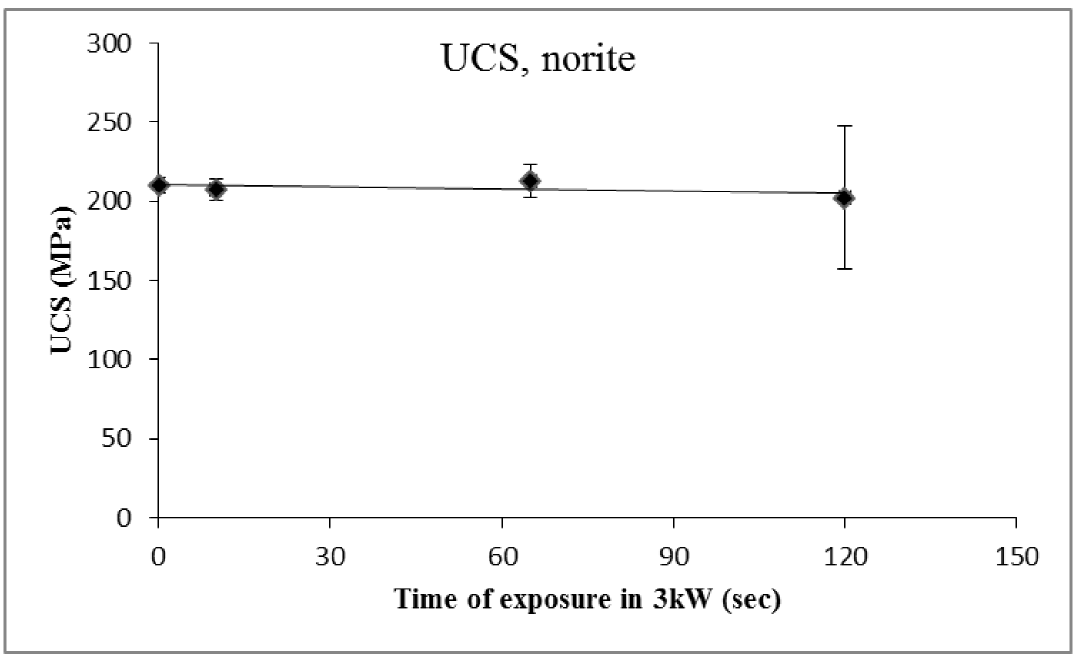

UCS, norite
UCS (MPa)
300
250
200
150
100
50
0
0
30
60
90
120
150
Time of exposure in 3kW (sec)

b)

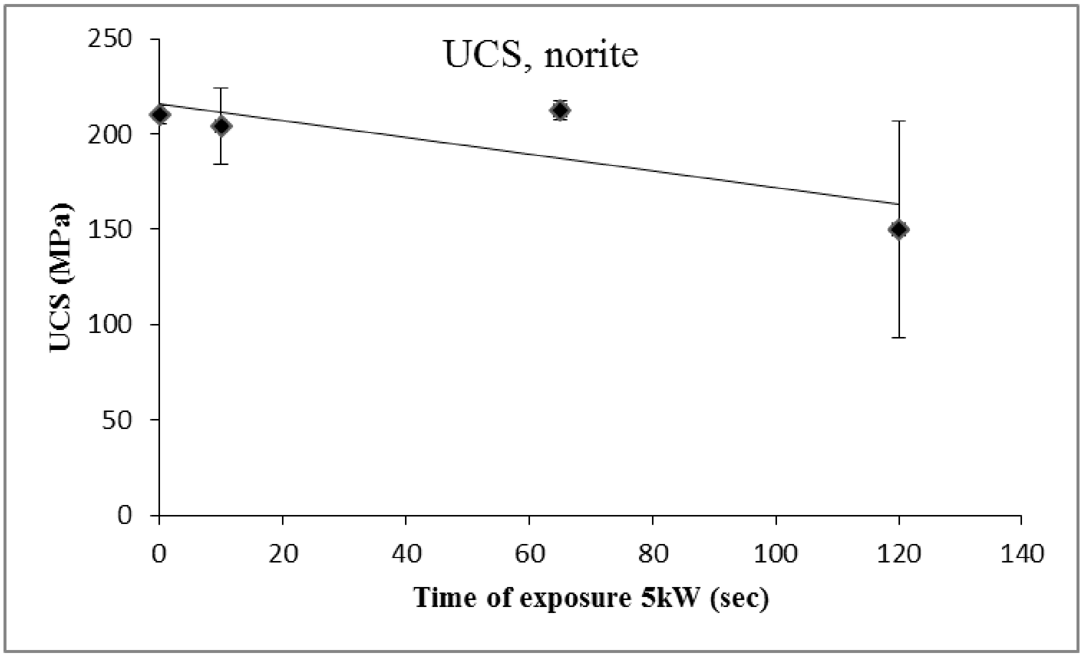

c)

Figure 4-23 Uniaxial compressive strength of norite treated at a) 1.2 kW, b) 3 kW and c) 5 kW microwave power

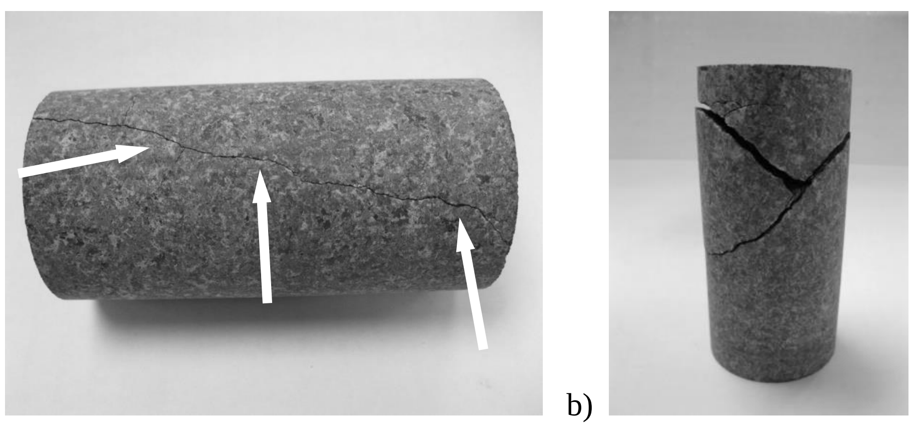

a) b)

Figure 4-24 Norite cylinder cracked at a) 65 s and b) 120 s at 5 kW power

As Figure 4-25 shows, likewise the basalt #1 sample, norite's CERCHAR abrassivity index value remains unchanged regardless of exposure time and power. This in fact reveals that the abrassivity of the rock is not affected by microwave energy emitted. It also understood from the literature that the abrassivity of rocks are directly related to the mineral composition of the rock. Since the microwave energy does not influence nor changes the mineral characteristics, logically the CERCHAR abrassivity index value of the rock is not supposed to change, as observed.

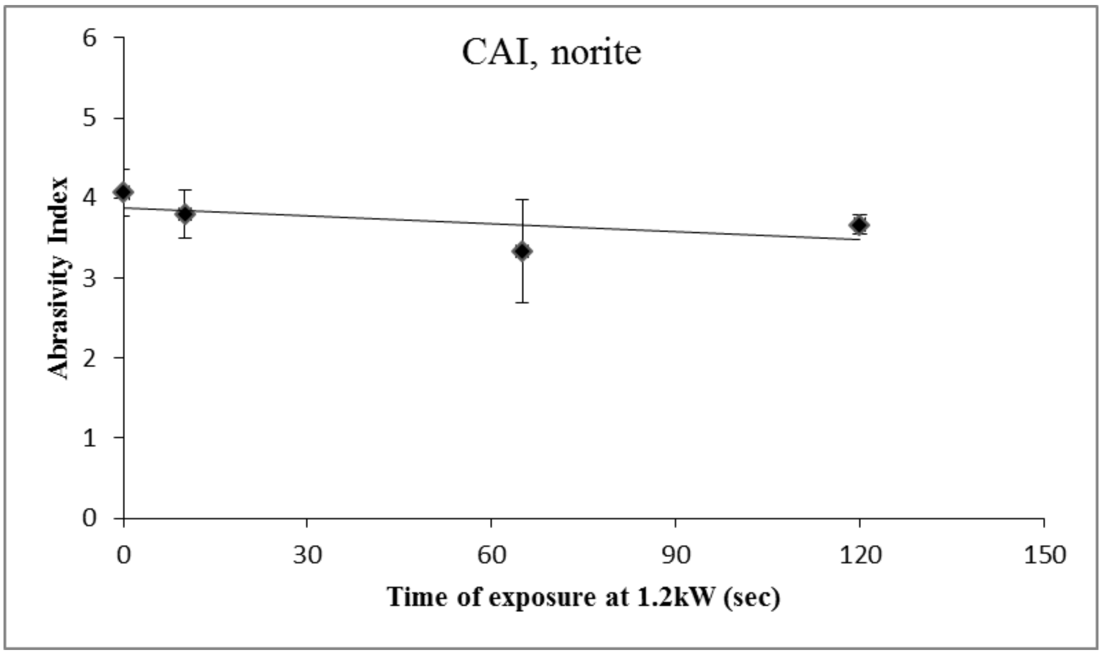

a)

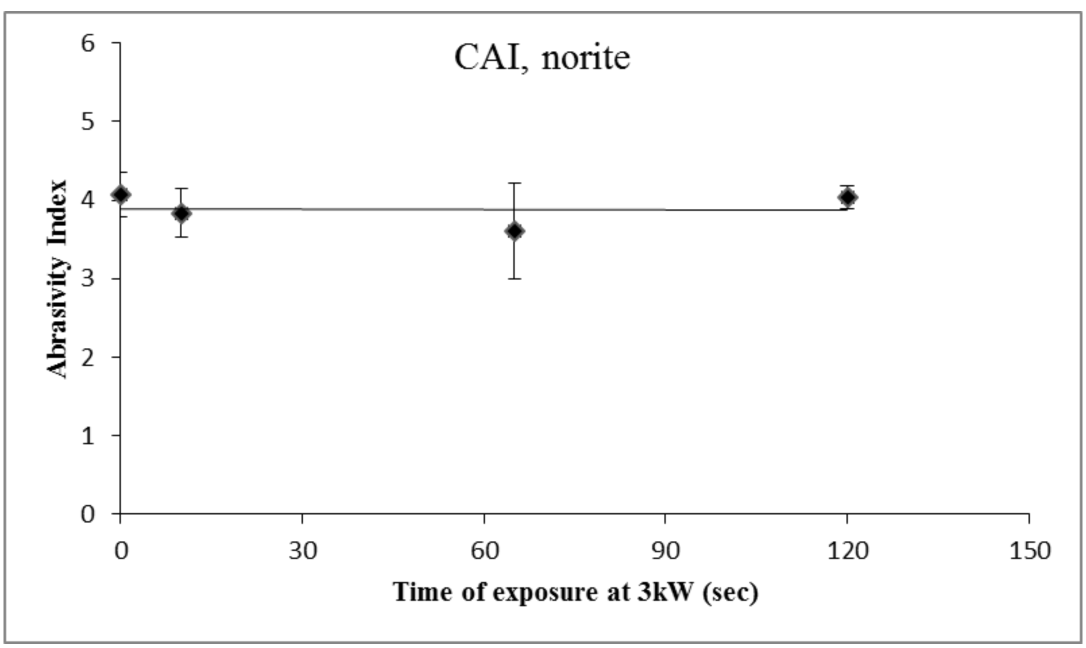

b)

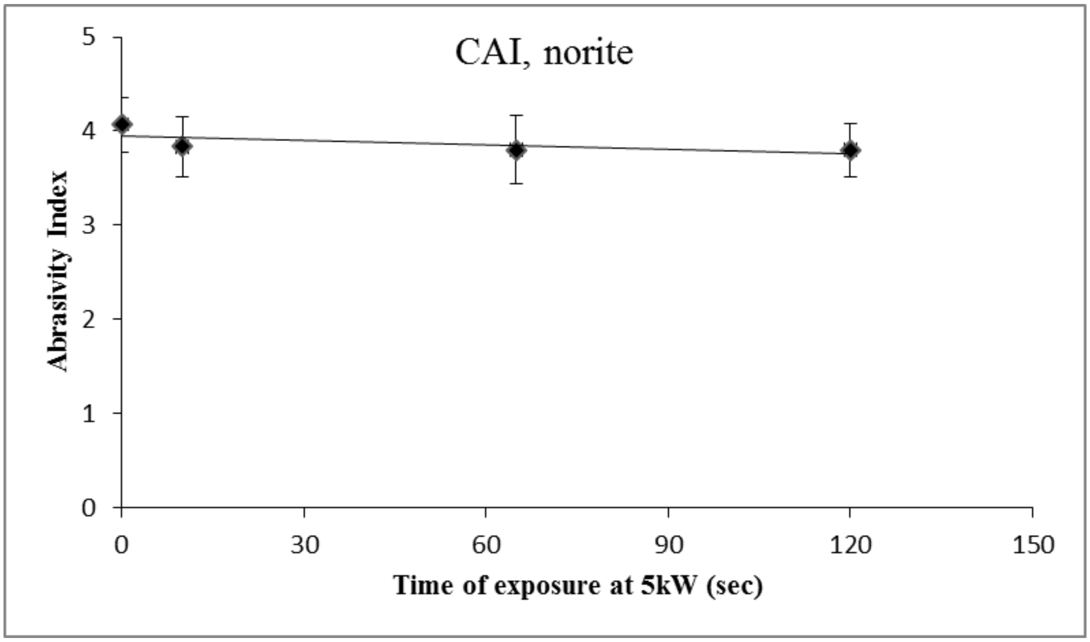

c)

Figure 4-25 CERCHAR abrasiveness index of norite treated at a) 1.2 kW, b) 3 kW and c) 5 kW microwave power

The influencing coefficients of the three surface response regression models are given in Table 4-3 for norite. Considering the multi-mode microwave conditions as a platform of multi-regression analysis for norite sample, two main controllable parameters or influencing factors are playing a crucial role affecting the rock specimens. Those primary factors are power that varies between 0.8 – 5 kW and exposure time of microwave treatment varying from 10 to 120 seconds.

Table 4-3 Factor coefficients of quadratic models for temperature of discs and cylinders of norite for CAI, BTS, as well as UCS responses on specimens exposed to microwaves in a multi-mode cavity

Factor	Parameter	Temperature of discs	CAI	BTS	Temperature of cylinders	UCS
Constant		213.36	3.533	12.428	130.57	211.67
A	Power (W)	104.20	0.33881	-1.792	97.033	3.295
B	Exposure time (s)	157.05	0.01903	-2.476	102.93	-1.237
AB		87.942	0.22472	-1.597	88.998	-3.829
AA		-31.923	-0.07275			-0.32787
BB			0.43045			-2.943
AAB			-0.25344			-17.044
ABB			-0.21709			-15.724
AABB			-0.16902			-23.822
R^2		0.9546	0.2947	0.8434	0.9760	0.4398

By evaluating the linear regression of coefficients it has been understood that variability among the CAI and UCS results were high. Hence the results of multi regression analysis is found to be inconclusive statistically. The BTS, however, shows significant influences of the power, exposure time as well as the interaction between those two. The models for the temperature response in disc and cylindrical shape specimens, as well as for BTS show high regression values. The variability of the results confirms the fact that materials are not uniformly affected in a multi-mode cavity, since there is a chaos of energy distribution in the cavity.

4.3.4 Basalt #2 Strength Parameters

A limited number of basalt #2 discs were treated because discs could not be exposed to the microwave energy for 120 s at 3 kW or more than 35 s at 5 kW power: the high power absorption of the rock caused it to melt (Figure 4-26). Specimens treated at 3 kW cracked at 65 s, and at 5 kW cracked at 25 s. The temperature increased at a much greater rate as the power level increased. For instance, specimens treated for 120 s at 1.2 kW, 65 s at 3 kW, and 35 s at 5 kW reached the same level of temperature (Figure 4-13). The temperature of cylinders increased linearly with increasing exposure time at each power level (Figure 4-13). Cylinders were not exposed for more than 65 s at 5 kW to avoid the risk of melting.

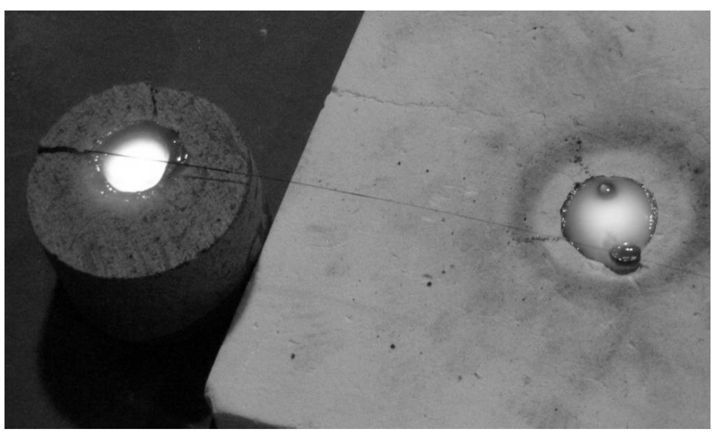

Figure 4-26 Basalt #2 discs melted in 120 s at 3 kW power

The BTS of untreated basalt #2 was 11 MPa. It was observed that a 1.2 kW power level of microwave energy caused a tensile strength reduction of 20% - 30% (Figure 4-27). At higher power levels of microwave irradiation, the specimen melted from the center of the specimen again at 3 kW power when exposed for 120 seconds and at 5 kW power when exposed for 35 seconds. Therefore, no test would be appropriate to be performed on those melted specimen.

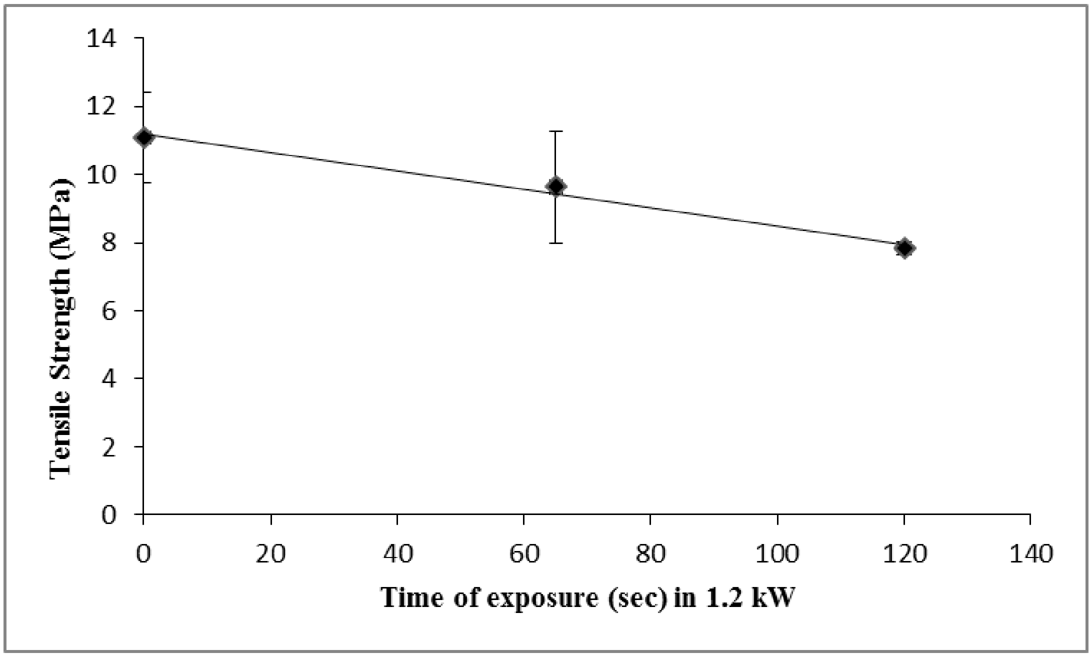

a)

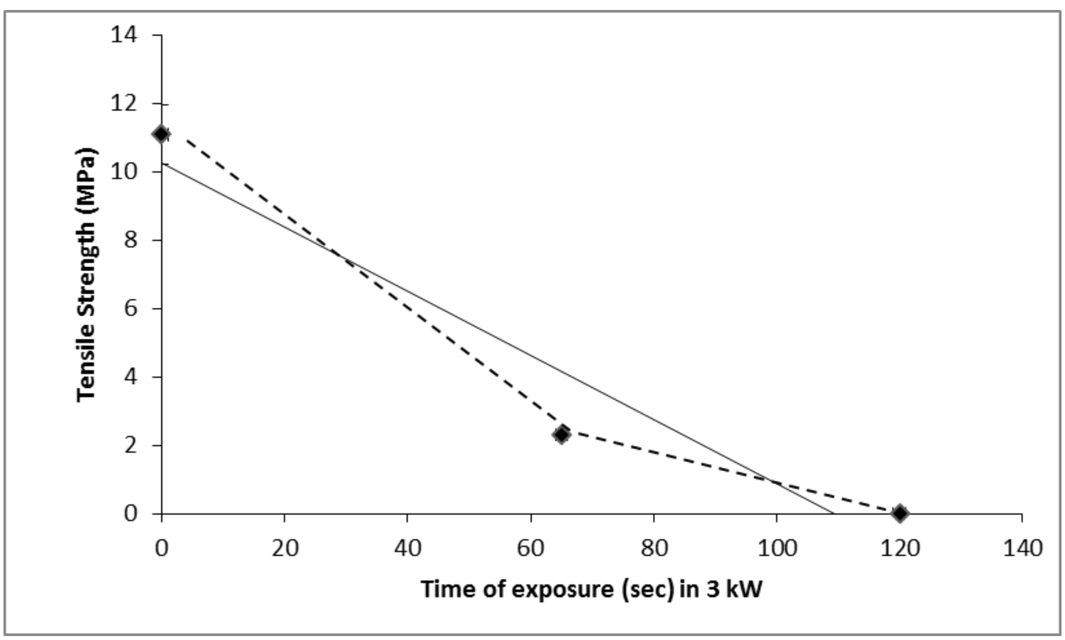

b)

c) 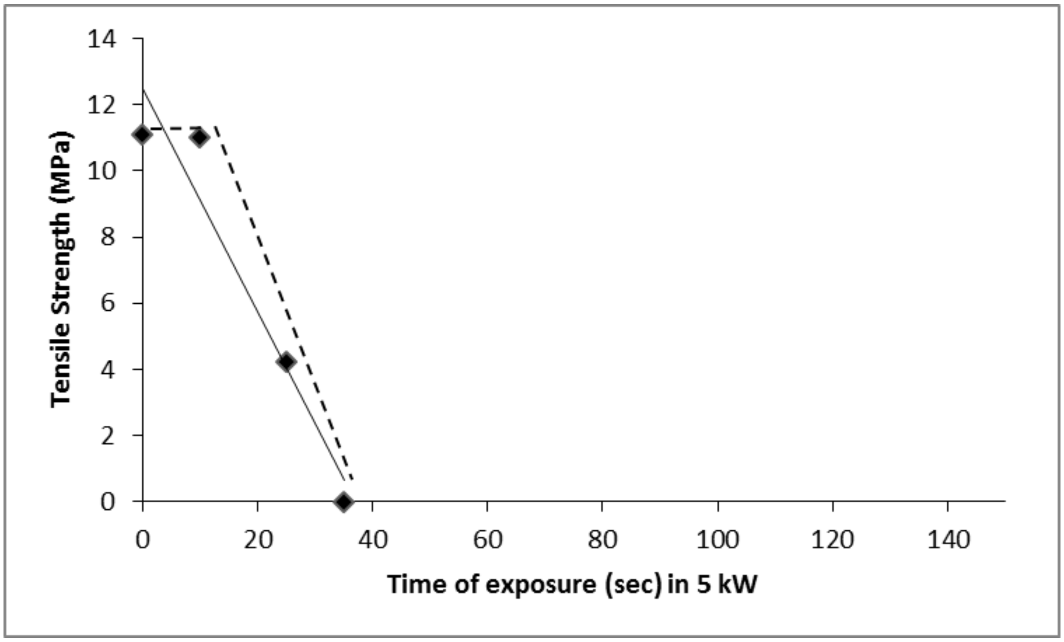

Figure 4-27 Brazilian tensile strength of basalt #2 treated at a) 1.2 kW, b) 3 kW and c) 5 kW microwave power

The influence of microwave energy on the uniaxial compressive strength of a number of cylindrical shaped specimens of basalt #2 sample has been analyzed. The low power microwave input of up to 3 kW had little effect on the uniaxial compressive strength value of specimens at different irradiation time (Figure 4-28a, b)s, whereas a high power microwave input of 5 kW reduced the uniaxial compressive strength values by approximately 30% after 65 seconds of exposure time (Figure 4-28).

a)
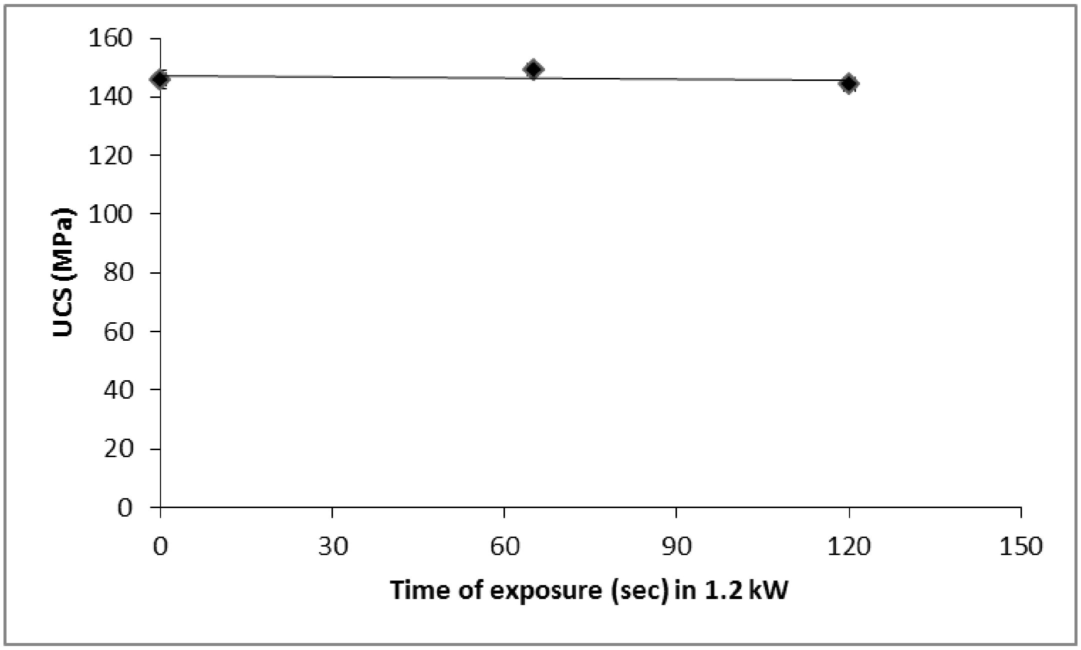

UCS (MPa)
160
140
120
100
80
60
40
20
0
0
30
60
90
120
150
Time of exposure (sec) in 1.2 kW

b)
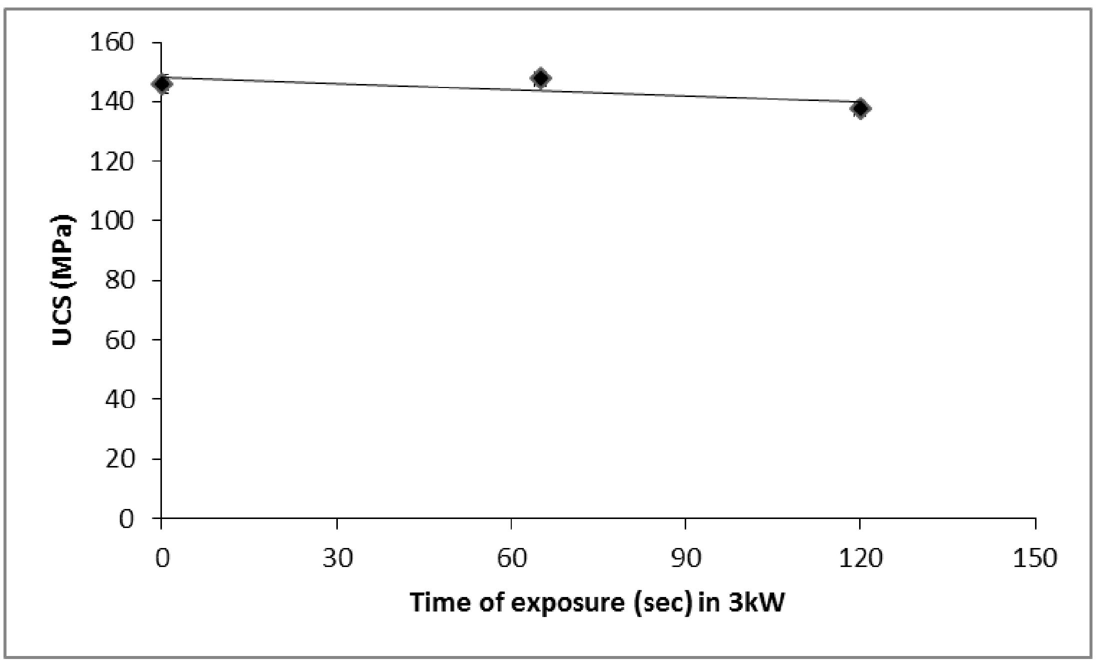

UCS (MPa)
160
140
120
100
80
60
40
20
0
0
30
60
90
120
150
Time of exposure (sec) in 3kW

c) 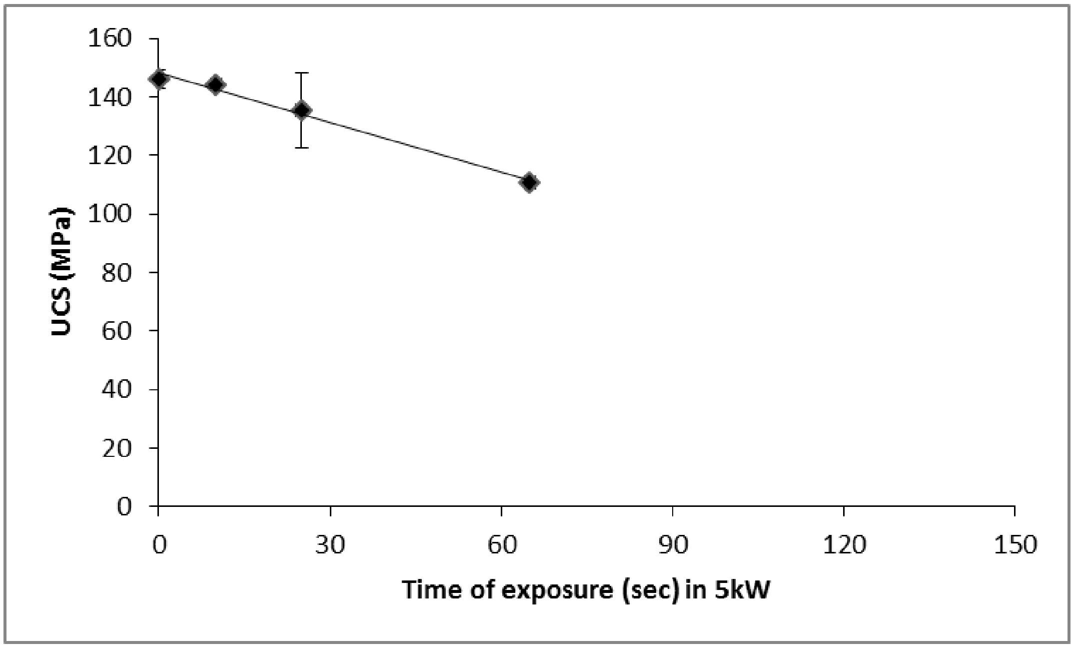

Figure 4-28 Uniaxial compressive strength of basalt #2 treated at a) 1.2 kW, b) 3 kW and c) 5 kW microwave power

By observing the influence of microwave energy on the compressive strength of the sample basalt #2, it is also possible to compare the influence of the power input of microwave energy at each time of exposure. Figure 4-29 demonstrates that the compressive strength of basalt #2 is reduced by increasing the power input of microwave energy. Basically, the higher the power input of microwave energy the more positive (detrimental) influence on mechanical properties of basalt #2, in terms of reducing the strength value.

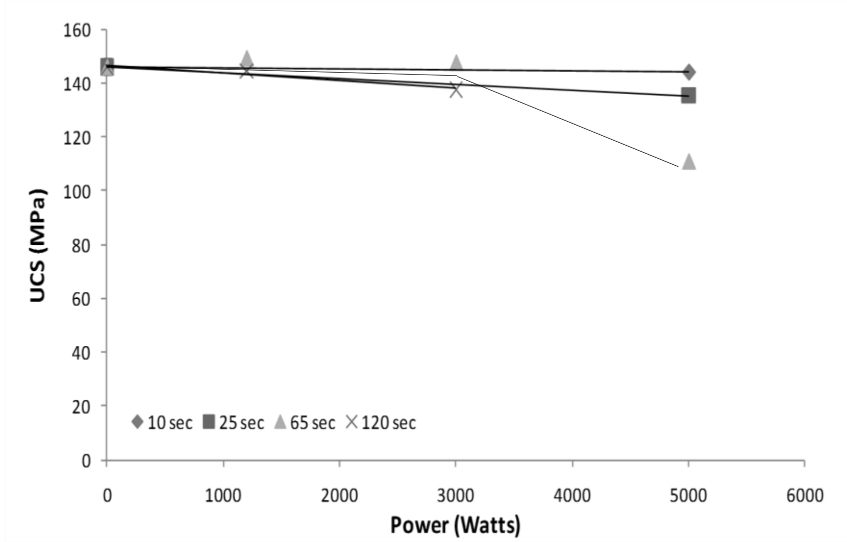

Figure 4-29 Uniaxial compressive strength of basalt #2 versus microwave power level

With reference to the first two samples, the CERCHAR abrassivity index value of this rock sample remain unchanged regardless the exposure time and power (Figure 4-30). This also signify that microwave energy would not have any effect on the surface abrassivity of subjected rocks exposed to microwave energy.

a) 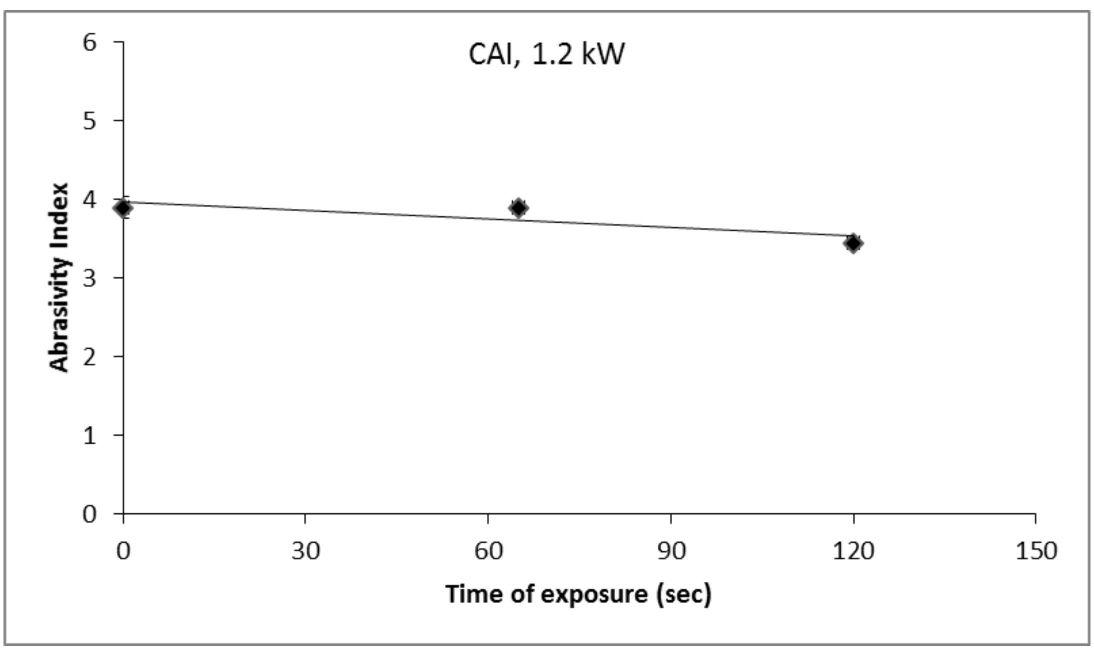

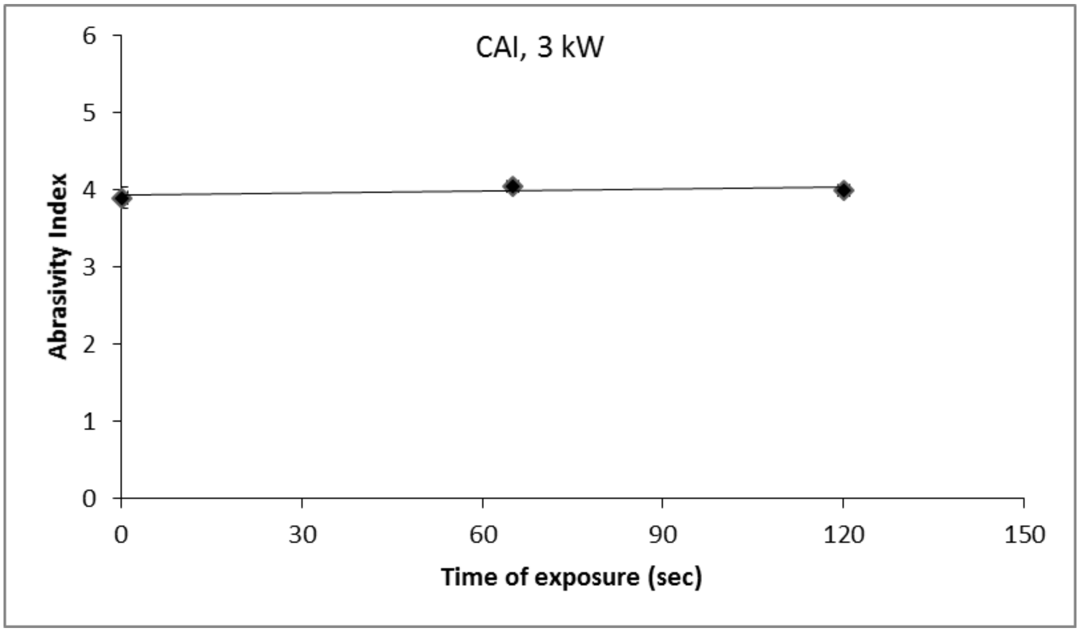

b)

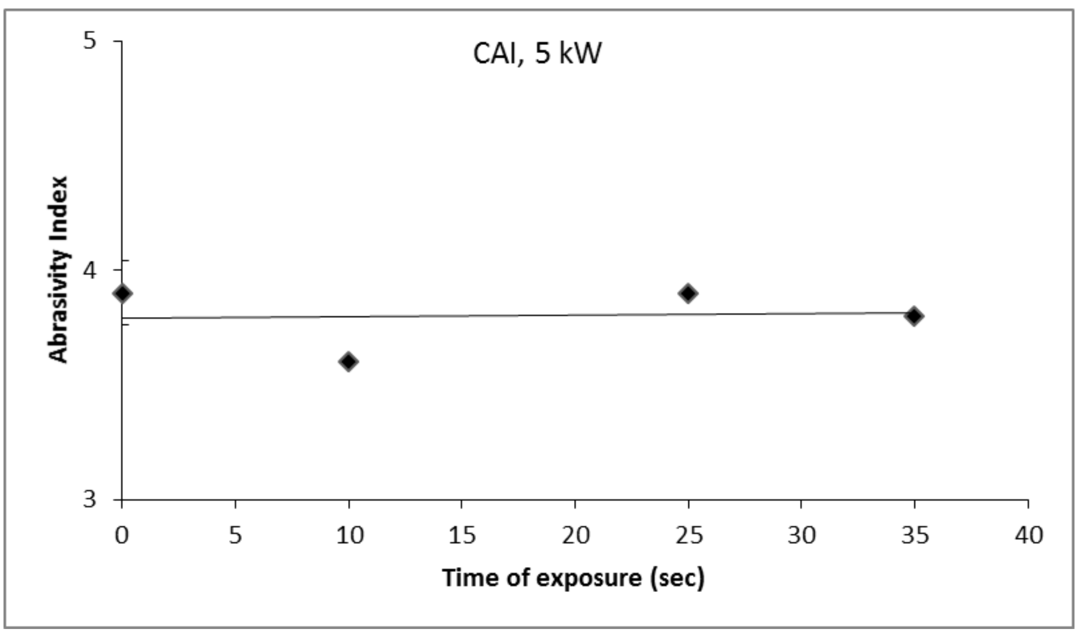

c)

Figure 4-30 CERCHAR abrasiveness index of basalt #2 treated at a) 1.2 kW, b) 3 kW and c) 5 kW microwave power

4.3.5 Granite Strength Parameters

Granite consists of high amount of silica minerals which previous researchers have found to be transparent to the microwave energy (Chen et al., 1984). This caused the generation of numerous sparks within the microwave cavity due to the fact that granite has very low absorption ability and acted as if there was no load in the microwave cavity; hence, granites temperature will not increase significantly.

After treating cylindrical and disc shaped specimens in microwave energy for predefined exposure times and power levels, uniaxial compressive and tensile strength test were conducted. The temperature increased approximately linearly with power level and exposure time for discs and cylinders. The temperature of discs increased much faster and higher compared to cylindrical specimens due to the volume of specimens. The bigger the load, the longer it takes for the energy to dissipate within the load; thus, the temperature of a cylinder is low relative to a disc at the same exposure time and power level. In other words, since the volume of the specimen is larger, more energy is required to rise the specimen’s temperature.

The BTS of untreated granite was 10.5 MPa. It has been observed that the microwave energy has no effect on tensile strength value of granite in 1.2 kW and 3 kW power level. However, higher power level (5 kW) shows significant reduction in tensile strength value after 120 seconds of microwave irradiation (Figure 4-31). This is also due to the final temperature of the specimen which hits about 350°C. At 450 degree Celsius temperature quartz reaches its max volume of expansion. The tensile strength of granite is reduced more than 20% in high power level after two minutes (Figure 4-31); therefore, it can be concluded that the higher the power level the more reduction on tensile strength of granite.

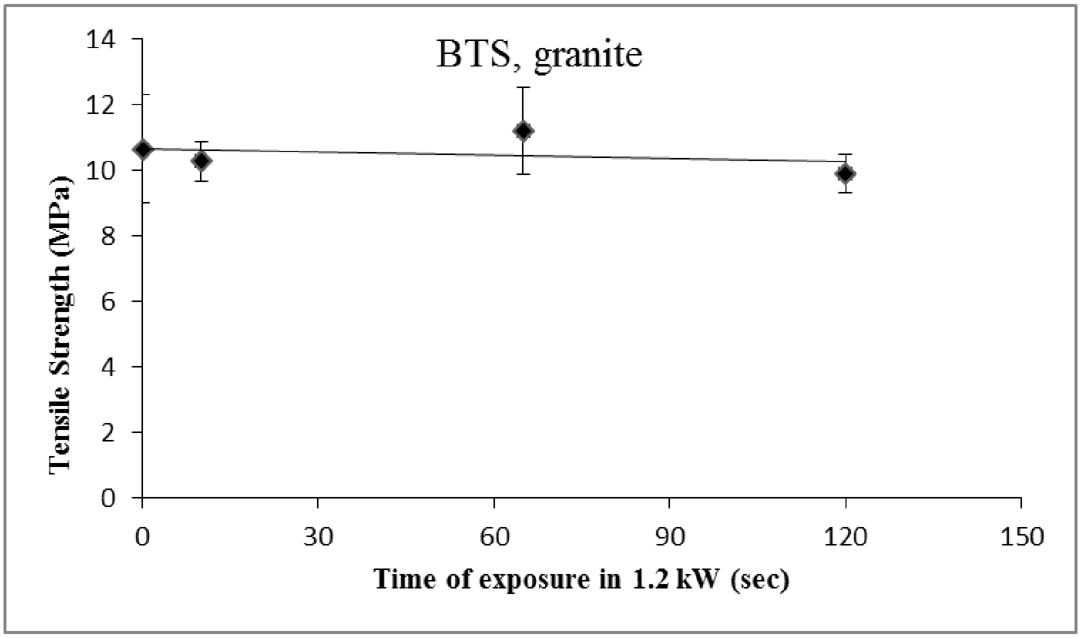
BTS, granite
Tensile Strength (MPa)
14
12
10
8
6
4
2
0
0
30
60
90
120
150
Time of exposure in 1.2 kW (sec)

a)

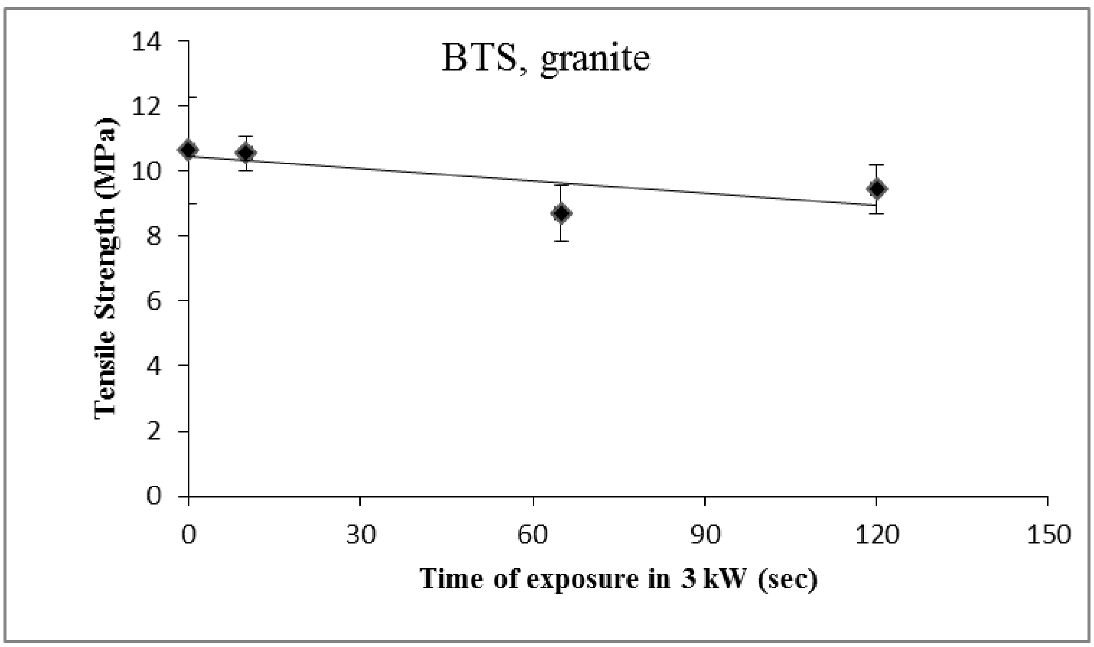
BTS, granite
Tensile Strength (MPa)
14
12
10
8
6
4
2
0
0
30
60
90
120
150
Time of exposure in 3 kW (sec)

b)

c) 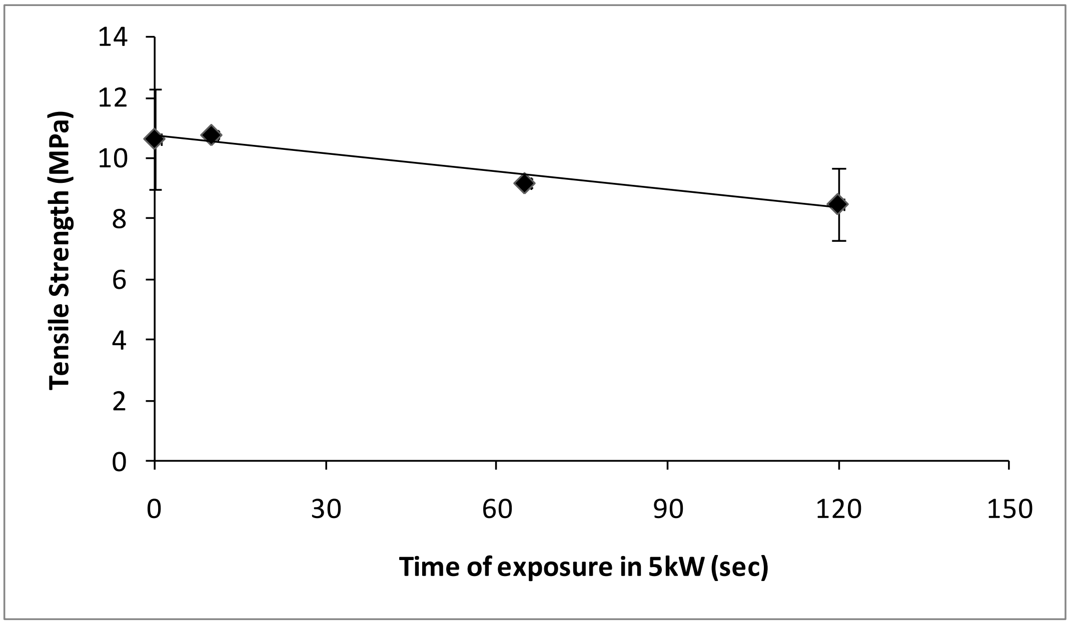

Figure 4-31 Brazilian tensile strength of granite treated at a) 1.2 kW, b) 3 kW and c) 5 kW microwave power

The UCS of untreated granite was approximately 175 MPa. Cylindrical specimens are larger than disc shape specimens. Since granite consist a large amount of quartz (silica mineral), which is one of the transparent minerals to microwave energy, and power absorption density of granite is relatively very low. It is observed from Figure 4-32 that Granite cylinders only reached approximately 200°C after 120 s of microwave irradiation in 5 kW power at which that temperature wouldn’t be enough to induce major physical influence on granite. Therefore, the UCS of granite remained unchanged at all tested power levels and exposure times (Figure 4-32). Since granite contains a large amount of quartz, which is transparent to microwave energy, the power absorption density is very low.

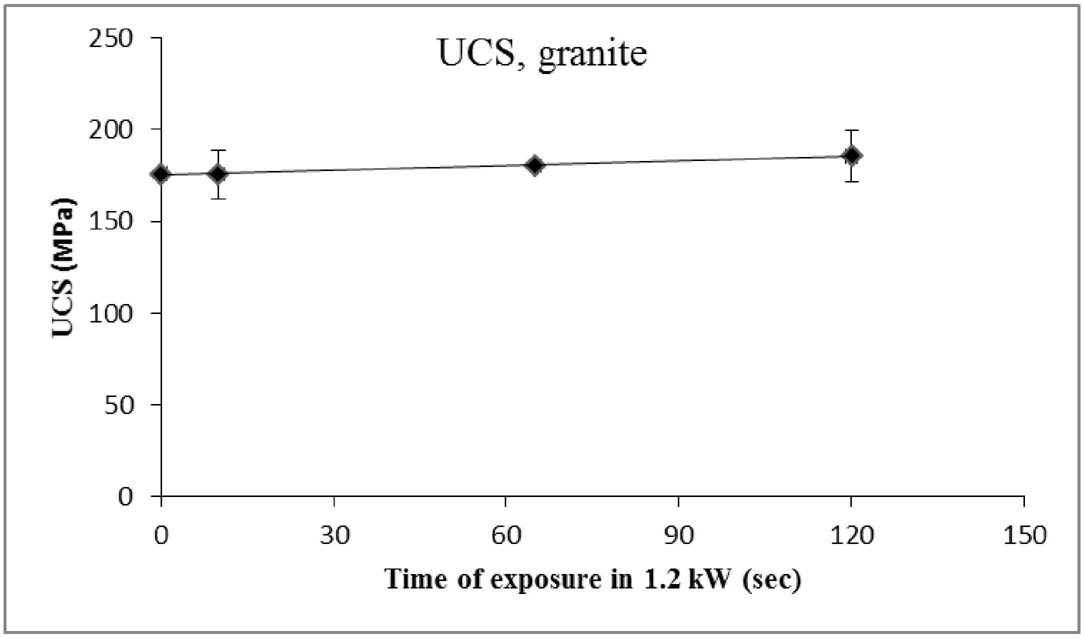
UCS, granite
UCS (MPa)
250
200
150
100
50
0
0
30
60
90
120
150
Time of exposure in 1.2 kW (sec)

a)

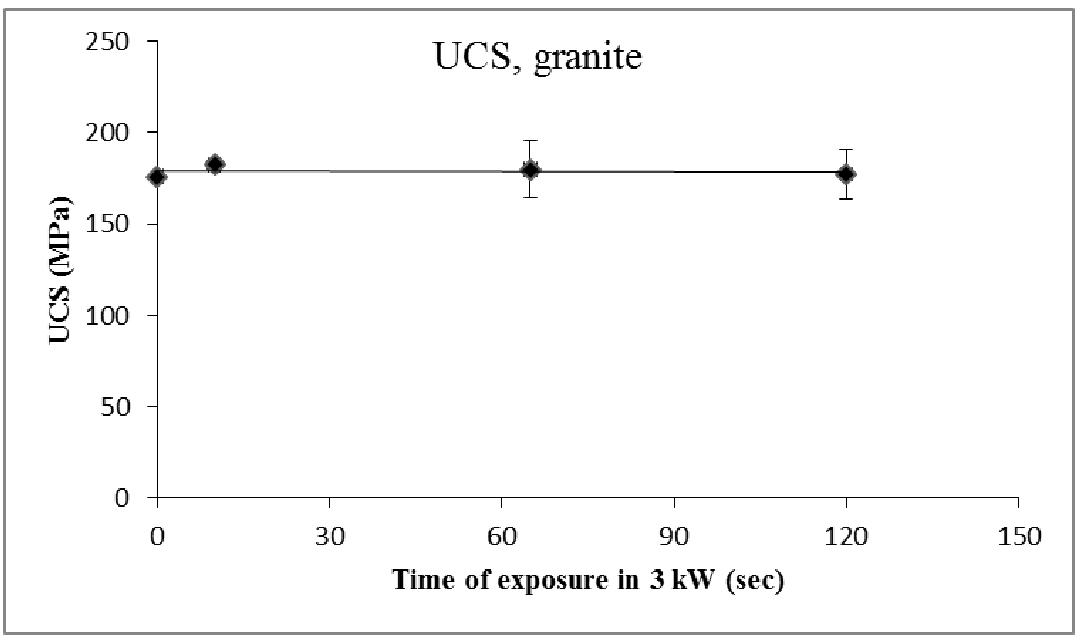
UCS, granite
UCS (MPa)
250
200
150
100
50
0
0
30
60
90
120
150
Time of exposure in 3 kW (sec)

b)

c) 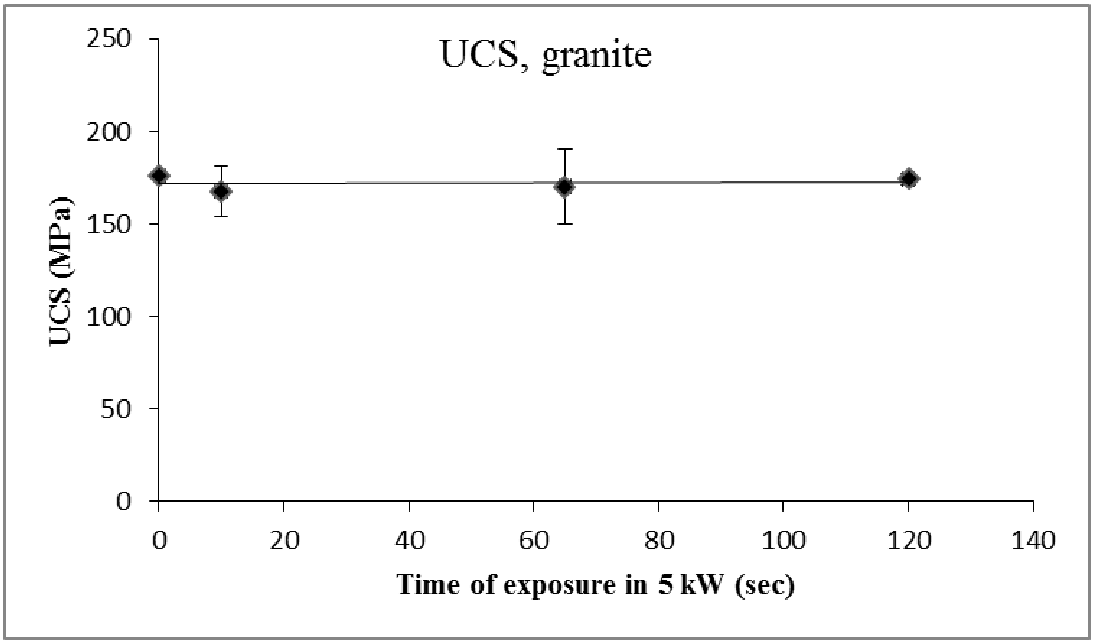

Figure 4-32 Uniaxial compressive strength of granite treated at a) 1.2 kW, b) 3 kW and c) 5 kW microwave power

Similarly, the CAI value of granite did not differ from the untreated value of 3.75, regardless of power level and exposure time (Figure 4-33). In fact, quartz, the most abrasive natural mineral, makes up a significant proportion of the minerals in the granite sample (70 %). Furthermore, quartz is the most transparent natural mineral to microwaves.

a)
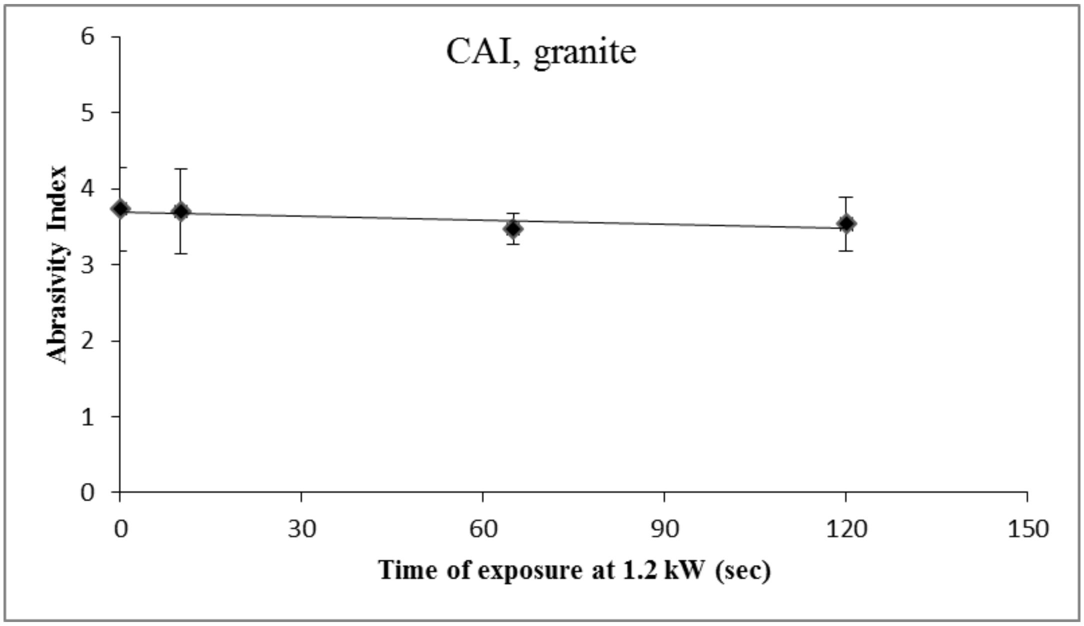
CAI, granite
Abrasivity Index
0
1
2
3
4
5
6
0
30
60
90
120
150
Time of exposure at 1.2 kW (sec)

b)
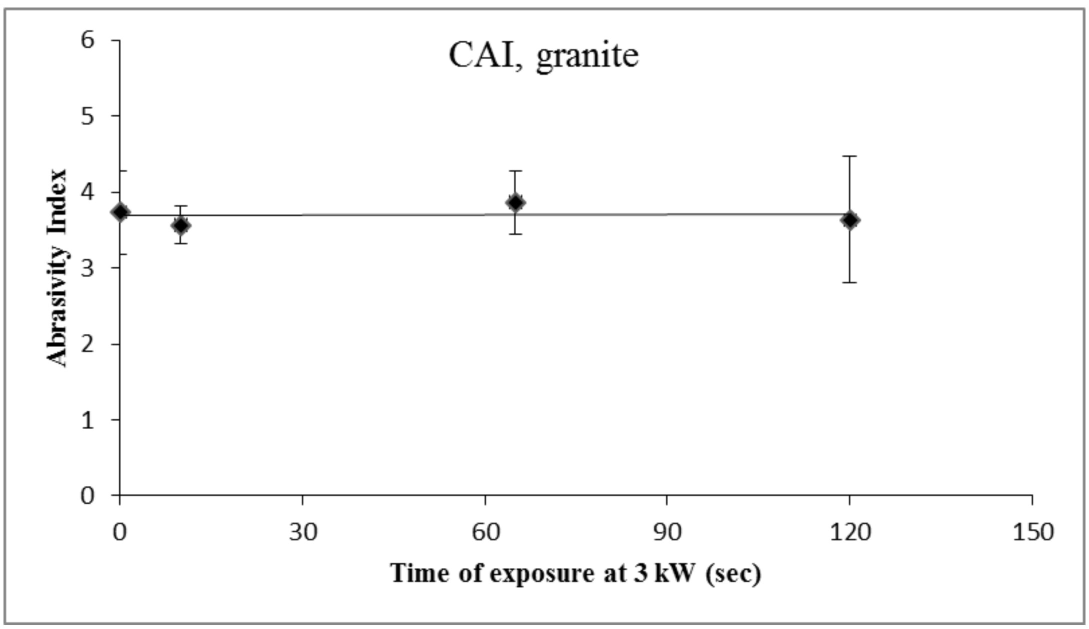
CAI, granite
Abrasivity Index
0
1
2
3
4
5
6
0
30
60
90
120
150
Time of exposure at 3 kW (sec)

c)

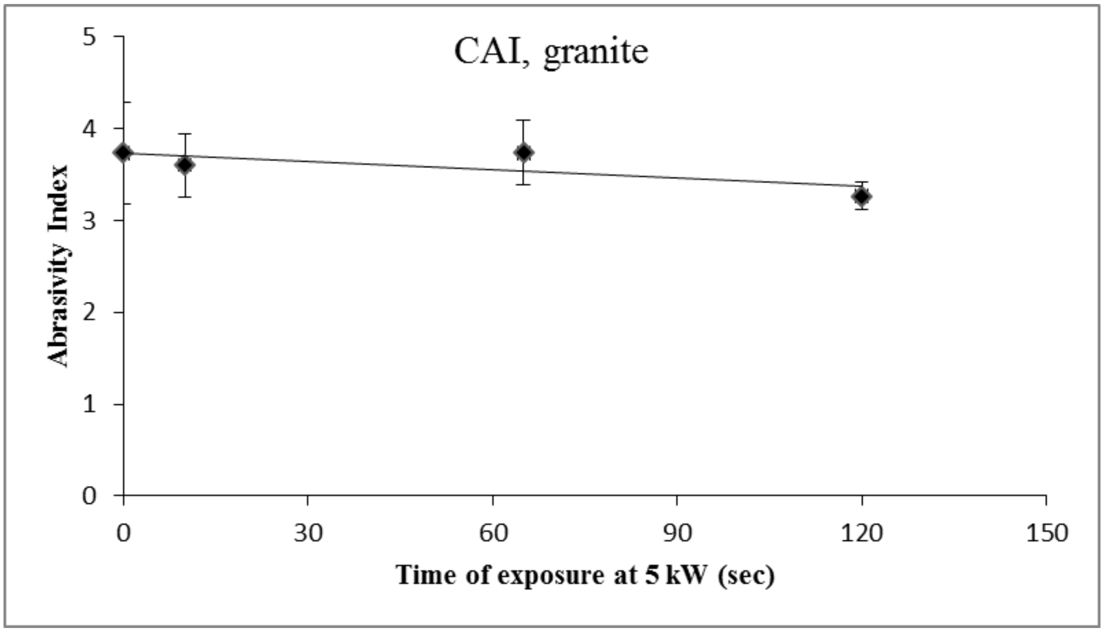

Figure 4-33 CERCHAR abrasiveness index of granite treated at a) 1.2 kW, b) 3 kW and c) 5 kW microwave power

The influencing coefficients of the three surface response regression models are given in Table 4-4 for granite.

Table 4-4 Factor coefficients of quadratic models for temperature of discs and cylinders of granite for CAI, BTS, as well as UCS responses on specimens exposed to microwaves in a multi-mode cavity

Factor	Parameter	Temperature of discs	CAI	BTS	Temperature of cylinders	UCS
Constant		99.343	3.790	9.795	59.365	182.06
A	Power (W)	91.293	0.35682	-1.634	42.534	-0.23205
B	Exposure time (s)	73.697	0.04001	-0.58560	39.135	-0.46565

AB		83.117	0.08160	-0.86664	44.276	-3.333
AA			-0.39571	0.65260		-12.040
BB			-0.17953	0.06956		-2.413
AAB			-0.23193			6.883
ABB			-0.41368	1.251		-6.522
AABB			0.21804			10.382
R^2		0.9671	0.1517	0.5008	0.9552	0.2200

By evaluating the linear regression of coefficients it has been understood that variability among all parameters are high. Hence the results of multi regression analysis is found to be inconclusive statistically. The temperature, however, shows significant influences of the power, exposure time as well as the interaction between those two. The models for the temperature response in disc and cylindrical shape specimens show high regression values but not for the remaining parameters. The variability of the results confirms the fact that materials are not uniformly affected in a multi-mode cavity, since there is a chaos of energy distribution in the cavity.

4.3.6 Tunnel Advancement Prediction

The BTS and UCS are the most important parameters affecting the performance of a TBM tunneling in hard rocks (equations 22 and 23). By reducing either type of strength, the TBM performance can be increased. The CAI value can also predict disc cutter life. In addition, micro- or macro-cracks play a significant role in predicting the TBM penetration rate.

Regardless of all influencing parameters predicting the penetration rate of a TBM, the results obtained from this research have been implemented in mentioned equations and observed the penetration rate results in Figure 4-34 for granite, Figure 4-35 for basalt #1, Figure 4-36 for basalt #2 and Figure 4-37 for norite samples.

Although some variations of the results are observed in the Brazilian tensile strength results of granite, the penetration rate prediction (considering only the BTS or the UCS values) shows no improvement nor decline (Figure 4-34). Figure 4-35 demonstrates the penetration rate prediction using only the BTS or the UCS values individually of basalt #1. The prediction shows improvement in penetration rate based on the BTS values but no improvement based on the UCS values of the rock sample. Moreover, the penetration rate improves at higher power level based on the BTS values. Figure 4-36 shows the penetration rate prediction of a TBM based on the BTS or the UCS values of basalt #2 individually. Since limited amount of basalt #2 were available, the BTS nor the UCS values were tests at 1.2 kW nor 3 kW for 10 seconds; however, the prediction rate shows significant increase over 3 kW power on the disc shaped and at 5 kW on the cylindrical shaped specimens treated. Figure 4-37 shows the penetration rate prediction of norite based on the BTS or the UCS individually. Norite shows reduction in strength or increase in penetration rate prediction at 5 kW power.

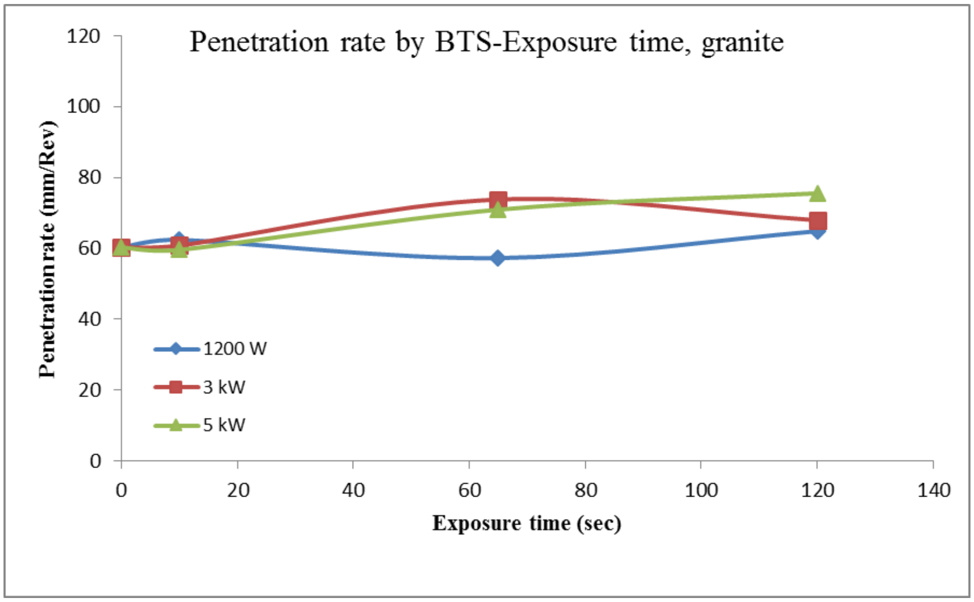

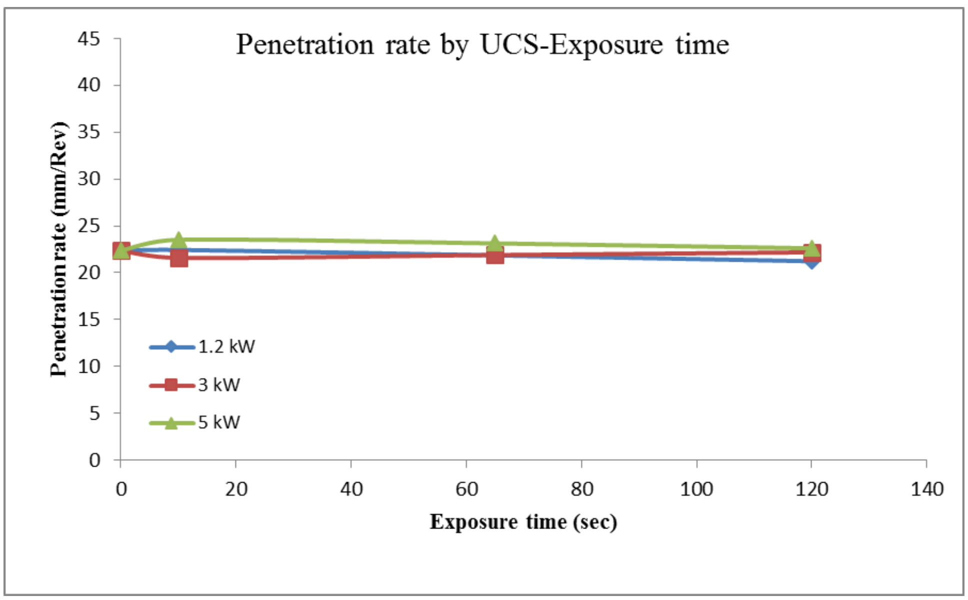

Figure 4-34 Predicted penetration rate of a TBM into granite based on a) Brazilian tensile strength and b) uniaxial compressive strength

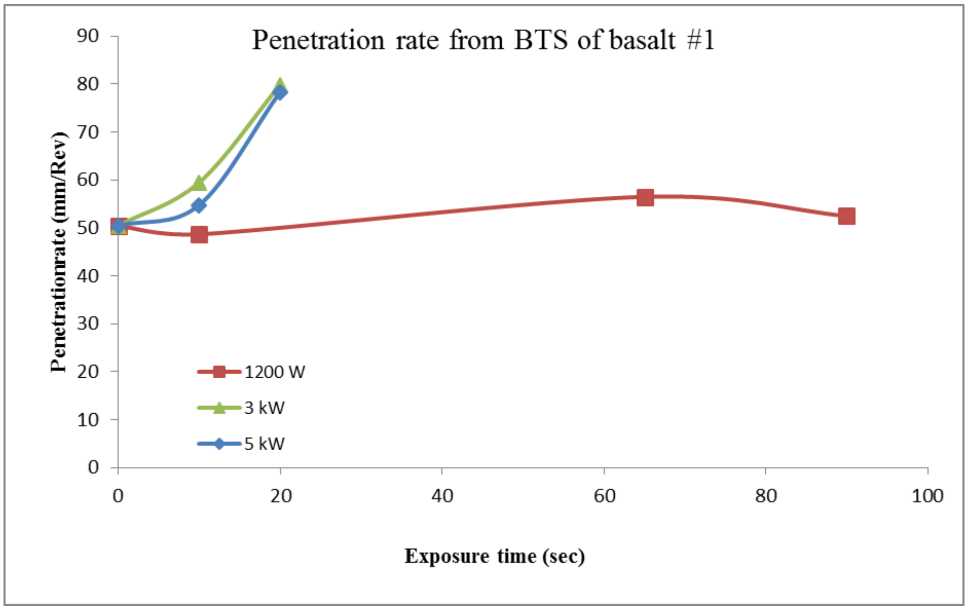

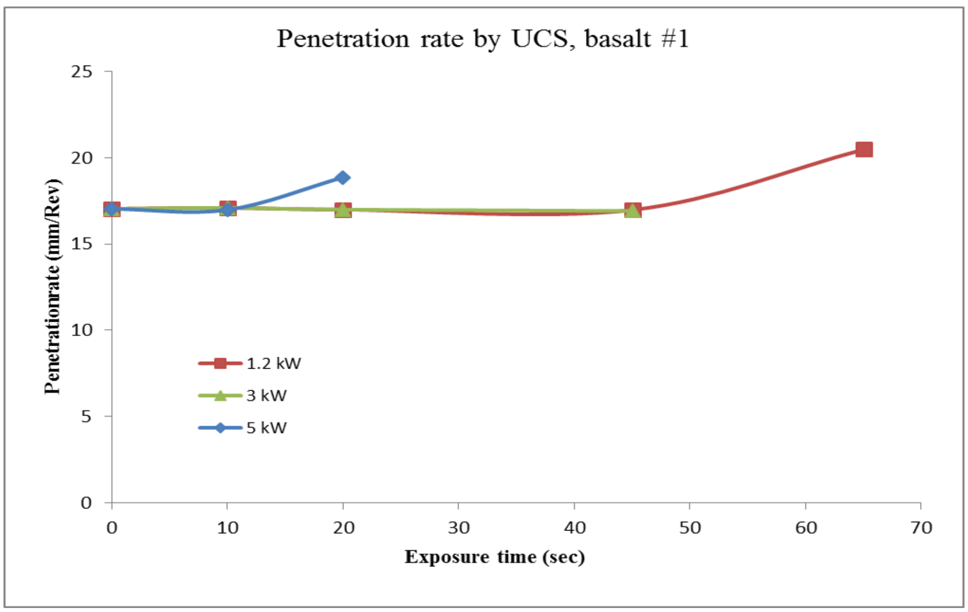

Figure 4-35 Predicted penetration rate of a TBM into basalt #1 based on a) Brazilian tensile strength and b) uniaxial compressive strength

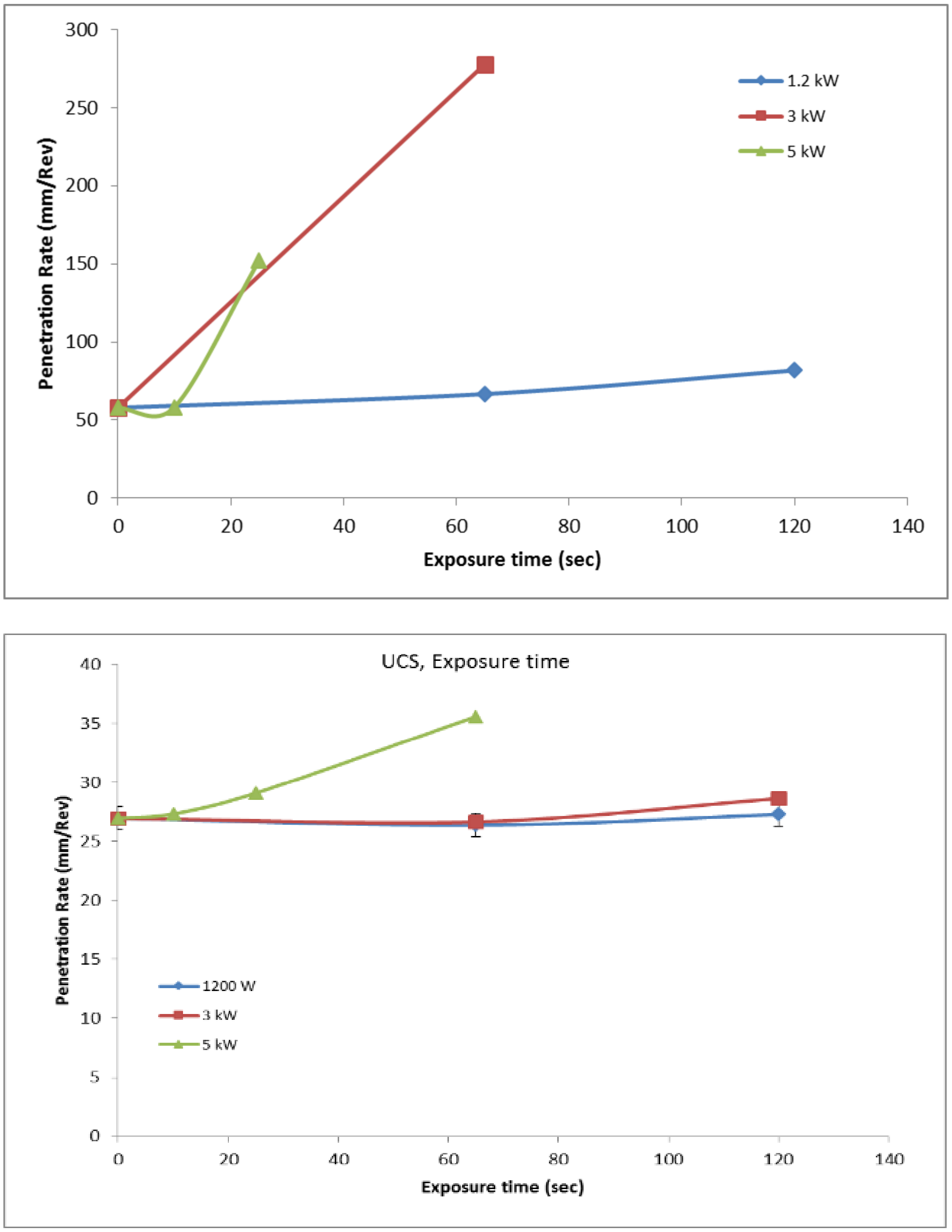

Figure 4-36 Predicted penetration rate of a TBM into basalt #2 based on a) Brazilian tensile strength and b) uniaxial compressive strength

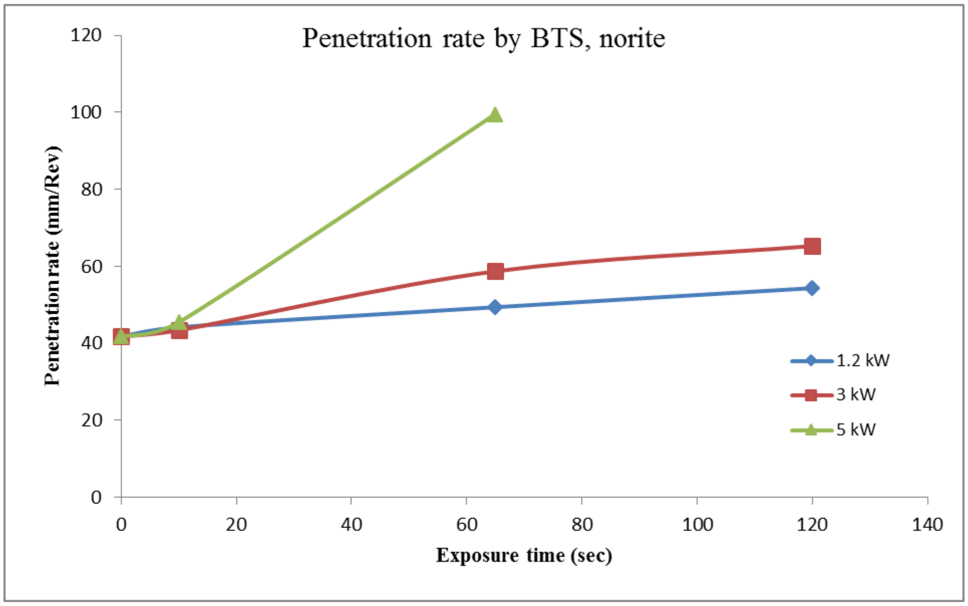

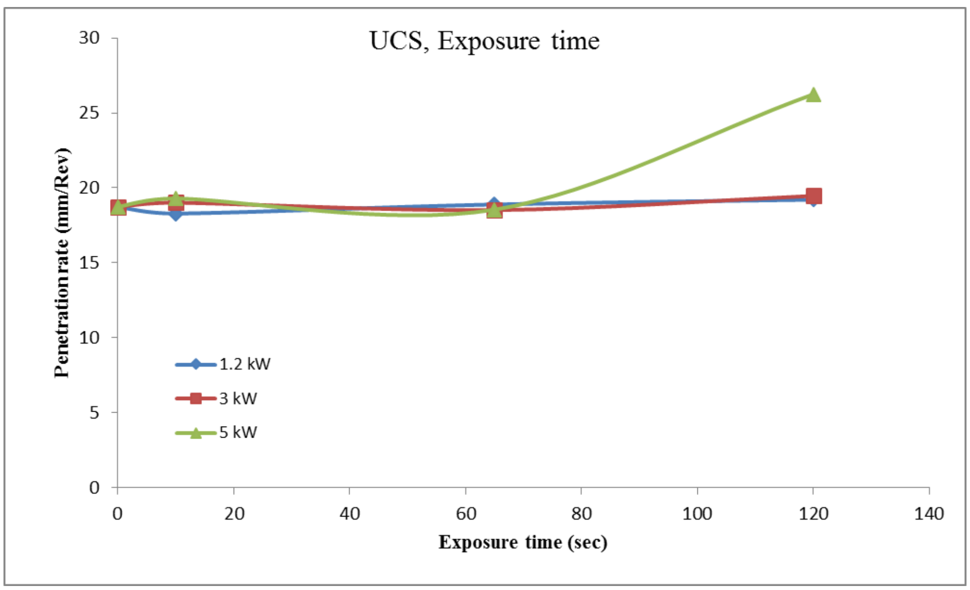

Figure 4-37 Predicted penetration rate of a TBM into norite based on a) Brazilian tensile strength and b) uniaxial compressive strength

The CAI values were not applied to equation 24, since the CAI values of the rock samples were not affected by microwave energy.

4.4 Treatment in Industrial Microwave Ovens (3 to 15 kW)

In addition to improving the efficiency and advancement rate of a TBM, microwave treatment has the potential to improve the efficiency of rock comminution and mineral processing. Since the rock mass in front of the cutter head of the TBM is irradiated with microwave energy, the pieces of rock being chipped out of the face are also affected by microwave energy. Therefore, the pieces conveyed out of the tunnel are already considered as treated rocks prior to the comminution or processing plant if the rock is mineralized.

4.4.1 Temperature Distribution in Dry vs. Wet Basalt #2, 3 kW Power

In order for the project to be relevant and applicable to its actual on site situation, all rock specimens were prepared in the form of slabs. The dimensions of the slabs were designed in a way to be considered larger than the largest dimension of the horn antenna aperture. The temperatures of dry basalt #2 slabs after exposure to continuous 3 kW microwaves power were highest at the rock surface and decreased exponentially with depth into the stacks of slabs, at both 60 s (Figure 4-38) and 120 s exposure times (Figure 4-39). It is seen that the closer is the rock surface to the aperture of horn antenna the higher its temperature is. The penetration depth of basalt #2 sample calculated with equation 18 for a frequency of 2.45 GHz is approximately 4.22 cm. The measure penetration depth was 5 cm for both exposure times. Recall this means that, at this depth, the microwave energy attenuated to 1/e [over Euler's number ($\frac{1}{e} = \frac{1}{2.72}$)] of the value at the rock surface. Higher maximum temperatures were achieved when the samples were closest to the antenna. For example, after 60 s exposure, the mean temperature at a distance of 3.5 cm was 150°C, versus 50°C at a distance of 19.5 cm (Figure 4-38). A longer exposure time also led to higher temperatures: the highest mean temperature (3.5 cm distance) was nearly twice as high after 120 s exposure (275°C; Figure 4-39) than after 60 s exposure (150°C; Figure 4-39).

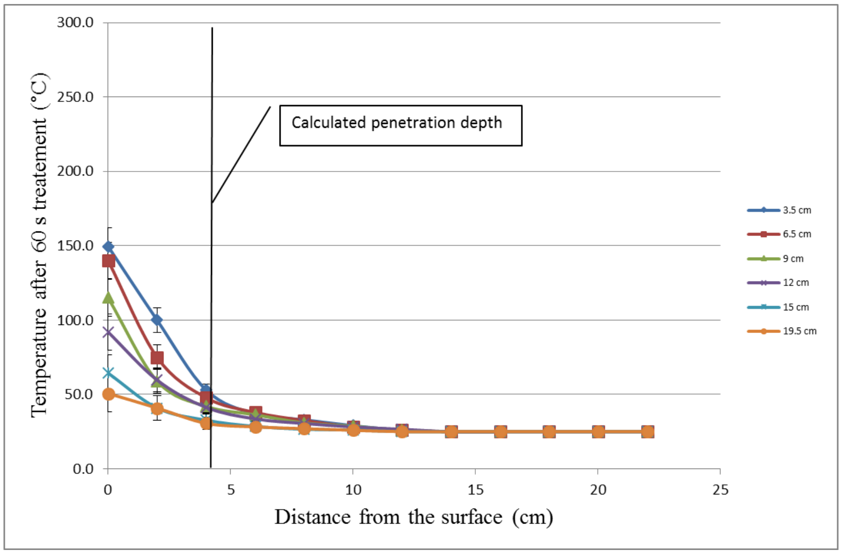

Figure 4-38 Dry basalt #2 temperature vs. depth into the stack of rock slabs after 60 s of microwave treatment at six distances from the antenna and 3 kW power.

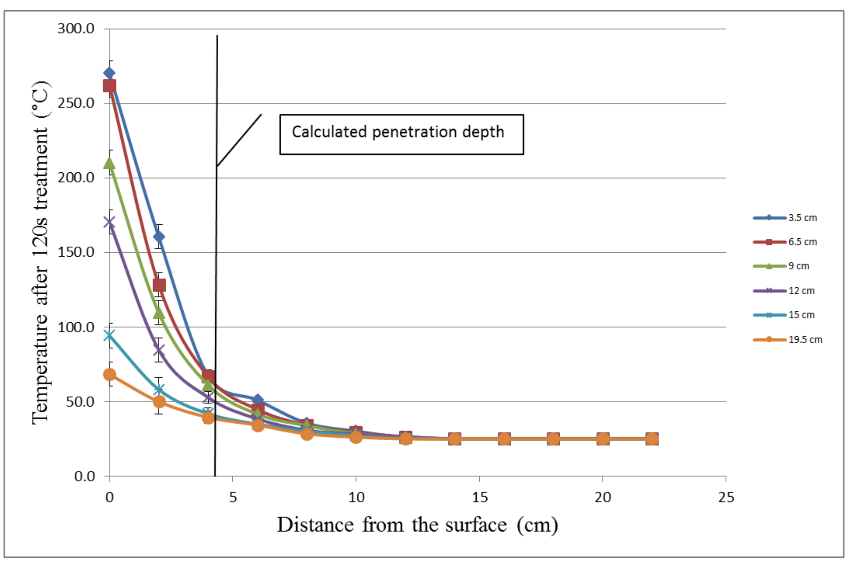

Figure 4-39 Dry basalt #2 temperature vs. depth into the stack of rock slabs after 120 s of microwave treatment at six distances from the antenna and 3 kW power.

The temperature distribution pattern and penetration depth did not differ between dry and saturated conditions (Figure 4-40 and Figure 4-41). However, a 20% higher maximum temperature (180 vs 150°C) was achieved at the closest distance from the antenna by wetting the samples for the 60 s exposure. The effect was negligible at 120 s exposure (295 vs. 275°C). At longer distances from the antenna, the temperatures of wet basalt were similar to or lower than dry basalt. The low porosity of basalt #2 meant that the small amount of water in the rock (no more than 1.5%) had little effect on the microwave absorption of the sample.

By definition t Figure 4-40 illustrates the temperature distribution within the simulated cubic block of rock formed by stacked slabs after being exposed to microwaves for 60 seconds as its distance increases from the antenna. The theory says that as microwaves penetrates into the rock, its power decays exponentially as it is observed in the graphs.

The same test is repeated but the time of exposure is set to 120 seconds at the same power intensity. At the same condition as the previous test but longer exposure time, it is observed that the temperature of the surface increased significantly; however, the temperature distributions within the block of rock decays exponentially as the previous test shown in.

Theoretically, the penetration depth of basalt sample used in this study is calculated to be 4.22 cm from the surface of the rock. Both Figure 4-40 and Figure 4-41 show that the temperature of the rock at 5 cm depth is around 50 degrees Celsius, which is very close to ambient temperature compare to the surface temperature, although time of exposure is different in both tests. This confirms that upon knowing the wavelength and electrical properties of the rock, the penetration rates can be approximately calculated.

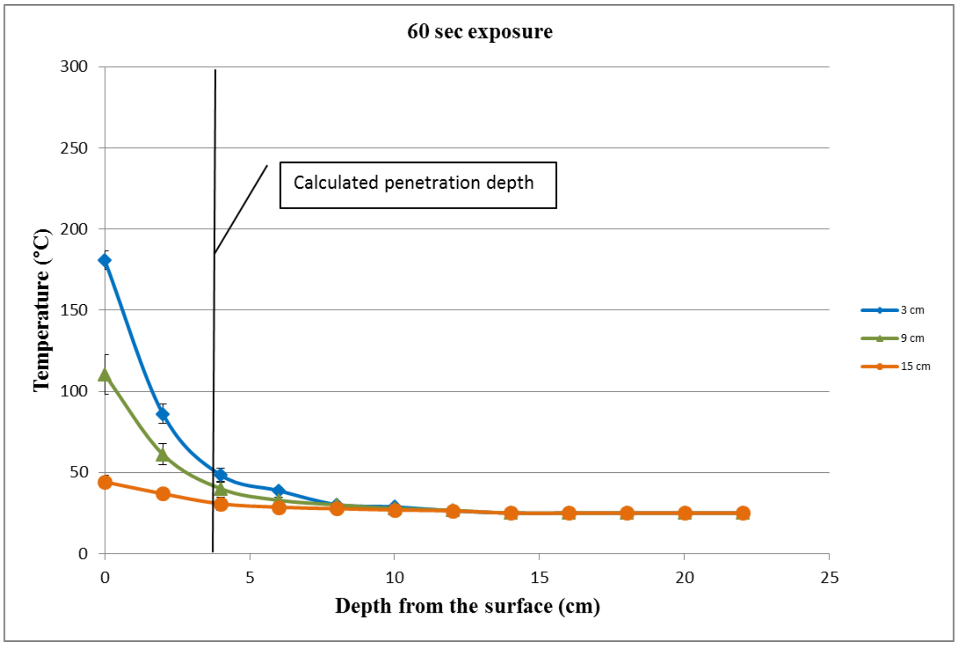

Figure 4-40 Wet basalt #2 temperature vs. depth into the stack of rock slabs after 60 s of microwave treatment at three distances from the antenna and 3 kW power

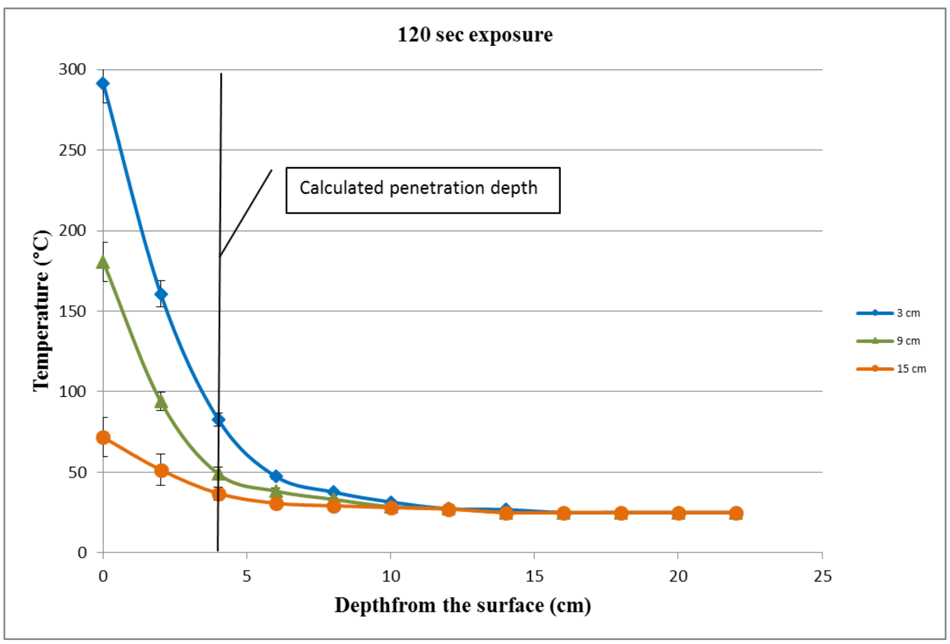

Figure 4-41 Wet basalt #2 temperature vs. depth into the stack of rock slabs after 120 s of microwave treatment at three distances from the antenna and 3 kW power.

The surface temperature decreased linearly as the distance from antenna increased. Figure 4-42 makes it easier to visualize the pattern noted above: as the distance from antenna increased, the surface temperature of wet basalt #2 decreased more rapidly than did dry basalt #2 at both 60 and 120 s. This phenomenon is due to the very thin layer of water on the surface of the first slab. Since water is a strong absorber of microwave energy, the temperature of the surface of the wet rock was higher than the dry rock. The closer the rock is to the antenna, the higher is the intensity of microwave energy; therefore, the higher is the temperature of the first slab. The water on the wet rock absorbed the energy reaching the surface and evaporated. This phenomenon is more highlighted when the distance between the horn antenna and rock specimens increases. As demonstrated in Figure 4-42 the temperature of rock specimen's surface in saturated rocks are lower than the temperature measured in dry condition as the Low power intensity reaching the surface of the specimen evaporates the very thin wet layer on the rock's surface first.

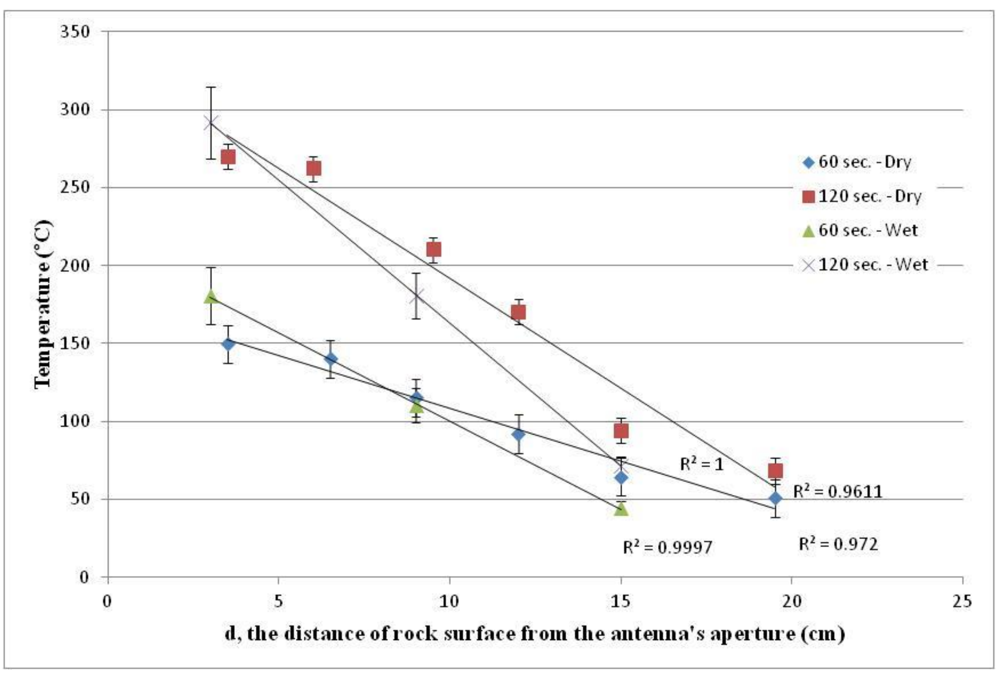

Figure 4-42 Temperature versus distance from antenna for top slabs of dry and wet basalt #2 treated with 3 kW microwave power

4.4.2 Temperature Distribution in Basalt #2, 5, 10 and 15 kW Power

Figure 4-43 to Figure 4-48 shows the temperature distribution along the z axis (normal to the surface of rocks) towards depth when exposed to 60 and 120 seconds of microwaves at four different power (3, 5, 10 and 15 kW). Each curve in the figures represents the temperature distribution toward depth at various distance from the pyramidal horn antenna's aperture. Every time the slabs are stacked on top of each other to form a block of rock in front of microwave antenna. The distance shown in the figures is the distance of the overall block's surface with the antenna.

The 3 kW power experiment above was repeated with a higher power apparatus using dry basalt #2. The penetration depth was approximately 4 cm, which is less than the theoretical penetration depth of 4.22 cm. From equations 16 and 17, it is evident the intensity of the electric field emitted by an electromagnetic device diminishes exponentially when it enters a medium (Metaxas, et al., 1983) and the power dissipated from that electric field also decreases exponentially. In other words, the higher the absorption capacity of the material, the quicker the power decreases. Air is a dielectric, but the losses in air are negligible. The electric field intensity affects the surface of a lossy material first and starts to increase the temperature at the surface first. Since the surface warms, the heat penetrates into the material by conductance. This phenomenon caused the measured depth of penetration to be shallower than theoretical depth.

The exponential decrease in temperature with depth into the specimen and the linear decrease in surface temperature with distance from the antenna seen in the 3 kW experiments were also observed in the higher power experiments (Figure 4-43 to Figure 4-48). Also similarly, at 5 and 10 kW power, temperatures were higher at 3 and 6 cm from the antenna than longer distances for both exposure periods (Figure 4-43 to Figure 4-48). The energy intensity at these distances is at its highest. In addition, 3 and 6 cm are equivalent to ¼ and ½, respectively, of the wavelength of 2.45 GHz frequency. At 15 kW power, only the 3 cm distance temperature was higher than longer distances (Figure 4-47 and Figure 4-48). From this graph it is also evident that high power at short distance rises the rock's surface temperature much higher compare to the other distances. Figure 4-43 to Figure 4-48 shows the temperature distribution within the overall block being exposed to.

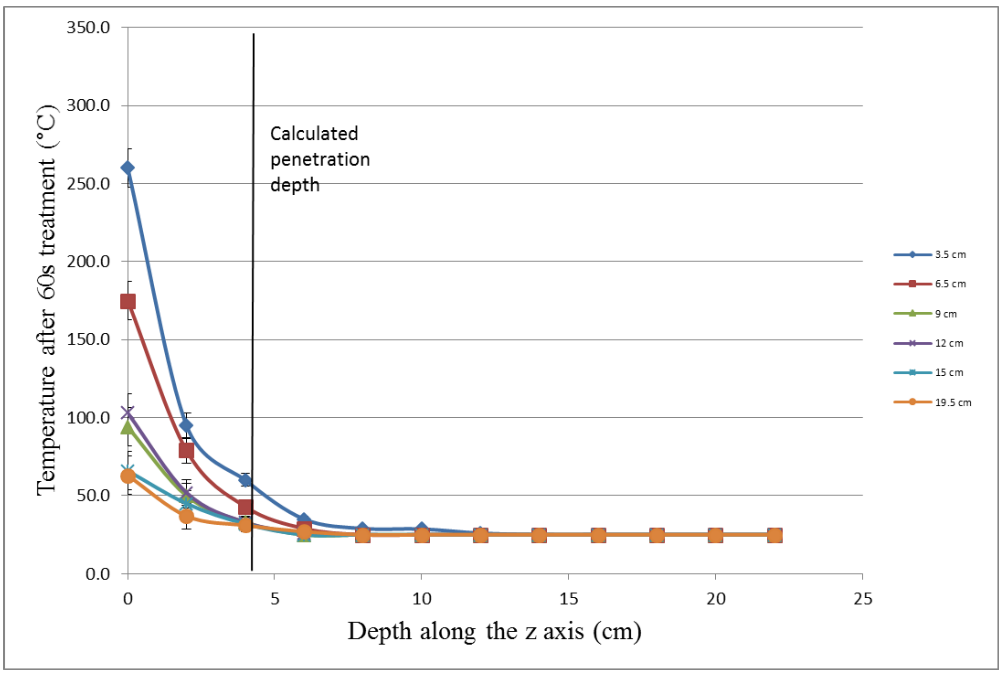

Figure 4-43 Basalt #2 temperature vs. depth into the stack of rock slabs after 60 s of microwave treatment at six distances from the antenna and 5 kW power.

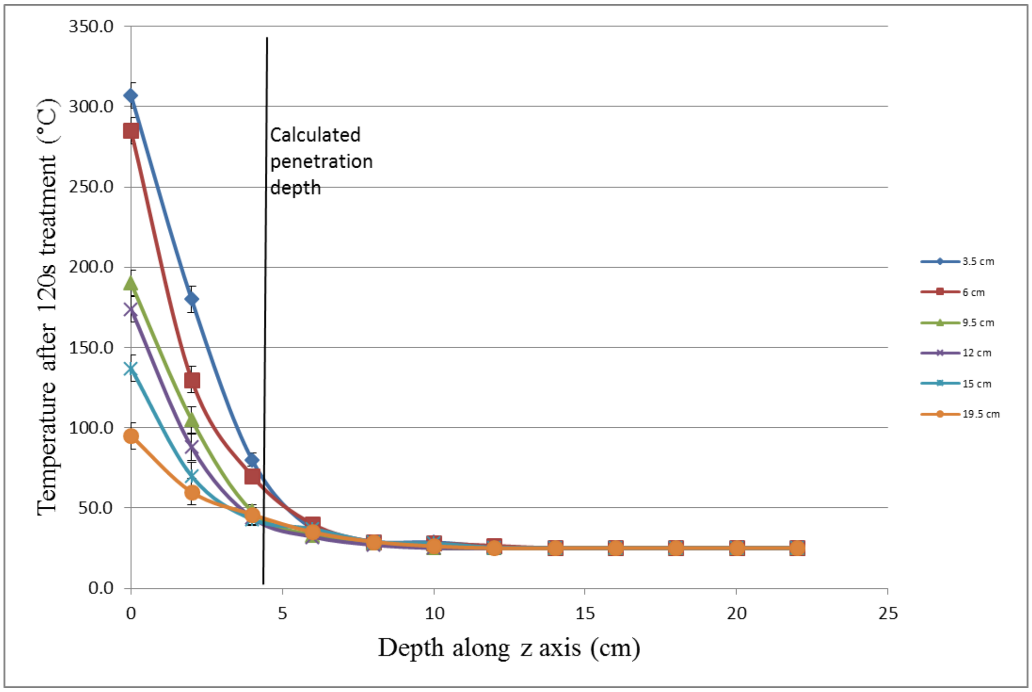

Figure 4-44 Basalt #2 temperature vs. depth into the stack of rock slabs after 120 s of microwave treatment at six distances from the antenna and 5 kW power.

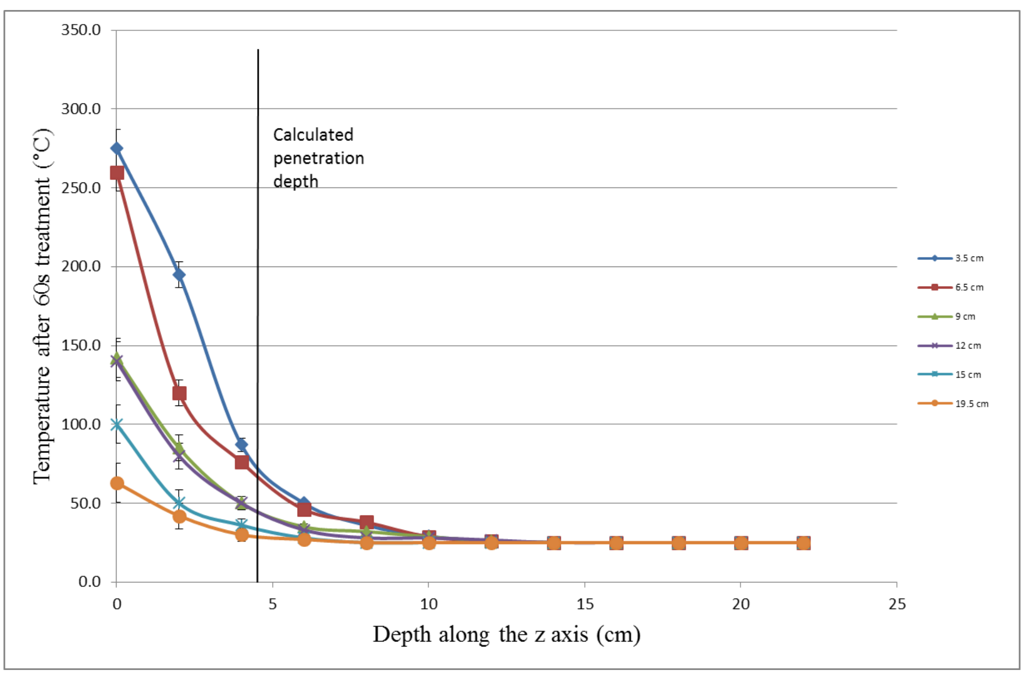

Figure 4-45 Basalt #2 temperature vs. depth into the stack of rock slabs after 60 s of microwave treatment at six distances from the antenna and 10 kW power.

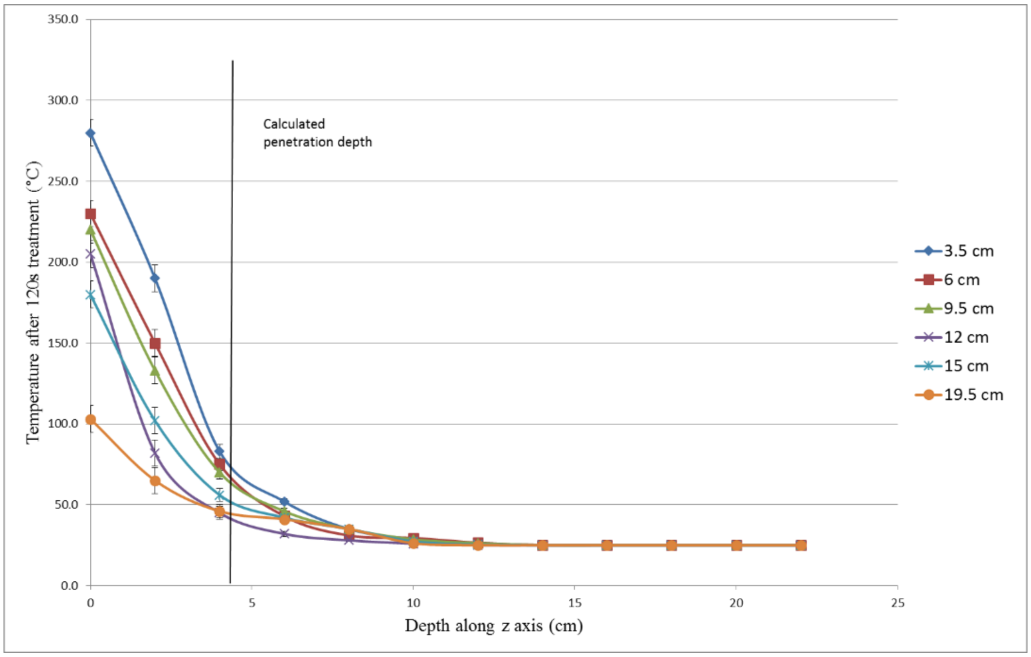

Figure 4-46 Basalt #2 temperature vs. depth into the stack of rock slabs after 120 s of microwave treatment at six distances from the antenna and 10 kW power.

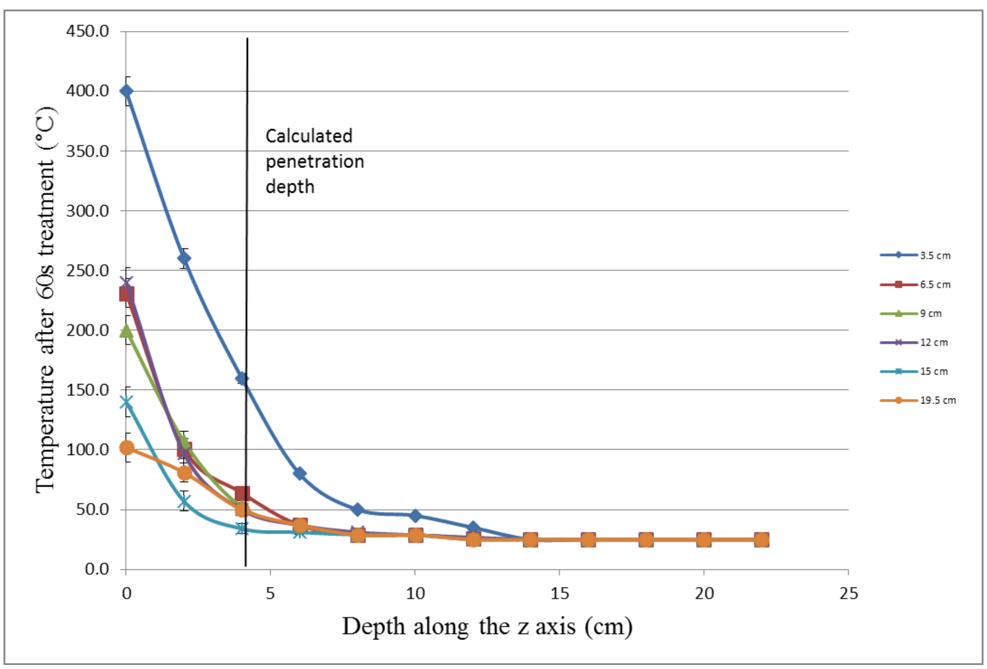

Figure 4-47 Basalt #2 temperature vs. depth into the stack of rock slabs after 60 s of microwave treatment at six distances from the antenna and 15 kW power.

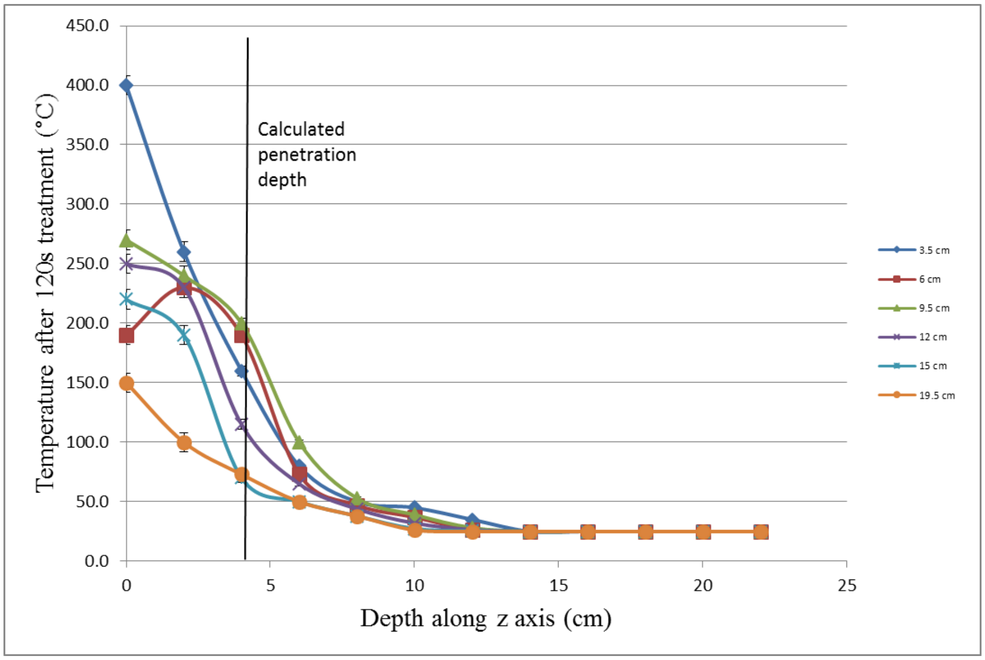

Figure 4-48 Basalt #2 temperature vs. depth into the stack of rock slabs after 120 s of microwave treatment at six distances from the antenna and 15 kW power.

As the exposure time increased, heat had more time to dissipate and conduct evenly toward deeper depths; therefore, the difference between the temperature at 3 and 6 cm distances and at 9, 12, 15 and 20 cm was less pronounced.

In the 5 kW treatment at the end of 60 s exposure, stress in the center of the top slab reached the failure threshold and it shattered into three pieces. The second slab cracked diagonally from the center to the edge. The slabs in all other distances stayed intact at 60 sec of exposure time except when the surface of the overall block is very close to the antenna. The spalling pieces had a thickness of 0.2–9 mm and varied in size and shapes. The width and length of spalled pieces vary a lot and have not definitive size. The quicker the rock reached its highest thermal gradient (i.e. high power), the smaller the sizes of spalling pieces. The highest thermal gradient happens normally when power increases at very short span of time.

An exposure time longer than 60 s meant that when the top slab shattered into three pieces, and the second slab was directly exposed to microwave energy: it began spalling at 90 s and shattered in two pieces by 120 s. At 6 cm distance the first slab cracked diagonally at 90 s and started spalling at the center at the end of exposure period. The second and third slabs cracked diagonally. At 9 cm distance the first slab cracked diagonally after 90 s and finally shattered in three parts from the center. The second slab cracked diagonally. At 12 and 15 cm distances from the antenna the first two slabs just cracked diagonally, but no physical damage was observed at 20 cm distance.

At 3 cm distance the first slab started to spall out from the center at 30th sec continuously from both sides, which ended up shattering in four pieces. At 6 cm distance the slab shattered in two pieces and went away. When the second slab got exposed since the first one went away, it started to spall out from the center then shattered in four pieces. At 9 and 12 cm distance the first slab shattered in two pieces at around 50 to 70 sec but not violently, so the shattered slabs remained stationary. At 15 and 19.5 cm distance the first slabs only cracked diagonally. At 10 kW power and 3 and 5 cm distances, the first slab of the block started spalling at 25 s from the center on both the top and bottom of the slab, resulting in a violent shattering of the slab into two pieces (Figure 4-49). The test had to be stopped at 48 s to avoid damaging the system. Too much energy was emitted to the surface of the slab at high power at a close distance. The energy is emitted to the top side of the slab, so smaller pieces were produced (Figure 4-49a), whereas at the bottom of the slab, one intact chip was separated from the slab (Figure 4-49b). Since the second slab was located beneath the first, confinement pressure from the weight of the first slab kept the chip beneath the first slab intact. The spallation sequence of the slab in front of the antenna is evident in Figure 4-49c and Figure 4-49d. Weak confinement pressure inside the rock due to the thinness of slabs (2 cm) compared to the width and length (40 cm) meant individual slabs tended to crack diagonally or shatter into multiple pieces.

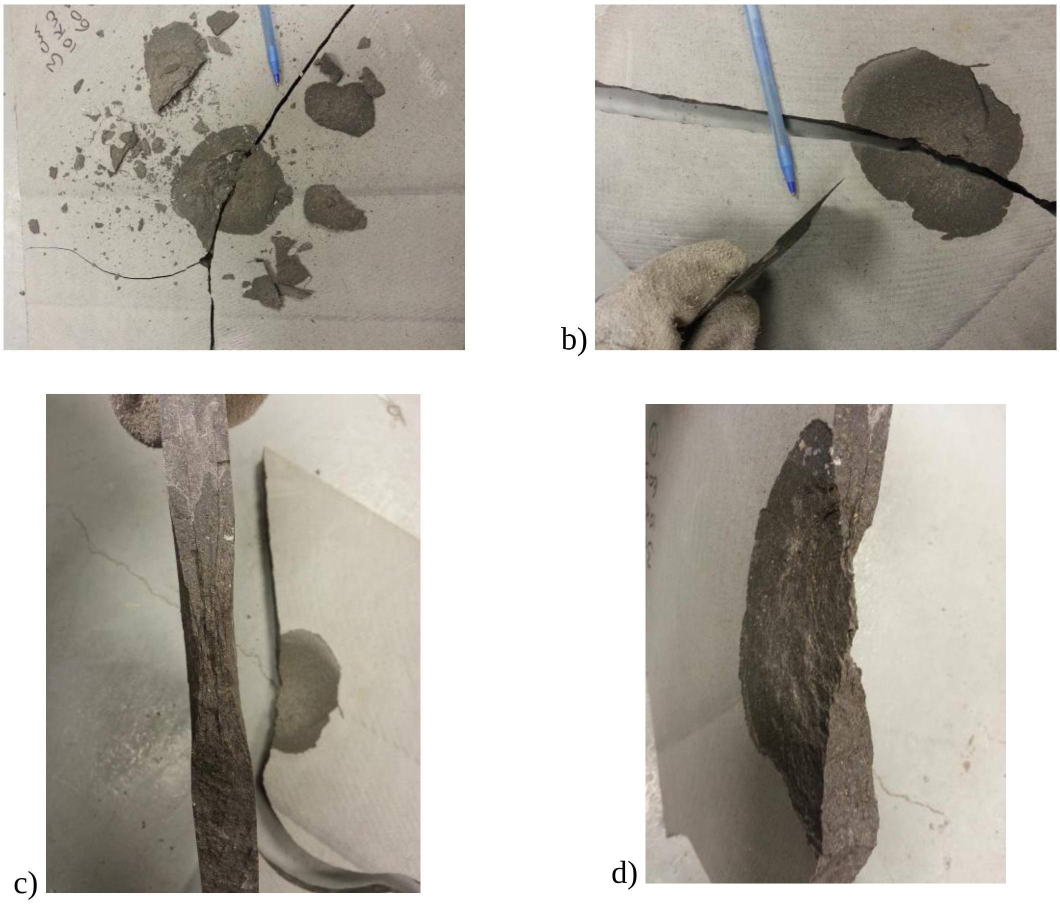

a) b) c) d)

Figure 4-49 First slab treated at 10 kW power, 3 cm distance from the antenna at 60 s exposure time a) spallation on the top; b) spall at the bottom; c and d) cross sections of the slab when shattered and spalled out

At 15 kW power at 3 cm distance, the first layer started to spall out at the center at 30 s. It shattered in pieces and exposed the second layer. Because the power was too high, the center of this layer turned red, stopped spalling out and started to burn. The rock had reached the chemical reaction stage (Figure 4-50). Since the rock continuously spalled out and slabs were violently shattered at this distance, the test was stopped at 45 s. The second layer spalled once exposed to microwaves after the top slab shattered. The second layer also shattered, but the third layer cracked diagonally. At 6 cm distance, the first layer started to spall continuously at 25 s. The test at this distance had to be stopped after 37 s, since the hot zone created between the rock surface and the horn waveguide generated a plasma zone. From 9–19.5 cm distance, the first layer shattered in half at 45–55 s.

So far, all the graphs had an organized and order respecting the distances at each power and time of exposure. The test was stopped, when slabs shattered while testing. The majority of the times slabs shattered almost at the end of the exposure time. At 15 kW and 120 sec of exposure time shown in Figure 4-50 the tests had not been stopped except at 3 and 6 cm distances, although the slabs were shattered violently.

Since the slabs continuously spalled out at 3 cm distance and were violently shattered in pieces, the test had to be stopped at 75 sec. The results recorded are the final results obtained at 75 sec of exposure time. At this distance the first layer started to spall out from the center as of the 30th second. It shattered in pieces and went away afterward. The center of this layer also turned red in color as it was getting burnt. The second layer continued spalling out continuously as it got exposed to microwaves when the first slab went away.

At 6 cm distance in between the hot zones created by the surface of the slabs and the horn antenna a plasma zone has been created at 65 sec; therefore, the test had to be stopped in order not to damage the machine. The temperature recorded are the temperatures at the time when the test had been stopped. The first layer started to spall out from the center. Since the thermal expansion was too quick the slab shattered in two pieces and went away violently. The second layer also started to spall out from the center as it was exposed following by being shattered in pieces. The third layer also shattered in pieces when it got exposed to microwaves when the second layer shattered away.

At 9 cm distance the four first layers shattered in pieces and went away one after the other in sequence. The third layer also stated spallation process from the center as the overall surface got distant from the antenna. At 12, 15 and 19.5 cm distances the two first layers shattered away in four pieces at about 55 to 65 sec and exposed the layer beneath. At 19.5 cm distance the second layer only cracked diagonally.

Figure 4-50 Top slab of basalt #2 after exposure to 15 kW power at 60 s from 3 cm distance

Figure 4-51 is an illustration of the spallation mechanism of a slab exposed to a microwave horn antenna. When a zone is heated by an in-depth source such as microwave energy, the lossy exposed material starts to heat up layer by layer from the surface toward deeper depths. The thermal expansion of the heated zone tends to expand more toward the weakest confinement zone; therefore, it creates a tension stress zone in the center and shearing stress zone around the edge of the potential chip to spall. The failure mechanism helps explain the phenomenon shown in Figure 4-49c.

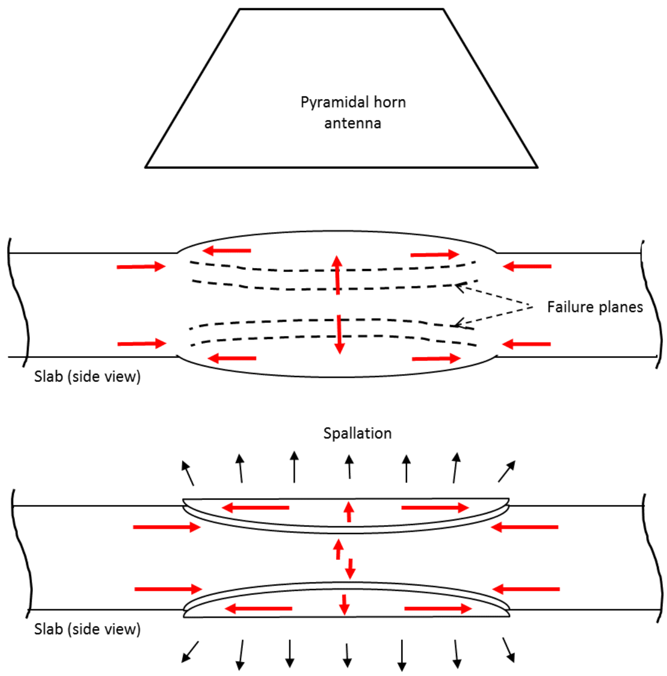

Figure 4-51 Spallation mechanism of a slab of basalt #2 in front of a microwave horn antenna

Figure 4-52 summarizes the three main behaviours (which could occur in combination) of basalt #2 slabs when exposed for 60 and 120 s at 3, 5, 10 and 15 kW power:

1. Continuous spallation from the center of the surface immediately in front of the antenna.
2. Diagonally cracking initiated from the center to the edge of the slab.
3. Violent shattering as the slab burst from the center.

Further than individual behaviour named any combination of two behaviours is also observed.

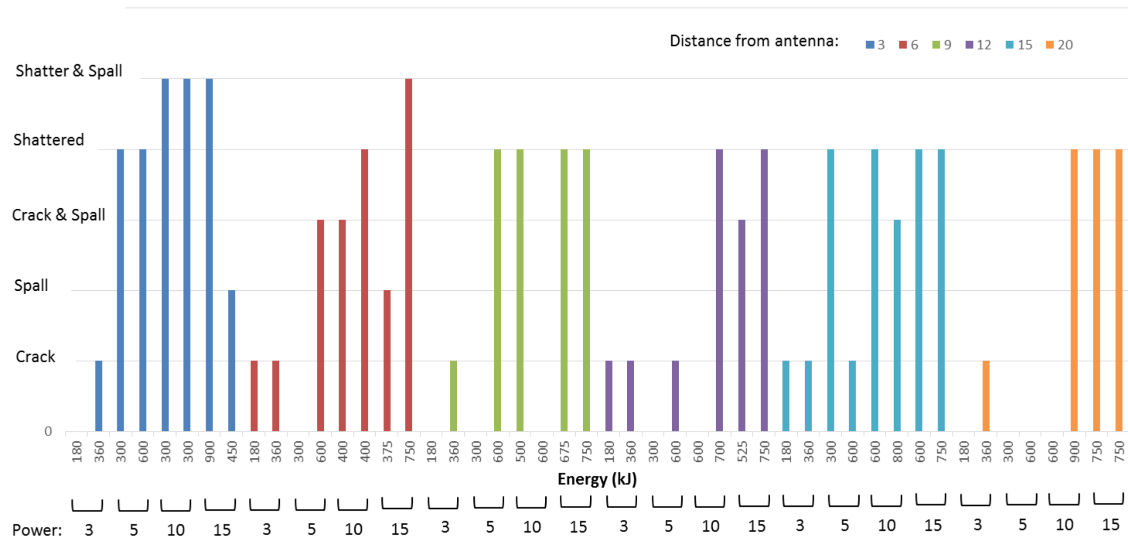

Figure 4-52 Basalt #2 cracking and spalling behaviour in response to microwave energy emitted for up to 120 s at 3, 5, 10,and 15 kW of power and at five distances from the antenna

Figure 4-53 shows a basalt #2 slab for each of the three behaviours. If the energy intensity— the electric field intensity, which refers to the power of microwave—is high, enough power will reach deeper depths of the dielectric. Therefore, a larger zone absorbs the energy and is heated, causing the potential failure plane for spallation to deepen further. Thus a larger zone is heated and expands instead of generating chips. When heat is generated at high power and for a short period, the high expansion rate of the hot zone creates a large amount of stress within the slab. Since an individual slab is weak (thin relative to its width and length), it shatters suddenly and violently (Figure 4-53b). As the power increased and the distance to the antenna decreased, the spallation pieces got smaller and the shattering more violent. The spalled pieces passing a 12.7 mm sieve increased from 10% at 10 kW power and 15 cm distance to 49% at 15 kW and 6 cm distance.

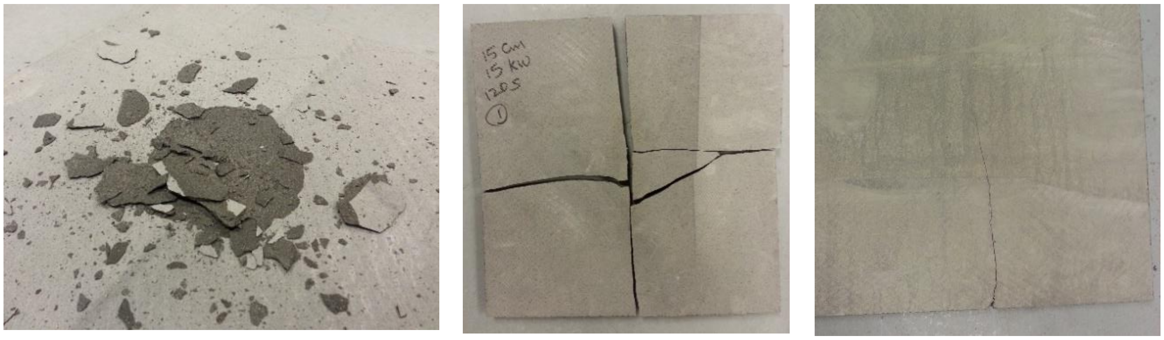

a) b) c)

Figure 4-53 Basalt #2 slab a) spalling chips at the center right in front of the antenna); b) shattering or violently divided into pieces; c) cracked diagonally from the center to the edge

When heat is generated rapidely, the heated zone expand rapidly and creates a high amount of compression stress zone around itself; therefore, causes the slab to shatter suddenly and violently shown in the right picture in Figure 4-55.

A small intact block of basalt #1 (30 cm (l) × 17 cm (w) × 20 cm (h)) was exposed to directional plane-wave microwaves as were the stacked slabs, at 3 kW power for 120 s from 3 cm distance (Figure 4-54a). The same spallation and chipping occurred on the surface in front of the antenna, as well as many open cracks in the body, as a result of thermal expansion of the heated zone (Figure 4-54b). This experiment showed that when confinement pressure is present—in contrast to the thin slabs with weak confinement pressure—spallation and chipping occur on the surface (Figure 4-54). The spallation of the surface is as if the open surface of the rock is subjected to a biaxial compressive stress, which the shearing failure zone all around the chips confirms.

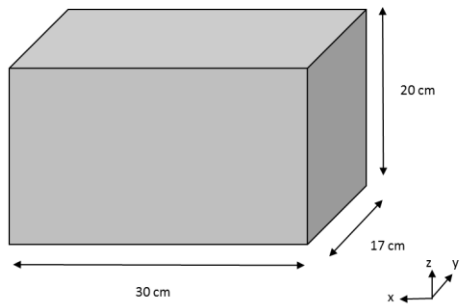

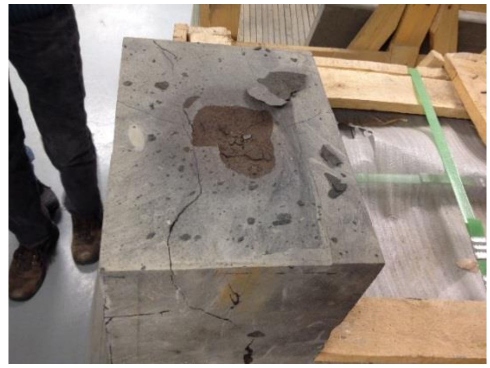

Figure 4-54 a) Schematic and b) photograph of an intact small block of rock sample exposed to directional plane-wave microwaves at 3 kW for 120 s from 3 cm distance

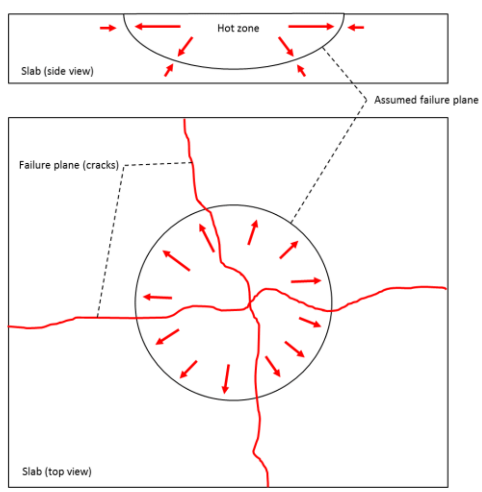

Figure 4-55 a) Schematic view of heated zone in front of the microwave antenna expanded rapidly and the resulting high compression stress zone caused the slab to shatter suddenly and violently; b) slabs shattered and fell away from the antenna and exposed the layers beneath (right)

Overall, the directional plane-wave experiments demonstrated that three main parameters influenced the rock surface exposed to microwaves:

1. power level from 3–15 kW,
2. exposure time of either 60 or 120 s, and
3. distance from the antenna to the surface of subjected rock (3.5 to 19.5 cm).

In order to have a good statistical analysis on the existing data obtained experimentally, a surface response regression was performed using a design of experiment software as an add-ins on Microsoft Excel. Temperature and violence of surface failure as a responses. A 3 full factorial design was analyzed. Distance explained the most variation in the temperature model (R^2 = 0.89) and power explained the most variation in the surface failure model (R^2 = 0.73). The influencing coefficients for quadratic models of regression are presented in Table 4-5.

Table 4-5 Factors coefficient of the quadratic model for temperature and violence of surface failure responses on the slabs exposed to directional microwave radiation

Factor	Parameter	Temperature	Violence of surface failure
constant		121.30	3.587
A	Power (kW)	40.894	2.191
B	Exposure time (s)	61.099	0.66716
C	Distance (cm)	-100.08	-0.86413
CC		31.641	

The surface response of temperature as function of power vs. exposure time, considering a fixed distance of 11.5 cm between the antenna and the rock's surface, is demonstrated as Figure 4-56. The temperature increased linearly with exposure time. By comparison, when the exposure time is kept constant at 60 s and the surface response of temperature is plotted as a function of power vs. distance, the temperature decreased exponentially with distance from the antenna (Figure 4-57).

By defining the levels of failure in Figure 4-52 on a scale of violence from unbroken (1) to a combination of spallation and shattering (6), the surface failure as a function of power vs. exposure time at a constant distance of 11.5 cm shows a linear increase

(Figure 4-58). The surface failure response is a linear decrease as a function of power vs. distance while exposure time is constant at 60 s (Figure 4-59).

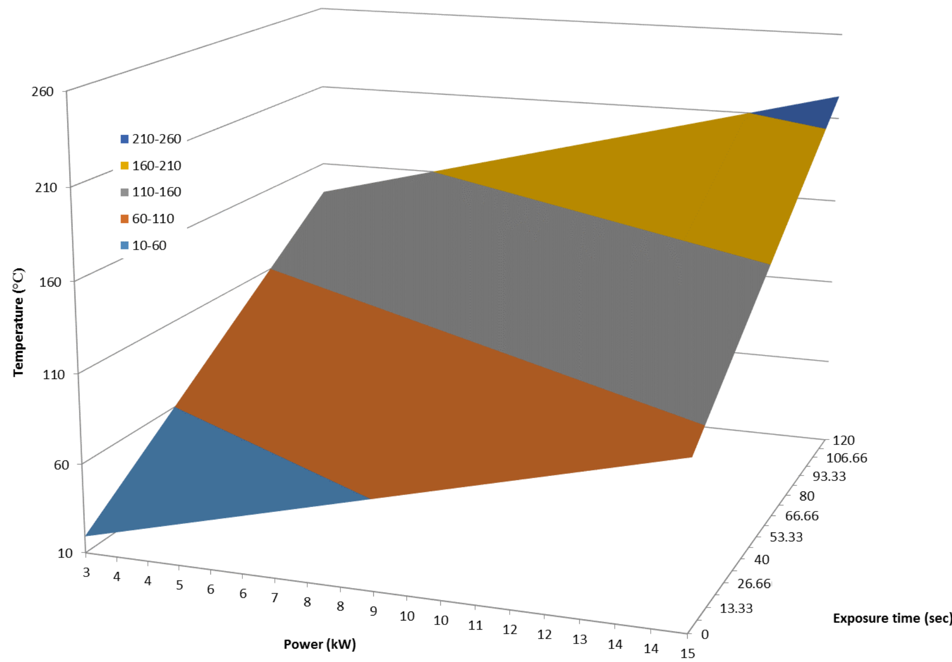

Figure 4-56 Surface temperature of basalt #2 at a constant distance of 11.5 cm in front of the microwave antenna as a function of power vs. exposure time

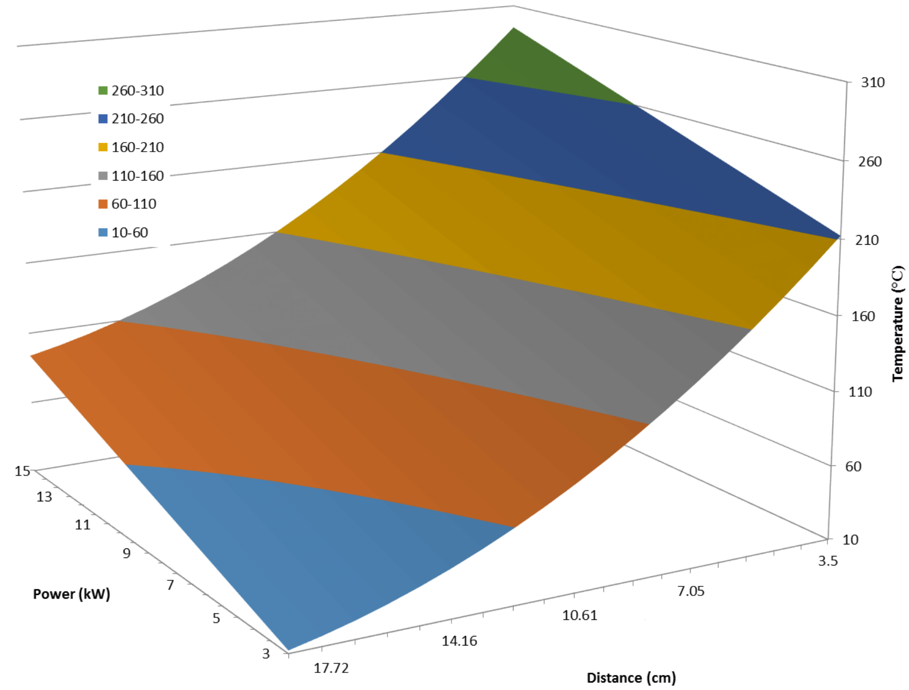

Figure 4-57 Surface temperature of basalt #2 at constant exposure time of 60 s as a function of power vs. distance from the microwave antenna

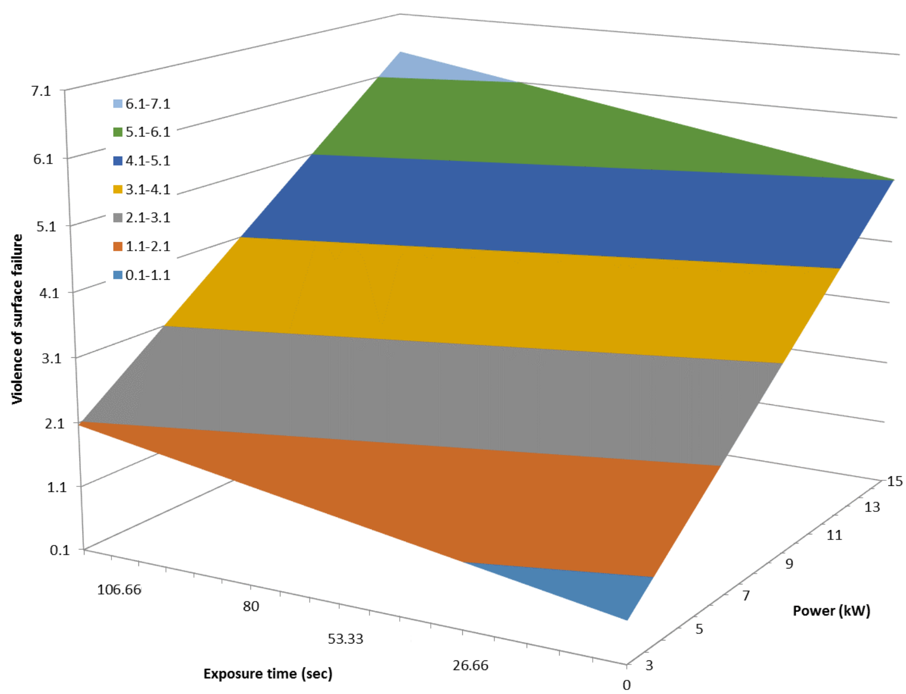

Figure 4-58 Violence of surface failure of basalt #2 at a constant distance of 11.5 cm from the microwave antenna as function of power vs. exposure time

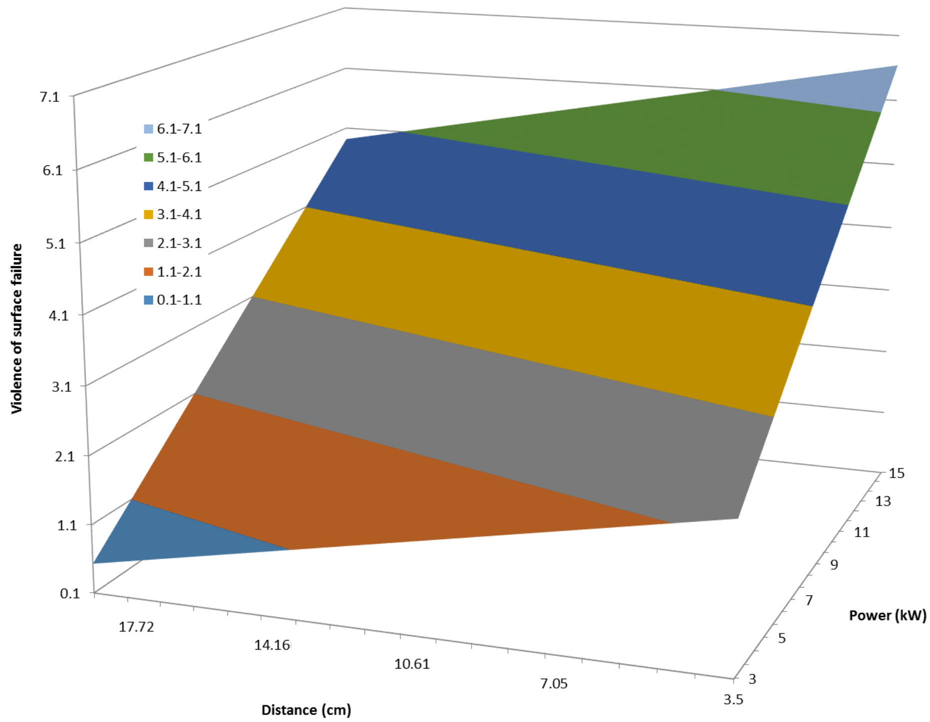

Figure 4-59 Violence of surface failure of basalt #2 at a constant exposure time of 60 s as function of power vs. distance from the microwave antenna

4.4.3 Power Reflection

When a block of rock is microwaved, energy reflects back from the rock surface to the magnetron. At short distances to the antenna, large amounts of energy are reflected, whereas at longer distances, the amount of reflected energy decreases (Figure 4-60). Longer distances provide more room for microwaves to bounce between the rock surface and the metallic walls of the closed cavity. Therefore, less energy is available to heat the rock surface in front of the antenna. According to energy propagation theory, the electromagnetic energy irradiated from an antenna into the free space loses intensity exponentially as the distance from the antenna increases. As the red line in Figure 4-60, was much less than the dry condition (blue line); however, tests at 6, 12 nor 19.5 cm from antenna in wet condition has not been conducted. Since there is no data at mentioned distances, the graph shows smooth decay in power reflection.

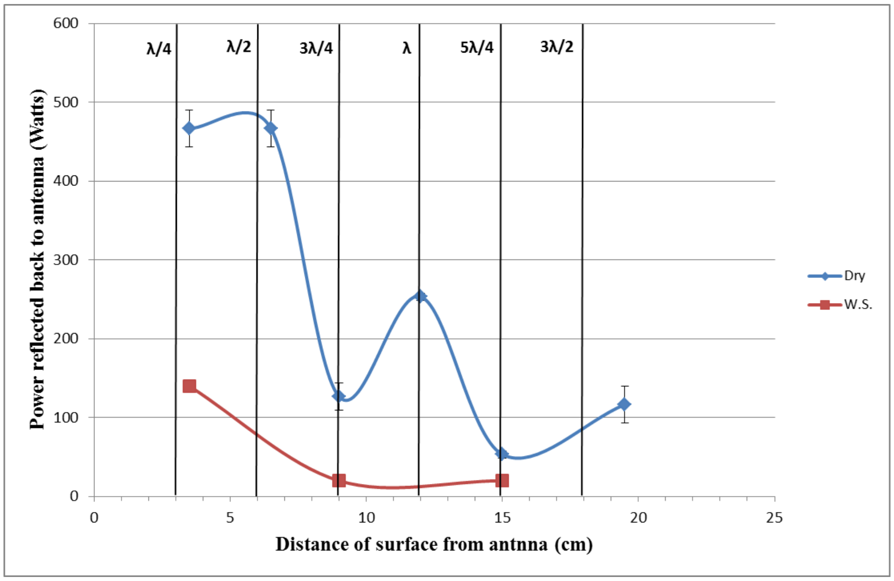

Figure 4-60 Power reflected from dry and wet basalt #2 surfaces during microwave treatment at 3 kW power at different distances from the antenna. Note: tests were not conducted on wet rock at 6, 12, or 19.5 cm distances.

When dry slabs of basalt #2 were exposed to microwaves at 3 kW power, the energy reflected back from the surface decreased exponentially with distance from the antenna (Figure 4-61). Furthermore, the amount of energy at each distance from the antenna fluctuated in a sinusoidal form while its attenuation decayed exponentially according to equation 16. When wet slabs were exposed to microwaves, less energy was reflected (Figure 4-61) because the very thin layer of water on the exterior surface of the rock absorbed a good portion of the energy emitted. At 6, 12 and 19.5 cm, the distance are equivalent to $\lambda/2$, λ and $3\lambda/4$ of the wave length for 2.45 GHz. Less amount of energy reflection in wet condition is due to more absorption by the rock. In wet condition the absorbed energy is very efficient by the rock sample exposed to microwave, which confirms a slight increase of the surface temperature of the first slab.

The experiments at higher power intensity showed similar results (Figure 4-61 to Figure 4-63): the power intensity decayed exponentially with distance from the antenna. The decay includes peaks and valleys in which the peaks in energy reflection at distances equivalent to λ/2, λ and 3λ/4 of the 2.45 GHz wavelength. Power reflection at various distances remained the same, regardless the exposure time. Combined, the graphs of 3, 5, 10 and 15 kW power levels show that power reflection intensity increased with power emitted. In other words, higher power emitted shows higher power reflection and reveals higher power absorption by the dielectric.

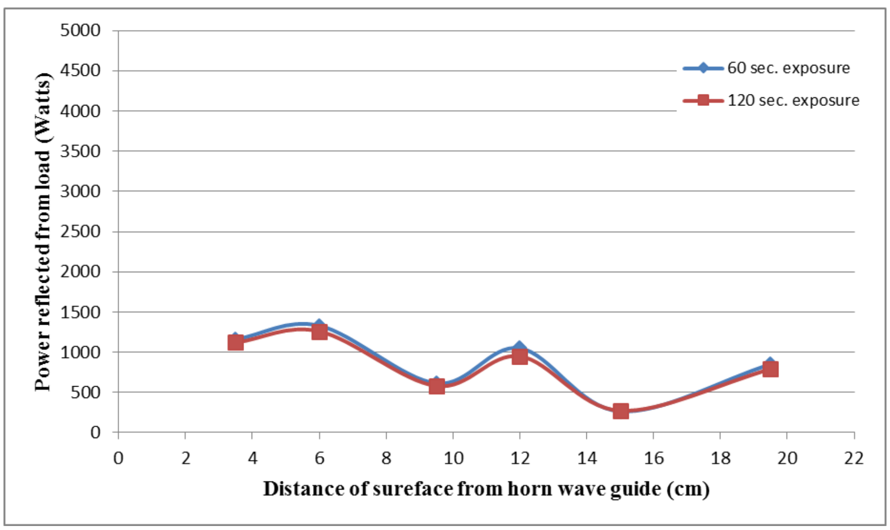

Figure 4-61 Power reflected from the surface of rock exposed to 5 kW microwave power at various distances from the antenna

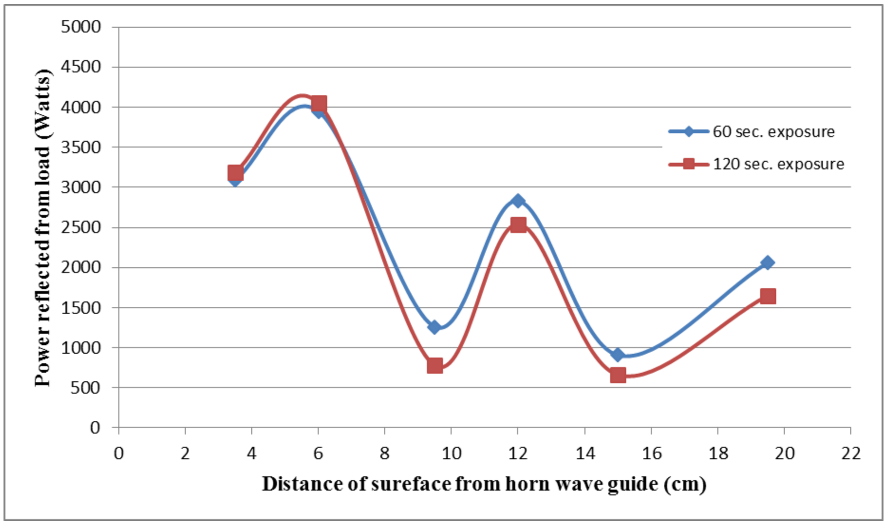

Figure 4-62 Power reflected from the surface of rock exposed at 10 kW microwave power at various distances from the antenna

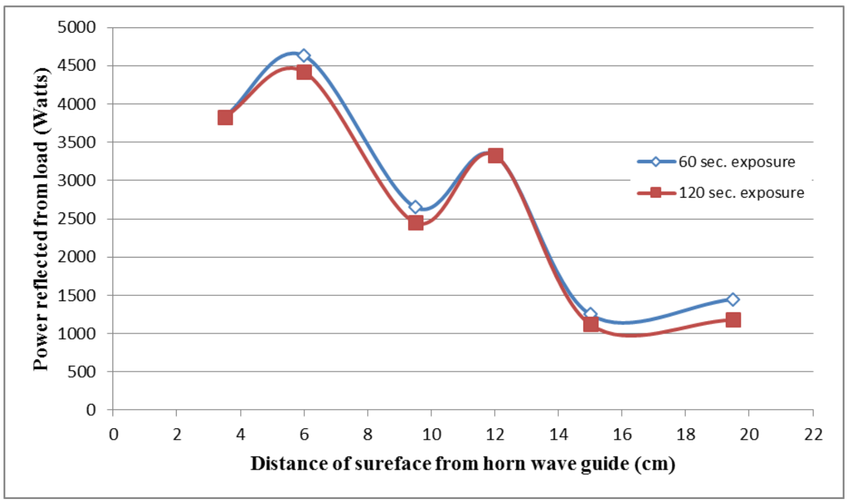

Figure 4-63 Power reflected from the surface of rock exposed to 15 kW microwave power at various distances from the antenna

4.4.4 Macro-Crack Density at 3 kW

Figure 4-64 shows the macro-crack density on the surface of each slab when the complete block was 3 cm from the antenna aperture. Two peaks of high crack density are evident at 6 and 12 cm distance (i.e., approx. ½× and 1× of the wavelength) from the horn antenna’s aperture. Since the working frequency is 2.45 GHz and the wavelength of this frequency is 12.2 cm, both peaks fall where the energy intensity was high. The high energy intensity at half wavelength distance from the antenna imposes higher impact on the surface of the rock being exposed; hence, higher macro-crack density is observed. Although the energy intensity is higher at half wavelength, the overall electric field intensity diminishes exponentially as microwave radiation propagates furthermore into the material known as load such as solid materials like rocks or gas like the air.

The test and macro-crack observation was performed within both dry and wet conditions. The results of macro-crack density induced on the surface of the slabs after each time of exposure, 60 and 120 seconds, are illustrated in both Figure 4-64 and Figure 4-65.

With respect to the Griffith theory, it is observed that as the temperature increased (when rocks get radiated by microwaves) macro-crack density increased. In contrast, as microwaves penetrated farther into the slabs, their power diminished, as did the macro-crack density. According to the Griffith theory (Hoek et al., 1965) for rock mass saying that with pre-existing micro and macro cracks within every rock mass, we can assume that up to 0.5% macro-crack density can be referred to as pre-existing micro and macro cracks within the subjected rock samples tested. This amount of pre-existing cracks have not been deducted from the results; therefore, the first 0.5% in each graph is assumed to be pre-existing cracks, and most of the crack density at the 60 s exposure of dry and wet basalt #2 was pre-existing.

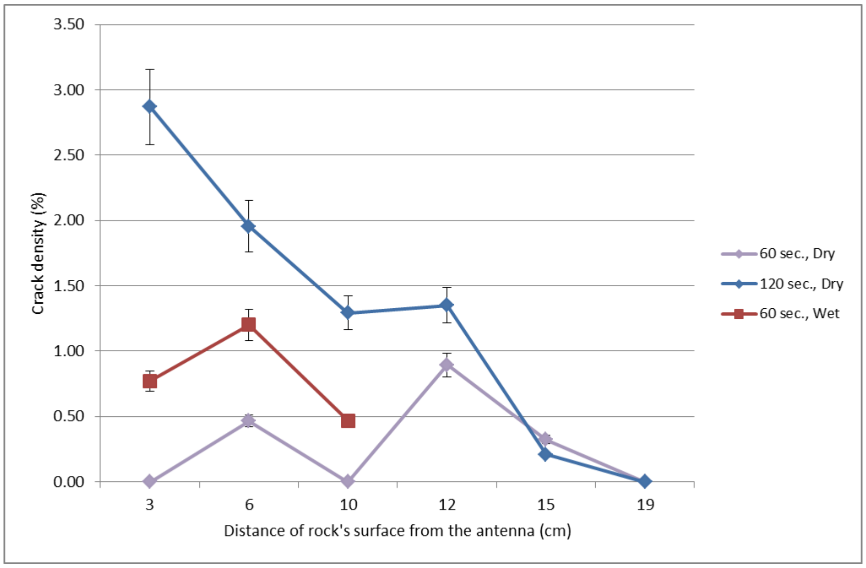

Figure 4-64 Macro-crack density in a unit area on the surface of the first slab of dry and wet basalt #2 at various distances from the antenna

Avoiding any macro-cracks observed under 0.5% density according to the Griffith theory, Figure 4-65 demonstrates that as the temperature increases due to microwave exposure, the macro-crack density on the surface in front of the antenna increased (ignoring first 0.5% density). The temperature of each layer in front of the antenna at various depths can be plotted along the normal line drawn from the antenna perpendicular to the rock surface. Since the power intensity of microwave energy decays exponentially as it penetrates and propagates into rock, less heat is generated at various depths within the rock, resulting in fewer macro-cracks due to low temperature. This phenomenon is precisely observed in Figure 4-65. As the distance increased, the physical impacts of microwave treatment decreased due to the reduction of electric field intensity of microwaves propagating through air. Although at the multiplication of half wavelength higher power reflection happens, higher crack density is observed on the surface of the slabs. Moreover, distances below the half wavelength results in a turbulent zone that signifies extreme high power density.

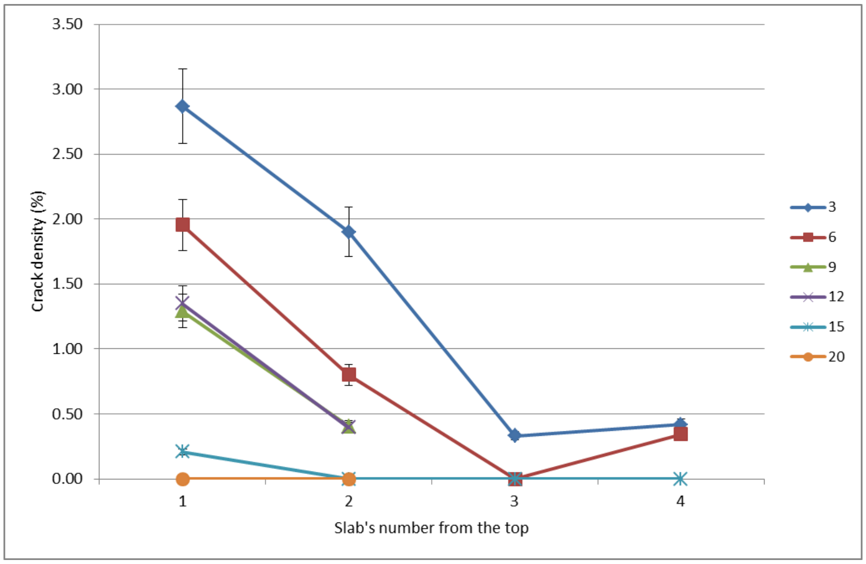

Figure 4-65 Macro-crack density of slab surfaces at various depths within the block and distance from the antenna in dry condition

4.4.5 Continuous versus Pulsed Microwave Irradiation

At constant 15 kW power and at 15 cm from the antenna, at the higher frequency pulsation mode (200 Hz), the duty cycle and temperature on the surface of the rock (Figure 4-66) than at 20 Hz pulsation. Both pulsation mode temperatures were lower than the continuous mode temperature (100% duty cycle).

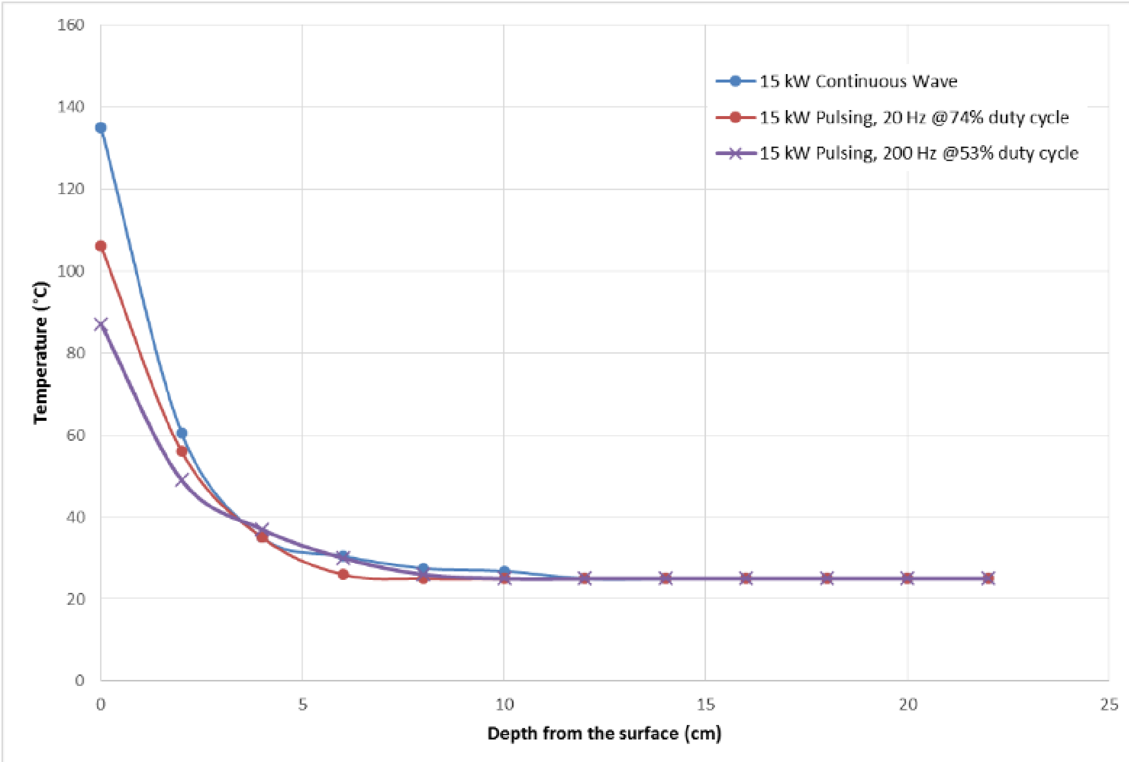

Figure 4-66 Temperature profile comparison of a block of rock exposed to 2.45 GHz frequency, 15 kW power from 15 cm distance from the antenna in continuous irradiation as well as pulsing in two different conditions

4.4.6 Errors

Two sources of error led to underestimates of rock sample temperature. The magnetron systems used were either water cooled or air cooled. In the latter systems, air is blown into the magnetron, and moves through the waveguides into the cavity from the horn antenna. Therefore, the rock sample was slightly cooled by the air as it was irradiated. This causes reduction of heat generated on the surface as the heat is conveyed the inside air of the cavity. In addition, microwave energy is categorized as in-depth heating source, which has the advantage of being turned ON and OFF quickly with a switch. The energy emitted to a dielectric turns into heat inside the load; therefore, heat is generated as long as the microwave energy is emitted. The moment the microwave system was turned OFF, the heat generated inside the rock started to dissipate by conduction through the material and by convection to the air inside the cavity. The higher the temperature of the material, the quicker the convection. As a result, the time required to measure the temperature after the microwave system was turned OFF allowed the temperature to decrease, especially when several layers were measured.

4.5 Theoretical Temperature and Stress Distribution

The mechanisms by which slabs thermally crack diagonally or shatter are driven mainly by lack of confinement pressure by the rock. By comparison, the spallation mechanism of rocks is the same as rock burst in rock masses (Brown, 1974), namely biaxial compression. Assuming an orthogonal coordinate in which x and y axis fall on a plane and z axis normal to that plane, the relationship between strain, stress and temperature are well defined by Boely and Weiner (1960). Under the conditions of biaxial stresses (σ_z = 0) the relationship $\sigma_x = \sigma_y = \frac{E\alpha T}{(1-\vartheta)}$ is extracted, from which it is understood that spallation process does not depend on the thermal gradient, but on the temperature itself. Carslaw and Jaeger (1959) defined the temperature distribution in a semi-infinite solid heated by a constant heat flux as a function of heat flux ($cal/cm^2/s$), time (s), depth (cm) and thermal diffusivity of rock ($/cm^2/s$) into the rock. This function was defined by applying a plasma torch to the rock surface. The spallation process appears to be similar in rocks treated by microwave (in-depth heating source) and rocks treated by a plasma torch (conductive heat source) (Kandev et al., 2013). Since directional plane-wave microwave heating is similar to a plasma torch heating, the heat flux can be replaced as the electric field intensity of microwave energy. Hence, if the electric field intensity of microwave energy increases, the heating rate of the material increases and it is as if the heating flux of a conductive heating source is increased.

4.6 Simulation of Microwave Irradiation

4.6.1 3D Simulation

The microwave applicator is simulated with COMSOL®, a powerful multi-physics software, simulating the scenarios experimented in practice. All the simulation results were compared with its equivalent practical tests. The simulation results confirmed the experimental foot print of microwave's influence on rocks.

Two scenarios were considered: 1) being intact cylindrical rock sample, and 2) being the same as scenario number (1) but having the specimens in the form of stacked disc shaped slices on top of each other (Figure 4-67). The disc shaped rock specimens stacked on top of each other's scenario allows us to reveal the temperature distribution profile within a cylindrical rock specimen. Both scenarios were simulated in various exposure time and validated them with the experimental results obtained with the multi-physics software in order to reproduce the results numerically. The stacked slabs have been positioned inside of the closed cavity in order to make various distances with the horn antenna. In addition to the temperature distribution profile obtained from the simulations, the power as well as the electric field intensities within the closed cavity is computed. Furthermore, the propagation of microwaves is demonstrated and discussed previously in order to better understand the pattern that microwaves propagates through a media (e.i. rock, air, etc).

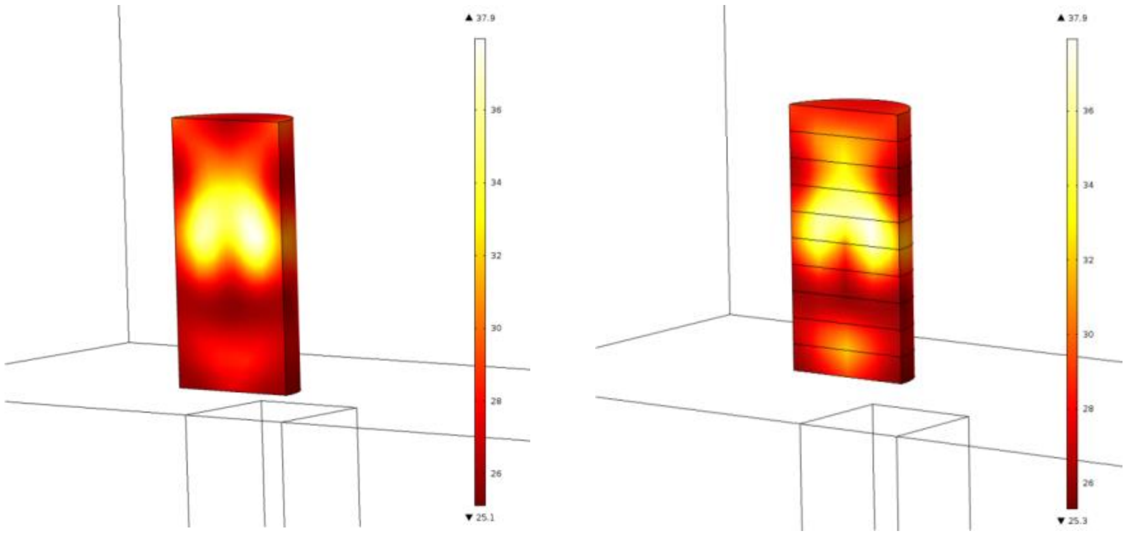

a) b)

Figure 4-67 Model of a) intact cylinder and b) stacked discs microwaved inside the 3 kW commercial cavity

Following the commercial microwave oven used to treat cylinder shape of rock samples, the industrial 3 kW power microwave oven is used to investigate the influence of microwave on the surface of the rock. The industrial microwave oven has an open ended horn wave guide known as its antenna inside of a closed cavity. All of the tests performed with that industrial microwave oven have been simulated The results of 3 kW industrial microwave oven came to a conclusion that higher power of microwave energy is required in order to treat the surface of the rock with higher power within lesser amount of tie. Therefore, a specialized fully costume made industrial microwave system is designed and purchased from a highly qualified supplier. The new high power microwave oven will have the ability to generate 15 kW power at 2.45 GHz frequency. This highly specialized microwave system not only has high power capacity but it also has the ability to emit microwaves within two modes of continuous and pulsation.

Due to the mesh generation limitation discussed earlier, an intact block of rock was considered in simulations, rather stacked slabs. Exposure to 3 kW power for 120 s revealed the same heating profile obtained experimentally, which explains clearly why the spalls or chips have the form of a flat bowl (Figure 4-68).

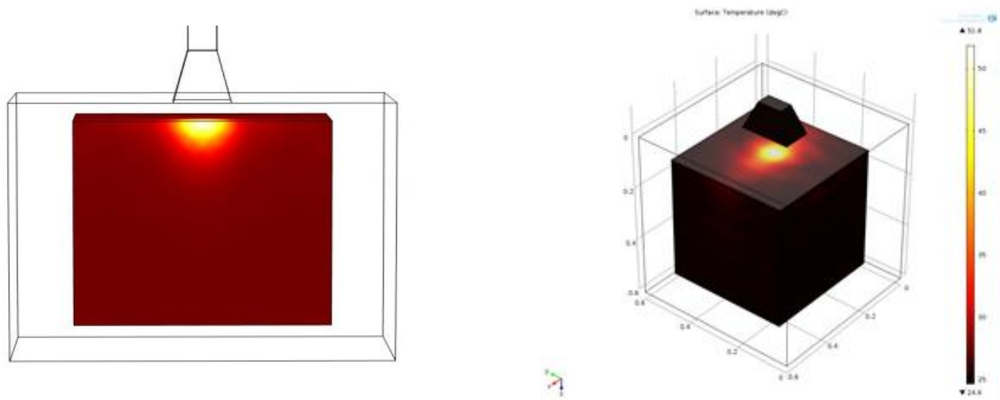

Figure 4-68 Pattern of heating when a block of dielectric is exposed to microwave energy: a) symmetrical half block showing how heat is dissipated and conducted with depth; b) zone affected by microwaves on the surface of the block in front of the antenna

4.6.2 Frequency

In the meantime, extensive simulations had been carried out by the COMSOL software to determine the amount of exposure time that a rock would require to be irradiated at high power intensity. In addition to the 2.45 GHz frequency that is commonly used throughout industries, 0.915 GHz of frequency was also simulated due to its interesting advantages for the research application. Both frequencies simulated were compared with one and the other to define their advantages and disadvantages within the current research application. In order to have a good comparison in between frequencies, a higher frequency is chosen (5.8 GHz) to examine the behavior of rocks in that frequency.

To visualize and better understand the difference of frequencies, the electric field intensity of the microwave energy is plotted along the z axis normal to the antennas aperture (Figure 4-69). This electric field intensity of each frequency is the result of 15 kW power. Eventually, it is understood that the higher the frequency, the higher the electric field intensity; therefore, higher power intensity. However, the application in which the appropriate frequency is supposed to be used, high frequency would not be a wise choice. Higher frequency requires smaller size of waveguide due to smaller wave length; therefore, a smaller size of area is affected on the dielectric by the plane wave application.

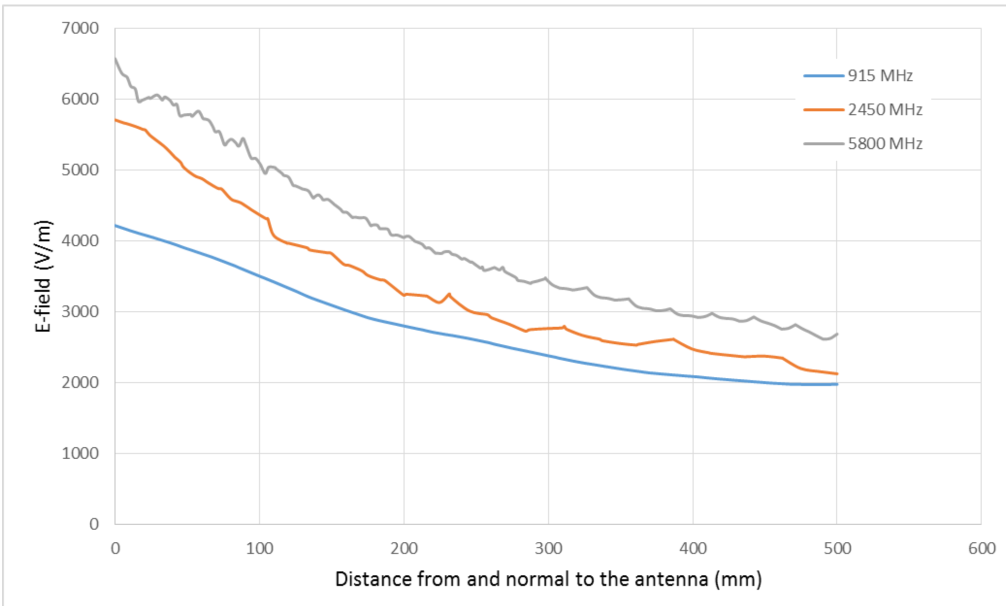

Figure 4-69 Electric field distribution of 0.915, 2.45 and 5.80 GHz frequencies versus distance and normal to the microwave antenna

4.6.3 Temperature Distribution Pattern

Experiments demonstrated that only a specific area (approximately 10 cm diameter) in front of the horn antenna is affected and heated during microwave treatment, because the energy is directed perpendicular to the aperture of the horn waveguide. Heat is concentrated into a small zone due to the very low thermal conductivity of the rock (i.e., more time is required for the heat to dissipate within the rock). Therefore, the diameter of the high temperature zone underneath of the first level (slab) is smaller in size. A lossy load in the vicinity of the antenna aperture absorbs most of the energy; little energy is reflected within the cavity. If the distance from the antenna aperture and the load surface increases, the larger volume of air allows part of the energy to be reflected from the load surface and to bounce around until it is absorbed by the load—by areas other than the spot immediately in front of the antenna. Since electromagnetic intensity decreases exponentially with distance from the waveguide, less energy will reach the load surface of the load; therefore, the chance of reflection of the energy from the surface of the load increases.

The spot heated on every layer observed by experimental procedure was in the center of the slabs, underneath of the antenna and the diameter of heated area corresponds to the dimension of the aperture of the horn wave guide. The diameter of heated spot on the slab on the top level is about 10cm. When the experiments were modelled with COMSOL, the heating distribution within the rock was visualized. Figure 4-70 and Figure 4-71 show the heating distribution along the width of the top slab after being irradiated to microwave for 60 s at 3 kW power and 3 cm from the aperture of the horn waveguide (10 and 15 cm wide, respectively) inside the cavity. . The interior dimensions of the aperture of a standard rectangular wave guide WR340 is 9 cm × 4.5 cm and expands to 15 cm × 10 cm with a horn wave guide. When the slab is exposed to microwave radiation the pattern of heat distribution along the width of the top slab is observed.

Figure 4-70 is showing the heat distribution on the surface of the top slab from the smaller dimension of the horn wave guide considered as the side show. The temperature distribution demonstrates a rapid rise of temperature in the center of the slab. Considering

100°C of temperature as significantly hot surface, in is observed that the significantly high temperature is almost along the small dimension of the horn wave guide. According to the temperature distribution pattern obtained by simulation as well as experimental observation, two zones of high and medium temperature zones can be defined. This is due to the mechanical reaction of the rock being exposed into microwave radiation. The high temperature zone is in the center of the rock's surface in front of the horn antenna that rises quickly as the exposure time increases. This is also observed in both Figure 4-70 and Figure 4-71 as the temperature distribution curves as extremely sharp in the center. In experimental procedure when the temperature of the center rises over 400 degree Celsius in a short period of time at 3 kW power, chipping starts to happen in the form of very thin bowl shape flakes. The maximum diameter these thin flakes can reach is about 5 cm. This zone is considered to be as a high temperature zone exactly in the center in front of the horn antenna. The same condition is applied when studying the Figure 4-71. The high temperature area is almost along the longer dimension of the horn wave guide.

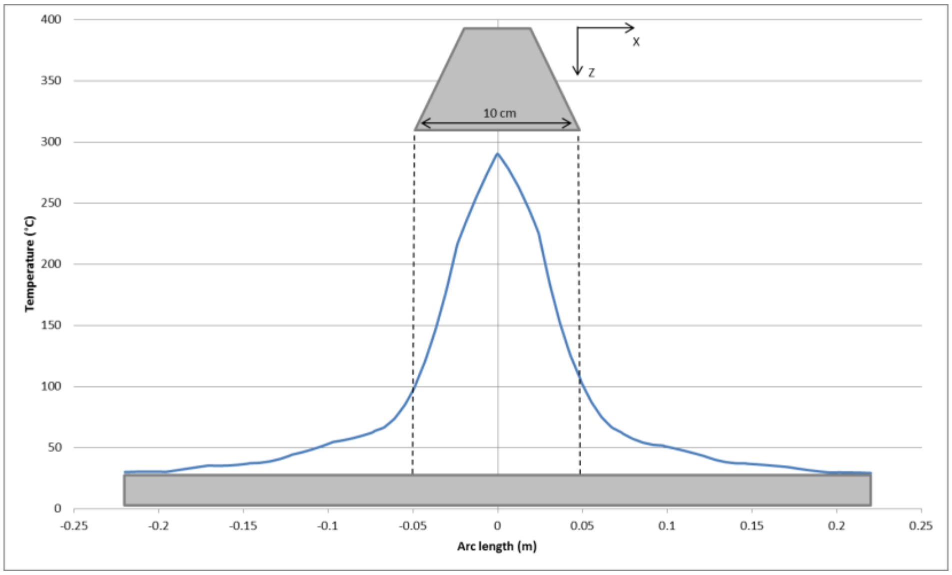

Figure 4-70 Temperature distribution on the rock surface along the length of the horn waveguide

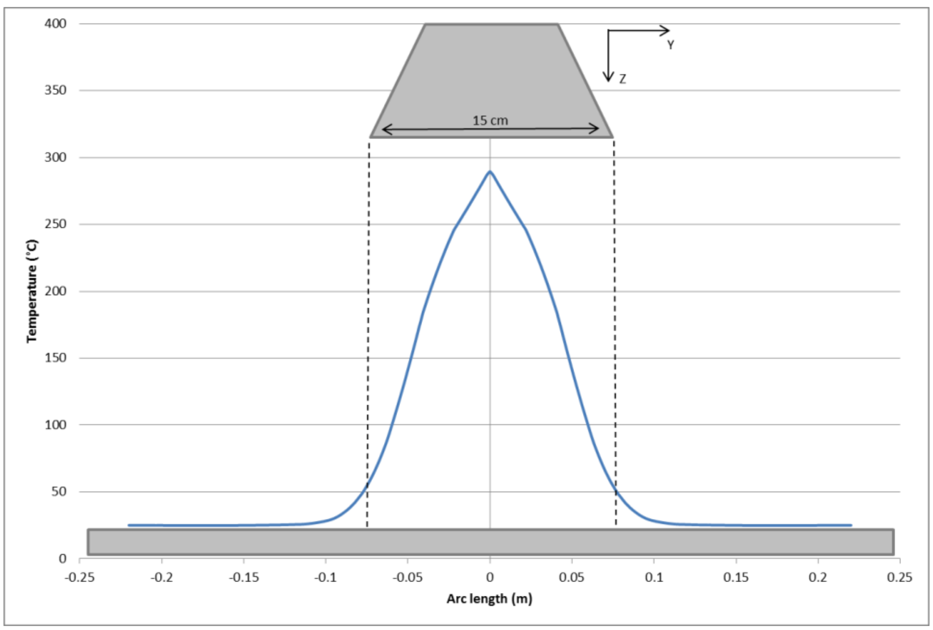

Figure 4-71 Temperature distribution on the rock surface along the width of the horn waveguide

A block of rock placed 3 cm from the antenna and treated at 5, 10 and 15 kW power for 120 s increased in temperature with time and at a faster rate with higher power levels (Figure 4-72). According to Bowen's reaction series (Appendix B), natural felsic silica rich rocks begin to melt at 700°C (gray area in Figure 4-72) (Tarbuck et al., 2011). For solid materials, an elastic and smoothness stage precedes melting; it is not the goal of this research to enter that stage.

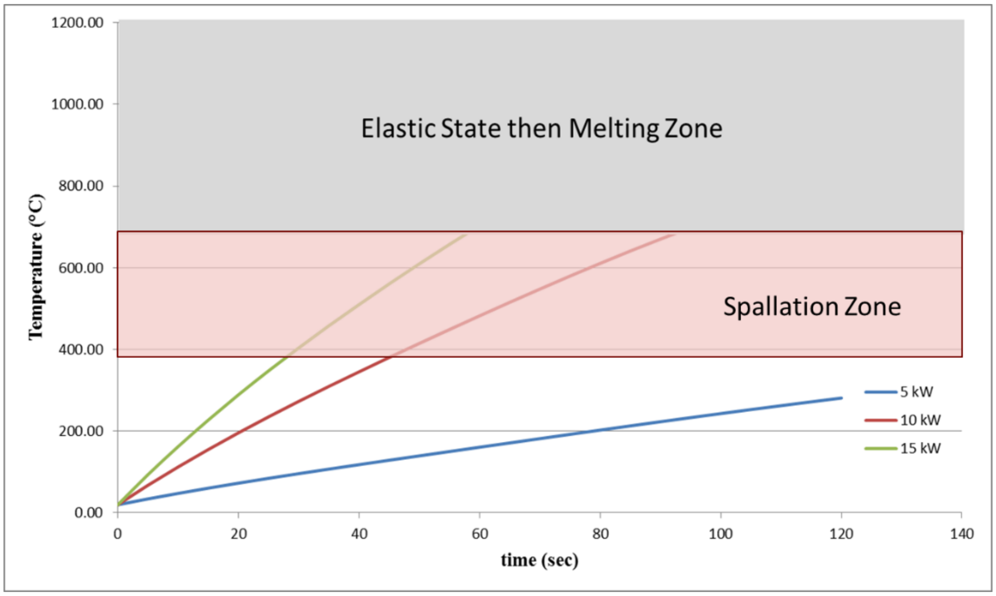

Figure 4-72 Temperature obtained by simulation versus time at three different powers (5, 10 and 15 kW) from 3 cm away from antenna

Interestingly, experiments on the behaviour of basalt #1 showed physical damage at higher power levels, rather than elevated temperature. Mechanical destruction due to thermal stresses occurred between approximately 400 and 700°C. This zone is defined as the spallation zone (pink area in Figure 4-73). The rate at which the rock temperature increases and reaches that zone is also very important. At low power intensities, temperature increases gradually, since heat has enough time to dissipate through the rock sample. At higher power, heat does not have time to dissipate, so the temperature increases rapidly and the spallation zone is reached more quickly.

To better understand how heat is dissipated and conducted within rock irradiated by a plane-wave microwave applicator, the temperature profile of the rock body is shown at every time increment in Figure 4-73. The surface absorbs much of the energy emitted, since the very low thermal conductivity of rock does not allow the heat to be dissipated quickly. As microwave irradiation continues, the surface temperature rises more quickly and higher compared to the inside of the block. This agrees with Mirkovich (1968), who showed the thermal conductivity of 19 igneous rocks was reduced significantly from 100 to 600°C.

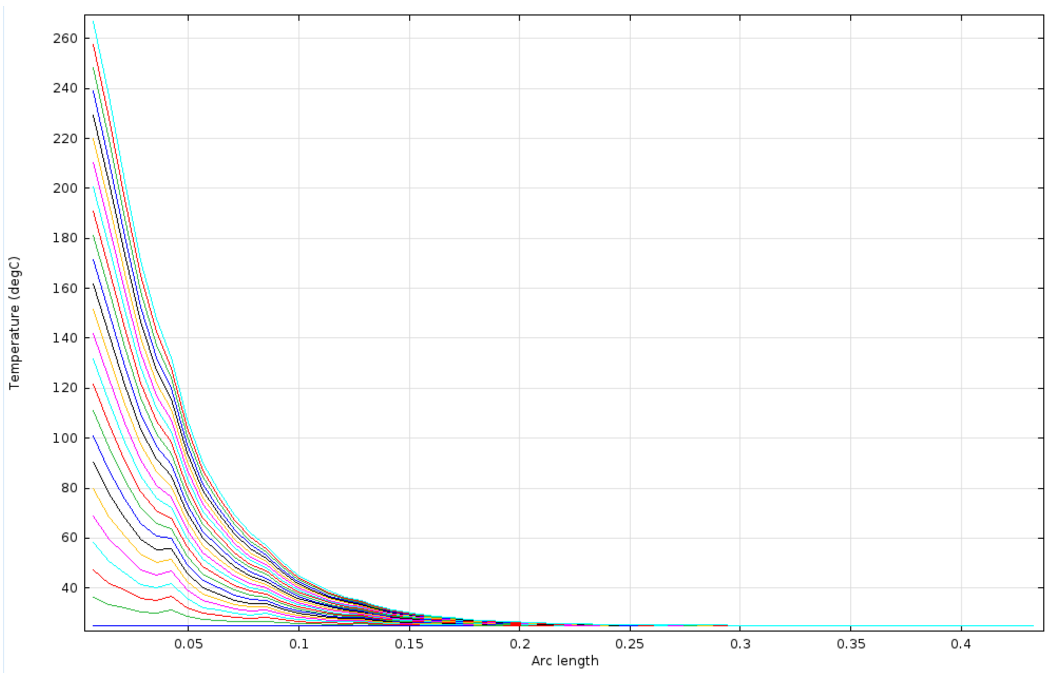

Figure 4-73 Temperature profile sequence within the block of rock for 120 s as the time passes while microwaved at 3 kW power and 3 cm distance.

The experiments at 3 kW power is reproduced numerically in order to have a good comparison with their experimental results. The microwave system set-up as well as the block of rock is defined and constructed accordingly. A fresh block is always used to be irradiated at 3 kW power. The blocks were exposed to microwave irradiation from various distances according to the experimental procedure (3.5, 6, 9.5, 12 and 15 cm). Two sets of experiments are performed one at 60 and the other 120 seconds. Figure 4-74 and Figure 4-75 demonstrate the temperature profiles after 60s and 120 s, respectively, within a block of rock in front of the antenna, normal to the surface towards the depth. The simulated temperature gradient was shallower than the one observed experimentally. Both temperature distributions from the surface toward the center of the block matched the temperature distribution obtained in experiments. The simulated temperatures at 5 cm depth from the surface (theoretical penetration depth) were slightly higher than measured temperatures because the simulated material is considered completely uniform and perfectly homogenous. In reality, the rock is made of different minerals of various particle sizes, each having their own physical, chemical and electrical properties. Each particle influences the amount of microwaves absorbed during treatment.

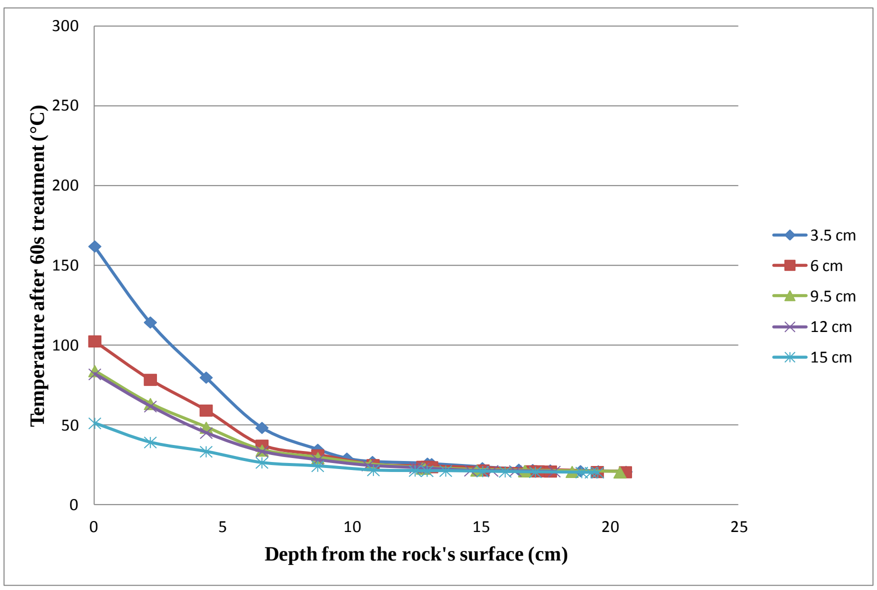

Figure 4-74 Simulated temperature distribution from the surface toward the center after 60 s at 5 distances from the antenna

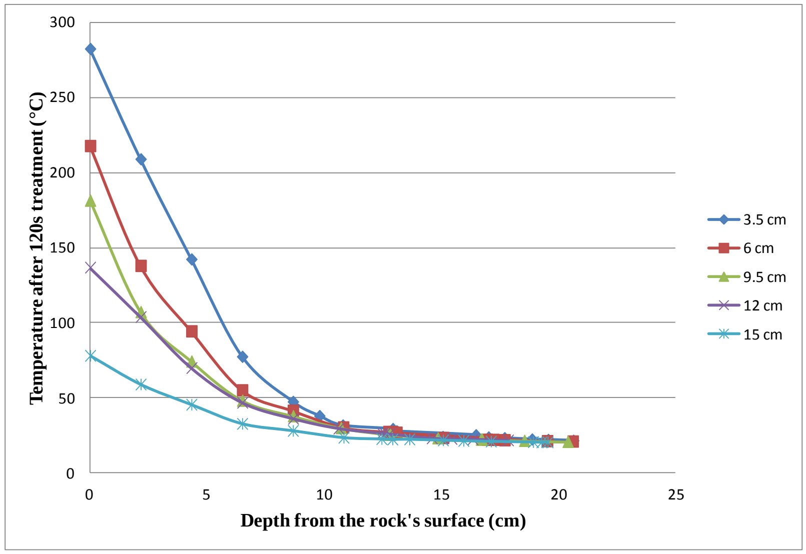

Figure 4-75 Simulated temperature distribution from the surface toward the center after 120 s at 5 distances from the antenna

Simulated and measured surface temperatures were in good agreement (Figure 4-76) after microwave treatment at 3 kW power, and at various distances from the horn aperture. The overall trend showed temperature reduction as the distance from the antenna increased. Energy reflection and losses were also considered in the simulation.

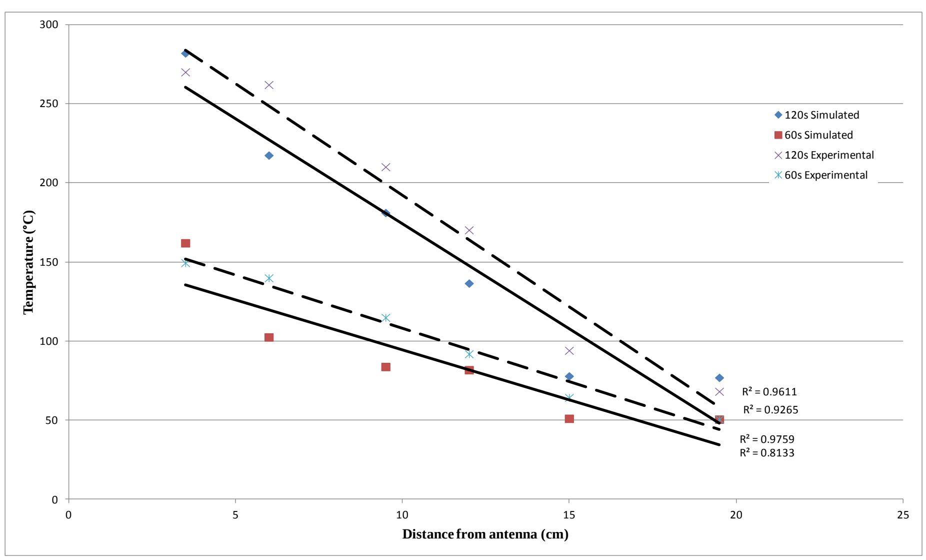

Figure 4-76 Experimental (dashed line) and simulated (solid line) temperature at 3 kW power and various distances from the antenna

The power absorbed and dissipated within a material is directly related to the heating rate of the material (equation 15). Thus, by computing the heating rate of the rock block being irradiated by microwaves in experiments and simulations, the power intensity can be obtained. Regardless of the exposure time, the heating rate and power intensity decreased linearly with distance from the antenna (Figure 4-77). This phenomena make sense, since microwave energy dissipates quickly and loses its intensity once it exits the waveguide into the open air. Although the block of rock is being radiated in a closed cavity larger than a standard wave guide (WR340), the microwave energy exits from a waveguide inside the closed cavity in one direction (perpendicular to aperture). If the subjected rock is closer to the antenna, microwaves lack room to dissipate away from the rock: they will be absorbed by the rock. However, as noted earlier, the power dissipated within the subjected rock is exponentially directed to the electric field at various depths according to equations 16 and 17. Since the electric field intensity diminishes exponentially within a material, the power absorbed also diminishes exponentially. This trend defines the penetration depth.

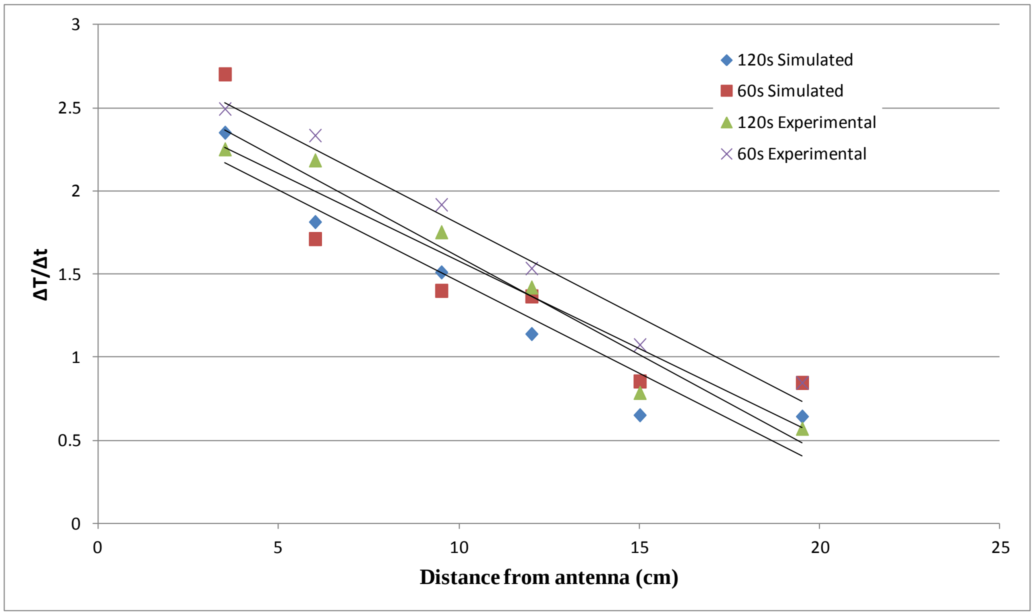

Figure 4-77 Experimental and simulation of temperature difference change on the rock surface over distance from the antenna at 60 s and 120 s of exposure time at 3 kW.

Increasing the power increased the heating rate. Imposing a higher heating rate on rock, which has very low thermal conductivity, induces strong thermal stresses within the rock due to differential expansion ratios of particles. Therefore, the rock surface will spall out more quickly and easily. This has important implications for TBM applications.

4.7 Applicability of Microwave-Assisted TBMs to Hard Rocks

Ongoing development requires more mineral extraction, faster excavations, and quicker project advancement in underground excavations applications. Although the quality of the mechanical equipment currently used to break hard natural rocks is of high quality, it has a limited life span. Weakening the rock prior to mechanical breakage could prolong equipment life and improve the rate and efficiency of excavations. Microwave-assisted mechanical rock breakage has been highlighted as a potential technique within a major collaborative research program between McGill University and NSERC, evaluating explosive-free rock breakage techniques (EFRB).

The objective of this research is to investigate the concept of a microwave-assisted TBM system. Microwave treatment in multi-mode and single mode cavities was investigated. Although cavity systems are not suitable for replicating field conditions, they are useful for small-scale experiments and to characterize samples. Directional plane waves from an open-ended waveguide emulate conditions in the field, where between the tunnel face and the TBM head, a disc-shaped cavity is created. One side is metallic (the TBM head including the disc cutters) and all remaining sides comprise the rock mass or dielectric (Figure 4-78). If using 2.45 GHz frequency horn antenna, a microwave antenna is required for every single disc cutter on the TBM cutter head such that they overlap, covering the complete radius of the tunnel. Each antenna would be placed in front of each disc cutter as shown in Figure 4-79.

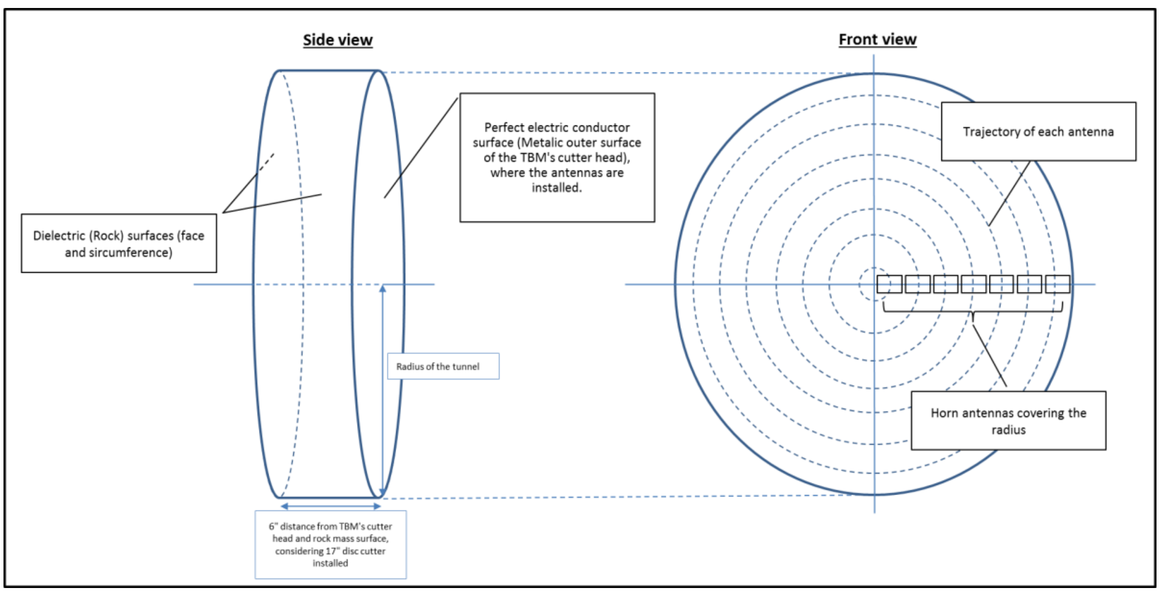

Figure 4-78 The disc-shaped space between the TBM cutter head and tunnel face, as well as disc cutter and antenna trajectory

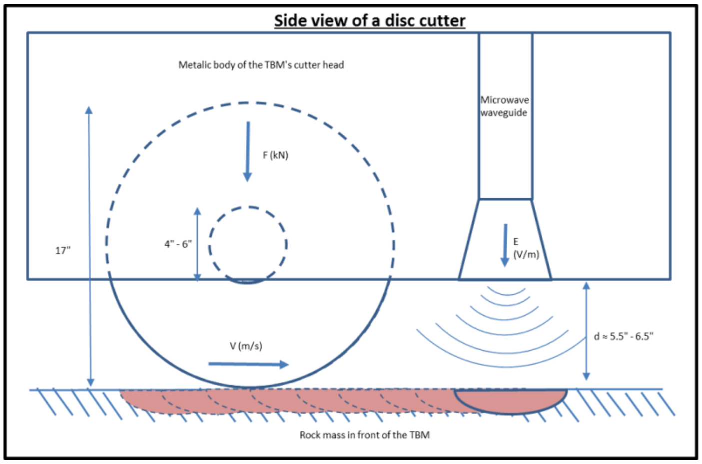

a)

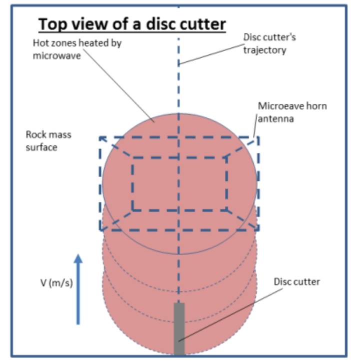

b)

Figure 4-79 a) Side view and b) top view of a horn waveguide antenna installed in front of a disc cutter, including the antenna footprint on the tunnel face

For a frequency of 2.45 GHz, a WR-340 rectangular waveguide is required. The appropriate open-ended horn waveguide installed on the TBM cutter head has a 9 cm × 15 cm base. In front of the antenna base, a circular zone approximately 10 cm in diameter is where the electric field affects the rock surface: heat is generated when the antenna is approximately 6 cm from the surface of the rock. Two proposed designs for a TBM head differ in terms of the antenna location and patterns of distribution. To be actualized, these designs require further investigation.

In design #1, a single horn antenna installed in front of all disc cutters irradiates the rock surface prior to cutting, creating a hot zone in front of the TBM (Figure 4-80). The temperature gradient from the rock surface inward causes thermal expansion, resulting in shear failure at the edges and chipping. Since the hot zone is directly in front of the disc cutters, the shearing stresses stored in the possible failure plane will add up to the shearing stresses caused by the disc cutter running on that zone. This mechanism eases the breakage and cutting procedure; less energy is used by the mechanical tool to break the rock surface.

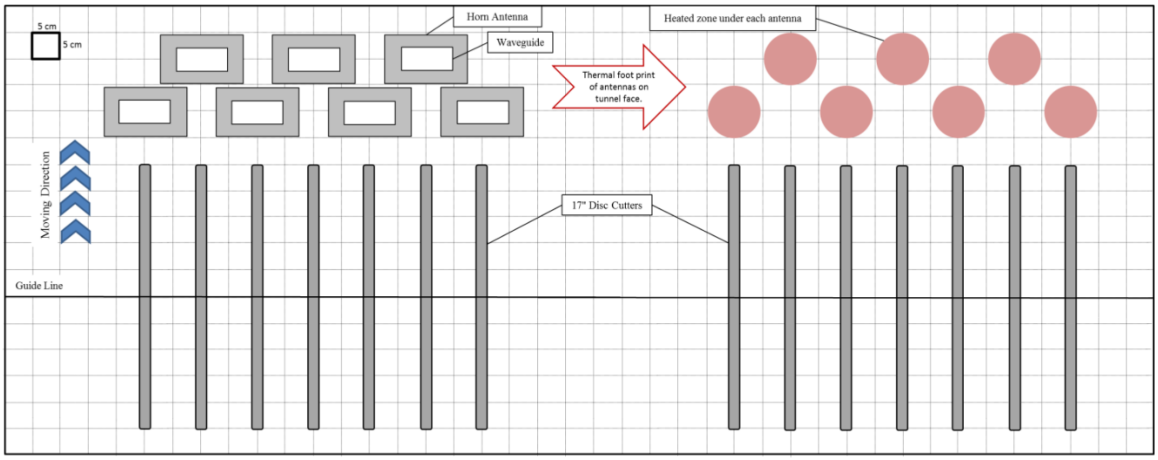

Figure 4-80 Design #1: Top views of a series of disc cutters, showing horn antennas installed in front of the cutters, as well as the antennas footprint

In design #2, a horn antenna installed in front of each disc cutter irradiates the rock surface between each disc cutter as the head rotates (Figure 4-81). The hot zones generated in the middle of the discs cause steep temperature gradients between layers, creating shear stresses on the edges of the hot zones beneath the disc cutter. Combined with the mechanical force of the disc cutter, the shear stresses cause the rock to fail. Relative to design #1, the amount energy required to cut the rock is low, because the hot zones are beneath the dis cutters (in line with the direction of force).

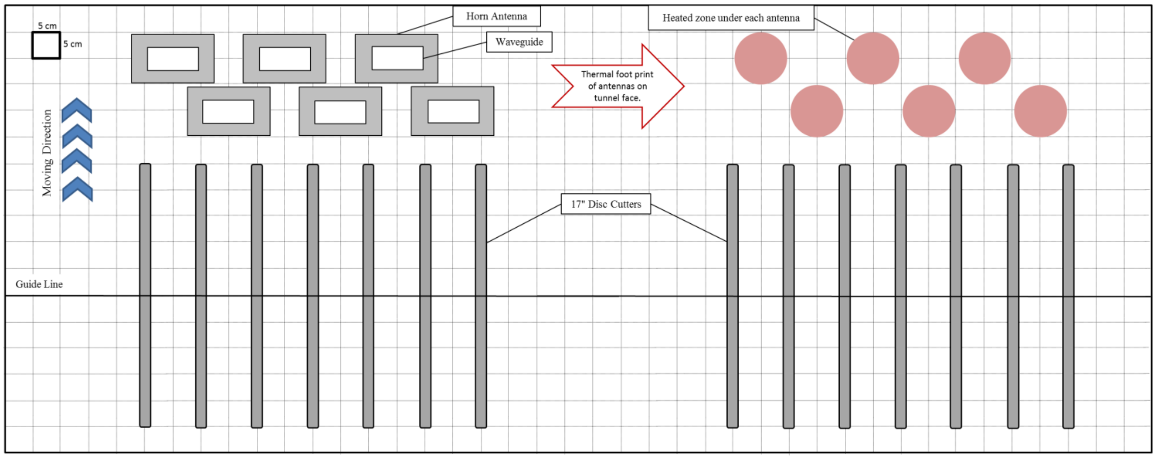

Figure 4-81 Scenario #2: Top views of a series of disc cutters including horn antennas installed in between discs as well as the antennas footprint

Another possible alternative is to use a lower frequency such as 0.915 GHz, since the electrical properties of rocks are independent of frequency. By using a lower frequency, the wavelength increases and the physical dimensions of the pyramidal horn waveguide increase to cover a larger footprint (Figure 4-82). The rock surface for more than one disc can be preconditioned by fewer microwave systems and antennas, saving capital costs. Further, higher power at a cheaper price is available for lower frequency (0.915 GHz) than higher frequency (2.45 GHz) microwave systems. The penetrations depth is deeper for lower frequency microwaves as well, due to the very low thermal conductivity of rocks. The influence of lower frequency microwaves on rocks needs to be investigated further.

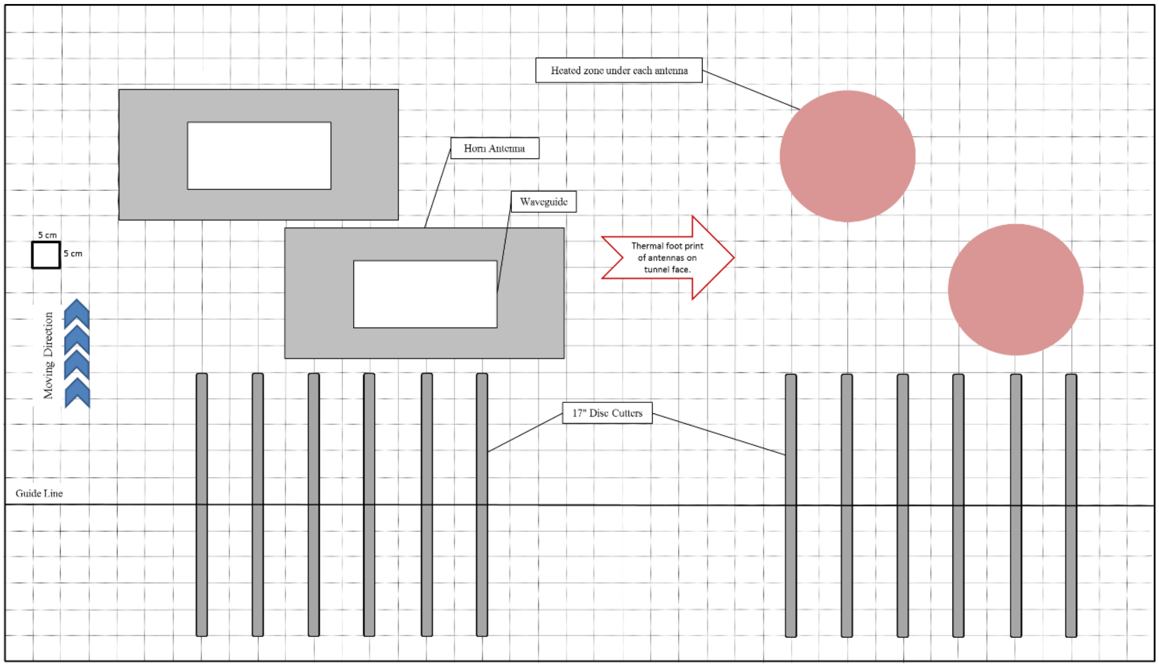

Figure 4-82 Top views of a series of disc cutters including 0.915 GHz horn antennas installed in front of the discs as well as the antennas footprint

Disc cutters on a TBM head are classified as the center cutters, edge cutters (known as gage cutters) and normal cutters distributed on the head in a specific pattern (Cigla et al., 2001). For instance, 7 m diameter TBM generally has 52 disc cutters: 6 center cutters, 10 gage cutters and 36 normal cutters. Microwave antenna(s) could be installed in front of the normal cutters to ease maneuverability. In general, a TBM head rotates at 4–7 rpm, penetrating 3–110 mm during each revolution in hard rock formations (Gertsch et al., 2007). Directional plan microwaves irradiating the surface ahead of the cutters would increase rock breakage and increase the penetration rate of the discs.

Since the electric field travels along the y axis through the waveguide, the smallest dimensions would be towards the rotation direction of the head. The smallest dimensions of a pyramidal horn waveguide for 0.915 GHz is 25 cm and for 2.45 GHz is 10 cm. Considering a TBM 8 m in diameter, with a rotation speed of 4 rpm, the time for the smallest dimension of the horn waveguide to pass a given point on the tunnel face can be calculated as in Figure 4-83. There is a time difference between antennas close to and farther from the center; the power for antennas close to the center can be adjusted down.

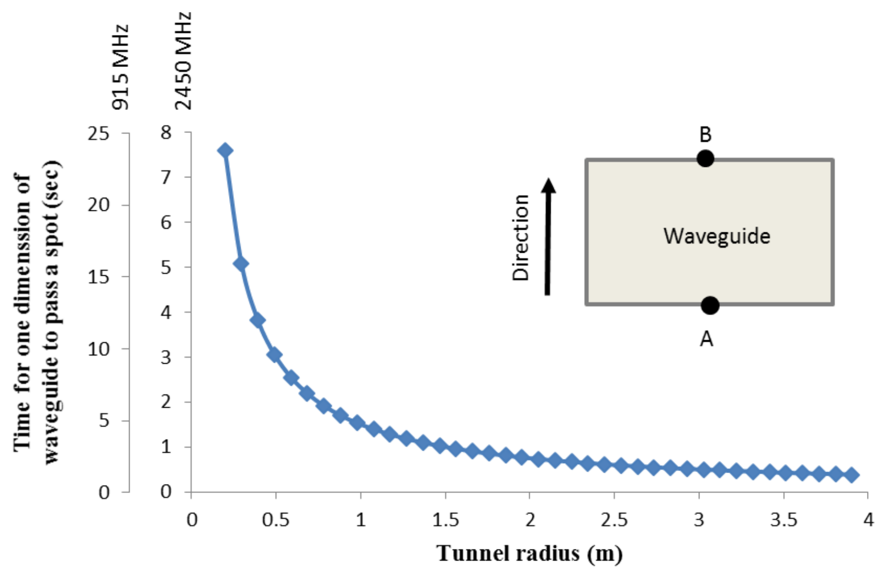

Figure 4-83 The time needed for the shorter dimension of a horn antenna to pass a point along the radius (the time for point A to reach point B) assuming 8 m diameter tunnel and 4 rpm

4.7.1 Benefits

The use of microwave-assisted TBMs to precondition the tunnel face prior to cutting has advantages such as:

- Rapid ON and OFF switching and quick warm-up
- Does not consume fossil fuel, saving operating costs
- Does not produce fossil fuel emissions in underground spaces, improving worker safety and saving emission control and ventilation costs
- Could increase the penetration rate
- Could decrease wear of mechanical parts on cutting machines

- The fractured pieces produced by the TBM are weakened by microwave irradiation and would require less energy to crush during processing. Moreover, recovery and liberation of valuable elements could be improved after the mineral processing sequence (Scott, 2006; Scott et al., 2008; Veasey & Wills, 1991; Fitzgibbon & Veasey, 1990).

Using 0.915 GHz of frequency instead of 2.45 GHz has its own advantage such as:

- 0.915 GHz has longer wavelength than the one of 2.45 GHz; therefore penetrates the rock further inside to pre-heat the face before the machine reaches it
- Has larger waveguide; therefore, its heating footprint is larger and covers an area for three disc cutter
- It is more common in other industries so it is easier to find one in the market
- Manufacturers have no difficulties building high power (over 100 of kW) at a reasonable price much cheaper than system at 2.45 GHz

4.7.2 Economics

The future leads today's mining and civil underground excavations to be more efficient, quick and productive. Many major corporations (e.g., Atlas Copco, Anglo American, Rio Tinto, Sandvik, Robbins Company) are collaborating to develop explosive-free mechanical equipment, which can continuously breaks rocks. Although using conventional explosives to break rocks is inexpensive, it has disadvantages (e.g., safety, environmental impacts, time-consuming) that limit the productivity and advancement rate of a project.

The most efficient technique, toward which underground civil project are advancing, is continuous excavation. TBMs are widely used in civil applications. Mining is also advancing toward using TBMs to increase productivity (Robbins Company, 2012). Microwave-assisted TBMs could make a project more economical. Although each microwave system to be installed can make the mechanical equipment more expensive, the project may become more economical as well as more efficient and productive by considering the section of mine – to – mill. BWI of the rock can be reduced up to 90% when the rock is subjected to microwave irradiation (Walkiewicz et al., 1988, 1991, 1993; Marland et al., 2000; Wang & Forssberg, 2000; Vorster et al., 2001; Kingman et al., 2004; Amankwah et al., 2005; Bradshawet al., 2007). Thus the resistance to crushing is reduced, saving energy consumption by the crushing sequence. Further, the liberation of elements and production recovery increases after rock is treated with microwave energy (Scott, 2006; Scott et al., 2008; Veasey & Wills, 1991; Fitzgibbon & Veasey, 1990).

This study shows that high-power microwave treatment induces mechanical damage to the rock surface, which should ease breakage for the mechanical disc cutter of the TBM and reduce disc cutter wear. The fresh feed for the mineral processing plant would already be in small sizes. Combined with the damage induced to the pieces of rocks, the size of the crusher in the mineral processing plant could be significantly reduced.

If TBMs are assisted by microwaves, the crushed pieces of rocks produced by the machine might also necessitate changes to the design of the mineral processing plant (Figure 4-84), making it more economical in terms of feasibility and production. In a conventional mineral processing plant, materials are sorted into appropriate sizes after crushing. Over-sized pieces are returned to the crusher (called the circulating load). The amount of circulating load determines the size of the crusher. Microwave-assisted TBMs have the potential to reduce the circulating load, leading to an even smaller crusher size and an energy savings. Since the pieces are already smaller in size, a primary screening could be performed before the crusher to classify the loads into two parts. One part would go through the crusher, but the undersized feed could go directly to the mill (passing fraction). The primary screening would reduce the load going through crushing and secondary screening.

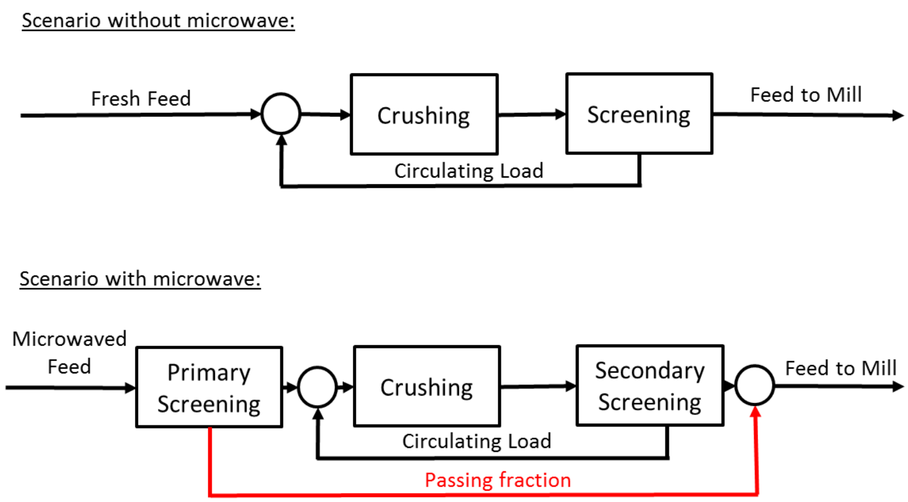

Figure 4-84 Mineral processing design without (top) and with (bottom) microwave treatment

4.7.3 Safety

Although microwaves are hazardous for human health, microwave ovens are in nearly every home kitchen and are regularly used. The very small amount of microwave leakage that occurs is not hazardous to human health. Domestic microwaves are well developed and designed for safe operation. The same attention could be devoted to microwave-assisted TBMs, so the underground environment can be safe. Furthermore, the microwave antennas irradiate only in front of the TBM head, which is metallic and totally reflects the microwaves. All other sides in front of the head are the rock mass, which either absorbs the microwaves or transmit them. To prevent the remaining small amount of microwaves from leaking from the head or the edge of the tunnel, perforated plates, chains or springs could be used to absorb excess microwaves.

Chapter 5 Conclusions and Future Work

Initial Physical properties (volumetric expansion ratio of minerals, mineralogy, petrology of rock samples, electrical properties) and mechanical properties (uniaxial compressive strength, Brazilian tensile strength tests) have been conducted on samples in treated and untreated conditions with microwave. A commercial microwave oven was used for initial experimentation to treat samples with microwaves, which is considered a multi-mode configuration. It is understood that physical and electrical properties are influencing parameter defining the amount of microwave energy absorption of rocks. Mineralogy of rocks can be a rough indicator whether a rock absorbs microwave energy or not. The electrical properties are the first most crucial parameters specifying the absorption of microwave energy.

The electrical properties of basalt, norite and granite were independent of frequency from 10 MHz to 12 GHz. The choice of apparatus and technique is important. The parallel plate method was suitable for frequencies < 1 GHz and the resonant cavity method was suitable for frequencies > 1 GHz. The coaxial probe method tended to overestimate the loss factor and was not accurate if water was present. Therefore, is not recommended to measure the electrical properties of the rock types tested. Basalt had a loss factor of approximately 1, which makes it a good absorber of microwaves. Granite has its loss factor of approximately 0.01 and considered as completely transparent to microwaves, since it contains >70% silicates.

Commercial microwave ovens are designed to have multi-mode cavity and a chaotic energy distribution inside the cavity. In the concept and scope of the current research a directional plane wave microwave irradiated from a horn waveguide antenna is designed in order to be a good representation of an actual in-field replica. Slabs of intrusive basalt sample have been stacked on top of each other in order to stimulate a complete intact block of basalt sample to be irradiated with microwaves. The surface of the rock sample had been designed to be much larger than the aperture of the microwave horn antenna so the waves would be irradiated toward one direction normal to the rock's surface. The surface of basalt specimens have been exposed to 2.45 GHz of frequency microwaves at 3 power level from 3 to 15 kilo-Watts power within 60 sec and 120 sec. The electric field and wave propagation have been investigated within a cavity when microwaves are radiated from an open ended horn wave guide as antenna. The temperature profile within the rock specimens are being investigated experimentally as well as simulation. It has been concluded that the results obtained from simulation are validated by experimental results. The influence of microwaves on dry and saturated conditions of the basalt sample have also been studied to. Although the extremely low permeability and porosity of basalt meant that the water content was low, even if saturated (<1.5%), a thin film of water on the surface of the rock increased surface temperatures relative to dry samples, particularly at longer distances from the microwave antenna.

Microwave power levels were the key factor influencing the rock surface temperature in terms of heating rate and maximum temperatures achieved. Higher power intensity for the microwave system is required in order to have the same damage at higher distances from antenna to the rock's surface as with lower power at shorter distance.

The heating rate strongly influenced the mechanical destruction of the rock. The spallation process is independent of the thermal gradient inside the rock but it is greatly affected by the temperature difference at a certain depth inside the rock; Brittle rocks are more susceptible to be spalled or shattered; whereas, ductile rocks tend to initiate cracks. Above 300 kJ energy emitted to the rock spallation is observed. The spallation mechanism is initiated by biaxial compressive stresses, as well as shear failure on the edges of spalled pieces. Furthermore, it has also been concluded that higher power intensity has greater influence on the rock's surface when exposed to microwaves. Therefore, higher power intensity for the microwave system is required in order to have the same damage at higher distances from antenna to the rock's surface as with lower power at shorter distance.

The concept of microwave-assisted TBMs appears to be potentially feasible. Microwaves greatly influence metal-based formations, since metal based minerals are strong absorbers of microwave energy. The current research showed the concept of using microwave is non-metallic based rocks to pre-condition the rock prior to be cut by a disc cutter. Considering the concept of mine – to – mill operation in continuous mining method, microwave-assisted TBM turns to be economically viable.

An electric field intensity of 0.915 GHz frequency is recommended, instead of the more commonly used 2.45 GHz frequency. The waveguide of 0.915 GHz frequency has a larger dimensions and can more efficiently treat a larger surface area of the rock mass; whereas, the 2.45 GHz waveguide's surface area coverage is about 12 times smaller.

5.1 Future Work

- Treat large intact blocks of basalt #1 sample at high power level to evaluate the effect of confinement pressure from the rock itself.
- Treat at least four types of granite samples into the microwave energy in order to have a good understanding on the difference of the granite composition and mineralogy.
- Conduct computerized axial tomography scan and image analysis to study the micro-crack distribution inside rocks treated by microwaves.
- Conduct scratch test and linear disc cutter on microwave treated blocks of rocks to obtain practical results on the performance of a mechanical rock cutter on rock surfaces preconditioned by microwave irradiation.
- Determine the relationship between temperature profile and crack density induced by microwaves to develop to aid simulations.
- Investigate the influence of microwave irradiation on mechanical properties of rocks at lower frequency (0.915 GHz).

Chapter 6 References

Agilent Technology Inc. (2006). Agilent basics of measuring the dielectric properties of materials. Application note. USA 5989-2589EN

Amankwah, R.K., Khan, A.U., Pickles, C.A. and Yen, W.T. (2005). Improved Grindability and Gold Liberation by Microwave Pretreatment of a Free-milling Gold Ore. Transactions of The Institution of Mining and Metallurgy Section C-mineral Processing and Extractive Metallurgy, 114, C30-C36.

Arrieta, A., Otaegui, D., Zubia, A., Cossio, F. P., Diaz-Ortiz, A., De La Hoz, A., Herrero, M.A., Prieto, P., Foces-Foces, C., Pizarro, J L. and Arriortua, M.I. (2007). Solvent-free thermal and microwave-assisted [3 + 2] cycloadditions between stabilized azomethine ylides and nitrostyrenes. An experimental and theoretical study. Journal of Organic Chemistry. 72: 4313-4322.

ASTM D3967-05, Standard test method for splitting tensile strength of intact rock core specimens. Annual book of ASTM standards, Soil and Rock D18.12 Rock Mechanics.

ASTM D7012-04, Standard test method for compressive strength and elastic moduli of intact rock core specimens under varying states of stress and temperatures. Annual book of ASTM standards, Soil and Rock D18.12 Rock Mechanics.

Atomic Energy of Canada Ltd. and Voss Associates Engineering Ltd. (1990). Microwave and minerals. Ottawa, ON: Queen`s Printer. ISBN 0-7729-6584-6.

Ayappa, K.G., Davis, H.T., Crapiste, G., Davis, E.J. and Gordon, J. (1991). Microwave heating: An evaluation of power formulations. Chemical Engineering Science, 46, 1005-1016.

Blindheim, O. (1979). Borability predictions for tunnelling. PhD thesis. Norwege: Department of Geological Engineering, The Norwegian Institute of Technology.

Boaly, B.A. and Weiner, J.H., (1960). Theory of Thermal Stresses, John Wiley and Sons, New York.

Bond, E.J., Li, X., Hagness, S.C. and Van Veen, B.D. (2003). Microwave imaging via space-time beam forming for early detection of breast cancer. IEEE Transaction on Antennas and Propagation. 51, 1690-1705.

Bradshaw, S., Louw, W., Van der Merwe, C., Reader, H., Kingman, S., Celuch, M. and Kijewska, W. (2007). Techno-economic considerations in the commercial microwave processing of mineral ores. Journal of Microwave Power & Electromagnetic Energy, Vol. 40, No. 4, pp. 228 – 240.

Brown, E.T. (1974). Fracture of rock under uniform biaxial compression. Proc. 3rd. International Society of Rock Mechanics Congress, Denver, Vol. 2A, pp. 111-117.

Cao, W. (2012). The development and application of microwave heating. InTech, Croatia. ISBN 978-953-51-0835-1. DOI: 10.5772/2619.

Carmichael, R. S. (1988). Practical handbook of physical properties of rocks and minerals. Boca Raton: CRC Press.

Carslaw, H.S. and Jaeger, J.C. (1959). Condition of heat in solids. Oxford University, United Kingdom, Press.

Chen, T.T.; Dutrizac, J.E.; Haque, K.E; Wyslouzil, W. and Kashyap, S. (1984). Relative trasparansy of minerals to microwave radiation. Canadian Metallurgical Quarterly, 23(3), 349-351.

Church, R.H., Webb, W.E. and Salsman, J.B. (1988). Dielectric properties of low-lost minerals. United-States Department of the Interior and The Bureau of Mines, Report of Investigation RI-9194.

Cigla, M., Yagiz, S., & Ozdemir, L. (2001). Application of tunnel boring machines in underground mine development. Proceedings of 17th International mining congress and exhibition of Turkey, (pp. 155-164). Ankara.

DeJonghe, L. and Rahaman, M. (2003). Sintering of Ceramics. In S. e. al., Handbook of Advanced Ceramics. Elsevier Inc.

Fitzgibbon, K.E. and Veasey, T.J. (1990). Thermally assisted liberation – A review. Minerals Engineering, 3(1/2), 181-185.

Fowel, R.J. and McFeat-Smith, I., (1976). Factors Influencing the Cutting Peerformance of Selective Tunnelling Machine. Tunnelling Institute of Mining and Metallurgy, UK, Vol. 76, pp. 3-11.

Frenzel, C., Kasling, H., & Thuro, K. (2008). Factors influencing disc cutter wear. In V. f. KG, Geomechanik und Tunnelbau (Vol. 1, pp. 55-60). Berlin: Ernst & Sohn.

Gabriel, C., Gabriel, S., Grant, E.H., Halstead, B.S.J. and Mingos, D.M.P. (1998). Dielectric parameters relevant to microwave dielectric heating. Chem. Soc. Rev., 27, 213-224. DOI: 10.1039/A827213Z

Gary Ong, K.C. and Akbarnezhad, A. (2015. Microwave-Assisted Concrete Technology: Production, Demolition and Recycling. CRC Press Taylor & Francis Group, Boca Raton, ISBN 13-978-1-4665-8394-8.

Gertsch, R., Gertsch, L. and Rostami, J. (2007). Disc cutting tests in Colorado re granite: Implications for TBM performance prediction. International Journal of Rock Mechanics and Mining Sciences. Vol. 44, pp. 238 – 246.

Gray, W.M. (1965). Surface spalling by thermal stresses in rock. Proc. Rock Mech. Symp. Mines Branch Dept. Mines and Technical Surveys, Ottawa, 85-106.

Griffiths, D. (1999). Introduction to electromagnetic (3rd edition). Prentice Hall, International.

Gwarek, W., and Celuch-Marcysiak, M. (2000). A review of microwave power applications in industry and research. Warszawa, ul.Nowowiejska: Instytut Radioelektroniki Politechniki Warszawskiej.

Haque, K.E. (1999). Microwave energy for mineral treatment processes—a brief review. International Journal of Mineral Processing, 57(1), 1-24.

Hartman, H.L. (1992). SME Mining engineering handbook (2nd edition). United States: Society for Mining, Metallurgy, and Exploration.

Hasselman D.P.H. (1969). Undefined theory of thermal shock fracture initiation and crack propagation in brittle ceramics. Journal of American Ceramic Society. Vol. 52 (11), pp. 600 - 604.

Heiniö, M. (1999). Rock excavation handbook. Sandvik Tamrock

Howarth, D.F., Adamson, W.R. and Berndt, R.J., (1986). Correlation of Model Tunnel Boring and Drilling Machine Performances with Rock Properties. International Journal of Rock Mechanics and Mining Science, Vol. 23, 2, pp. 171-175.

Hoek, E. M. and Bieniawski, Z. T. (1965). Brittle fracture propagation in rock under compression. International Journal of Fracture Mechanics, 1(3), 135-155.

IEEE International Committee on Electromagnetic Safety (SCC39). (2006). IEEE Standard for safety levels with respect to human exposure to radio frequency electromagnetic fields, 3 kHz to 300 GHz. New York: The Institute of Electrical and Electronics Engineers Inc.

ISRM, (1978). Suggested methods for determining tensile strength of rock materials. International Journal of Rock Mechanics and Mining Science and Geomechanics Abstracts, 15, 99-103.

ISRM, (1979). Suggested methods for determining the uniaxial compressive strength and deformability of rock materials. International Journal of Rock Mechanics and Mining Science and Geomechanics Abstracts, 16(2), 137-140.

Jerby, E. and Dikhtyar, V. (2000). Method and device for drilling, cutting, nailing and jointing solid non-conductive materials using microwave radiation. United States Patent 6,114,676.

Jerby, E. and Thompson, A.M. (2004). Microwave Drilling of Ceramic Thermal-Barrier Coatings. Journal of American Ceramic Scociety, 87(2), 308 – 310.

Jerby, E.; Aktushev, O. and Dikhtyar, V. (2004). Theoretical analysis of the microwave drill near-field localized heating effect. Journal of Applied Physics, 97, 1-7.

Jerby, E.; Dikhtyar, V. and Aktushev, O. (2003). Microwave drill for ceramics. Ceramic Bulletin, 82(35), 1 – 7.

Jerby, E., Dikhtyar, V., Aktushev, O. and Grosglick, U. (2002). The microwave drill. Science, 298, 587-589.

Jing Tao, S. and Tianxing W. (2011). Review of China's bioethanol development and a case study of fuel supply, demand and distribution of bioethanol expansion by national application of E10. Biomass and Bioenergy, Elsevier. 35 (9), 3810 - 3829.

Jones, D. A., Lelyveld, T. P., Mavrofidis, S. D., Kingman, S. W. and Miles, N. J. (2002). Microwave heating applications in environmental engineering — a review. Resources, Conservation and rRcycling, 34, 75-90.

Jones, D.A.; Kingman, S.W.; Whittles, D.N. and Lowndes, I.S. (2007). The influence of microwave energy delivery method on strength reduction in ore samples. Chemical Engineering and Processing, 46, 291 – 299.

Kandev, N., Lemire, C., Auger, S., Cote, D., Betournay, M.C. and LeBlanc, G., (2013). Design of a new plasma torch starter for mining applications. Canada Center for Mineral and Energy Technology (Canmet) Mining report 013-012(CF).

Kingman, S. W. (2005). Pre-treatment of multi-phase materials using high field strength electromagnetic waves. United States Patent: 0,236,403.

Kingman, S.W. and Rowson, N.A. (1998). Microwave treatment of minerals. Minerals Engineering, 11(11), 1081 – 1087.

Kingman, S.W., Corfield, G.M. and Rowson, N.A. (1998). Effects of microwave radiation upon the mineralogy and magnetic processing of a massive Norwegian ilmenite ore. Magnetic and Electrical Separation, 9, 131-148.

Kingman, S.W., Vorster, W. and Rowson, N.A. (2000). The influence of mineralogy on microwave-assisted grinding. Minerals Engineering, 13 (3), 313 - 327.

Kingman, S.W., Jackson, K., Cumbane, A., Bradshaw, S.M., Rowson, N.A. and Greenwood, R. (2004a). Recent developments in microwave-assisted comminution. International Journal of Mineral Processing, 74, 71-83.

Kingman, S.W., Jackson, K., Bradshaw, S.M., Rowson, N.A. and Greenwood, R. (2004b). An investigation into the influence of microwave treatment on mineral ore comminution. Powder Technology, 146, 176-184.

Klauenberg, B., & Miklavčič, D. (2000). Radio Frequency Radiation Dosimetry and Its Relationship to the Biological Effects of Electromagnetic Fields. The Netherlands: Kluwer Academic Publishers.

Lauriello, P.J. (1974). Application of a convective heat source to the thermal fracturing of rock. International Journal of Rock Mechanics and Mining Science and Geomechanics Abstracts, 11, 75-81.

Lauriello, P.J. and Fritsch, C.A. (1974). Design and Economic Constraints of Thermal Rock Weakening Techniques. International Journal of Rock Mechanics and Mineral Science & Geomechanics, 11, 31 – 39.

Lindroth, D.P., Berglund, W.R., Morrell, R.J. and Blair, J.R. (1992). Microwave-assisted drilling in hard rock. Mining Engineering Journal, 44, 1159-1163.

Lindroth, D.P., Berglund, W.R., Morrell, R.J. and Blair, J.R. (1993). Microwave assisted drilling in hard rock. Tunnels and Tunnelling, 25(6), 24-27.

Lindroth, D.P., Berglund, W.R., Morrell, R.J. and Blair, J.R. (1991). Microwave-assisted hard rock cutting. United States Patent 5,003,144.

Marland, S., Han, B., Merchant, A. and Rowson, N. (2000). The effect of microwave radiation on coal grindability. Fuel, 79, 1283-1288.

Maurer, W.C. (1968). Novel Drilling Techniques. London: Pergamon Press.

McFeat-Smith, I. (1977). Rock property testing for the assessment of tunnelling machine performance. 29-33.

Meredith, R. (1998). Engineers' Handbook of Industrial Microwave Heating. Institution of Electrical Engineers, 1st Edition, London, ISBN 0852969163.

Metaxas, A.C. and Meredith, R.J. (1983). Industrial Microwave Heating. Peter Peregrinus, 1st Edition.

Michalakopoulos, T. N., Anagnostou, V. G., Bassanou, M. E. and Panagiotou, G.N. (2006). The influence of steel styli hardness on the CERCHAR abrasiveness index value. International Journal of Rock Mechanics and Mining Sciences, 43, 321-327.

Mirkovich, V.V. (1968), Experimental study relating thermal conductivity to thermal piercing, International Journal of Rock Mechanics and Mining Science, Pergamon Press, Vol. 5, pp. 205-218

Nejati, H. (2014). Analysis of physical properties and thermos-mechanical induced fractures of rocks subjected to microwave radiation. Unpublished doctoral dissertation, McGill University, Canada.

Osepchuck, J.M. (1984). A History of Microwave Heating Applications. Raytheon Research Division.

Pang, S., Goldsmith, W., and Hood, M. (1989). A force indentation model for brittle rocks. Journal of Rock Mechanics and Rock Engineering, 22, 127-148.

Passchier, C.W. and Trouw, R.A.J. (2005). Micro-Tectonics. Germany: Springer.

Pfafflin, J. (1992). Encyclopedia of Environmental Science and Engineering, 3rd edition, updated and revised (Vol. 2). Taylor & Francis.

Plinninger, R. J. and Restner, U. (2008). Abrasiveness testing, Quo Vadis? – A commented overview of abrasiveness testing methods. Geomechanik und tunnelbau, 1(1), 61-70.

Plinninger, R. J.; Kasling, H. and Thuro, K. (2004). Wear prediction in hard rock excavation using the CERCHAR abrasiveness index (CAI). EUROCK 2004 and 53rd Geomechanics Colloquium.

Plinninger, R. J.; Kasling, H.; Thuro, K. and Spaun, G. (2003). Testing conditions and geomechanical properties influencing the CERCHAR abrasiveness index (CAI) value. International journal of rock mechanics and Mining Science, 40, 259-263.

Raytek Corporation, (1999). High Performance Infrared Thermometer Manual. Rayteck Corporation, USA.

Res, J., Wladzielczyk, K. and Ghose, A.K. (2003). Environment-Friendly Techniques of Rock Breaking. India: A.A. Balkema.

Robbins Company, (2012). Mechanized Mining: Are TBMs the Way into the Future? Munnel Magazine, 05/2012, 12-18.

Roxborough, F.F. and Philips, H.R., (1975). Rock Excavation by Disc Cutter. International Journal of Rock Mechanics and Mining Science and Abstracts. Vol. 12, pp. 361-366.

Santamarina, J. C. (1989). Rock excavation with microwaves; A literature review. Foundation engineering: current principles and practices proceedings, Evanston, Illinois, 459 – 473.

Satish, H. (2005). Exploring microwave-assisted rock breakage for possible space mining applications. Mechanical Engineering, Masters of Engineering Thesis, McGill University.

Satish, H.; Ouellet, J.; Raghavan, V. and Radziszewski, P. (2006). Investigating microwave-assisted rock breakage for possible space mining applications. Mining technology, 115(1), 34 – 40.

Saxena, A.K. (2009). Electromagnetic Theory and Applications. Alpha Science International, 1st Edition.

Schön, J.H. (2004). Physical Properties of Rocks: Fundamentals and Principles of Petrophysics. Amsterdam: Elsevier.

Scott, G. (2006). Microwave pretreatment of a low grade copper ore to enhance milling performance and liberation. Chemical Masters of Science in Engineering, Stellenbosch University.

Scott, G., Bradshaw, S.M. and Eksteen, J.J. (2008). The effect of microwave pretreatment on the liberation of a copper carbonatite ore after milling. International Journal of Mineral Processing, 85, 121 – 128.

Somerton, W. (1992). Thermal properties and temperature-related behavior of rock/fluid systems. Amsterdam; New York: Elsevier, ISBN 0444890017.

Steneck, N., Cook, H., Vander, A., & Kane, G. (1980). The origin of U.S. safety standards for microwave radiation. Science, 208, 1230-1237.

Suana, M and Peters, T. J. (1982). The CERCHAR abrasivity index and its relation to rock mineralogy and petrography. Rock Mechanics, 15, 1-7.

Sutton, W.H. (1989). Microwave Processing of Ceramic Materials. Ceramic Bulltin. 68(2), 376-386

Tarbuck, E.J., Lutgens, F.K., Tsujita, C.J. and Hicock, S. (2011). Earth: An Introduction to Physical Geology, 3rd Canadian Ed., Pearson Canada, ISBN 978-0-13-704776-5

Ulaby, F.T., Bengal, T.,East, J.,Dobson, M.C., Garvin, J. and Evans, D. (1988). Microwave Dielectric Spectrum of Rocks. NASA/GSFC Grant NAG-5-843 and JPL Contract 947450, Ann Arbor, Michigan

Veasey, T.J. and Wills, B.A. (1991). Review of methods of improving mineral liberation. Minerals Engineering, 4(7-11), 747-752.

Venkatesh, M.S. and Raghavan, G.S.V. (2005). An overview of dielectric properties measuring techniques. Journal of Canadian Biosystem Engineering, 47, 15-30.

Vorster, W., Rowson, N.A. and Kingman, S.W. (2001). The effect of microwave radiation upon the processing of Neves Corvo copper ore. International Journal of Mineral Processing, 63, 29-44.

Walkiewicz, J.W., Clark, E. and McGill, S.L. (1991). Microwave-assisted grinding. Institute of Electrical and Electronics Engineering Transaction on Industrial Applications, 27(2), 239-243.

Walkiewicz, J.W.; Kazonich, G. and McGill, S.L. (1988). Microwave heating characteristics of selected minerals and compounds. Mineral and Metallurgical Processing, 5(1), 39-42.

Walkiewicz, J.W., Lindroth, D.P. and Clarck, A.E. (1993). Grindability of taconite rod mill feed enhanced by microwave induced cracking. SME Annual Meeting, Reno, NV.

Wang, G., Radziszewski, P. and Ouellet, J. (2005). Exploring DEM model development for the simulation of thermal effects on ore breakage. Mechanical Engineering Department Report, McGill Univ., 1-8.

Wang, Y. and Forssberg, E. (2000). Microwave-assisted Comminution and Liberation of Minerals. Özbayoğlu et al. (Ed.) Mineral Processing on the Verge of the 21st Century. Balkema, Rotterdam.

West, G. (1989). Rock abrasiveness testing for tunneling. International Journal of Rock Mechanics and Mining Science and Geomechanics Abstracts, 26(2), 151-160.

Whittles, D.N., Kingman, S.W. and Reddish, D.J. (2003). Application of numerical modelling for prediction of the influence of power density on microwave-assisted breakage. International Journal of Mineral Processing, 68, 71-91.

Wijk, G. (1992). A model of tunnel boring machine performance. Geotechnical and Geological Engineering, 10, 19-40.

Wilkinson, M. and Tester, J. (1993). Experimental measurement of surface temperatures during flame-jet induced thermal spallation. Rock Mechanics and Rock Engineering., 26(1), 29-62.

Znamenácková, I., Lovás, M., Hájek, M. and Jakabský, Š. (2003). Melting of andesite in a microwave oven. Journal of Mining and Metallurgy, 39(3-4) B, 549-557.

Appendix A: Electrical Permittivity of Rocks

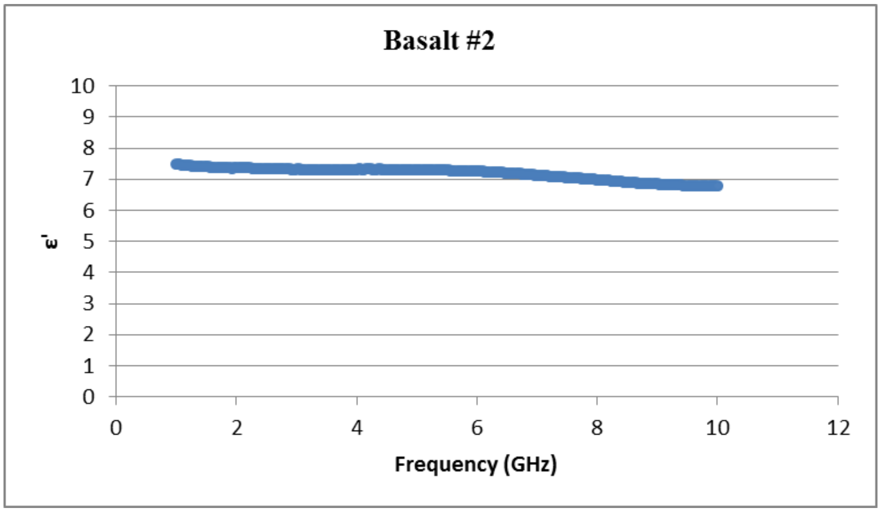

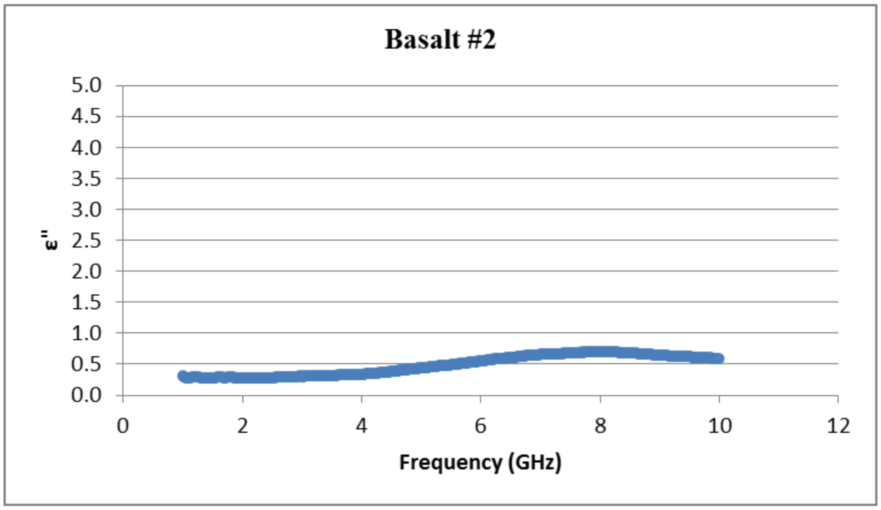

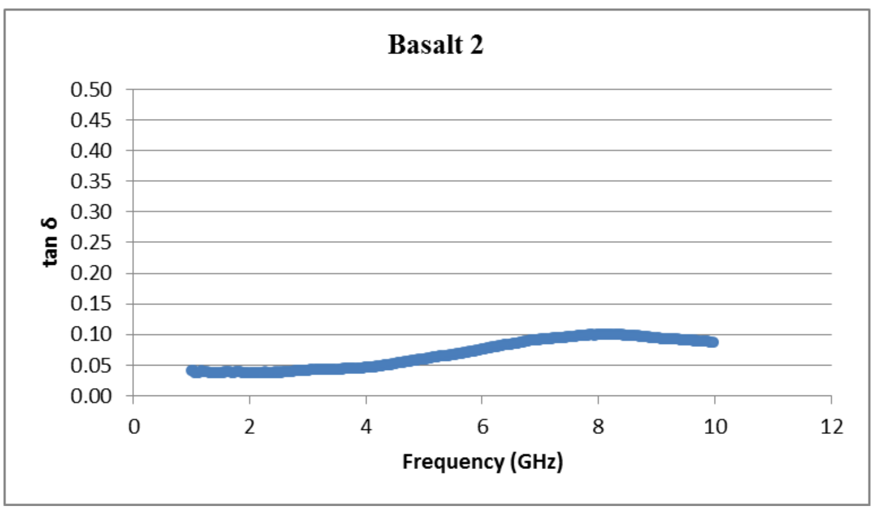

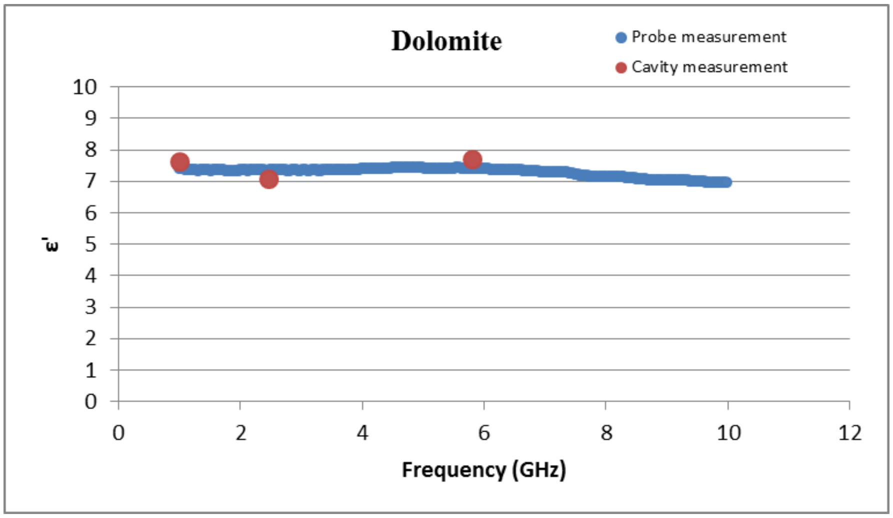
Dolomite
Probe measurement
Cavity measurement
ε'
10
9
8
7
6
5
4
3
2
1
0
0
2
4
6
8
10
12
Frequency (GHz)

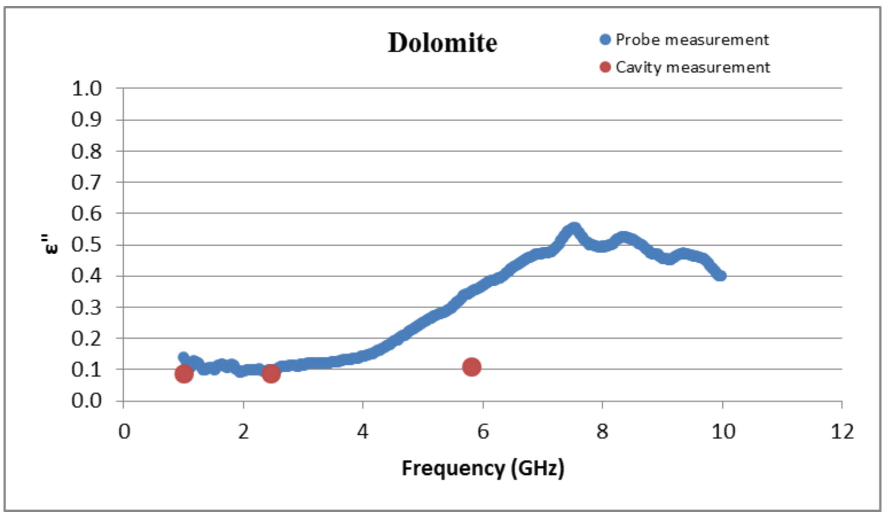
Dolomite
Probe measurement
Cavity measurement
ε''
1.0
0.9
0.8
0.7
0.6
0.5
0.4
0.3
0.2
0.1
0.0
0
2
4
6
8
10
12
Frequency (GHz)

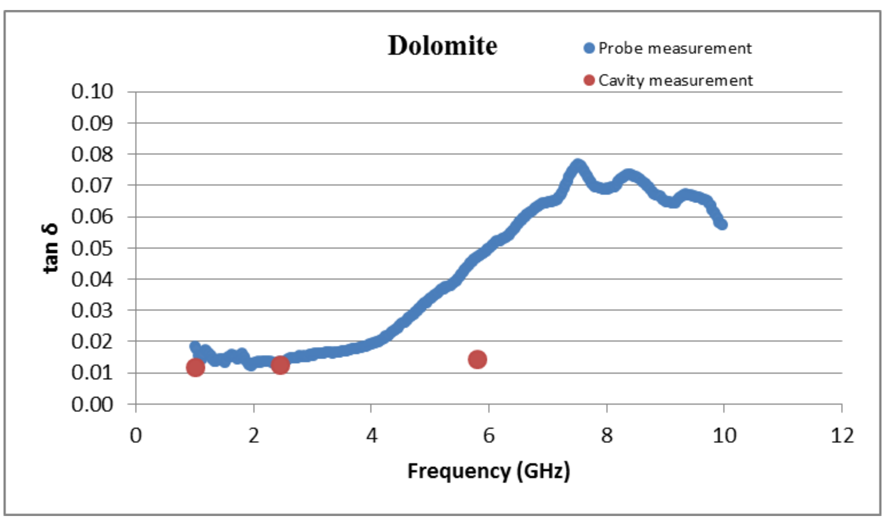
Dolomite
Probe measurement
Cavity measurement
tan δ
0.10
0.09
0.08
0.07
0.06
0.05
0.04
0.03
0.02
0.01
0.00
0
2
4
6
8
10
12
Frequency (GHz)

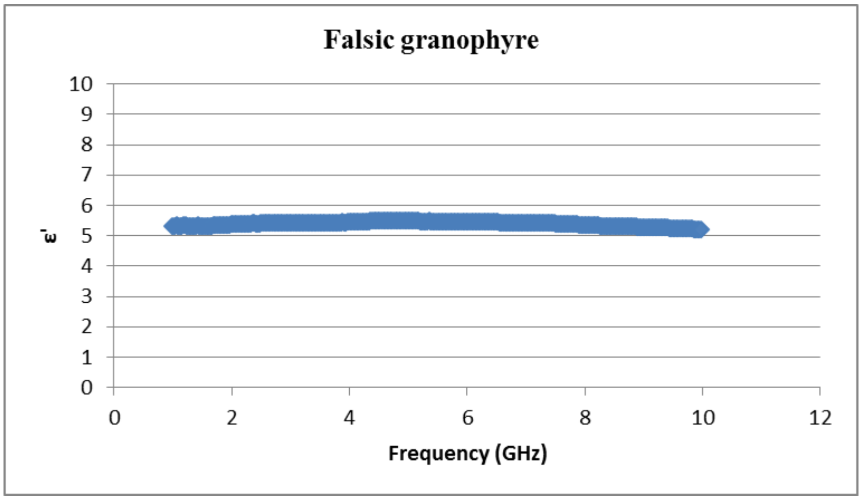
Falsic granophyre
ε'
0
1
2
3
4
5
6
7
8
9
10
0
2
4
6
8
10
12
Frequency (GHz)

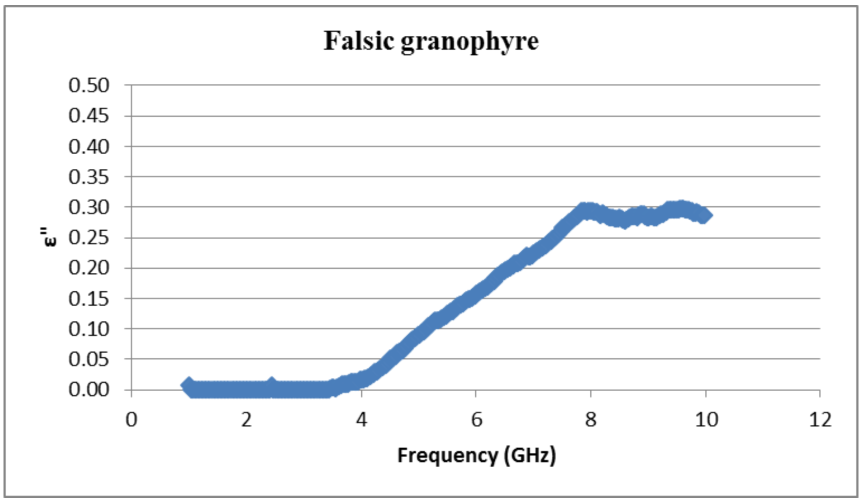
Falsic granophyre
ε''
0.00
0.05
0.10
0.15
0.20
0.25
0.30
0.35
0.40
0.45
0.50
0
2
4
6
8
10
12
Frequency (GHz)

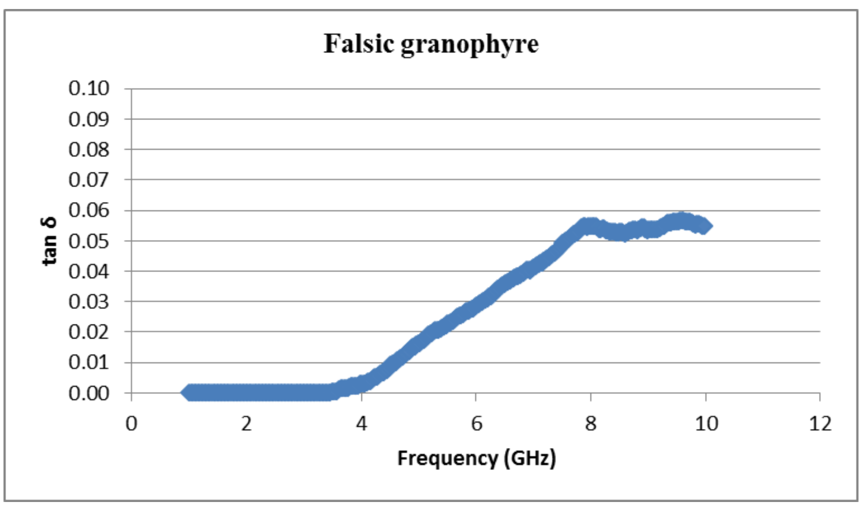
Falsic granophyre
tan δ
0.00
0.01
0.02
0.03
0.04
0.05
0.06
0.07
0.08
0.09
0.10
0
2
4
6
8
10
12
Frequency (GHz)

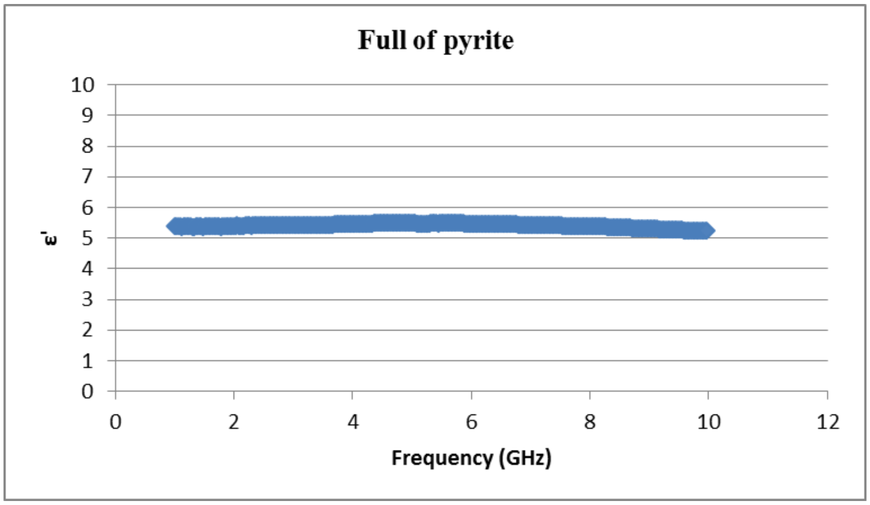
Full of pyrite
ε'
10
9
8
7
6
5
4
3
2
1
0
0
2
4
6
8
10
12
Frequency (GHz)

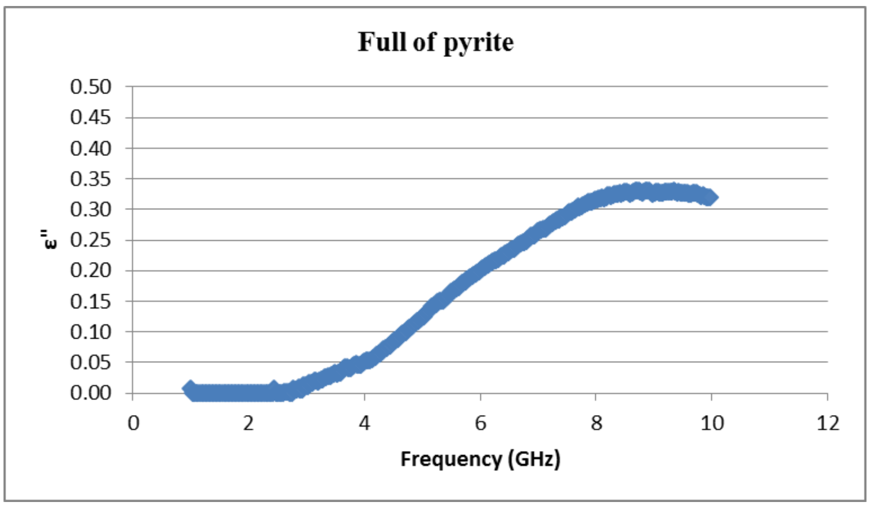
Full of pyrite
ε''
0.50
0.45
0.40
0.35
0.30
0.25
0.20
0.15
0.10
0.05
0.00
0
2
4
6
8
10
12
Frequency (GHz)

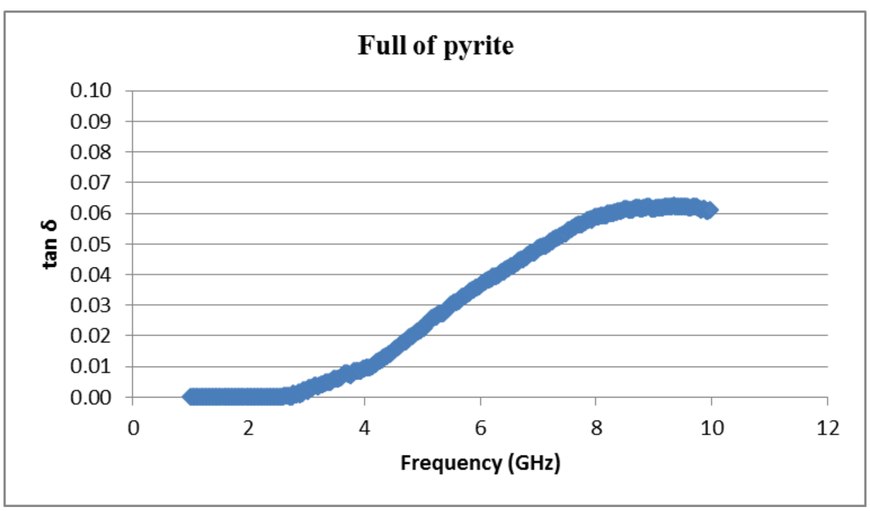
Full of pyrite
tan δ
0.10
0.09
0.08
0.07
0.06
0.05
0.04
0.03
0.02
0.01
0.00
0
2
4
6
8
10
12
Frequency (GHz)

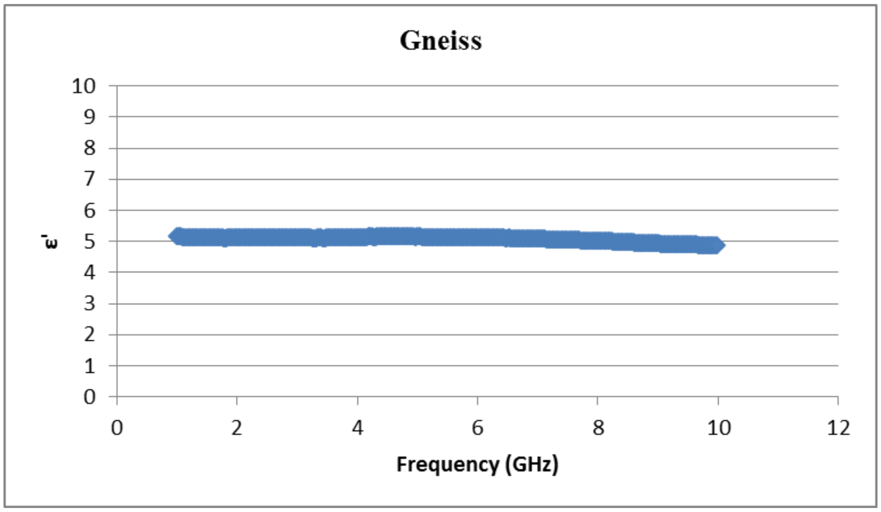
Gneiss
ε'
Frequency (GHz)

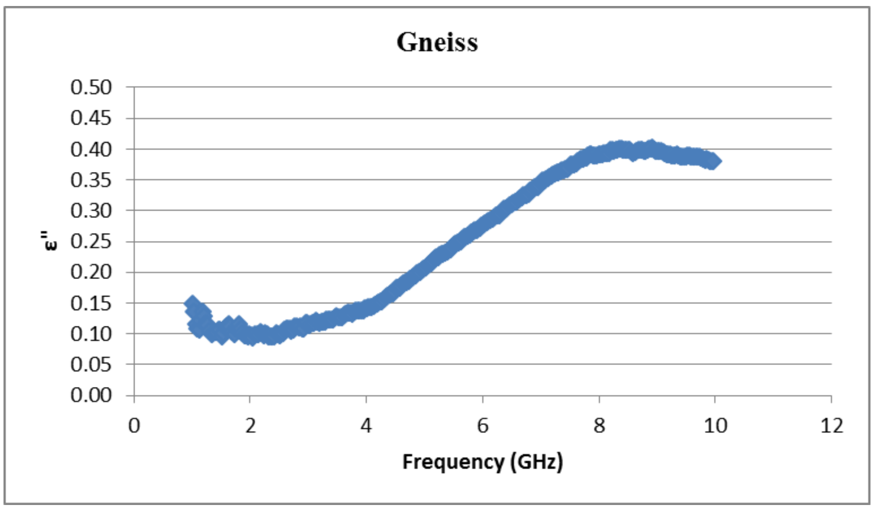
Gneiss
ε''
Frequency (GHz)

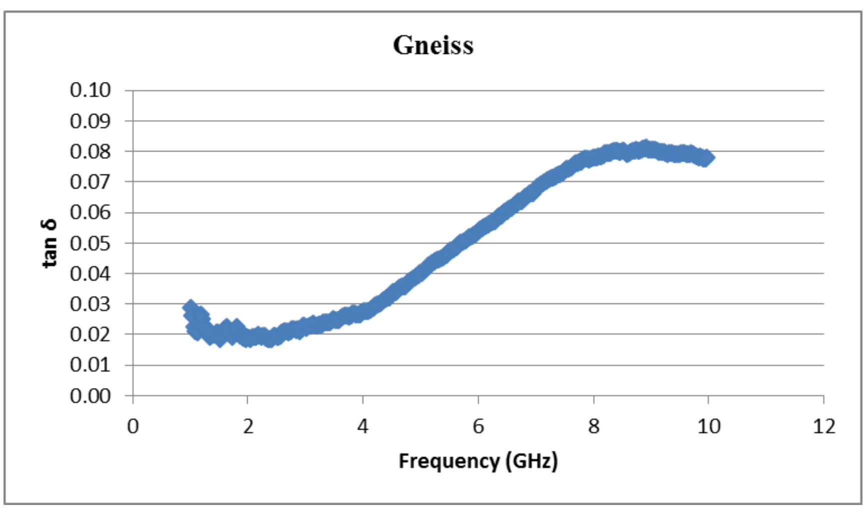
Gneiss
tan δ
Frequency (GHz)

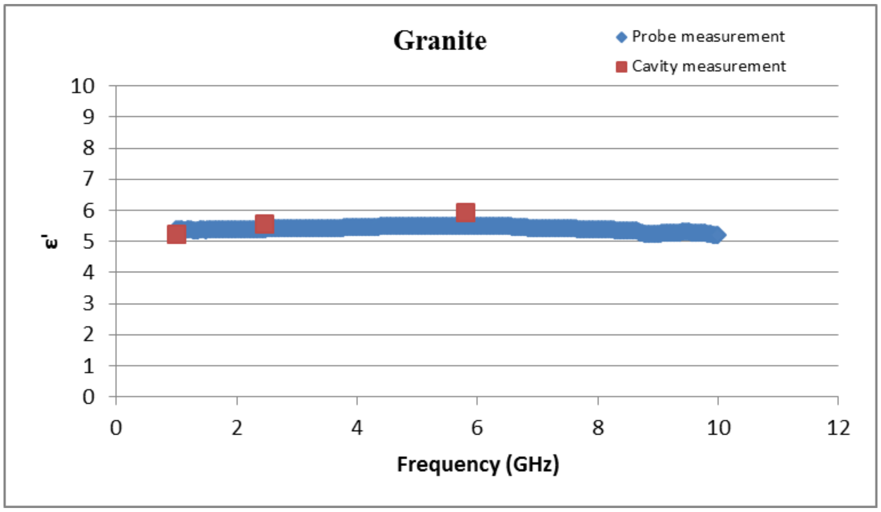
Granite
Probe measurement
Cavity measurement
ε'
Frequency (GHz)

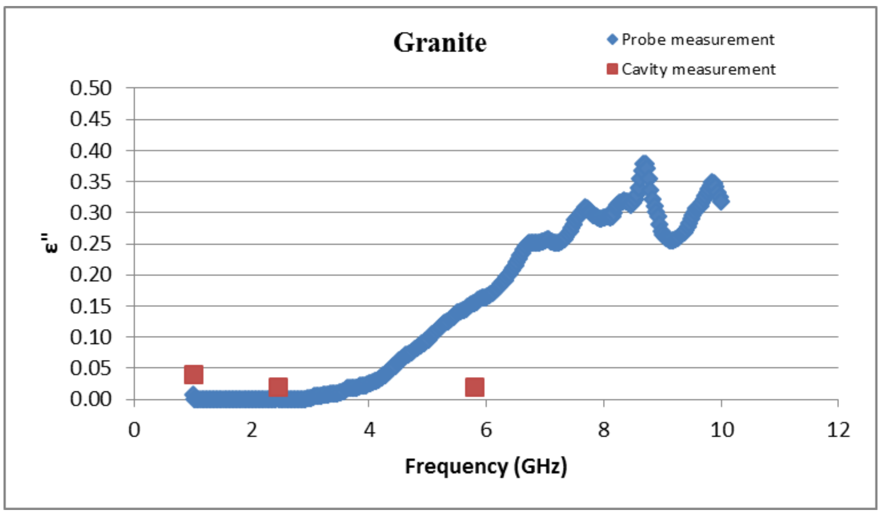
Granite
Probe measurement
Cavity measurement
ε''
Frequency (GHz)

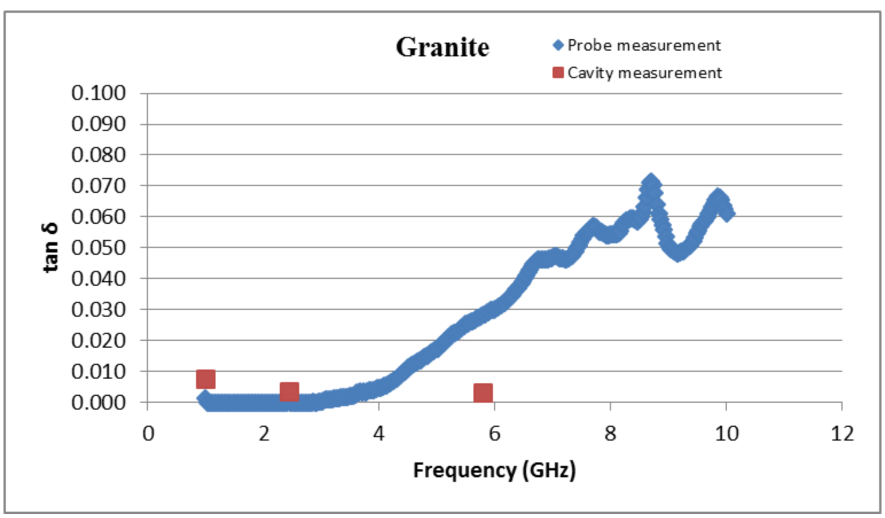
Granite
Probe measurement
Cavity measurement
tan δ
Frequency (GHz)

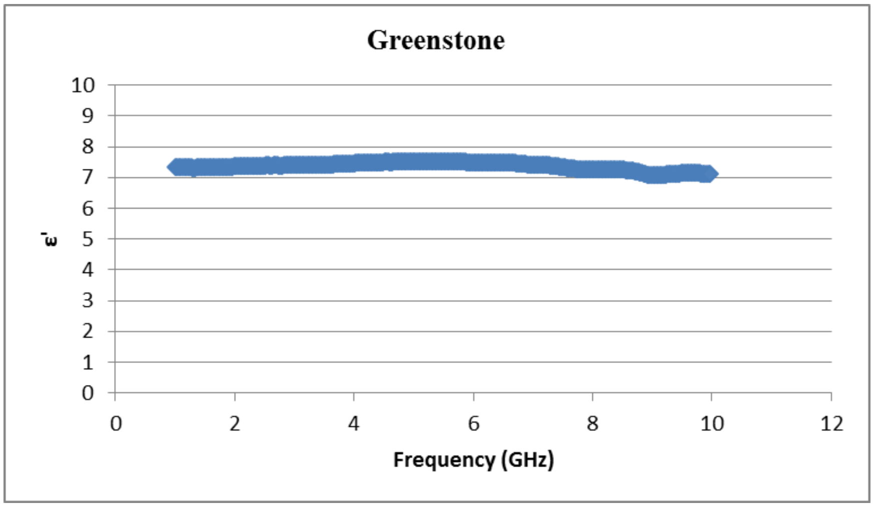
Greenstone
ε'
Frequency (GHz)
0
1
2
3
4
5
6
7
8
9
10
0
2
4
6
8
10
12

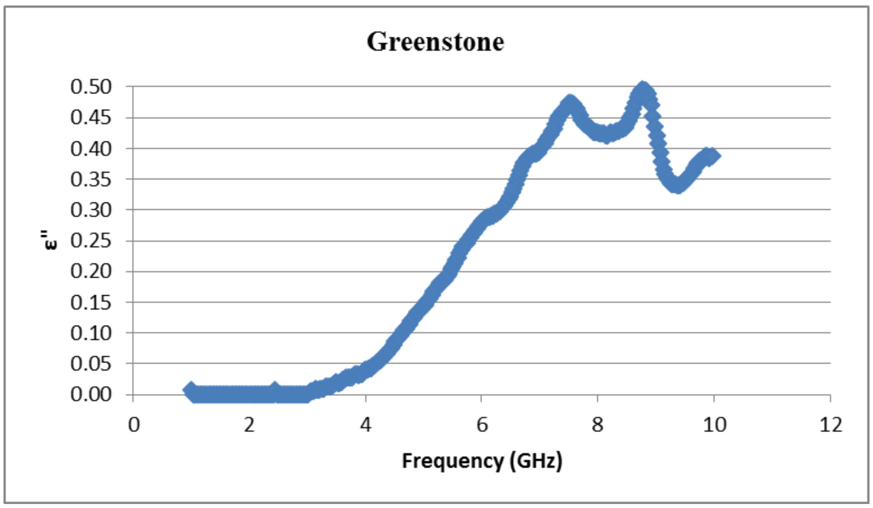
Greenstone
ε''
Frequency (GHz)
0.00
0.05
0.10
0.15
0.20
0.25
0.30
0.35
0.40
0.45
0.50
0
2
4
6
8
10
12

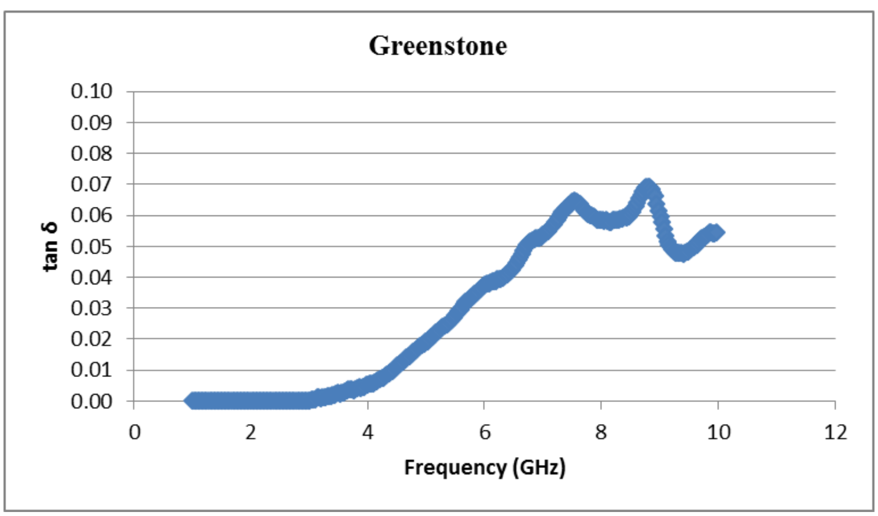
Greenstone
tan δ
Frequency (GHz)
0.00
0.01
0.02
0.03
0.04
0.05
0.06
0.07
0.08
0.09
0.10
0
2
4
6
8
10
12

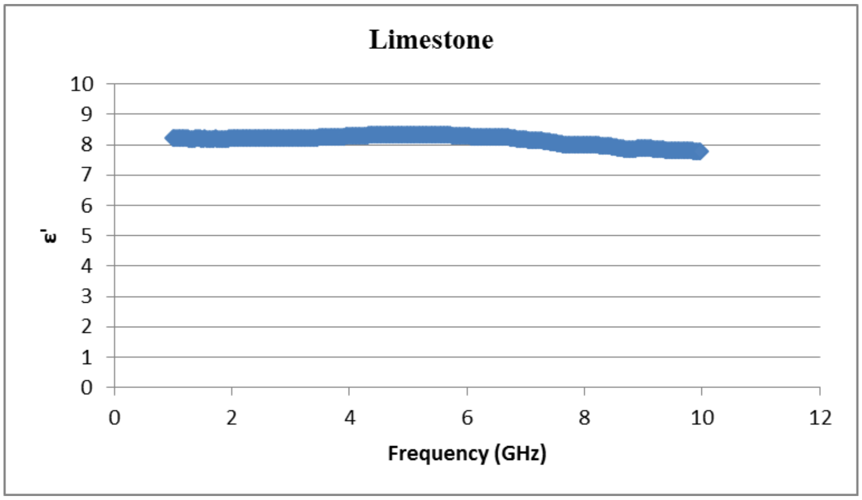
Limestone
10
9
8
7
6
5
4
3
2
1
0
ε'
0
2
4
6
8
10
12
Frequency (GHz)

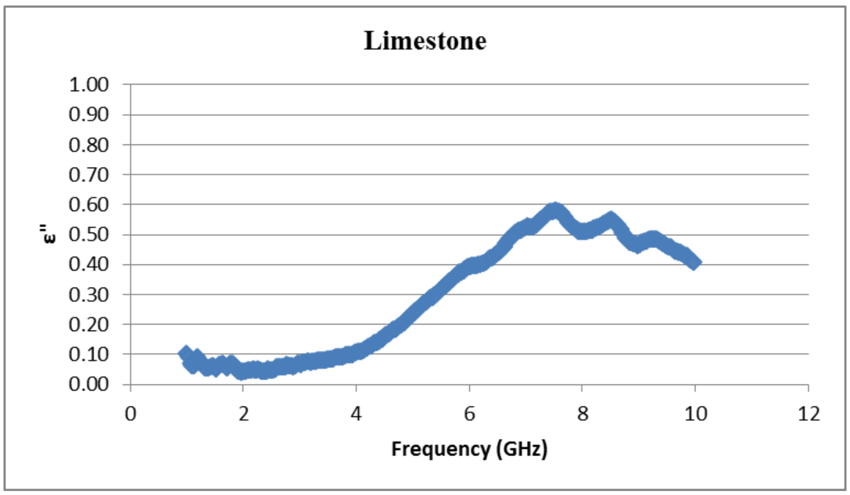
Limestone
1.00
0.90
0.80
0.70
0.60
0.50
0.40
0.30
0.20
0.10
0.00
ε''
0
2
4
6
8
10
12
Frequency (GHz)

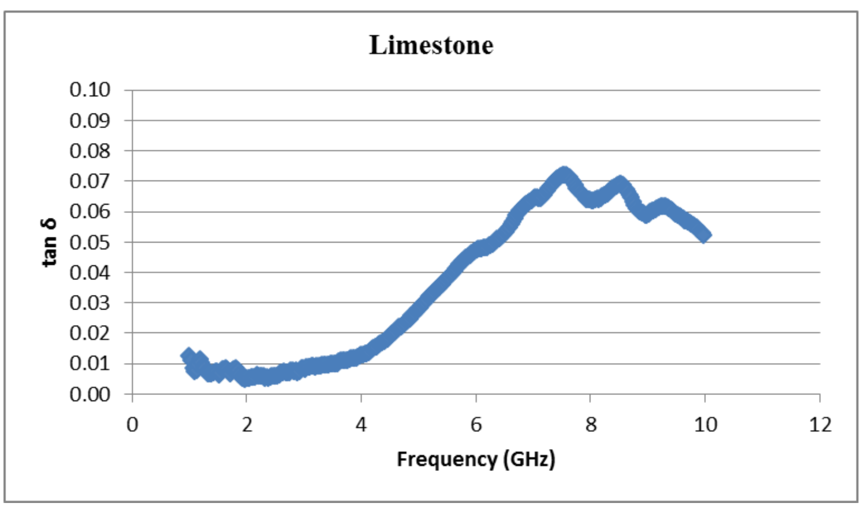
Limestone
0.10
0.09
0.08
0.07
0.06
0.05
0.04
0.03
0.02
0.01
0.00
tan δ
0
2
4
6
8
10
12
Frequency (GHz)

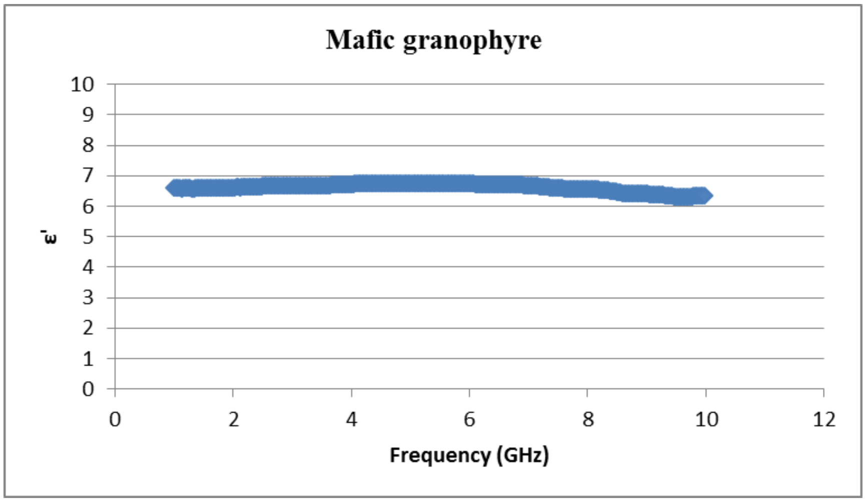
Mafic granophyre
10
9
8
7
6
5
4
3
2
1
0
ε'
0
2
4
6
8
10
12
Frequency (GHz)

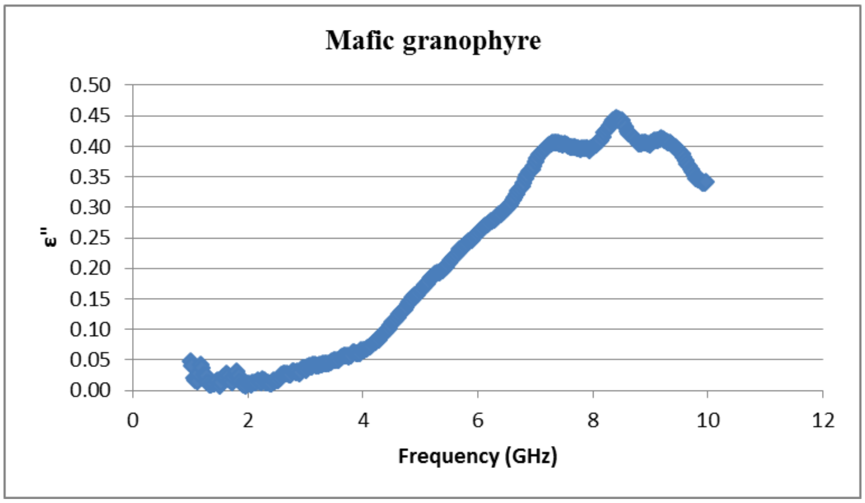
Mafic granophyre
0.50
0.45
0.40
0.35
0.30
0.25
0.20
0.15
0.10
0.05
0.00
ε''
0
2
4
6
8
10
12
Frequency (GHz)

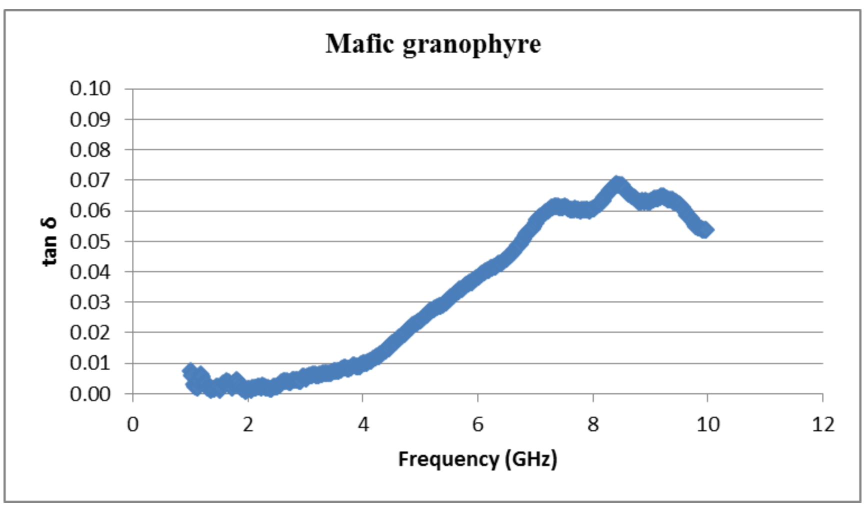
Mafic granophyre
0.10
0.09
0.08
0.07
0.06
0.05
0.04
0.03
0.02
0.01
0.00
tan δ
0
2
4
6
8
10
12
Frequency (GHz)

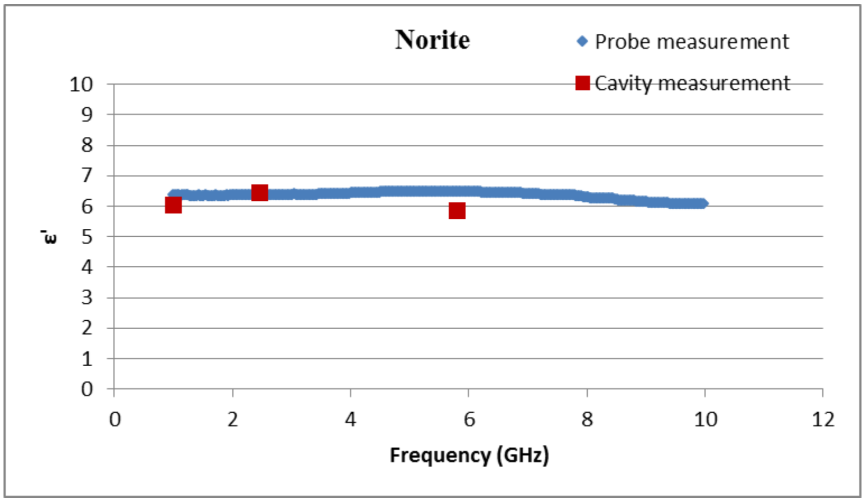
Norite
Probe measurement
Cavity measurement
ε'
Frequency (GHz)

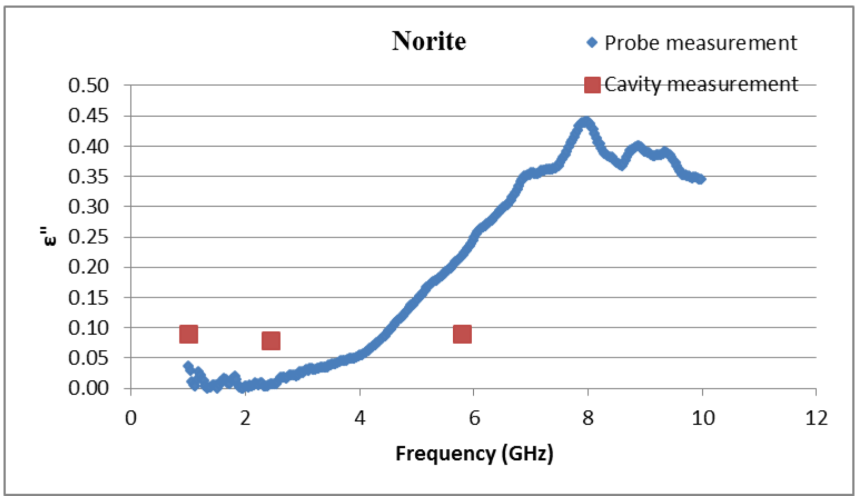
Norite
Probe measurement
Cavity measurement
ε''
Frequency (GHz)

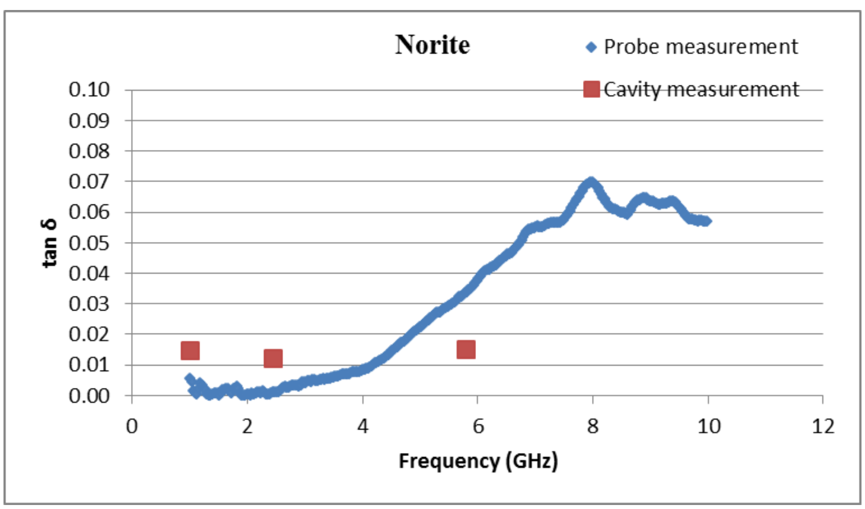
Norite
Probe measurement
Cavity measurement
tan δ
Frequency (GHz)

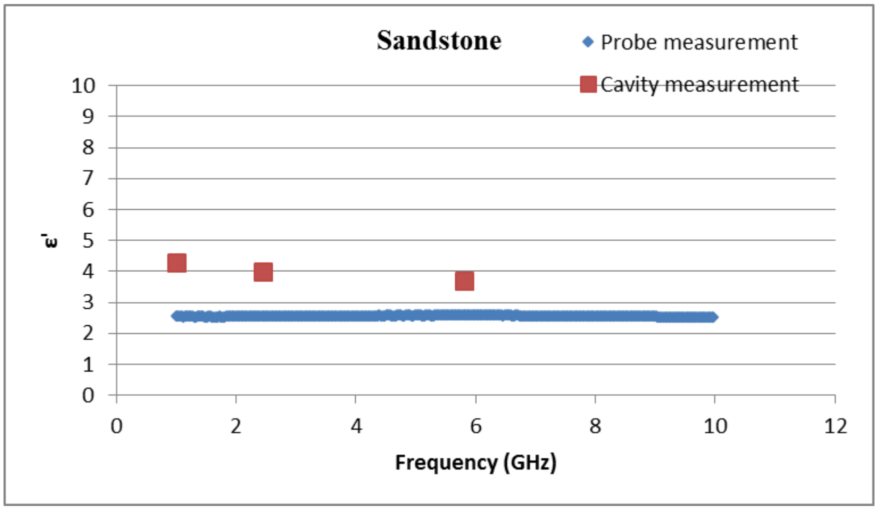
Sandstone
Probe measurement
Cavity measurement
ε'
Frequency (GHz)

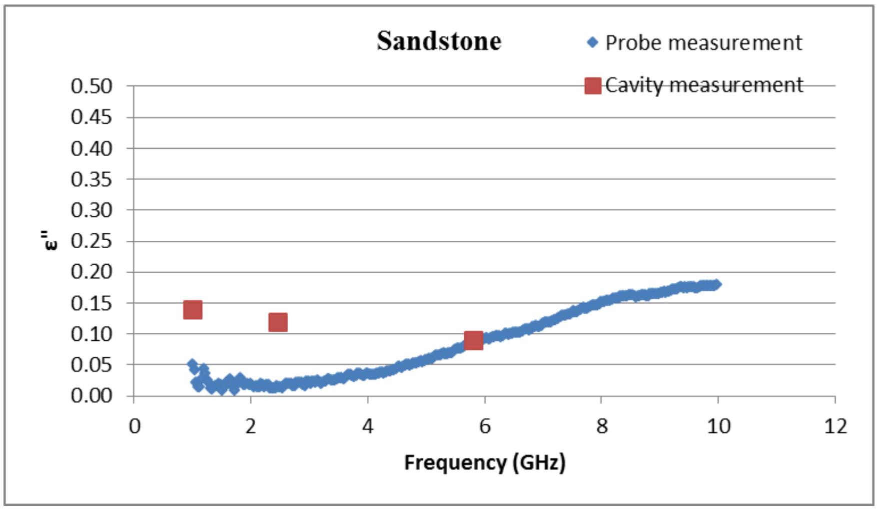
Sandstone
Probe measurement
Cavity measurement
ε''
Frequency (GHz)

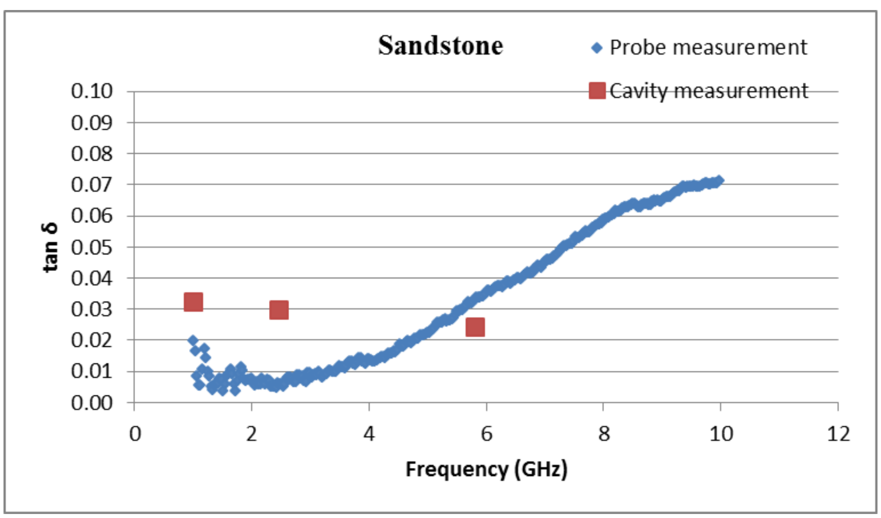
Sandstone
Probe measurement
Cavity measurement
tan δ
Frequency (GHz)

Appendix B: Bowen Reaction Series (Reprinted from Tarbuck et al., 2011)

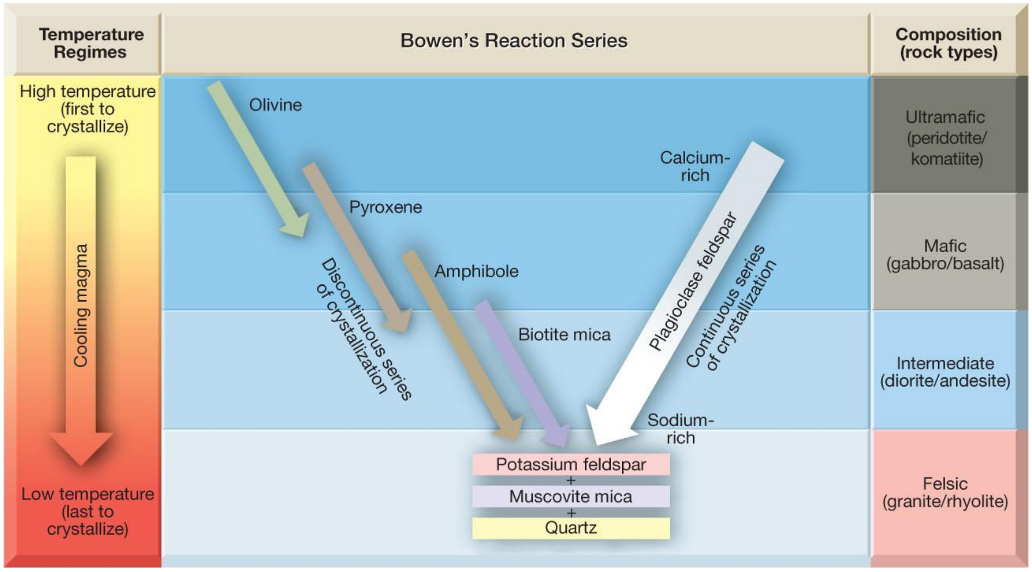

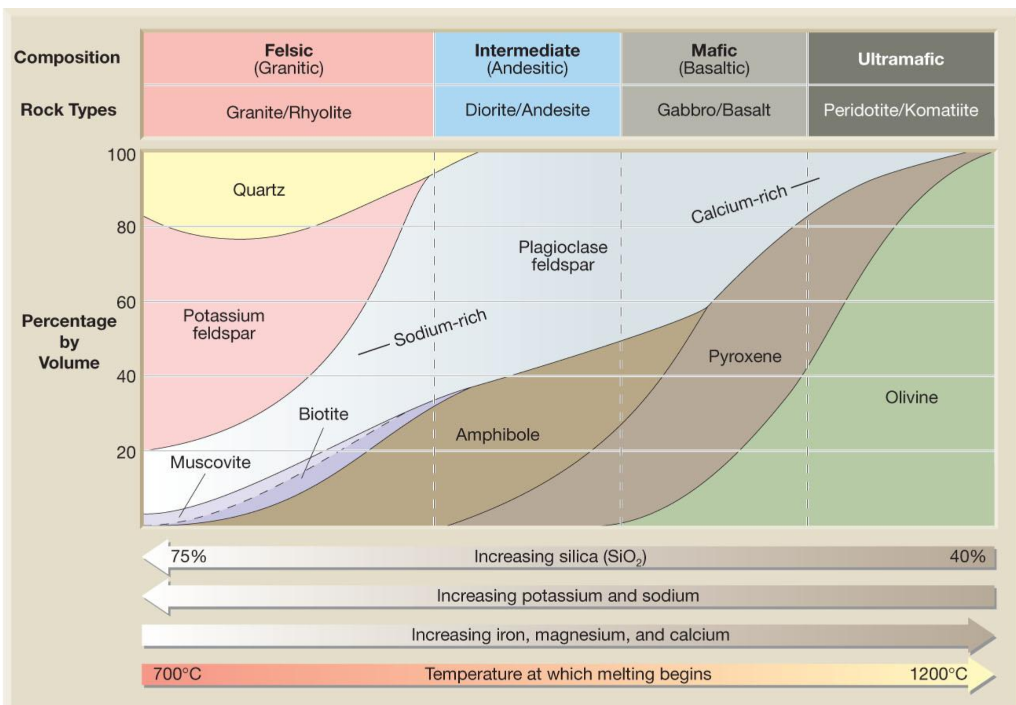

Appendix C: Temperature Distribution, UCS, BTS and CAI of Samples at 0.8, 1.25 and 3.0 kW Power

Granite: Temperature distribution

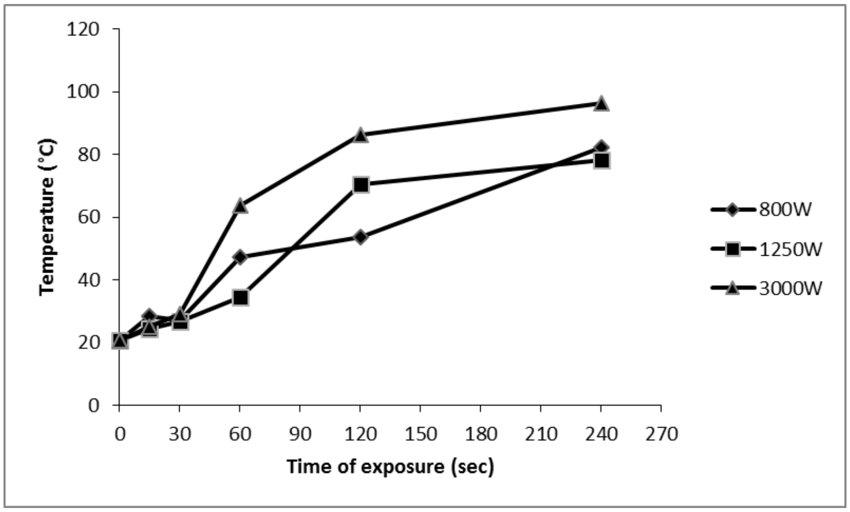

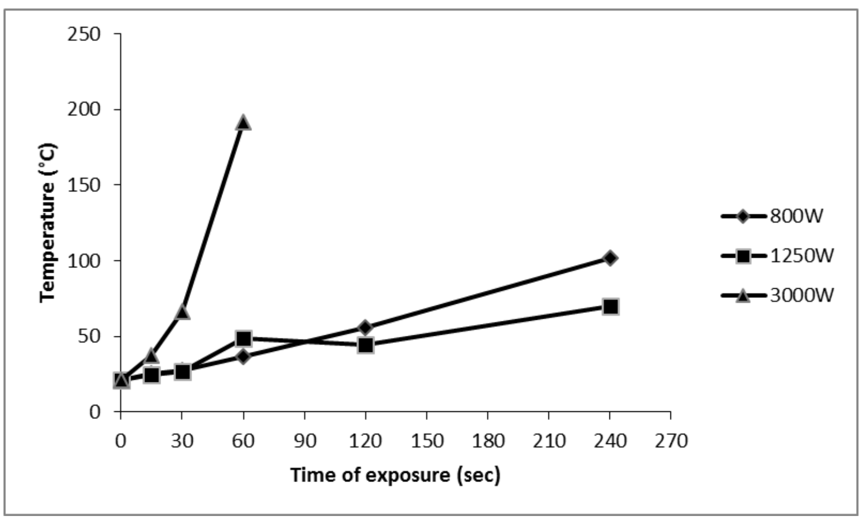

Granite: BTS

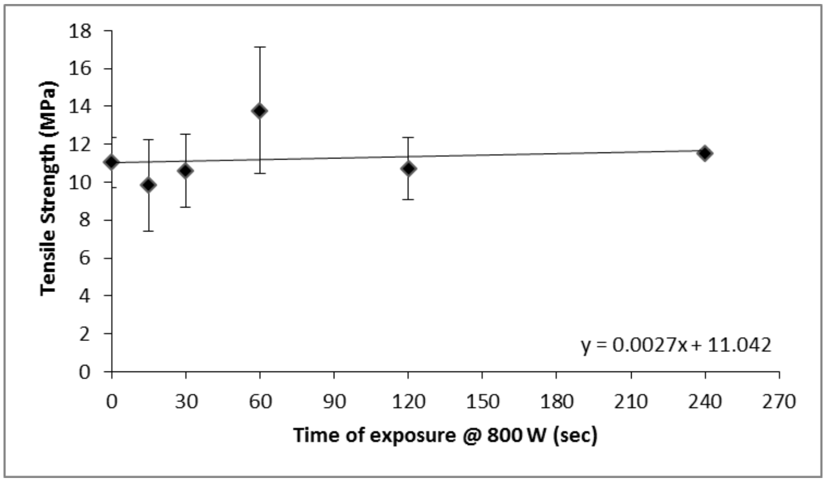

Tensile Strength (MPa)
18
16
14
12
10
8
6
4
2
0
y = 0.0027x + 11.042
0
30
60
90
120
150
180
210
240
270
Time of exposure @ 800 W (sec)

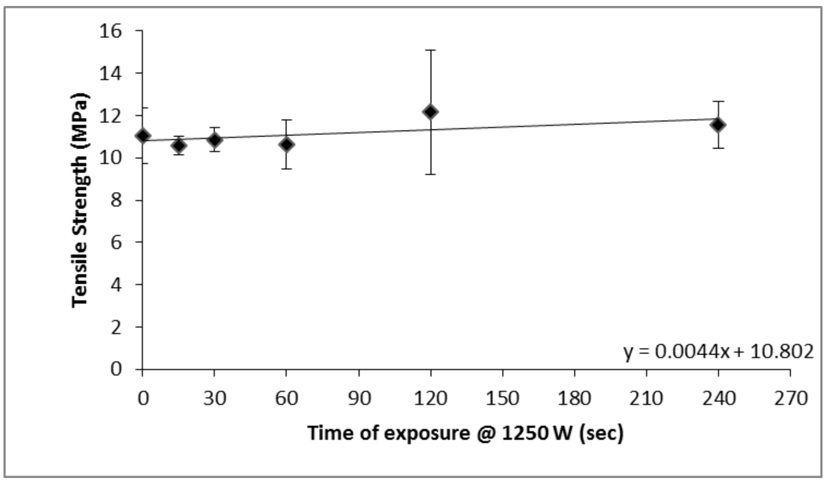

Tensile Strength (MPa)
16
14
12
10
8
6
4
2
0
y = 0.0044x + 10.802
0
30
60
90
120
150
180
210
240
270
Time of exposure @ 1250 W (sec)

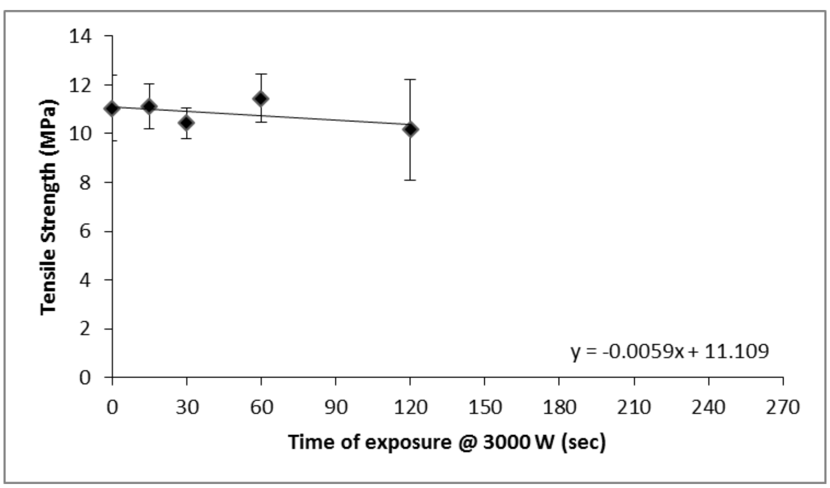

Tensile Strength (MPa)
14
12
10
8
6
4
2
0
y = -0.0059x + 11.109
0
30
60
90
120
150
180
210
240
270
Time of exposure @ 3000 W (sec)

Granite: CAI

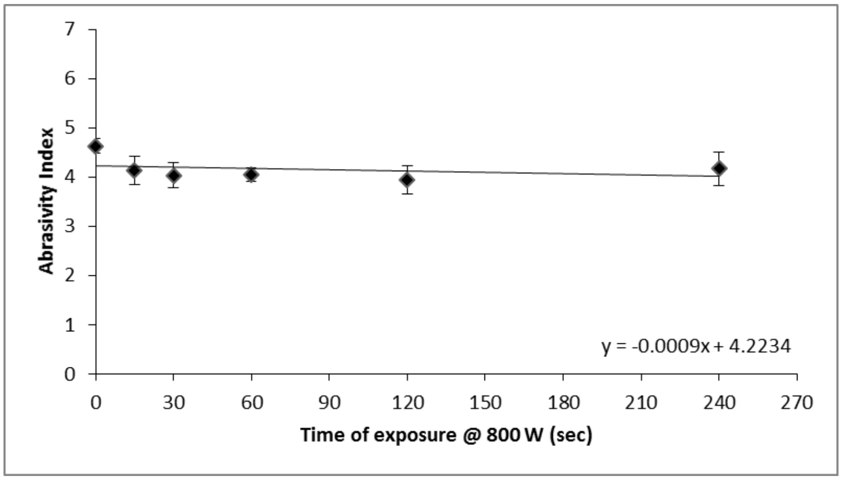
Abrasivity Index
Time of exposure @ 800 W (sec)
y = -0.0009x + 4.2234

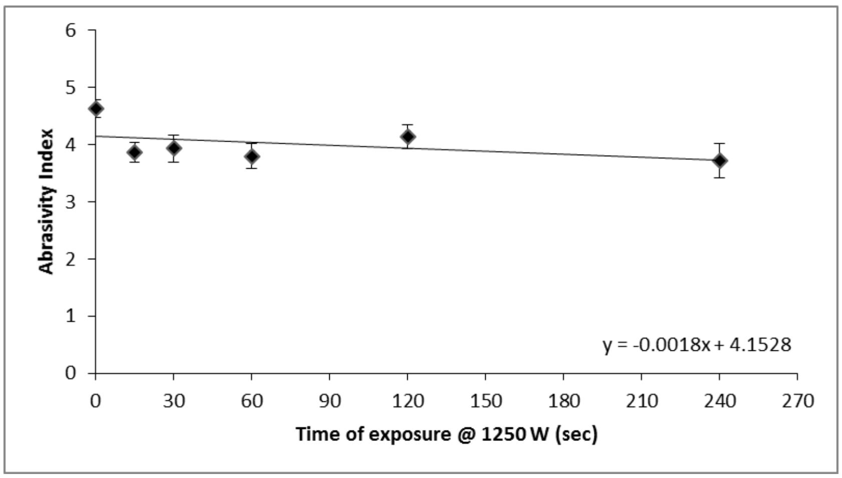
Abrasivity Index
Time of exposure @ 1250 W (sec)
y = -0.0018x + 4.1528

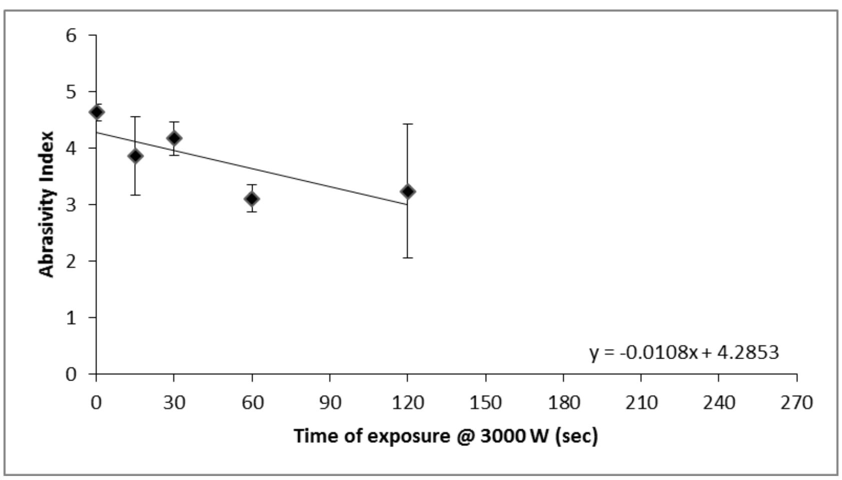
Abrasivity Index
Time of exposure @ 3000 W (sec)
y = -0.0108x + 4.2853

Granite: UCS

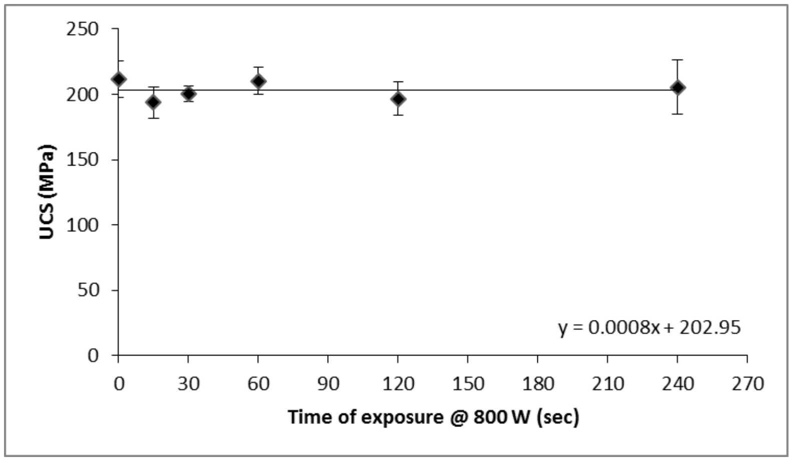

250
200
150
100
50
0
UCS (MPa)
y = 0.0008x + 202.95
0
30
60
90
120
150
180
210
240
270
Time of exposure @ 800 W (sec)

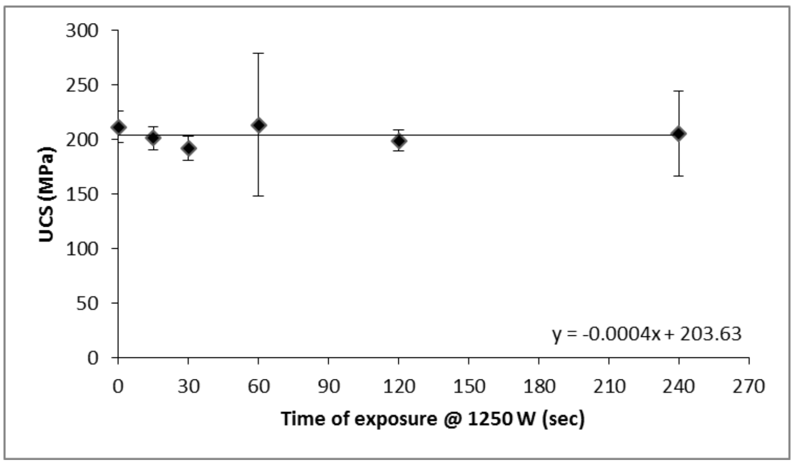

300
250
200
150
100
50
0
UCS (MPa)
y = -0.0004x + 203.63
0
30
60
90
120
150
180
210
240
270
Time of exposure @ 1250 W (sec)

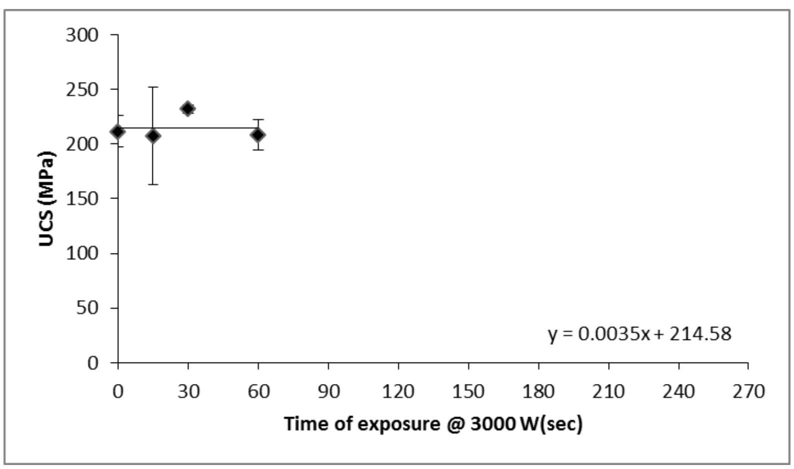

300
250
200
150
100
50
0
UCS (MPa)
y = 0.0035x + 214.58
0
30
60
90
120
150
180
210
240
270
Time of exposure @ 3000 W(sec)

Mafic Granophyre: Temperature distribution

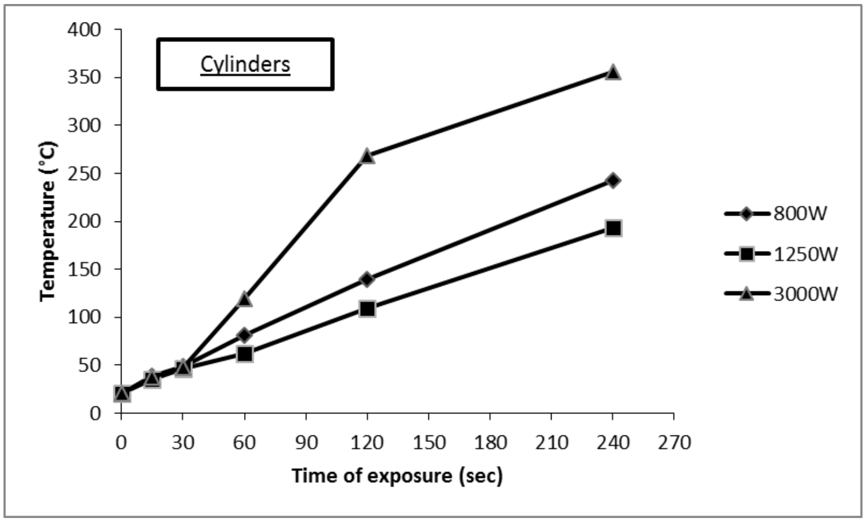

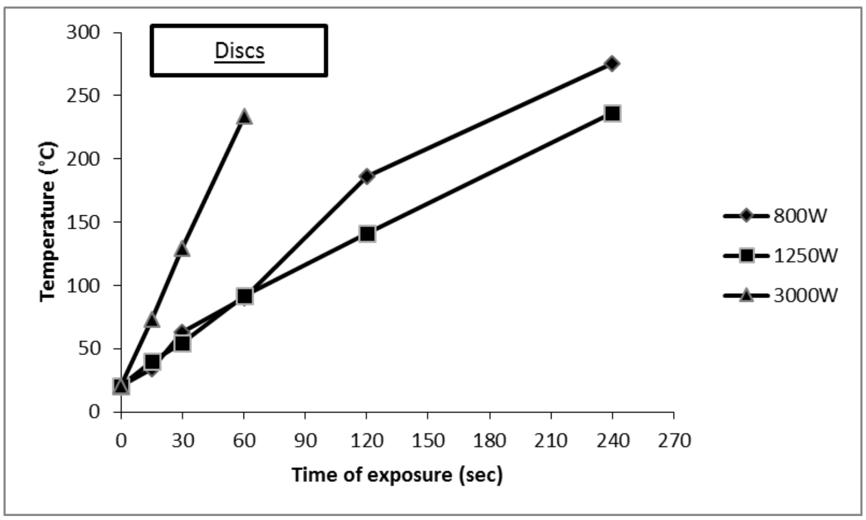

Mafic Granophyre: BTS

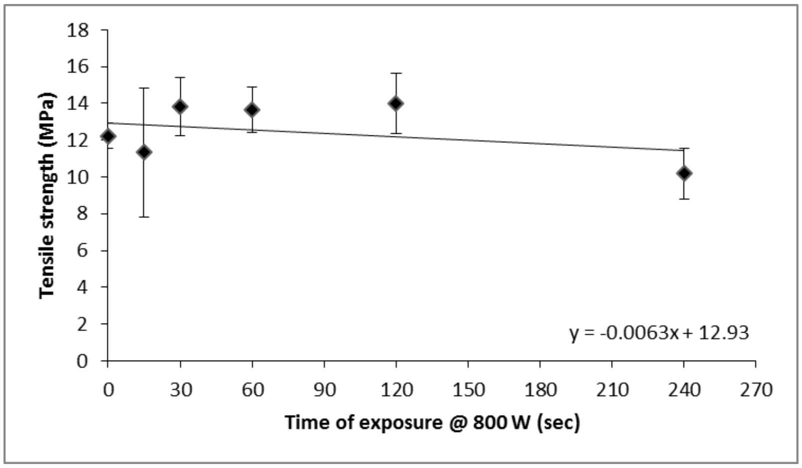

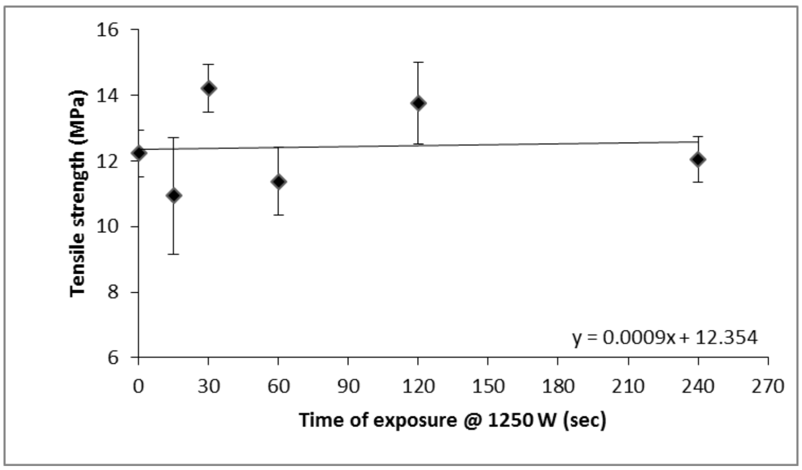

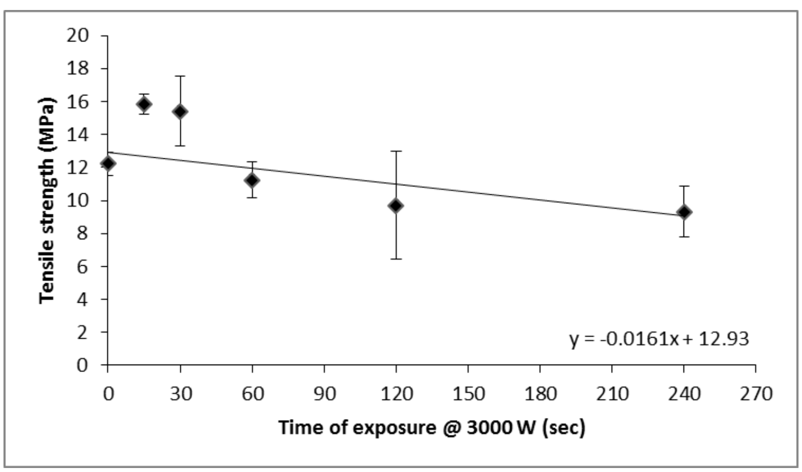

Mafic Granophyre: CAI

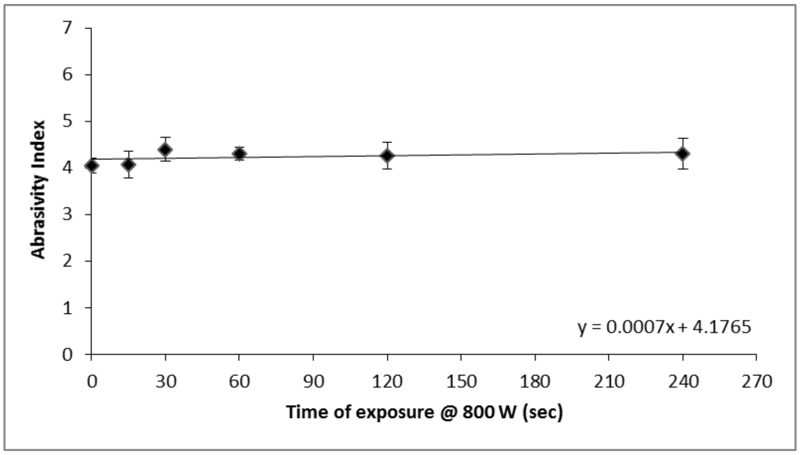

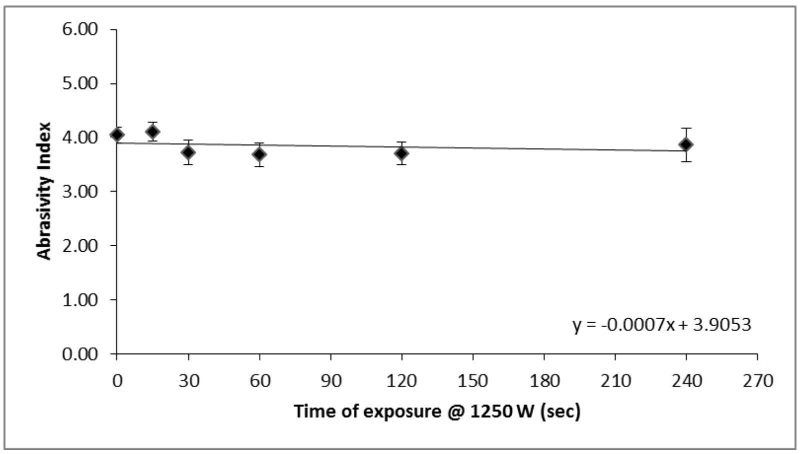

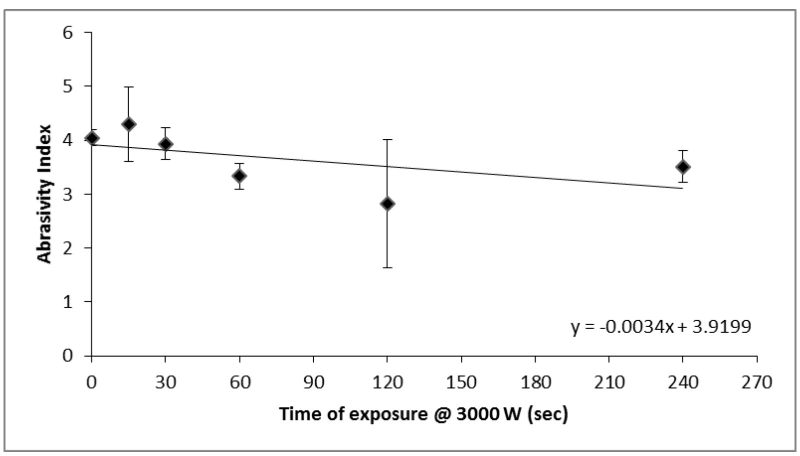

Mafic Granophyre: UCS

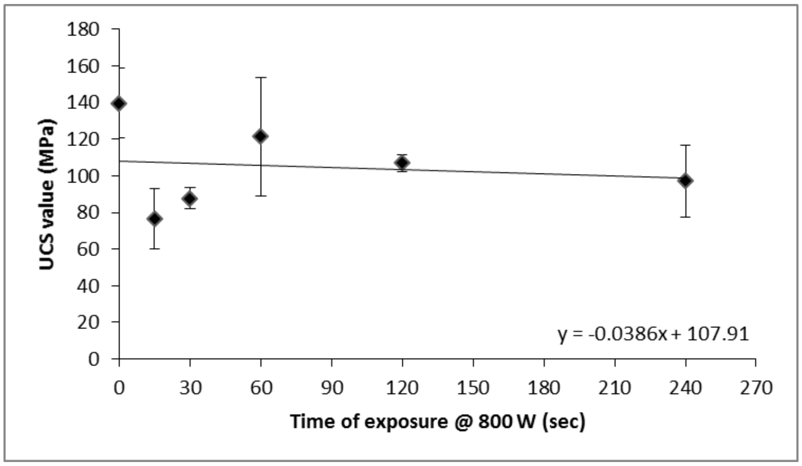

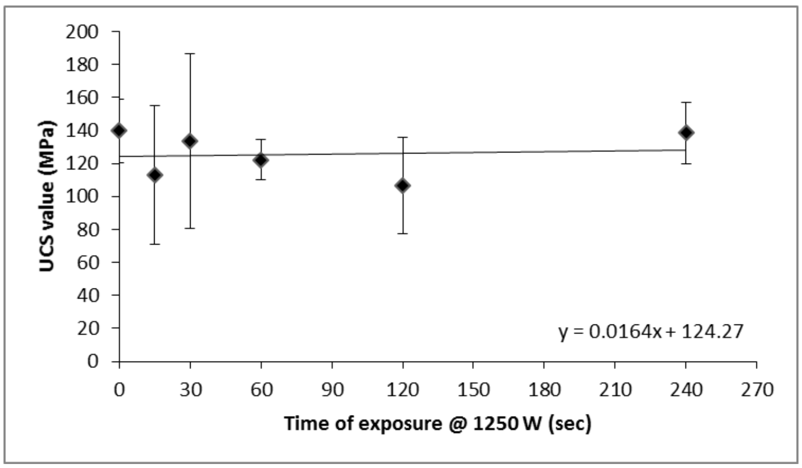

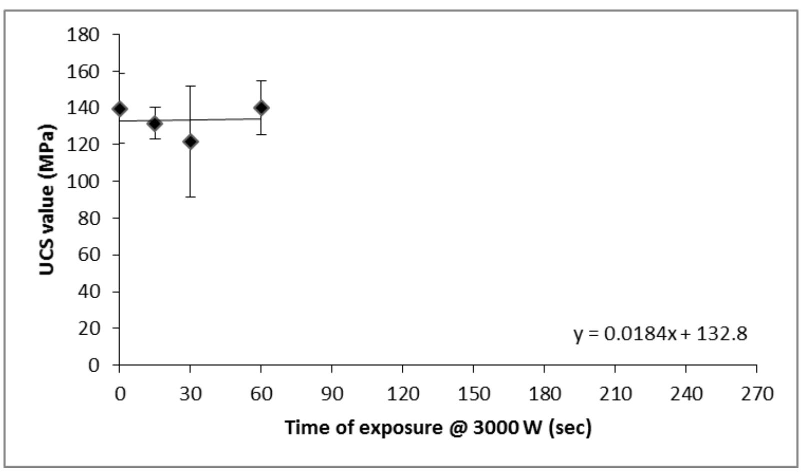

Falsic Granophyre : Temperature distribution

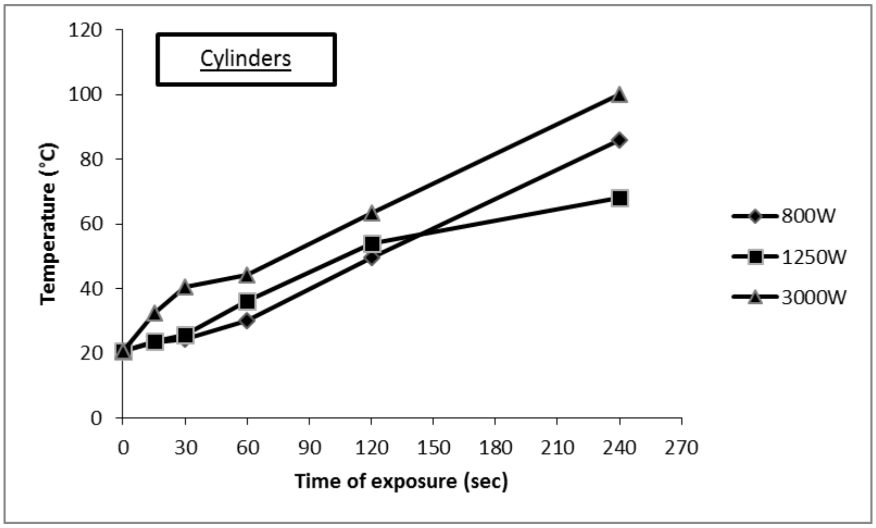

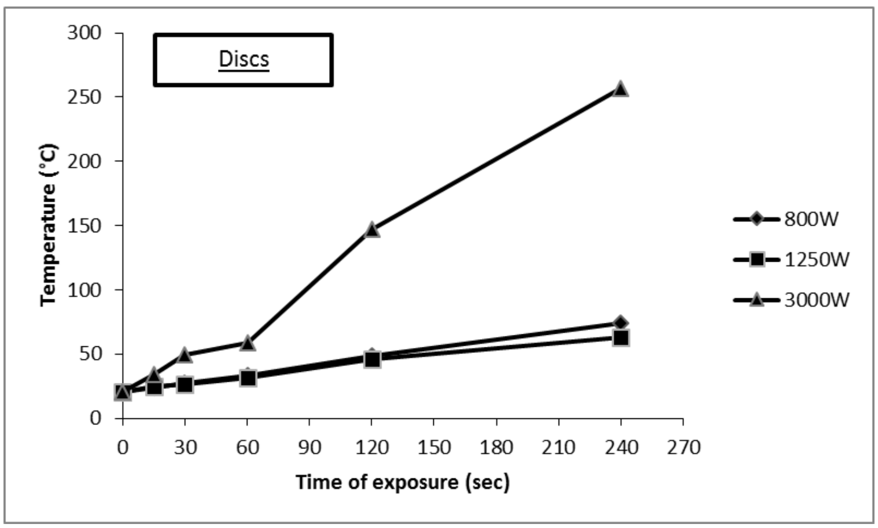

Falsic Granophyre : BTS

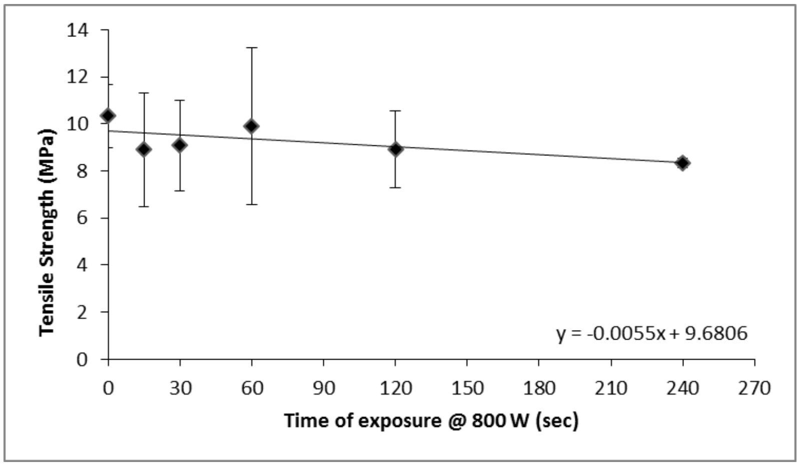

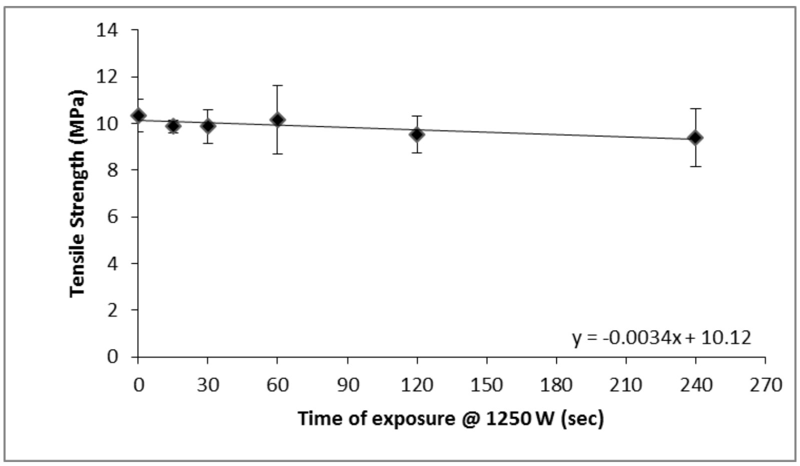

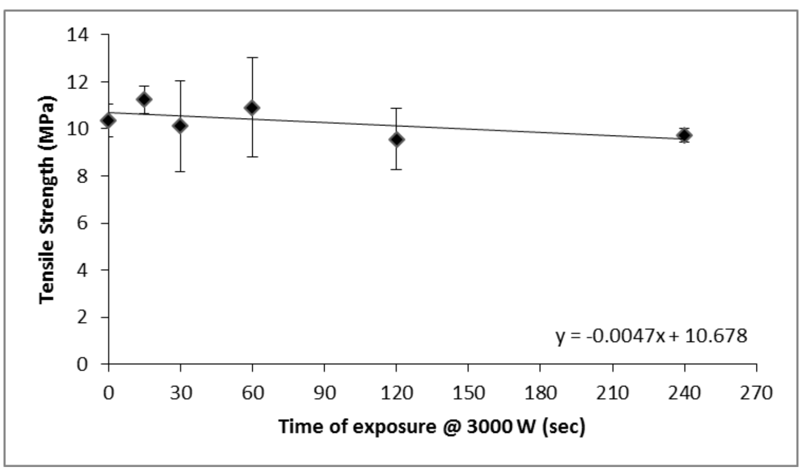

Falsic Granophyre : CAI

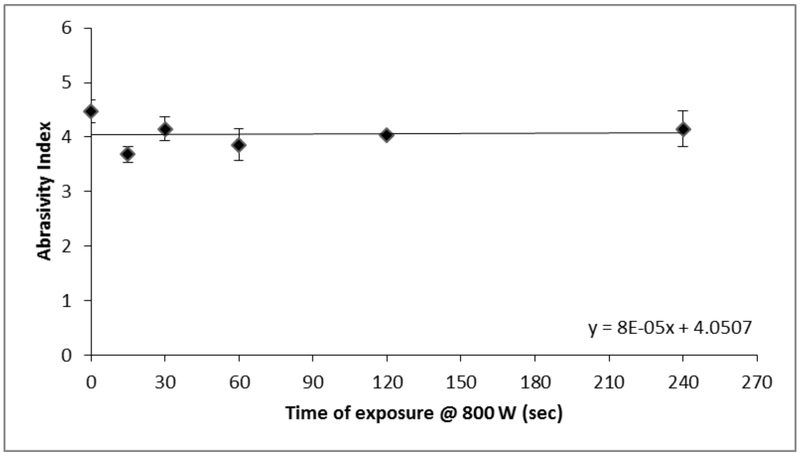

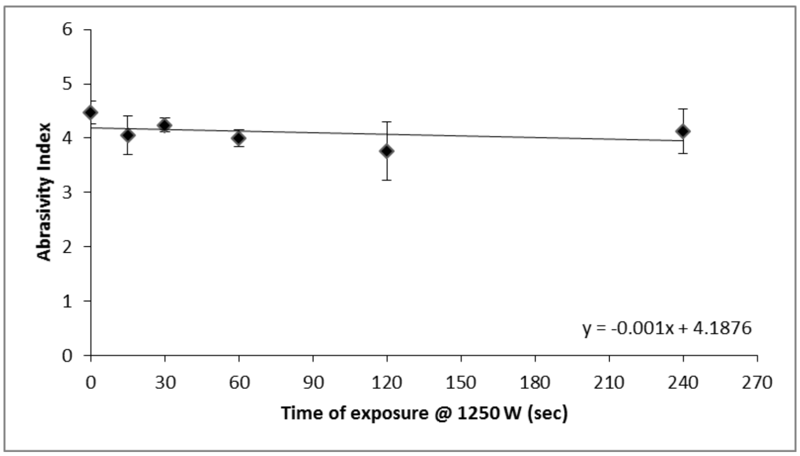

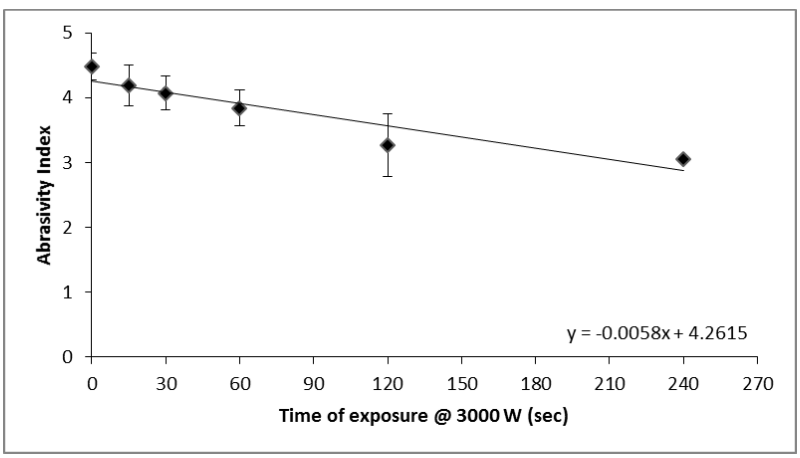

Falsic Granophyre : UCS

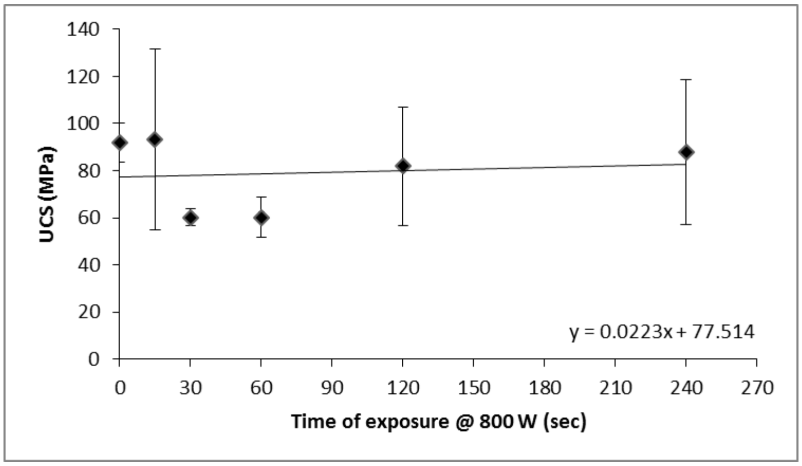

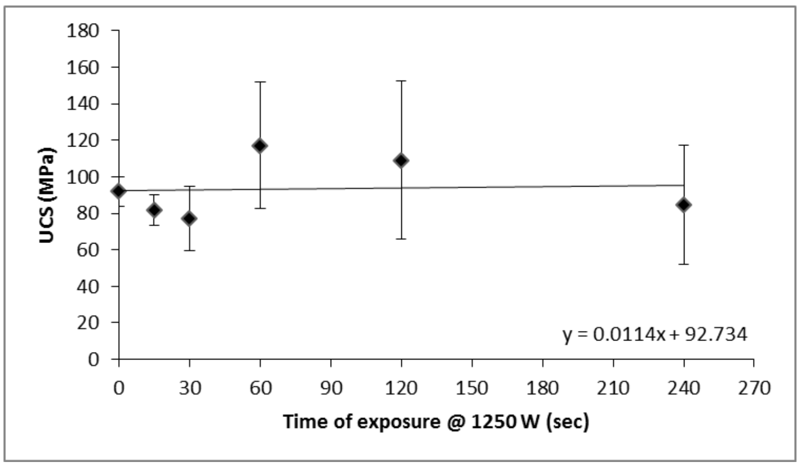

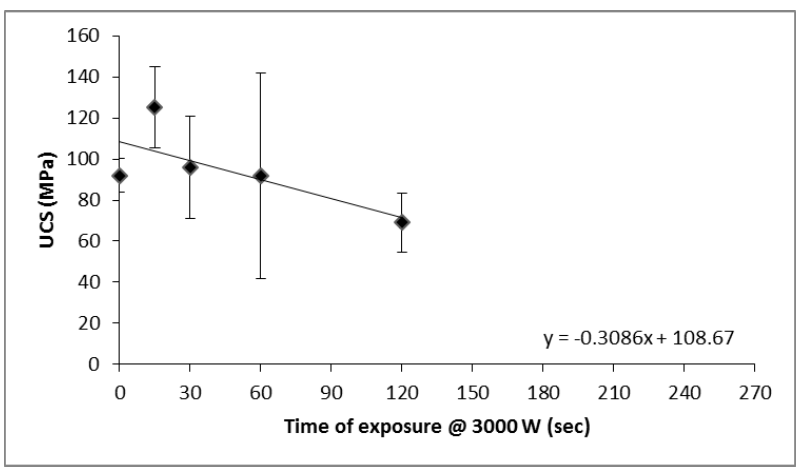

Gneiss : Temperature distrbution

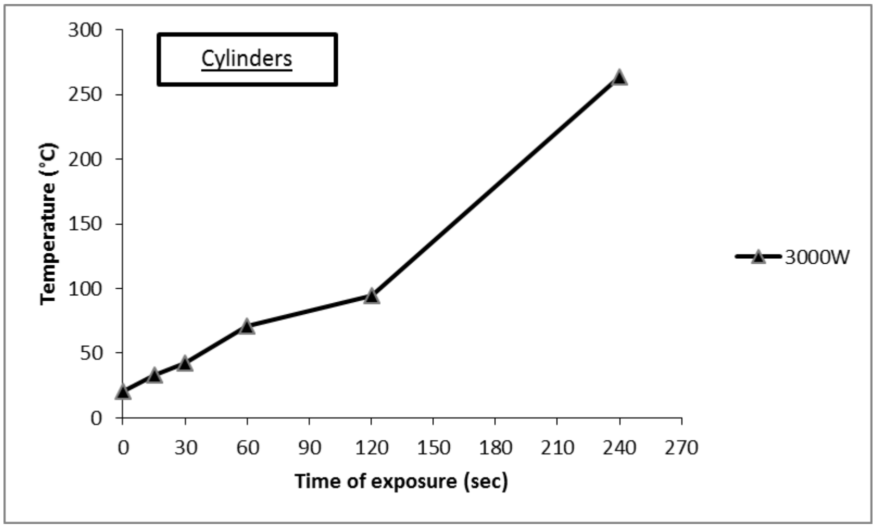

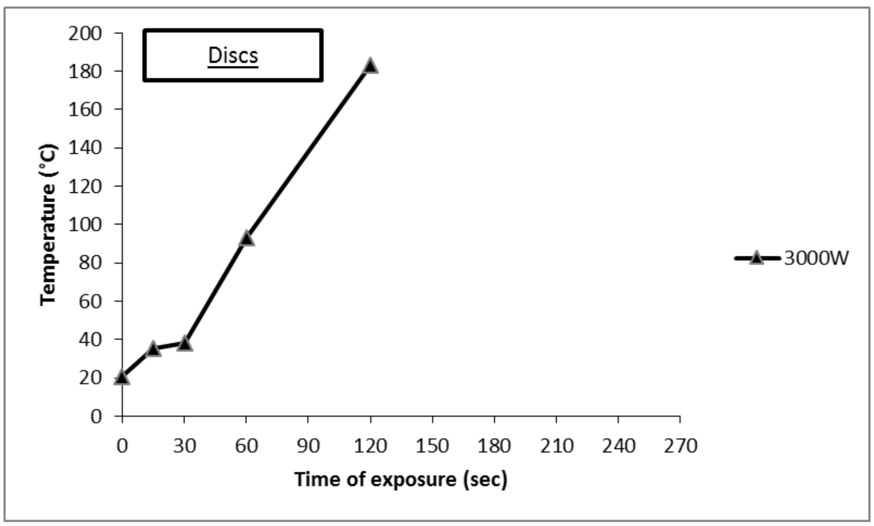

Gneiss : BTS

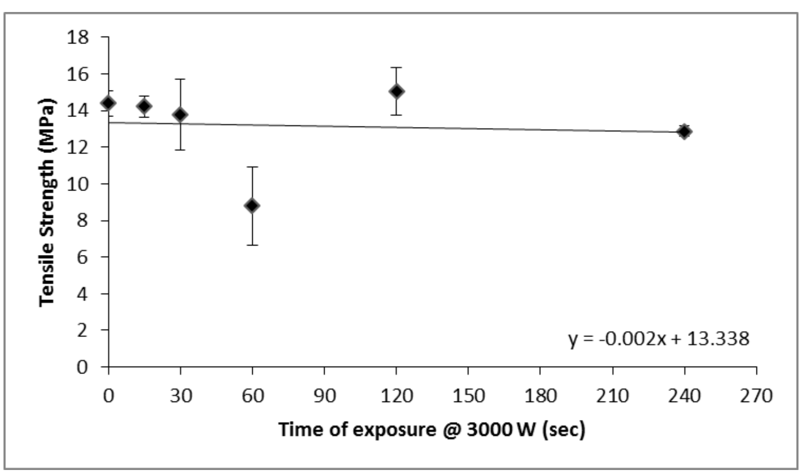

Gneiss : CIA

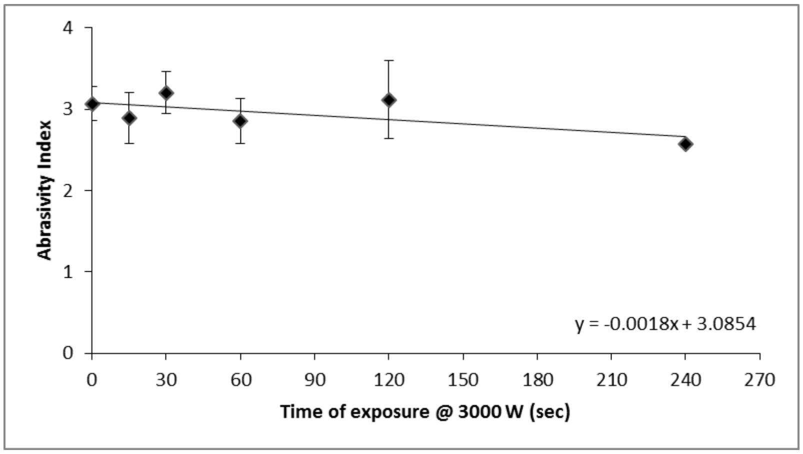

Gneiss : UCS

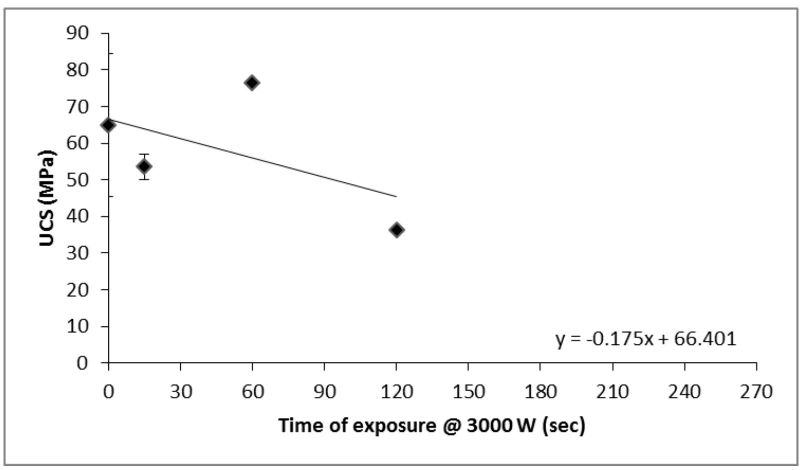

Gabbro : Temperature distrbution

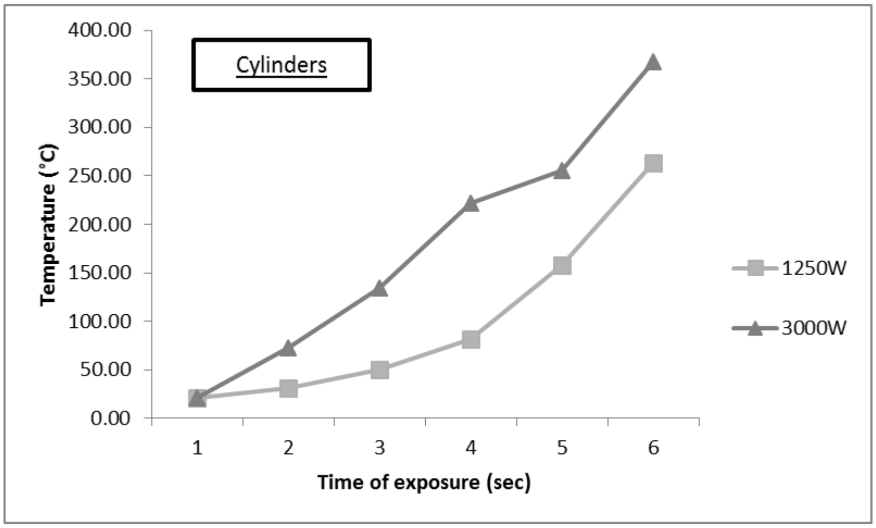

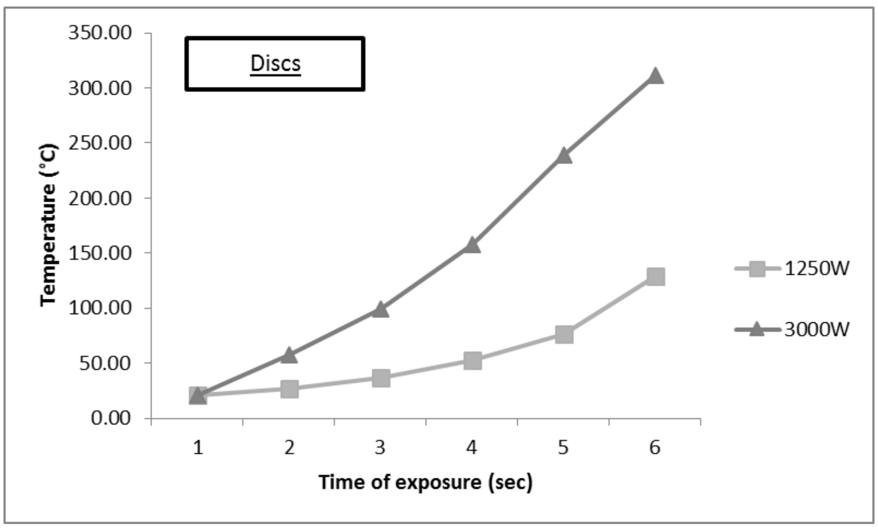

Gabbro : BTS

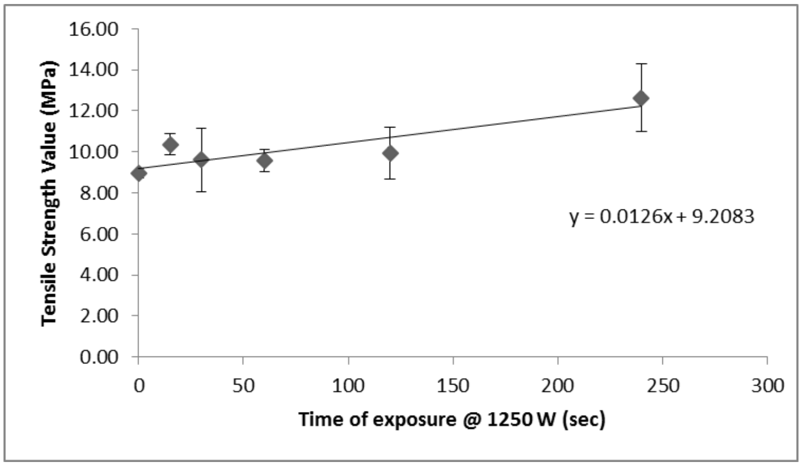

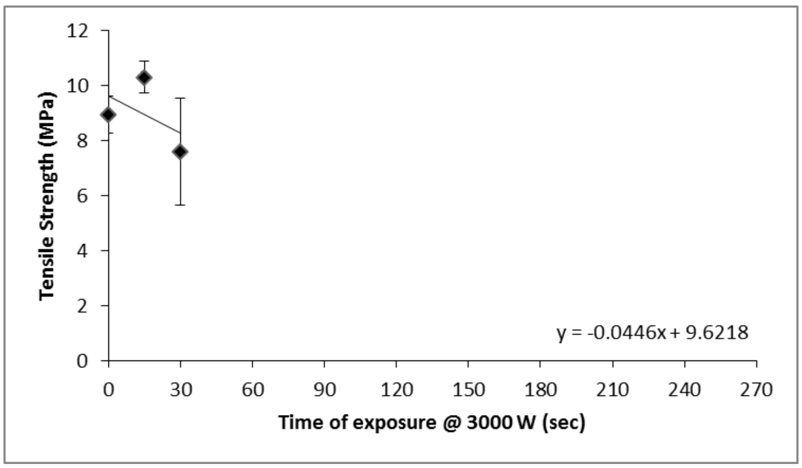

Gabbro : CAI

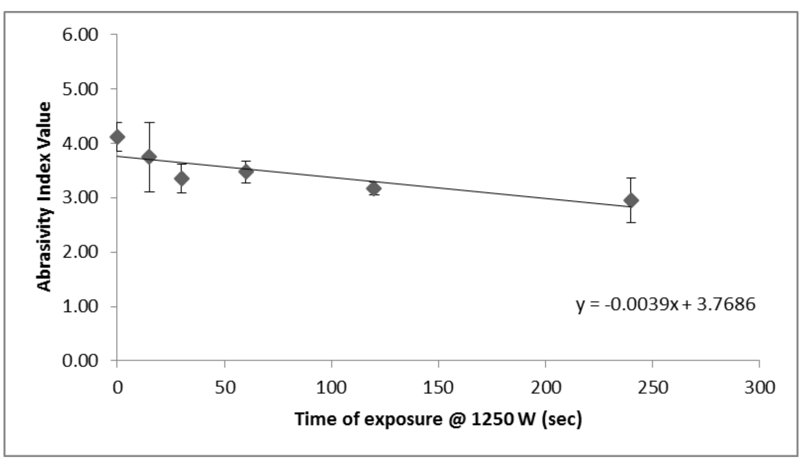

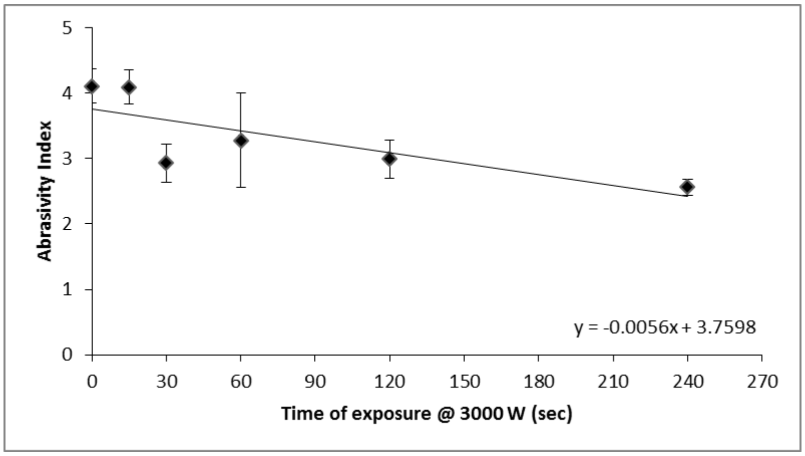
Abrasivity Index
y = -0.0056x + 3.7598
Time of exposure @ 3000 W (sec)

Gabbro : UCS

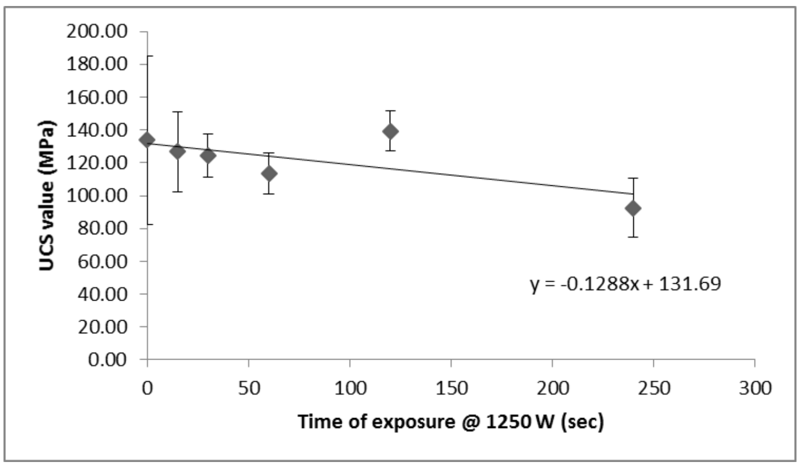
UCS value (MPa)
y = -0.1288x + 131.69
Time of exposure @ 1250 W (sec)

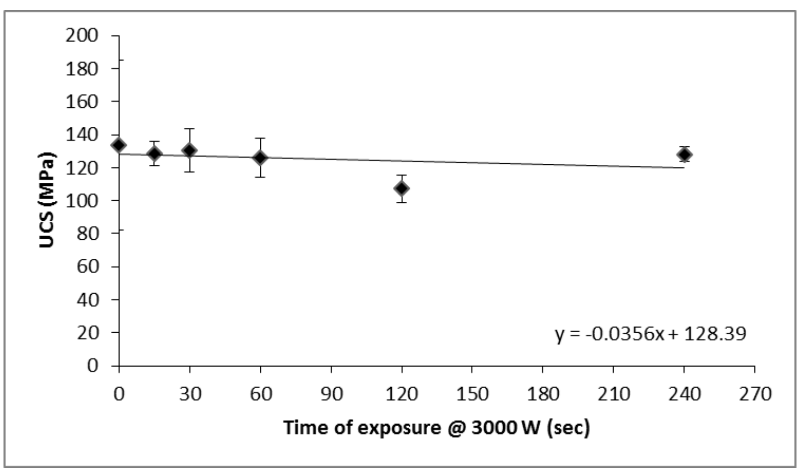
UCS (MPa)
y = -0.0356x + 128.39
Time of exposure @ 3000 W (sec)

Limestone: Temperature distribution

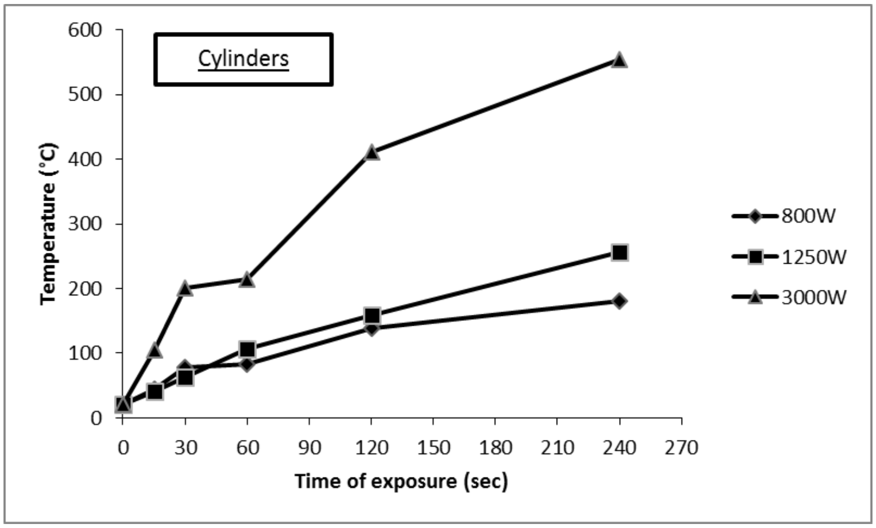

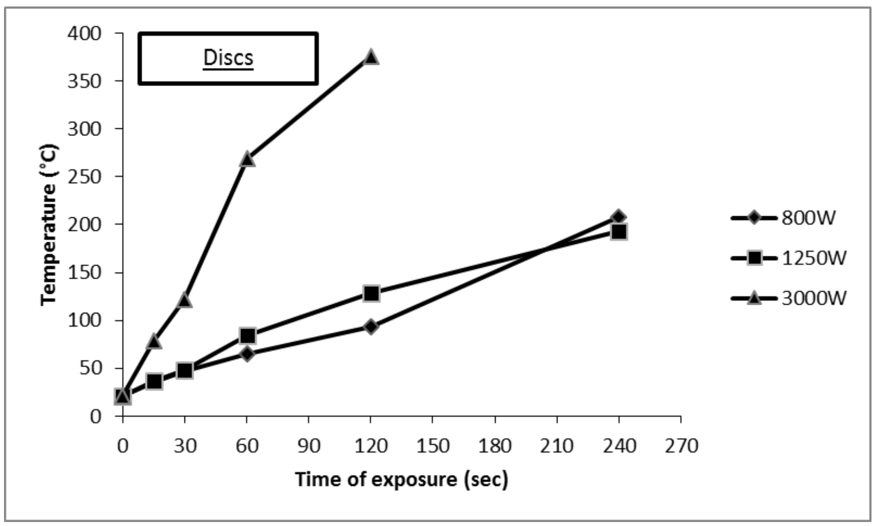

Limestone: BTS

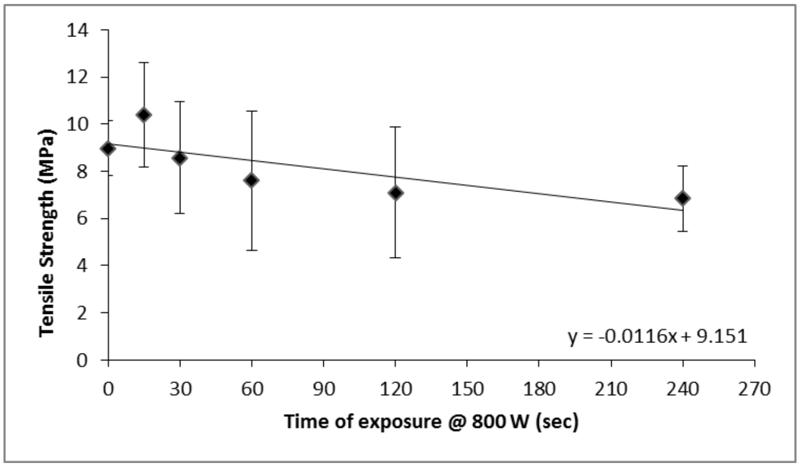

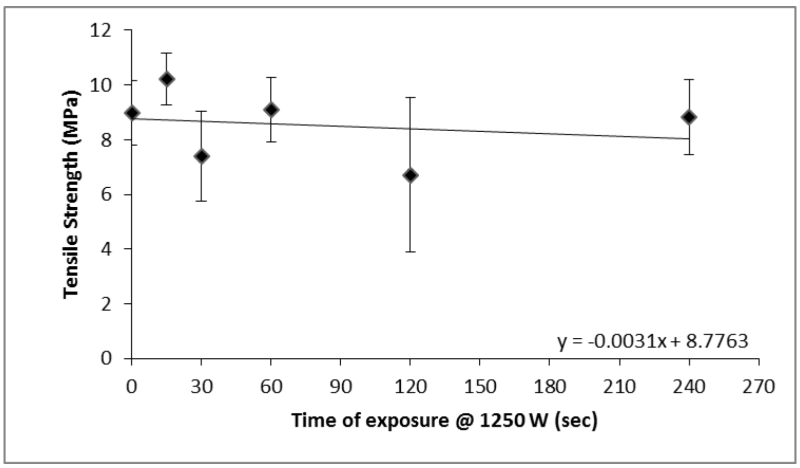

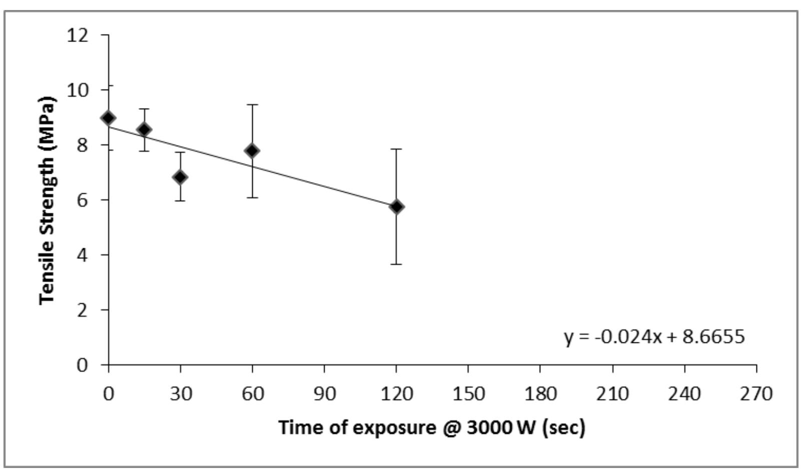

Limestone: CAI

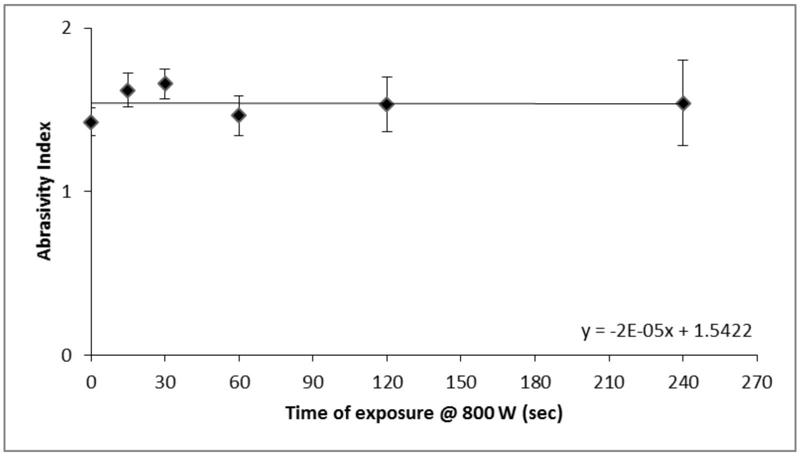

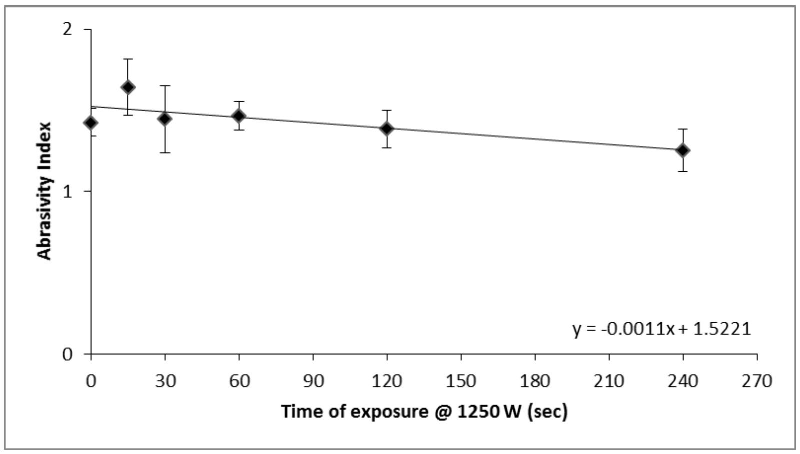

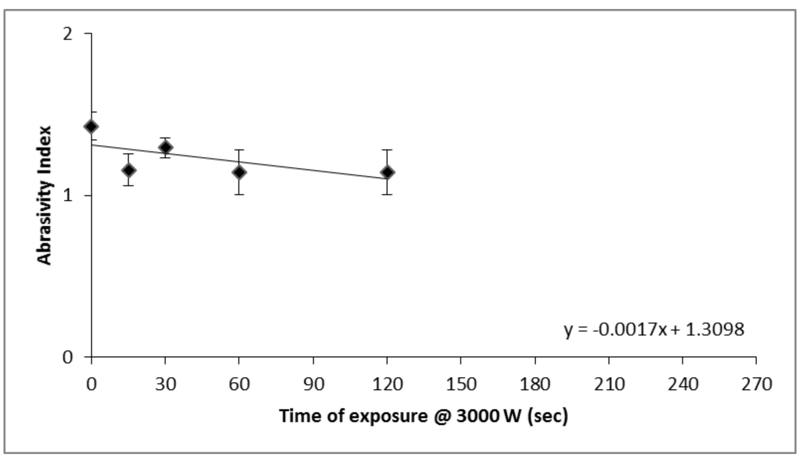

Limestone: UCS

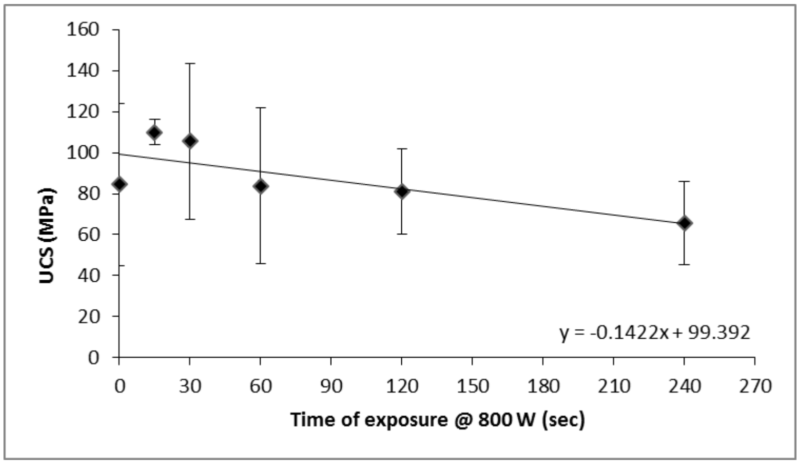

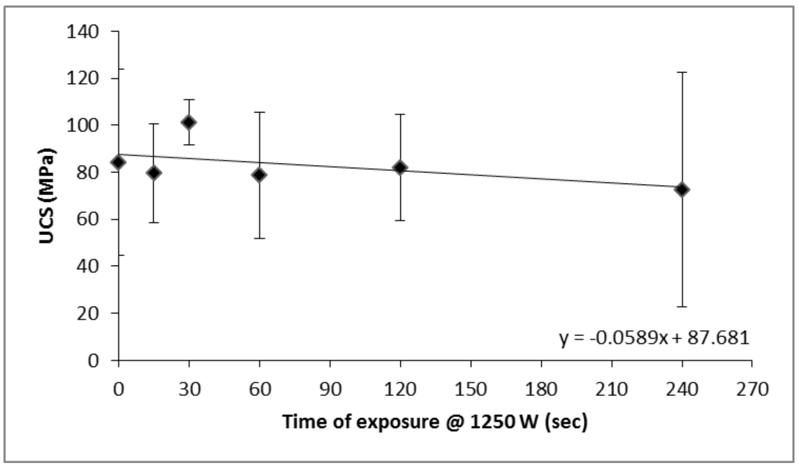

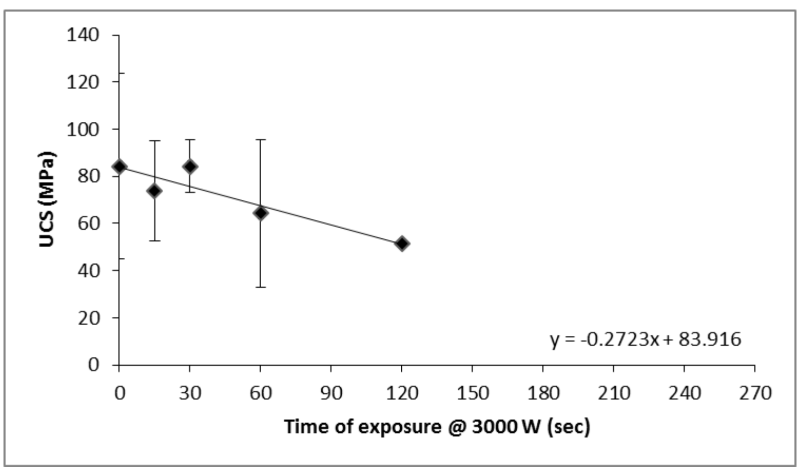

Appendix D: Penetration Depth vs. Loss Tangent

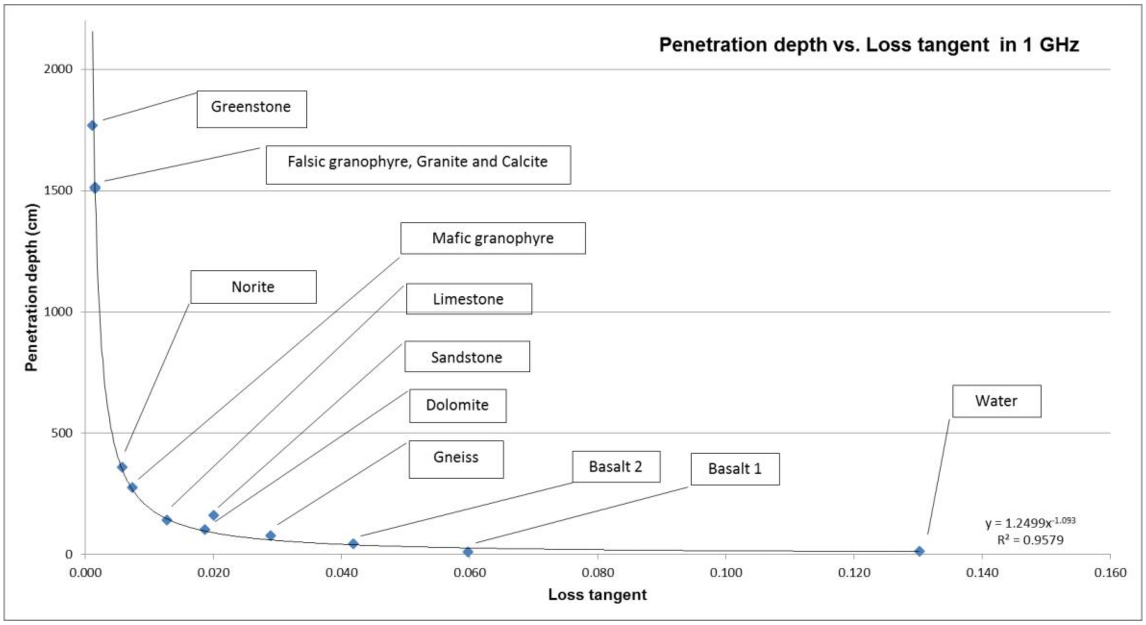

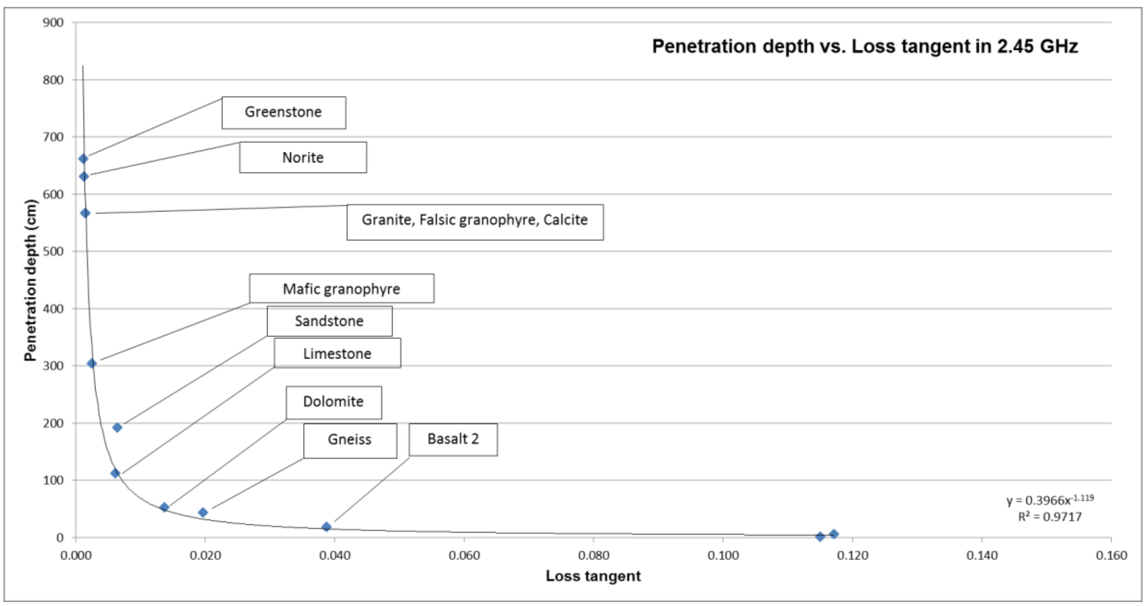

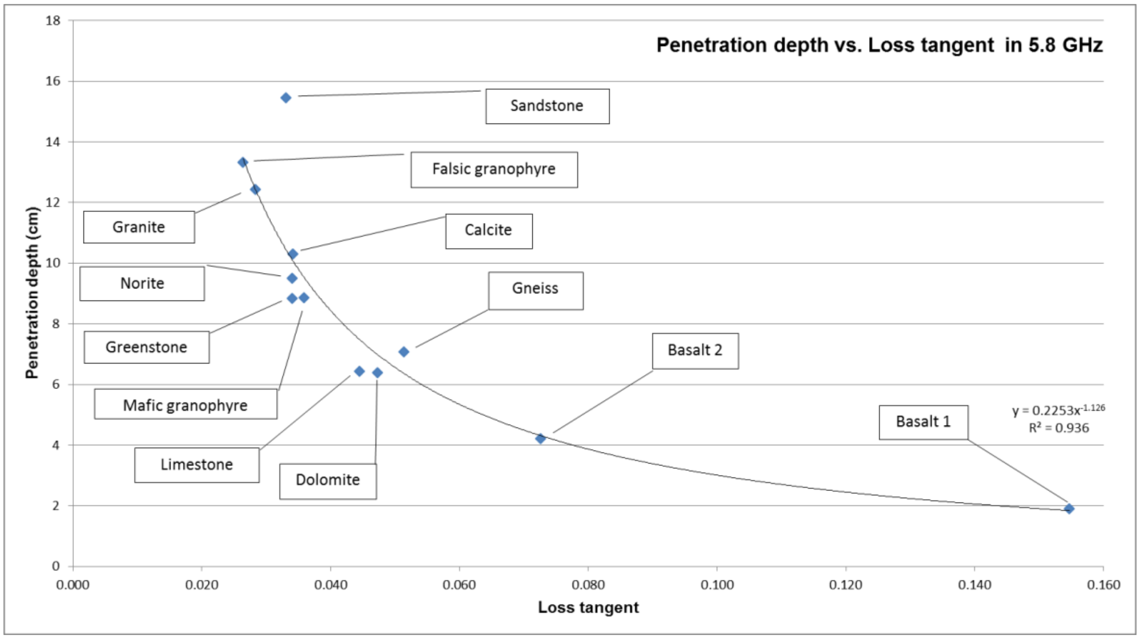
Penetration depth vs. Loss tangent in 5.8 GHz
Penetration depth (cm)
Loss tangent
0
2
4
6
8
10
12
14
16
18
0.000
0.020
0.040
0.060
0.080
0.100
0.120
0.140
0.160
Sandstone
Falsic granophyre
Granite
Calcite
Norite
Gneiss
Greenstone
Basalt 2
Mafic granophyre
Basalt 1
Limestone
Dolomite
y = 0.2253x-1.126
R² = 0.936

Appendix E: Ramp-up of Power over Time